



Virginia Commonwealth University
VCU Scholars Compass

Theses and Dissertations

Graduate School

2014

The Role of ADAM10 in the Immune System: Maintenance of Lymphoid Architecture, MDSC Development and Function, B cell Derived Exosomal Antigen Presentation, and B1 cell IgE Production.

Rebecca Martin
Virginia Commonwealth University

Follow this and additional works at: <https://scholarscompass.vcu.edu/etd>



Part of the [Medicine and Health Sciences Commons](#)

© The Author

Downloaded from

<https://scholarscompass.vcu.edu/etd/588>

This Dissertation is brought to you for free and open access by the Graduate School at VCU Scholars Compass. It has been accepted for inclusion in Theses and Dissertations by an authorized administrator of VCU Scholars Compass. For more information, please contact libcompass@vcu.edu.

© Rebecca K. Martin 2014

All Rights Reserved

The Role of ADAM10 in the Immune System: Maintenance of Lymphoid Architecture,
MDSC Development and Function, B cell Derived Exosomal Antigen Presentation, and
B1 cell IgE Production.

A dissertation submitted in partial fulfillment of the requirements for the degree of Doctor
of Philosophy at Virginia Commonwealth University

by

Rebecca Kelley Martin
B.S., Virginia Commonwealth University 2009

Director: Daniel H. Conrad, PhD
Professor
Department of Microbiology and Immunology
School of Medicine
Virginia Commonwealth University
Richmond, VA
April 25, 2014

Dedication

This dissertation is dedicated to my children: Natalie, Savannah, and Garrett Martin. I hope that one day they invest themselves in something they truly love. I also dedicate this dissertation to my husband, Tim Martin, and to my parents, Kemper and Susan Smith. Without them, all of this would not be possible.

Acknowledgements

First, I would like to thank my advisor, mentor, and friend, Daniel H. Conrad, Ph.D. He encouraged me to think for myself, push myself intellectually, and pursue science in a passionate way. He was always available to discuss an idea or help me troubleshoot a problem. Beyond financially supporting my research, Dr. Conrad provided me with many great opportunities for growth as a scientist. He expanded my horizons by sending me to several national and international meetings. He additionally sent me abroad to work with a collaborator in Uppsala, Sweden. Dr. Conrad's enthusiasm for scientific discovery has motivated me to continue pursuit of a career in academic research.

Second, I would like to thank all the past and current Conrad lab members. I am especially thankful to Sheinei Saleem, Ph.D., for her initial work on the ADAM10Tg mouse and for her collaboration on the MDSC/MC project. She always provided brevity and humor to every situation. She is a wonderful friend. Hannah Zellner, my friend and co-worker, provided unparalleled technical and emotional support. Lauren Folgosa-Cooley coached me in qPCR, western blotting, and delicious food. Her dedication to research is motivating and inspiring. Sheela Damle collaborated on the IL-13/MDSC project and always provided lots of late night laughter. Keith Brooks worked with me on the exosome project and always kept me on my toes. Natalia Chaimowitz collaborated on the ADAM10^{B/-} project. All of my independent study, summer and rotation students contributed to my project, allowed me to share my research with them, and hopefully learned something. I wish them all the upmost success in their careers. Emily Boice, PhD, an honorary Conrad lab member, embarked with me on exciting expeditions,

spent many late hours on encouragement sessions, and was my partner in crime, committing general shenanigans. She helped me capture my 'science spirit.'

Third, I thank our collaborators on the exosome project. Birgitta Heyman, Ph.D. is known for her work on IgE/Ag IC feedback responses. She hosted me for several weeks in Uppsala, Sweden to work on our collaboration. Zhoujie Ding introduced me to the 'Swedish' ways of doing science and became my tour guide whilst in Uppsala. I additionally thank all of our collaborators at VCU. Harry D. Bear, MD/Ph.D. provided weekly guidance and feedback on the tumor project at his lab meetings. Masoud Manjili, DVM/Ph.D., Anne-Marie Irani, MD, Mohey El Shikh, Ph.D., and John Tew, Ph.D. all provided excellent advice, collaboration and help with review of my manuscripts.

Fourth, I am truly thankful to my graduate committee members, Suzanne Barbour, Ph.D., John Ryan, Ph.D., Francine Cabral, Ph.D., and Andrew Lerner, Ph.D. I am especially thankful to Dr. Ryan for his collaboration and insight while working on the MDSC/MC project.

Next, I am thankful to the American Association of Immunologists for the two travel awards to attend and present at the 2013 meeting in Hawaii, USA. I am also thankful to the International Society of Extracellular Vesicles for the travel award to attend and present at the 2012 meeting in Gothenburg, Sweden.

Lastly, I would like to thank my family for their unwavering love and support.

Table of Contents

List of Tables	xv
Table of Figures	xvi
List of Abbreviations	xxi
Abstract	ii
Section 1	1
Chapter 1: ADAM10 and the Maintenance of Secondary Lymphoid Architecture	1
1.1.1 Introduction to ADAM10.....	1
1.1.2 ADAM10 in lymphocyte development	4
1.1.3 Introduction to secondary lymphoid tissues	6
Chapter 2: Materials and Methods	12
1.2.1 Mice	12
1.2.2 PCR and Quantitative PCR.....	12
<i>PCR</i>	12
<i>Quantitative PCR</i>	12
1.2.3 Immunization	13
1.2.4 Cell Isolation	14
<i>Tissue preparation</i>	14
<i>Magnetic Bead Isolation</i>	14
1.2.5 Enzyme Linked Immunosorbant Assay (ELISA)	15

<i>Total antibody levels</i>	15
<i>NP-specific ELISA</i>	15
1.2.6 Flow cytometry, immunofluorescence and confocal microscopy	16
<i>Flow cytometry</i>	16
<i>Immunofluorescence and confocal microscopy</i>	16
<i>Antibodies</i>	17
1.2.7 <i>In vitro</i> activation	19
1.2.8 Statistical analysis	19
Chapter 3: B cell ADAM10 deficient mice have altered responses to T-dependent antigens	22
1.3.1 Generation of mature B cell specific ADAM10 deficient mice	22
1.3.2 ADAM10 is essential for secondary lymphoid architecture	27
<i>ADAM10 is highly expressed in GC B cells</i>	27
<i>Humoral immune responses in ADAM10^{B-/-} mice</i>	27
<i>Germinal Center formation is impaired in ADAM10^{B-/-} mice</i>	28
<i>ADAM10^{B-/-} mice have altered splenic and lymph node architecture</i>	28
<i>ADAM10^{B-/-} mice have dysregulated chemokine expression following antigen challenge</i>	42
<i>Defect in humoral in ADAM10^{B-/-} mice is Notch2 and CD23-independent</i>	42
1.3.3 Discussion	50

<i>ADAM10 is important for B cell follicle formation and maintenance of lymphoid architecture</i>	52
<i>Conclusions</i>	53
Chapter 4: B cell ADAM10 expression and activity is increased during active allergy	55
1.4.1 Introduction to CD23	55
1.4.2 ADAM10 in allergic asthma models	56
1.4.2 ADAM10 in allergic patients	57
Chapter 5: Materials and Methods	58
1.5.1 Human studies	58
1.5.2 Flow cytometry	58
<i>Staining protocol</i>	58
<i>Antibodies</i>	59
1.5.3 <i>In vitro</i> cultures	59
1.5.4 Enzyme Linked Immunosorbent Assay	59
<i>sCD23 ELISA</i>	59
1.5.5 Reagents	60
1.5.6 Statistical analyses	60
Chapter 6: Characterizing ADAM10 in allergic patients PBMC	62
1.6.1 Allergic Patients B cells have increased ADAM10 levels and activity.	62

<i>Allergic patients have increased total B cell ADAM10</i>	62
<i>ADAM10 is not elevated on T cells or monocytes of allergic patients</i>	63
<i>sCD23 is increased in culture supernatant of stimulated allergic patient PBMC over control in an ADAM10 dependent manner.....</i>	63
Section 2	71
Chapter 1: ADAM10 in MDSC development and function.....	71
2.1.1 ADAM10 and myeloid cell development	71
2.1.2 Development of MDSCs	72
2.1.3 Development of the ADAM10Tg mouse	75
2.1.4 Introduction to MDSC Function.....	76
2.1.5 Survival and Proliferation	80
2.1.6 Polarization and differentiation.....	81
2.1.7 Oxidative Metabolism of MDSCs	82
2.1.8 Cytokine production	84
2.1.9 Cell Signaling.....	85
<i>STAT signaling</i>	85
<i>Notch signaling.....</i>	85
2.1.10 Cytokine induced MDSC expansion	86
2.1.11 Subset accumulation in pathological conditions.....	87
<i>Neoplasia.</i>	87

<i>Infection</i>	89
2.1.12 Interaction with cells other than T cells	91
<i>Macrophages</i>	91
<i>Dendritic Cells</i>	92
<i>Mast Cells</i>	93
2.1.13 Introduction to the Mast Cell	93
<i>Mast Cell secreted histamine on MDSC function</i>	94
<i>Mast Cell secreted IL-13 on MDSC function</i>	94
Chapter 2: Methods and Materials	97
2.2.1 Mice	97
2.2.2 Cell Lines	97
2.2.3 Isolation of MDSCs and AT, T cell depletion, and dye labeling.....	98
2.2.4 Arginase1 and iNOS detection.....	98
2.2.5 T cell suppression assays.....	98
2.2.6 BMMC co-culture with ADAM10Tg MDSCs	99
2.2.7 Migration Assays	99
2.2.8 Survival curve and proliferation assays	99
2.2.9 Adoptive immunotherapy of B16 melanoma	100
2.2.10 PCR and quantitative PCR	100
<i>PCR</i>	100

<i>qPCR</i>	100
2.2.11 Flow cytometry.....	101
<i>Sample preparation</i>	101
<i>Immunohistochemistry</i>	101
<i>Antibodies</i>	101
2.2.12 <i>N. brasiliensis</i> infection, GEM treatment, CET treatment, CIM treatment, B16 melanoma or LLC injection, and AT of MDSCs	104
<i>Eggs per gram of feces enumeration</i>	104
<i>L4 and L5 enumeration</i>	104
<i>Serum collection, drug administration, and AT of MDSCs</i>	105
<i>B16 melanoma or LLC injection</i>	105
2.2.13 Human MDSCs	106
2.2.14 Statistical analysis	106
Chapter 3: Results	107
2.3.1 Mast Cells critically augment MDSC activity	107
<i>MDSCs from ADAM10Tg mice are phenotypically and functionally analogous to tumor-induced MDSCs</i>	107
<i>Monocytic MDSCs promote B16 metastasis</i>	108
<i>MDSCs enhance the immune response against N. brasiliensis</i>	116
<i>Mast Cells are essential for MDSC-mediated parasitic clearance</i>	118

<i>MCs also contribute to MDSC-mediated immune suppression in B16 melanoma</i>	119
<i>MCs promote MDSC trafficking and parasite clearance</i>	120
<i>MDSC interaction with MCs maintains the granulocytic population in vitro.</i>	121
2.3.2 Mast cell histamine promotes immunoregulatory activity of MDSCs	156
<i>MDSCs express HR1 and HR2</i>	156
<i>Histamine induces MDSC proliferation and differential gene expression in monocytic versus granulocytic MDSCs</i>	156
<i>Histamine antagonist prevents MDSC-mediated N. brasiliensis expulsion and tumor progression</i>	157
<i>MDSCs are increased in allergic patients</i>	158
<i>IL-13^{-/-} mice have reduced MDSC accumulation in the periphery</i>	159
2.3.3 Discussion	187
Section 3	195
Chapter 1: B1 B cell IgE production in helminth infection	195
3.1.1 Introduction to B1 cells	195
3.1.2 Introduction to IgE	198
3.1.3 Correlation between allergy and helminth infections	199
Chapter 2: Methods and Materials	201
3.2.1 Mice	201

3.2.2 Isolation of MDSCs and AT, T cell depletion, and dye labeling.....	201
3.2.3 ELISA	202
<i>Total IgE ELISA</i>	202
<i>Total IgG1 ELISA</i>	202
3.2.4 Flow cytometry, cell sorting and immunohistochemistry	203
<i>Flow cytometry</i>	203
<i>Cell sorting</i>	203
<i>Immunohistochemistry</i>	203
<i>Antibodies</i>	203
3.2.5 B1 cell culture	205
CHAPTER 3: Th2 helminth infected mice induce a strong B1 cell IgE response that is augmented by MDSCs.....	206
3.3.1 ADAM10Tg mice lack B2 cell development, but elicit a strong IgE response during <i>N. brasiliensis</i> infection	206
<i>ADAM10Tg mice lack B2 cells but have an intact B1 cell compartment</i>	206
<i>ADAM10Tg mice have increased B1 IgE production</i>	211
<i>B1 cells have augmented IgE production that is independent of IgG1 and GCs228</i>	
<i>ADAM10Tg mice lack GC development</i>	211
<i>B1 cells from WT <i>N. brasiliensis</i> infected mice stain positive for IgE</i>	212

<i>B1 cells from N. brasiliensis infected mice make IgE in vitro after stimulation with IL-4 and anti-CD40</i>	212
<i>MDSCs enhance B1 IgE production in WT mice</i>	228
<i>MDSC AT into naïve mice increases IgE production by B1 cells</i>	228
3.3.2 Discussion	235
Section 4	238
Chapter 1: CD23 ⁺ B cell-derived exosomes mediate IgE-antigen complex mediated immune stimulation	238
4.1.1 Introduction	238
Chapter 2: Materials and Methods	241
4.2.1 Mice	241
4.2.2 Exosomal Cell Cultures	241
4.2.3 Exosomal Isolation.....	242
4.2.4 Western Blotting	242
4.2.5 Specific T cell proliferation:	243
<i>In vitro</i>	243
<i>In vivo</i>	243
4.2.6 Flow Cytometry/Immunohistochemistry	244
4.2.7 BMDC culture	244
4.2.8 Statistical Analysis	244

Chapter 3: IgE/Antigen Complexes stimulate OVA specific T cell proliferation	245
4.3.1 Results and Discussion	245
<i>IgE is associated with bexosomes in a CD23 dependent manner.....</i>	<i>245</i>
<i>Increased in vivo antigen specific T cell proliferation is seen with bexosomes from anti-CD40/IL4 activated B cells when IgE/antigen complexes are present in the culture.....</i>	<i>246</i>
<i>Bexosomes must first go through DCs in order to stimulate T cells in vivo.</i>	<i>247</i>
References	263

List of Tables

Table 1. Primer sequences.....	18
Table 2. Flow cytometry and immunohistochemistry antibodies.....	20
Table 3. Antibodies for flow cytometry.....	61
Table 4. List of primers used for PCR and qPCR.....	102
Table 5. List of antibodies used for flow cytometry.....	103
Table 6. Antibodies used in section 3.....	204

Table of Figures

Figure 1. ADAM10 and Notch signaling	23
Figure 2. ADAM10 B cell-specific knockout.....	25
Figure 3. ADAM10 expression on GC B cells.....	30
Figure 4. ADAM10 ^{B-/-} mice have impaired humoral responses.	32
Figure 6. GC formation after T-dependent immunization	36
Figure 7. Immunohistochemistry analysis of GC formation and LN architecture after T-dependent immunization	38
Figure 8. Immunohistochemistry analysis of GC formation and splenic architecture after T-dependent immunization.....	40
Figure 9. Chemokine expression in draining LNs.....	44
Figure 10. Defects in humoral responses in ADAM10 ^{B-/-} mice seem to be Notch2-independent	46
Figure 11. CD23Tg mice have a normal IgG response to NP-KLH	48
Figure 12. Allergic patients have increased total B cell ADAM10	65
Figure 13. ADAM10 is not elevated on T cells or monocytes of allergic patients	67
Figure 14. sCD23 is increased in culture supernatant of stimulated allergic patient PBMC over control in an ADAM10 dependent manner	69
Figure 15. MDSCs from ADAM10Tg mice are phenotypically and functionally analogous to tumor-derived MDSCs.....	110

Figure 16. MDSC depletion restores the antitumor response and prevents metastatic progression of B16 melanoma in ADAM10Tg mice.....	112
Figure 17. Gemcitabine selectively depletes MDSCs, which allows for effective AIT with tumor specific T cells.....	114
Figure 18. ADAM10Tg mice are resistant to <i>N. brasiliensis</i> infection	122
Figure 19. ADAM10Tg MDSCs have increased cytokine expression over WT during <i>N. brasiliensis</i> infection.	124
Figure 20. MDSCs accumulate in mesenteric lymph nodes in <i>N. brasiliensis</i> infection	126
Figure 21. Gemcitabine depletion of MDSCs restores WT response to <i>N. brasiliensis</i> infection to ADAM10Tg mice.....	128
Figure 22. Adoptive transfer of MDSCs from ADAM10Tg mice or LLC-tumor bearing mice induce increased parasitic clearance of <i>N. brasiliensis</i>	130
Figure 23. Granulocytic MDSCs are responsible for MDSC enhanced parasitic clearance in a T cell independent manner.....	132
Figure 24. T cell depleting antibodies completely deplete T cells.....	134
Figure 25. Monocytic MDSCs promote B16 melanoma colonization to the lungs.	136
Figure 26. MCs are required for MDSC-mediated <i>N. brasiliensis</i> clearance	138
Figure 27. MC/MDSC interaction augments cytokine production.	140
Figure 28. MC/MDSC interaction is required for MDSC-mediated immune suppression.	142

Figure 29. MDSCs preferentially migrate to the liver in a MC-dependent manner	144
Figure 30. PKH26GL ⁺ MDSCs are functional.....	146
Figure 31. MDSCs do not traffic to livers of MC-deficient mice during <i>N. brasiliensis</i> infection.....	148
Figure 32. MDSCs migrate preferentially to mast cells.....	150
Figure 33. MCs are required for MDSC-mediated tumor progression	152
Figure 34. Mast cells help maintain the granulocytic population of MDSCs <i>in vitro</i>	154
Figure 35. MDSCs express HRs	161
Figure 36. Histamine increases MDSC survival and proliferation.....	163
Figure 37. Histamine influences MDSC gene expression	165
Figure 38. Ly6C ⁺ MDSCs express increased Arg1 protein with Histamine	167
Figure 39. HR1 and HR2 antagonists blocks MDSC mediated <i>N. brasiliensis</i> clearance	169
Figure 40. HR antagonization inhibits MDSC mediated tumor progression.....	171
Figure 41. Allergic patients have increased circulating MDSCs. Symptomatic allergic patients were compared with non-allergic controls.....	173
Figure 42. MDSC gating strategy for allergic patient study.	175
Figure 43. Human MDSCs have increased survival in the presence of histamine.	177
Figure 44. IL13 is important for MDSC-driven suppression of tumor immunity	179
Figure 45. IL13 deficiency decreases MDSC accumulation in the liver	181

Figure 46. IL13 deficiency decreases MDSC accumulation in the spleen	183
Figure 47. IL13 deficiency does not affect committed progenitor cells of the bone marrow	185
Figure 48. Model of MDSC/MC interaction	193
Figure 49. ADAM10 Overexpression blocks B2 B cell development	207
Figure 50. ADAM10 overexpression does not affect B1 cell development	209
Figure 51. ADAM10Tg mice make increased IgE during <i>N. brasiliensis</i> infection	214
Figure 52. ADAM10Tg mice lack GCs.....	216
Figure 53. ADAM10Tg mice lack normal secondary lymphoid architecture	218
Figure 54. Peritoneal lavage and spleens from <i>N. brasiliensis</i> infected mice contain B1a, B1b and B2 cells	220
Figure 55. B1a cells from peritoneal lavage and spleens of <i>N. brasiliensis</i> infected WT mice stain for IgE	222
Figure 56. B1 cells sorted from peritoneal lavage fluid of <i>N. brasiliensis</i> infected mice make IgE <i>in vitro</i> after stimulation	224
Figure 57. Naïve B1 cells secrete very little IgE without <i>N. brasiliensis</i> infection	226
Figure 58. ADAM10Tg mice make increased IgE during <i>N. brasiliensis</i> infection that is reduced upon GEM treatment	229
Figure 59. ADAM10Tg mice do not make increased IgG1 and GEM does not affect total IgG1 levels in <i>N. brasiliensis</i> infection	231

Figure 60. Adoptive transfer of MDSCs into Naïve WT mice induces B1 IgE production	233
Figure 61. IgE and CD23 are associated with bexosomes.....	249
Figure 62. Bexosomes express co-stimulatory molecules CD80 and CD86	251
Figure 63. B cell derived exosomes by electron micrograph	253
Figure 64. Bexosome-induced antigen specific T cell proliferation is enhanced by IgE, only when CD23 is present and <i>in vivo</i> IgE immune complex T proliferation is enhanced in ADAM10B ^{-/-} mice.....	255
Figure 65. Bexosome-induced antigen specific T cell proliferation is enhanced by IgE in C57BL/6 model of OVA-specific T cell proliferation.....	257
Figure 66. Increased <i>in vivo</i> T proliferation with <i>i.v.</i> injected DCs incubated with bexosomes.....	259
Figure 67. Model for the mechanism of IgE immune complex mediated humoral immunity enhancement	261

List of Abbreviations

-/-	Homozygous deletion of a gene
2.4G2	mAb recognizing the stalk region of murine CD23
5-LO	5-Lipoxygenase
ADAM	A disintegrin and metalloproteinase
ADAM-TS	ADAM-thrombospondins
AID	Activation induced cytosine deaminase
AIT	Adoptive Immunotherapy
Ag	Antigen
APC	Allophycocyanin
APC	Antigen Presenting Cell
AP	Alkaline Phosphatase
AT	Adoptive transfer
Arg1	Arginase-1
ASC	Antibody secreting cell
AT	Adoptive transfer
BALF	Bronchiolar lavage fluid
BALT	Bronchiolar-associated lymphoid tissue

BBS	Borate buffered saline
BCR	B cell Receptor
BM	Bone marrow
BMDC	Bone marrow derived dendritic cell
BMMC	Bone marrow derived mast cell
BMP	Bovine metalloprotease
Breg	B regulatory cell
BSA	Bovine serum albumin
CCL	Chemokine ligand
CCR	Chemokine receptor
CD	Clusters of differentiation
C/EBP- β	CAAT/enhancer binding protein β
CHO	Chinese hamster ovary
CIM	Cimetidine
CK2	Casein Kinase 2
CLP	Common lymphoid progenitor
CMEP	Common myelo-erythroid progenitor

CMLP	Common myelo-lymphoid progenitor
CMP	Common myeloid progenitor
CNS	Central nervous system
CPM	Counts per minute
CSR	Class switch recombination
CoA	Co-Activators
CoR	Co-Repressors
CTL	Cytotoxic T lymphocyte
CT	Cetirizine
CYP	Cyclophosphamide
DC	Dendritic Cell
DLL	Delta-like Notch ligand
DLN	Draining lymph node
DMSO	Dimethyl sulfoxide
DNP	Dinitrophenol
EAE	Experimental autoimmune encephalomyelitis
ELISA	Enzyme linked immunosorbent assay

EMT	Epithelial-mesenchymal transition
EPG	Eggs per gram of feces
ER	Endoplasmic reticulum
FACS	Fluorescence active cell sorting
FBS	Fetal bovine serum
FcεRI	The high affinity IgE receptor
FDC	Follicular dendritic cell
FITC	Fluorescein isothiocyanate
FO	Follicular
FSC	Forward scatter
GALT	Gut-associated lymphoid tissue
GATA3	GATA-binding protein 3
G-CSF	Granulocyte-colony stimulating factor
GEM	Gemcitabine
GI	Gastrointestinal
GM-CSF	Granulocyte macrophage-colony stimulating factor
GMP	Granulocyte macrophage progenitor

GPCR	G-protein coupled receptors
GVHD	Graft versus host disease
HDC	Histidine decarboxylase
HEV	High endothelial venule
HGF	Hepatocyte growth factor
HLX	H2.0-like homeobox
HNSCC	Head and neck squamous cell carcinoma
HR	Histamine receptor
HRP	Horseradish peroxidase
HSC	Hematopoietic stem cells
ICD	Intracellular domain
IFN	Interferon
Ig	Immunoglobulin
IL	Interleukin
iNOS	Inducible nitric oxide synthase
i.p.	Intra-peritoneal
IRF-8	Interferon regulatory factor 8

ITAM	Immunoreceptor tyrosine-based activation motif
ITIM	Immunoreceptor tyrosine-based inhibitory motif
i.v.	Intravenous
Jak	Janus kinase
kuz	Kuzbanian
L-Arg	L-arginine
Lin	Lineage
LLC	Lewis lung carcinoma
LPS	Lipopolysaccharide
LM	Littermate
LN	Lymph node
LSK	Lineage ⁻ Sca ⁺ c-Kit ⁺ bone marrow cells
LT	Lymphotoxin
LTi	Lymphoid tissue inducer
M1	Classically activated macrophage
M2	Alternatively activated macrophage
mAb	Monoclonal antibody

MACS	Magnetic cell sorting
MCs	Mast cells
MCP-1	Monocyte Chemotactic Protein 1
M-CSF	Macrophage-colony stimulating factor
MDSCs	Myeloid derived suppressor cells
MEF	Mouse embryonic fibroblast
MFI	Mean fluorescence intensity
MHC	Major histocompatibility complex
MEP	Myeloid erythroid progenitor
MIF	Macrophage inhibitory factor
MLN	Mesenteric Lymph node
MMP	Matrix metalloprotease
MM	Multiple myeloma
MPP	Multipotent progenitor
mRNA	Messenger ribonucleic acid
MS	Multiple sclerosis
MVB	Multi-vesicular bodies

MZ	Marginal zone
ND	No difference
NICD	Notch intracellular domain
NKT	Natural killer T cell
NO	Nitric oxide
NP-KLH	4-Hydroxy,3-Nitrophenylacetyl Keyhole limpet hemocyanin
NS	Not significant
OCT	Optimal Cutting Temperature medium
ONOO ₂	Peroxynitrites
OVA	Ova albumin
PALS	Peri-arteriolar lymphoid sheath
PB	Peripheral blood
PBMC	Peripheral blood mononuclear cells
PBS	Phosphate buffered saline
PC	Plasma cell
PCR	Polymerase chain reaction
PE	Phycoerythrin

PerCP	Peridinin chlorophyll protein
PIR-A/B	Paired immunoglobulin-like receptors A and B
PL	Peritoneal lavage
PMN	Polymorphonuclear
PNA	Peanut agglutinin
PP	Peyer's patches
RAG1	Recombination activation gene 1
RASV	<i>Salmonella enterica</i> Seroovar <i>Typhimurium</i> vaccine
RBC	Red blood cell
RBP-Jk	Canonical Notch transcription factor
RCC	Renal cell carcinoma
RIP	Receptor intramembrane proteolysis
RNA	Ribonucleic acid
ROS	Reactive oxygen species
RTK	Receptor tyrosine kinase
RUNX3	Runt-related transcription factor 3
s.c.	Subcutaneous

SCF	Stem cell factor
SD	Standard deviation
SDF-1 α	stromal cell derived factor 1 α
SEM	Standard error of the mean
SHP-1	SH ₂ -homology-containing protein-tyrosine phosphatase-1
SHM	Somatic hypermutation
SSC	Side scatter
STAT	Signal transducer and activator of transcription
TACE	TNF- α converting enzyme
T-ALL	T cell acute lymphocytic leukemia
TCR	T cell receptor
TFH	T follicular helper
Tg	Transgenic
TGF- β	Transforming growth factor - Beta
Th1	T helper cell type 1
Th2	T helper cell type 2
TIMP	Tissue inhibitor of metalloprotease

TLR	Toll-like receptor
TNF	Tumor necrosis factor
TNP	Trinitrophenol
VCU	Villus/Crypt Unit
VEGF	Vascular endothelial growth factor
WPG	Whole β -glucan particle
WT	Wild type
YFP	Yellow fluorescent protein

Abstract

THE ROLE OF ADAM10 IN THE IMMUNE SYSTEM: MAINTENANCE OF LYMPHOID ARCHITECTURE, MDSC DEVELOPMENT AND FUNCTION, B CELL DERIVED EXOSOMAL ANTIGEN PRESENTATION, AND B1 CELL IGE PRODUCTION.

Rebecca Kelley Martin

B.S., Virginia Commonwealth University, 2009

A dissertation submitted in partial fulfillment of the requirements for the degree of Doctor of Philosophy at Virginia Commonwealth University.

Virginia Commonwealth University 2014

Director: Daniel H. Conrad, PhD

Professor

Department of Microbiology and Immunology

School of Medicine

ADAM10 is a zinc-dependent metalloprotease. ADAM10 has emerged as a key regulator of cellular processes by cleaving and shedding extracellular domains of multiple transmembrane receptors and ligands. In this study, we examined the role of ADAM10 in the immune system. Here, we show that knocking out ADAM10 on the mature B2 cell causes a defect in the development of secondary lymphoid architecture that becomes more severe post-immunization. We also show that overexpression of ADAM10 leads to a defect in hematopoiesis, which eliminates B2 lymphocyte development. This defect additionally induces accumulation of myeloid derived suppressor cells, MDSCs. ADAM10Tg MDSCs function synonymous to tumor MDSCs. Of the two subpopulations of MDSCs, granulocytic MDSCs increase parasitic clearance in a model of *N. brasiliensis*. Monocytic MDSCs are more immunosuppressive in regards to tumor. Both subpopulations are dependent on the presence of mast cells for activity. It is thought that this relationship is mediated through histamine and IL-13. During *N. brasiliensis* infection, ADAM10Tg mice, lacking B2 B cells but having intact B1 B cells, makes increased IgE over WT mice. This production of IgE is thought to be produced by the B1 cells. Of the two types of B1 cells, B1a cells make the majority of the IgE. This IgE production is enhanced by MDSC accumulation and can be induced by MDSC adoptive transfer in a parasite-free mouse. Lastly, ADAM10 is the key sheddase for CD23 on B2 cells. When IgE is bound to its antigen to form an immune complex, IC, it binds CD23 and is internalized. After CD23 bound to IgE ICs is internalized, it is sorted into bexosomes. These bexosomes are transferred to dendritic cells which are responsible for presenting to T cells and inducing an increased antigen-

specific immune response. Overall, ADAM10 is important for many aspects of the immune response

Section 1

Chapter 1: ADAM10 and the Maintenance of Secondary Lymphoid Architecture

1.1.1 Introduction to ADAM10

ADAM10 is a member of a family of a disintegrin and metalloproteases (ADAMs). ADAMs belong to the metzincin superfamily, along with matrix metalloproteases (MMP) and ADAM-thrombospondins (ADAM-TS). While all functionally active metzincin proteases contain a zinc binding motif, ADAMs are unique in that they also contain a transmembrane domain and are active while membrane bound. ADAMs are membrane-anchored and are therefore responsible for the processing of receptors and ligands expressed on the membrane surface, known as ectodomain shedding. ADAMs can mediate ectodomain shedding and regulated intramembrane proteolysis (RIP) of transmembrane proteins. ADAMs cleave mainly type I and type II transmembrane proteins and shedding of these extracellular domains releases soluble fragments into the extracellular space¹. This ectodomain shedding can lead to down-regulation of events that depend on transmembrane receptor-ligand expression or can activate paracrine and/or autocrine signaling by the production of a soluble mediator. Typical substrates of ADAMs are growth factors, cytokines, chemokines and their receptors, as well as cell adhesion molecules and differentiation factors^{1,2}. While ectodomain shedding is thought to occur constitutively, RIP requires receptor-ligand interaction³. ADAMs are widely expressed and are key in many developmental processes. ADAMs regulate cell-cell and cell-matrix interactions, they modulate differentiation, migration, receptor-ligand signaling or repulsion^{1,4}. The prototypical ADAM is composed of a

prodomain, metalloprotease domain, a disintegrin domain that confers substrate specificity, a cysteine-rich region, a transmembrane domain, and a cytoplasmic tail^{5,6}.

ADAMs were initially discovered as type I transmembrane proteins with shared homology to snake venom integrin ligands⁷. ADAMs and ADAM-related proteins have been described in many different species. These include everything from the yeast, *Schizosaccharomyces pombe* to the nematode worm, *Caenorhabditis elegans*, and the fruit fly, *Drosophila melanogaster*⁸⁻¹⁰. Forty different ADAM family members have been currently identified in the mammalian genome, with 37 expressed in the mouse and 22 in humans^{11,12}. ADAMs shown to possess zinc-dependent protease activity are termed active 'shedases'^{13,14}. These are ADAMs 8,9,10,12,15,17,19,20,21,28,30 and 33. All of these ADAMs share a typical consensus sequence (HEXGHXXGXXHD)¹⁵.

ADAM10 was characterized through study of its homolog, *Kuzbanian* (*kuz*), in *Drosophila*. In 1996, *kuz* was initially identified and studies of embryos deficient in *kuz* elucidated essential roles in lateral inhibition required for development of peripheral and central nervous systems¹⁶. Cloning and sequencing of *kuz* demonstrated the presence of disintegrin and metalloproteinase domains highly homologous to bovine metalloprotease (BMP)¹⁶. BMP was later named ADAM10 and was found to have α -secretase activity and cleave myelin basic protein. It was then well characterized in the cleavage of amyloid plaque proteins and Alzheimer's disease¹⁷. Through subsequent studies involving dominant negative mutants of *kuz*, it was demonstrated that *kuz* initiated RIP of Notch and the nervous system defects seen in initial studies were due to defective Notch signaling¹⁸. Murine studies of ADAM10-deficient embryos reveal early mortality at embryonic day 9.5, resulting from multiple defects in the cardiovascular and

central nervous systems^{19,20}. In the beginning, it was highly controversial that ADAM10 was responsible for Notch cleavage^{21,22}. ADAM17, or TNF α converting enzyme (TACE), was thought to be responsible for S2 cleavage of the Notch1 receptor and was reported by several groups^{23–27}. It is now thought that ADAM10 and ADAM17 may be functionally redundant and when one is absent, a compensatory mechanism will increase the other one and visa-versa^{28,29}. Increased evidence emerged that ADAM10 was exclusively involved in Notch signaling by examination of murine embryos deficient in ADAM10. These embryos mimicked features of Notch1-deficient murine embryos^{22,30}. This was further supported by ADAM17-deficient embryos, as they lacked similarity to the Notch1-deficient embryo³¹. Following these observations, two groups utilizing ADAM10-deficient mouse embryonic fibroblasts (MEFs) reported that while multiple proteases can perform ligand-independent proteolysis of Notch1, ADAM10 is required for ligand-dependent cleavage^{27,32}. Thus, ADAM10 may play a more critical role in Notch signaling than earlier *in vitro* studies predicted.

Some of ADAM10's most well characterized substrates are Notch receptors, such as Delta-like 1-4 and Jagged 1-2. Notch receptors regulate cellular differentiation. Notch signaling is initiated by ADAM10 mediated proteolysis of the extracellular domain of the Notch receptor. The extracellular domain is released and endocytosed by adjacent ligand-expressing cells. This cleavage event, termed S2 cleavage, produces a substrate that can be cleaved by the γ -secretase complex (S3 cleavage). This releases the Notch intracellular domain (NICD), that translocates to the nucleus where it complexes with transcription factor RBP-Jk and induces transcription of Notch target genes, such as CD21, Hes 1, Hes 5 and Deltex-1 as diagramed in **Figure 1**³³.

Other substrates for ADAM10 include CD23, TNF α , and many others^{3,5}. It is well accepted that ADAM10 mediates cleavage of membrane-bound substrates, but recent evidence shows that ADAM10 is not restricted to the plasma-membrane and can cleave substrates on the exosomal membrane^{34,35}. Additionally, ADAM10 is highly expressed in the endoplasmic reticulum (ER), providing a potential new location of activity³⁶. ADAM10 normally cleaves in *cis*, but recent studies of the substrate, ephrin, have shown that *trans*-cleavage is possible³⁷. Little is known about the regulation of ADAM10. ADAM10 is expressed as a zymogen and activation occurs after the pro-domain is cleaved by a furin protease^{38,39}. Following activation, *in vitro* ADAM10 activity can be inhibited by tissue inhibitors of metalloproteases (TIMP)-1 and TIMP-3^{17,40}. Additionally, enhancement of proteolytic activity can be achieved by calcium influx, retinoic acid receptor signaling, PKC signaling, cholesterol depletion, kainite receptor signaling and N-glycosylation^{41–46}.

1.1.2 ADAM10 in lymphocyte development

Notch1 signaling is essential for the commitment to T cell lineage, thus ADAM10 is important given its role in Notch signaling^{47,48}. Enforced Notch1 signaling in bone marrow (BM) progenitors, expressing the constitutively active NICD, promote T cell development⁴⁸. In fact, human mutations surrounding the S2 cleavage site of Notch1 results in ligand-independent proteolysis and excessive Notch1 activation. This ultimately leads to T cell acute lymphocytic leukemia (T-ALL). This mutation accounts for approximately 50 percent of all T-ALL cases²¹.

B2 lymphocytes comprise the majority of circulating B cells. They develop from common lymphoid progenitors (CLPs) and differentiate into pro-, pre-, and ultimately

immature B cells prior to exiting the BM. Given that the Notch1 cleavage site recognized by ADAMs is not present in murine Notch2, and that B cells express Notch2 rather than Notch1, ADAM10 was initially not thought to be involved in B2 cell development^{24,25,49–52}. Just as Notch signaling promotes CLP commitment to the T cell lineage, it prevents B lineage fate. Thus, multiple studies have demonstrated that enforced expression of active NICD in BM progenitors completely abrogates B2 cell development^{48,52}. Following exit from the BM, B2 cells enter a transitional stage and undergo further maturation in the spleen, where the majority differentiates into follicular (FO) B cells. A small subset of these cells, develop into the marginal zone (MZ) B cell lineage, including pre-MZ B cells and MZ B cells. By generating B cell-specific Notch2 knockout mice, it was demonstrated that Notch2 signaling is required for the balance in development of the MZ B cell lineage versus the FO B cell lineage. MZ B cells initiate immune responses to blood-borne infections and assist in transporting antigen into the splenic follicles^{25,53}. B cell specific deletion of the downstream transcription factor RBP-J κ , which binds the NICD fragment released after S3 cleavage, also resulted in a severe loss of MZ B cell development with a concomitant increase in FO B cell development⁵⁴. It is thought that Notch signaling induces a high turnover of E proteins, HEB, E2A, and E2-2, which are implicated in the regulation of peripheral B cell maturation⁵⁴. In mouse models where B cell-E proteins are deleted, an increase in MZ B cell lineages occurs to the detriment of the FO B cell lineage^{54,55}. Moreover, by deleting ADAM10 in a mature B cell-specific manner using the CD19-cre (ADAM10^{B-/-}), Gibb et al. demonstrated an absolute requirement for ADAM10 in MZ B development⁵⁶. Analysis of Notch target gene expression in these mice revealed a dramatic defect in Notch2 signaling. Furthermore,

in contrast to WT B cells, ADAM10-null cells were completely unresponsive to DLL-1-induced Notch stimulation. These findings not only revealed the importance of ADAM10 in B cell development, but also demonstrated that ADAM10 is responsible for activating RIP-mediated signaling through Notch2. No compensatory cleavage of Notch2 by other proteases occurs, thus ADAM10 may be the only protease that can recognize the Notch2 cleavage site, which is distinct from the Notch1 site²⁴. Notch signaling has also been implicated in other B cell functions. Notch signaling alongside B cell receptor (BCR) and CD40 signaling enhances B cell activation as well as, B cell differentiation into antibody secreting cells (ASC) *in vitro*. Notch signaling has also been implicated in germinal center (GC) formation^{50,57,58}. This is thought to be due to defects in development of follicular helper T cells (T_{FH}), which are essential to the GC response and T cell specific Notch1 and Notch2 defects lead to reduced GC B cell numbers and decreased high affinity antibody⁵⁹.

1.1.3 Introduction to secondary lymphoid tissues

Secondary lymphoid tissues are the primary sites of adaptive immune responses. Most lymphocytes within these tissues are mobile and transitory, yet secondary lymphoid structure is highly organized and tightly maintained. The development of these tissues occurs when hematopoietic lymphoid tissue inducer cells (LTi) expressing lymphotoxin $\alpha\beta$ (LT) and mesenchymal cells expressing LT β receptor interact^{60–62}. LT-deficient mice completely lack LNs, peyer's patches (PP) and have disrupted splenic architecture^{60–64}. LT signaling induces mesenchymal cells to differentiate into stromal organizer cells and to induce chemokine expression, leading to the recruitment of naïve

lymphocytes⁶². Disruptions in the TNF α level, a cytokine in the same family as LT, results in abnormal LN and splenic architecture as well^{29,65,66}.

Secondary Lymphoid organs consist of lymph nodes (LN), spleen, bronchiolar-associated lymphoid tissues (BALT), gut-associated lymphoid tissues (GALT), tonsils, PP and other organized lymphoid tissues associated with mucosal surfaces. These organs are located at strategic sites where they can trap foreign antigens entering the body^{61,67–69}. The segregation of cells within these organs is thought to enhance the efficiency of immune responses by arranging B and T cells into zones that provide them interaction with certain antigen presenting cells (APC) and regulatory cells⁶¹. It is also thought that the organization provides a framework for circulating naïve lymphocytes to encounter concentrated foreign antigen⁶¹.

Lymphatic vasculature delivers antigen-presenting cells from the periphery, as well as foreign antigen into the LN. This lymph enters the LN through the afferent lymphatics into the marginal sinuses, directly underneath the LN capsule. Under the marginal sinuses lies the outer cortex, or B cell zone consisting of B cell follicles. Directly beneath this is the paracortex or T cell zone. Underneath this lies the medullary chords containing macrophages and plasma cells, and in the center of the LN medullary sinuses are where the efferent lymphatics remove lymph fluid from the LN^{61,62}.

Circulation enters the LN through high endothelial venules (HEV) in the paracortex, bringing naïve lymphocytes in contact with antigen on APCs⁷⁰. A dendritic cell (DC) or other APC carrying an antigen migrates to the paracortex⁷¹. This is dependent on the chemokine CCR7 binding to its ligands CCL19 and CCL21^{72,73}. This

DC up-regulates CD80/CD86 co-stimulatory molecules as well as processes and presents the antigen on major histocompatibility class (MHC) II. MHC II binds to the specific T cell receptor (TCR) providing the initial signal needed for an immune response. Co-stimulation of CD28 by CD80/CD86 provides the second signal that is essential for the activation of the T cell. An additional specific cytokine milieu induces differentiation of the T helper (Th) cell^{60,74,75}.

Three lineages of CD4⁺ Th cells diverge at this point with respect to the antigen type and signals from APC. The Th1 lineage responds to intracellular pathogens and when inappropriate responses occur, can result in autoimmunity^{76,77}. Differentiation to Th1 cell is initiated by signal transducer and activator of transcription 1 (STAT1) activation through interferon γ (IFN- γ) and or (interleukin) IL-27. This induces the transcription factor T-bet up-regulation. In conjunction with H2.O-like homeobox (HLX) and other transcription factors activated post TCR signal, *ifn γ* transcription is increased and the transcription factor GATA-binding protein 3 (GATA3) is antagonized. This leads to the downstream up-regulation of IL-12 receptor that binds to IL-12 produced by the APC. This IL-12 signaling induces the transcription factor STAT4 and paired with runt-related transcription factor-3 (RUNX3), drives Th1 differentiation^{78–83}. The Th2 lineage responds to helminthes, but when responding to innocuous particles can lead to allergic disease⁷⁷. Th2 cell differentiation involves STAT5 and STAT3 and/or Notch mediated immunoglobulin- κ J region (RBPJ) induction of GATA3 through STAT6 and IL-4. A positive feedback loop drives Th2 differentiation and IL-4, IL-5, IL-13 production^{84–86}. A third Th cell lineage, the Th17 cell responds to extracellular bacteria and fungi. This differentiation is started with activation of STAT3, inducing IL-21. IL-21 signaling in

conjunction with transforming growth factor β (TGF β) by the APC induces the expression of transcription factor retinoic-acid-receptor-related orphan receptor- γ t (ROR γ t), IL-17, and IL-23R. IL-21 and IL-17 drive Th17 cell differentiation^{87–91}.

Th cells then up-regulate CXCR5 and traffic to the B-T border of the B cell follicle, where Th cells activate B cells^{92–94}. The initial signal is delivered via antigen specific BCR binding native epitopes on the antigen and the second signal is co-stimulation with Th cell CD40 ligand binding CD40 on the B cell⁹⁵. This is also influenced by particular Th lineage cell-secreted cytokine milieu. These B cells can then choose three particular fates: a short-lived extra FO plasma cell that secretes low affinity antibody, an early memory B cells, or give rise to the GC reaction^{60,74,75,96}.

GC reaction occurs in the B cell follicles of the LN. Within the GC, B cells undergo extensive differentiation and proliferation during the process called affinity maturation⁹⁶. The GC is divided into two zones morphologically, the light zone and dark zone^{60,97}. B cells were traditionally thought to move through the GC from dark zone to light zone, but can move from light to dark or intra-zonally⁹⁸. Within the dark zone, the B cell undergoes extensive proliferation, somatic hypermutation (SHM) and class switch recombination (CSR)⁶⁰. Initially, the B cell moves to the center of the follicle, where they rapidly divide as centroblasts⁹⁹. This is where B cells begin SHM, the result of point mutations in the variable regions of heavy and light chain in an attempt to create higher affinity antibody^{19,99}. CSR allows replacement of the μ gene with either γ , α , or ϵ ⁶⁰. Different cytokines drive CSR to different antibody classes¹⁰⁰. This occurs through a process of excising loops of DNA involving activation induced cytidine deaminase (AID) and results in the same antibody specificity with new antibody classes, thus new

antibody function^{60,100}. CSR is rare outside the GC reaction, but can occur⁶⁰. Follicular dendritic cells (FDCs) are essential for the GC reaction^{60,92-94}. FDCs and T_{FH} are found mainly in the light zone and are essential for positive selection and affinity maturation^{60,74,101}. After SHM and CSR, centroblasts exit the cell cycle and move to the light zone of the GC as centrocytes⁹⁶. Centrocytes sample antigens bound to immune complexes on FDCs or antigen on T_{FH} cells. This drives the positive signal through the BCR for high affinity, antigen-binding B cells to survive^{74,102,103}. Low affinity or self-reactive B cells are deleted from the GC by apoptosis¹⁰⁴⁻¹⁰⁶. These B cells move on to become long-lived plasma cells, memory B cells or reenter the dark zone for further rounds of SHM and CSR^{107,108}.

The spleen, as a secondary lymphoid organ, undergoes many of the same processes as the LN. It is organized differently as it contains two types of tissue. The red pulp is mainly a filter for damaged and aging erythrocytes, and the white pulp contains the peri-arteriolar lymphoid sheaths (PALS)⁶¹. Directly surrounding the central arteriole is a T cell rich compartment. This compartment is encircled by B cell follicles containing pockets of FDCs^{61,68}. The red pulp is separated from the white pulp by a MZ made up of MZ B cells and MZ macrophages⁶¹. MZ B cell development requires CD19, Notch2 and ADAM10 protein expression and signaling as reviewed earlier^{25,56,109}.

Regardless of the organ, B cells and T cells segregate into specific zones based upon chemokine secretion by stromal cells and chemokine receptor expression. When these chemokine gradients are disrupted, B and T cell positioning changes, which cripples the adaptive immune response.

Here we aim, in this section, to address the role of ADAM10 in secondary lymphoid architecture and GC formation. We utilize ADAM10 deletion in mature B cells utilizing the CD19-cre (ADAM10^{B-/-}) to show dramatic defects in GC formation and antibody responses, accompanied with changes in splenic and LN architecture¹¹⁰.

Chapter 2: Materials and Methods

1.2.1 Mice

ADAM10^{B-/-} mice were previously described⁵⁶. To generate ADAM10^{B-/-} N2ICD-Tg^{B+}. ADAM10^{B-/-} were mated to N2ICD-Tg^{flox/flox} mice¹¹¹. CD19-cre mice were wild type (WT) littermates of ADAM10^{B-/-} and ADAM10^{B-/-}N2ICD-Tg^{B+} mice. CD23Tg mice have been previously described¹¹². BALB/CJ mice were used as littermate controls of CD23Tg mice.

1.2.2 PCR and Quantitative PCR

PCR

For genotyping, DNA was isolated using Direct Tail PCR Solution as directed by the manufacturer (Viagen). Mangomix (Bioline) was used for amplification of CD19 cre-lines, ADAM-10 floxed alleles, YFP-Rosa and N2ICD transgenes. Cycling conditions were as follows, 95°C for 3 minutes then 35 cycles of 94°C for 1 minute, 55°C for 1 minute, 72°C for 2 minutes, and a final extension at 72°C for 10 minutes. Sequences of all primers described above are listed in **Table 1**.

Quantitative PCR

Total RNA was extracted and purified from draining and non-draining mouse LNs using TRIzol reagent (Invitrogen). Samples were treated with DNase (Takara Bio), mixed with phenol/chloroform/isoamyl alcohol solution (25:24:1 USB), and precipitated with ethyl alcohol. The purity of RNA was quantified by a spectrophotometer (ND-100; NanoDrop). One microgram of RNA was reverse transcribed using High Capacity cDNA RT kit (Applied Biosystems). Real-time quantitative PCR was performed with a

real-time PCR machine (iQ5; Bio-Rad Laboratories). Primers and probes for running a TaqMan quantitative PCR assay were purchased from Applied Biosystems. Taqman gene expression assays used included: CCL19: Mm00839967_g1, IL-21: Mm00517640_m1. Primers for CCL21 were synthesized by IDT as previously described¹¹³. PCR products, labeled with 6-FAM-conjugated probes, were amplified with 18S as an internal control. Reaction parameters were as follows: hold at 48°C for 30 minutes and hold at 95°C for 10 minutes, followed by 40 cycles of 95°C for 15 seconds and 60°C for 60 seconds. Results were analyzed with iQ5 real-time PCR software (version 2.0). Sequences of all primers and probes, except those included in purchased Taqman gene expression assays described above, are listed in **Table 1**.

1.2.3 Immunization

For all immunization protocols, mice were of 6-12 weeks of age, unless otherwise stated. When experiments were terminated, mice were euthanized via isofluorane inhalation and cervical dislocation. All mouse protocols were approved by Virginia Commonwealth University's Institutional Animal Care and Use Committee.

Mice were immunized with a single 10µg 4-Hydroxy-3-nitrophenylacetyl injection coupled to keyhole limpet hemocyanin at a ratio of 27:1 (NP₂₇KLH – from this point called NP-KLH) (Biosearch Technologies). For intra-peritoneal injections, mice were given 200µL of immunization mixture, made as follows: 10µg of NP-KLH in 100µL of PBS and 100µL of alum (4mg). For footpad injections, mice were given 25µL of immunization mixture, made as follows: 10µg of NP-KLH in 10µL of PBS and 15µL of alum (0.6mg). Mice were bled weekly via tail vein nick and cardiac punctured when the experiment was terminated.

1.2.4 Cell Isolation

Tissue preparation

Single cell suspensions of peripheral LN cells and splenocytes were generated by disrupting tissue between frosted glass slides. Red blood cells (RBCs) were then lysed using ACK lysis buffer (Quality Biological). Cells were plated or stained depending on experimental design.

Magnetic Bead Isolation

Cellular isolations were carried out using magnetic bead selection (Miltenyi Biotec). Briefly, single cell suspension was generated as described above. Cells were resuspended in MACS buffer (PBS pH 7.2, 0.5% BSA, and 2mM EDTA) and incubated with the corresponding magnetic beads for 15 minutes at 4°C. Cells were then washed and passed through a magnetic column via manufacturer's protocol (Miltenyi Biotec). When cells were isolated via negative selection, LD columns were used and flow-through was harvested. On the other hand, when cells were isolated via positive selection, LS columns were used. In this case, after cells were passed through the column, columns were washed and flushed with MACS buffer and the eluted cells were utilized for experiments. For B cell isolation, cells were isolated via positive selection (B220⁺ cells) for all cells or via negative selection (CD43⁻) for isolation of naïve or untouched B cells.

1.2.5 Enzyme Linked Immunosorbant Assay (ELISA)

Total antibody levels

For total Ig ELISAs, ELISA plates were coated with 5µg/mL of goat-anti Ig (Southern Biotech) in BBS (0.15M sodium chloride, 0.01 M borate buffer, pH=8.5). Plates were then incubated at 37°C for an hour or at 4°C overnight. Plates were then washed three times with ELISA wash (PBS with 0.02% Tween20). Blocking solution (PBS with 0.02% Tween20 and 2% FBS) was added to plates. Plates were then washed three times with ELISA wash and samples were added, diluted in block. For standard curve, normal mouse Ig (Southern Biotech) was used. Plates were then incubated at 37°C for an hour or at 4°C overnight. Plates were washed three times with ELISA wash and goat-anti Ig-AP was diluted in block (1:400 dilution) (Southern Biotech). After 1 hour incubation at 37°C, plates were washed and developed with phosphate tablets (Sigma-Aldrich) dissolved in substrate buffer (0.1g $\text{MgCl}_2 \cdot 6\text{H}_2\text{O}$, 0.2 NaN_3 , 50mL diethanolamine, pH to 9.8 per 500mL). Absorbance at 405nm was measured.

NP-specific ELISA

For NP-specific ELISAs, ELISA was carried out as previously described with minor modification. Plates were coated with NP₁₄BSA (Biosearch Technologies) (15µg/mL in PBS) for samples and with 5 µg/mL of goat-anti-Ig (Southern Biotech) in BBS for standards. The remaining steps were carried out as previously described (see total antibody levels). For measurement of high affinity antibodies, the protocol was carried out as described except that plates were coated with NP₄-BSA (both low and high affinity antibodies bind NP₁₄BSA). The described NP-specific ELISA protocol allows for the relative quantification of high vs. low affinity antibodies¹¹⁴.

1.2.6 Flow cytometry, immunofluorescence and confocal microscopy

Flow cytometry

Cell isolation was conducted as previously described (1.2.4). Cells were labeled following RBC lysis and filtered through 40µm cell strainers. For surface staining, cells were washed in FACS buffer (2% FBS in PBS). $1-3 \times 10^6$ cells were resuspended in 50-100µL. Cells were then incubated on ice with 1-5µg of Fc block (2.4G2) for 10 minutes to prevent non-specific staining. Subsequently, cells were incubated for 30 minutes on ice with different combinations of 0.25-0.5µg of anti-mouse antibodies. Cells were then washed with FACS buffer and analyzed. Flow cytometry analysis was performed using a Canto or Aria II (BD Biosciences) using DIVA software at the Flow Cytometry Core at Virginia Commonwealth University. Flow cytometry data analysis was conducted with Flowjo v8.8.7 (Tree Star).

Immunofluorescence and confocal microscopy

Spleen and LNs were flash frozen on dry ice in OCT compound (Tissue-Tek; Sakura). Serial 10µm sections were cut from frozen blocks using a cryostat (Frigocut 2800E; Jung), mounted on Superfrost Plus slides (VWR), fixed in absolute acetone for 15 minutes, and air-dried. Slides were blocked with 10% Normal Horse Serum with 3% BSA in PBS for 20 minutes to prevent background staining and then washed in ice cold PBS. Antibody was incubated in block solution for 60 minutes in the dark with different anti-mouse antibodies (concentrations varied for each antibody, see **Table 2**). Slides were washed in ice cold PBS 3 times for 5 minutes on oscillation in the dark. Slides were mounted with #1 cover slips (CORNING) using Vectashield Hardset mounting medium (Vector Labs). Slides were allowed to dry in the dark at room temp for 2 hours

before storage at 4°C until visualization. Slides were examined with a confocal laser scanning microscope (TCS-SP2 AOBS; Leica) fitted with an oil Plan-Apochromat 40x objective. Two lasers were used: argon (488nm) for FITC, and HeNe (543 nm) for PE and APC. Parameters were adjusted to scan at a 512x512 pixel density and an 8-bit pixel depth. Emissions were recorded in three separate channels. Digital images were captured, overlayed, and processed with the Confocal and LCS Lite programs (Leica).

Antibodies

All antibodies used for flow cytometry are listed in **Table 2**.

Table 1. Primer sequences

S- sense, AS- anti-sense

PCR	5' > 3'
ADAM10: Intron8	CAGTGTAATGTGAACTCACCC
ADAM10: Intron9	CGTATCTCAAACTACCCTCCC
N2ICD: N2AD1	CCTTATGATGTTCCCGATTATGC
N2ICD: N2AD2	AGTACACCCATCTGGGCCTCG
YFP: oMIR4982	AAGACCGCGAAGAGTTTGTC
YFP: oMIR8545	AAAGTCGCTCTGAGTTGTTAT
YFP: oMIR8546	GGAGCGGGAGAAATGGATATG
CD19-cre: oMIR1084	GCGGTCTGGCAGTAAAACTATC
CD19-cre: oMIR1085	GTGAAACAGCATTGCTGTCACTT
Quantitative PCR	
18S S	AAAATTAGAGTGTTCAAAGCAGGC
18S probe	CGAGCAGCCGCCTGGATACCGC
18S AS	CCTCAGTTCCGAAAACCAACAA
CCL21 S	AGACTCAGGAGCCCAAAGCA
CCL21 AS	GTTGAAGCAGGGCAAGGGT
CCL21 probe	CCACCTCATGCTCCAATAAGT

1.2.7 *In vitro* activation

For IgG1 and IgE production, B cells or splenocytes were cultured with CD40L-transfected Chinese hamster ovary (CHO) cells as a B cell stimulant (6×10^4 cells/well) or with 1 μ g/mL of stimulating anti-CD40 antibody (Invitrogen) and IL-4 (10,000 U/mL; NIH) for seven days. Supernatants were then harvested and analyzed for IgG1 and IgE production by ELISA. Cells were also stimulated with 50 μ g/mL of LPS (Sigma-Aldrich). Four days later, supernatants were harvested and analyzed for IgM and IgG3 production.

1.2.8 Statistical analysis

When dealing with two groups, p-values were calculated using unpaired two-tailed Student's t-tests in GraphPad Prism, unless samples did not form a Gaussian distribution, indicated by a failed D-Agostino and Pearson omnibus normality test. In the case of non-parametric populations, p-values were calculated using two-tailed Mann-Whitney test. When more than two were compared, p-values were calculated using a one-way analysis of variance with a Tukey post-test. Error bars represent the standard error of the mean (SEM) between samples. $p < 0.05$ is considered significant.

Table 2. Flow cytometry and immunohistochemistry antibodies

Specificity	Clone	Label	Source	Concentration Used
Immunohistochemistry				
B220/CD45R	RA3-6B2	FITC, PE	Biolegend	3µg/mL
CCL21	59106	Unlabeled	R&D	7.5µg/mL
CD19	6D5	PE	Biolegend	3µg/mL
CD21/CD35	7G6	FITC	Biolegend	3µg/mL
CD3ε	17A2	PE, FITC	Biolegend	2µg/mL
GL7 (B and T activation marker)	GL7	FITC	eBioscience BD Bioscience	3µg/mL
IgD	11-26c.2a	PE	Biolegend	3µg/mL
Thy1.2	30-H12	FITC, PE	Southern Biotech	3µg/mL, 5µg/mL
Rat IgG		Dylight 549	AbD Serotec	1:200
ADAM-10	139712	FITC	R&D	3µg/mL
Flow cytometry				
ADAM-10	139712	FITC, PE	R&D	
B220/CD45R	RA3-6B2	FITC, PE, APC, PE/Cy7	Biolegend	
CD16/CD32	2.4G2	Unlabeled	In house	

CD38	90	PE/Cy7	Biolegend
CD21/CD35	7G6	PE	Biolegend
IgG1	A85-1	APC, PE	BD Biosciences
IgD	11-26c.2a	PE, PerCP/Cy5.5	BD Biosciences
IgM	RMM-1	PE, APC, APC/Cy7, PerCP/Cy5.5	Biolegend

All made against mouse unless otherwise noted

Chapter 3: B cell ADAM10 deficient mice have altered responses to T-dependent antigens

1.3.1 Generation of mature B cell specific ADAM10 deficient mice

Our lab generated B cell-specific ADAM10 knockout mice (ADAM10^{B-/-}). These mice were generated by crossing homozygous floxed ADAM10 animals with CD19-cre animals¹¹⁵. These ADAM10^{B-/-} mice lacked MZ B cells, had drastically reduced numbers of pre-MZBs and a significant increase in FO B cells⁵⁶. In order to follow recombination in the CD19⁺ cells, ADAM10^{B-/-} mice were crossed with the YFP reporter mouse. This mouse only expresses YFP after cre-driven recombination, in cells where the recombination occurs⁵⁶. The generation of these mice is outlined in **Figure 2**.

The CD19-cre mediates efficient recombination of loxP-flanked gene sites in mature cells¹¹⁶. CD19 is expressed starting at the pro-B cell stage, but CD19-cre recombination is limited in the immature B cell, the pre-B cell¹¹⁷. Only ten percent of CD19⁺ B cells in CD19-cre⁺ YFP⁺ mice have undergone cre-mediated recombination in the BM¹¹⁸.

Figure 1. ADAM10 and Notch signaling

ADAM10 mediated RIP of Notch2 is required for MZ B cell development²⁵. The Notch2 heterodimer on B cells binds ligands Jagged 1-2 and Delta-like-1 that are present on stromal cells or APCs. Binding initiates sequential cleavage events by ADAM10 (S2 cleavage) and γ -secretase complex (S3 cleavage). Cleavage releases the Notch2 intracellular domain (N2ICD). Transport of the N2ICD to the nucleus followed by binding to the transcription factor RBP-Jk allows the release of co-repressors (CoR) and attraction of co-activators (CoA) to the transcriptional complex. The activated complex transcribes Notch target genes, including CD21/35, Deltex-1, Hes 1, and Hes 5, that promote development of MZ B cells. Deletion of ADAM10, Notch2, and RBP-Jk from B cells, or Delta-like 1 from stromal cells prevents MZ B cell development.

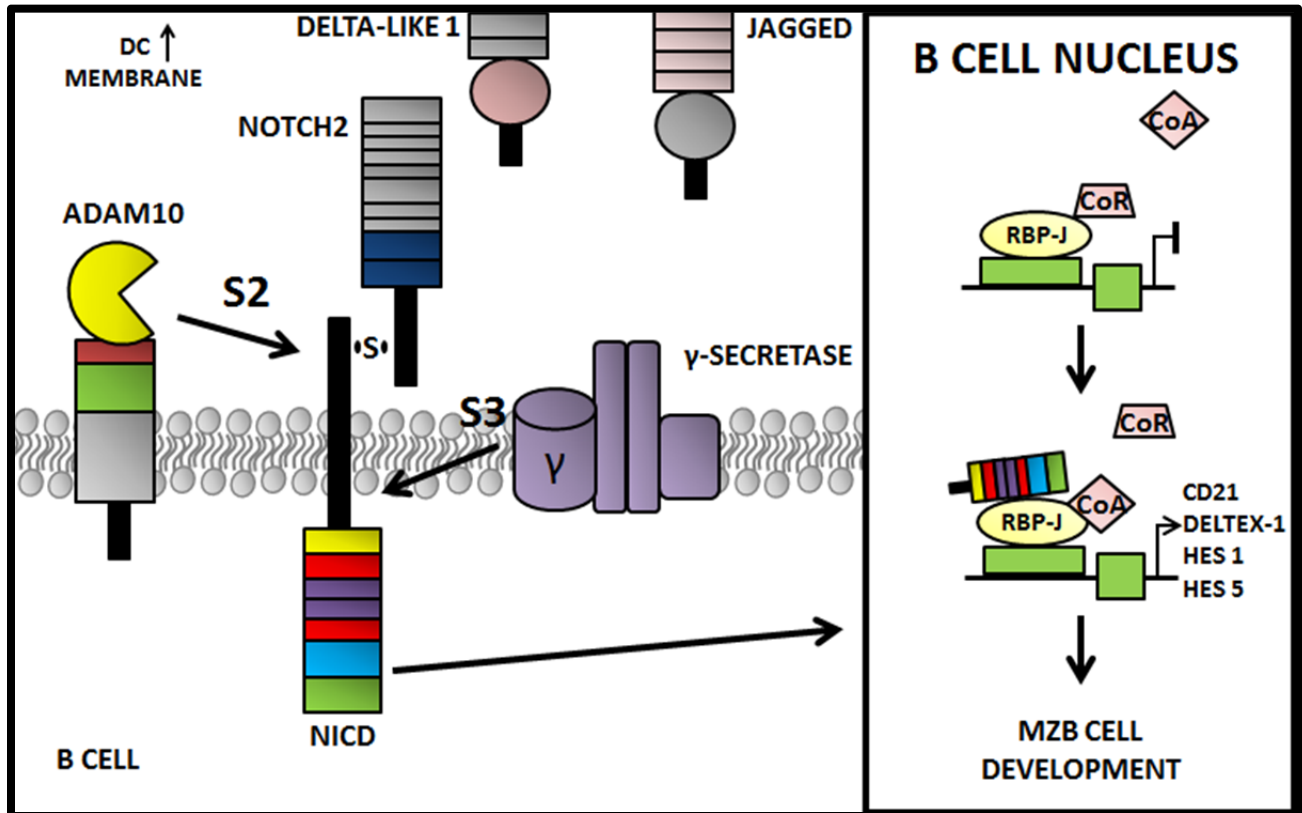


Figure 2. ADAM10 B cell-specific knockout

CD19-cre mice express cre-recombinase under the CD19 promoter. When CD19 expression is turned on in cells that normally express CD19, such as mature B cells, cre is expressed. Note, that this allele is kept heterozygous with the WT CD19 allele to avoid disruption in CD19 expression. In our ADAM10 floxed mice, loxP sites flank the ADAM10 gene. Upon expression of cre, recombination occurs at loxP sites, excising the gene and knocking out ADAM10. Additionally, these mice utilize the YFP reporter gene. With expression of cre, recombination occurs at loxP sites flanking a STOP sequence upstream of the YFP-Rosa gene. With the excision of the STOP sequence, the YFP-Rosa gene is transcribed. This yellow fluorescent molecule allows cre expression to be monitored as well as ADAM10-deletion. (A) Normal ADAM10 expression occurs without cre-recombinase. Thus, ADAM10 is not deleted and YFP expression is not induced. (B) Cre-recombinase is expressed when CD19 is turned on, this ADAM10 is knocked out and YFP is expressed.

1.3.2 ADAM10 is essential for secondary lymphoid architecture

ADAM10 is highly expressed in GC B cells

ADAM10 cleaves many substrates closely linked to humoral immune responses, not only Notch1 and 2, but TNF α and CD23 as well^{28,47,119}. We therefore sought to examine the role of B cell ADAM10 in humoral responses. First, in collaboration with Joanna Cichy from Jagiellonian University, Krakow, Poland, we examined the expression of ADAM10 within secondary lymphoid tissue undergoing GC response. PPs are located in the gut and have a high level of GC activity. Flow cytometry of PPs demonstrated that while less than 2% of naïve B cells expressed ADAM10, over 80% of GC B cells were ADAM10⁺ (**Figure 3A,B**). These results were confirmed by immunofluorescent staining of sectioned PPs for ADAM10, PNA, and IgD. Consistent with the flow cytometry results, ADAM10 was highly expressed by cells within GCs (**Figure 3C**).

Humoral immune responses in ADAM10^{B-/-} mice

Given the significant expression of ADAM10 in GC B cells, we investigated its role in humoral responses by using B cell-specific ADAM10-deficient mice (ADAM10^{B-/-}). Basal levels of serum IgM, IgG1, IgG2a, and IgG2b were significantly reduced in ADAM10^{B-/-} mice when compared with WT, suggesting a defect in antibody production (**Figure 4A**). To directly assess antigen-specific antibody production, we immunized ADAM10^{B-/-} mice intra-peritoneally (*i.p.*) with NP-KLH and examined serum levels of NP-specific antibody. ADAM10^{B-/-} mice showed reduced levels of NP-specific IgM 7 d post-immunization. However, levels reached control values by day 14 and through the remainder of the experiment (**Figure 4B**). In contrast, NP-specific IgG

levels, both total and high affinity, were reduced 4 weeks post-immunization (**Figure 4B**). This reduction in IgG was not specific to a particular isotype, as antigen-specific IgG1, IgG2a, and IgG2b were dramatically reduced in ADAM10^{B-/-} mice (**Figure 5A**). Furthermore, even when immunization with a high antigen dose, 1 mg NP-KLH, was performed, ADAM10^{B-/-} mice failed to mount a normal antibody response, demonstrating that the defect in antibody production cannot be overcome by simply providing more antigen (**Figure 5B**).

Germinal Center formation is impaired in ADAM10^{B-/-} mice

As demonstrated in Figure 5, antigen-specific ASCs were reduced in immunized ADAM10^{B-/-} mice. Being that long lived plasma cells (PC) and memory cells are generated within the GC¹²⁰, GC formation in ADAM10^{B-/-} mice was examined. GC B cells, defined as IgM^{lo}IgD^{lo}B220⁺IgG1⁺CD38^{lo}, were enumerated by flow cytometry¹²¹ (**Figure 6A**). Remarkably, the number and percentage of GC B cells within the spleen was dramatically decreased in ADAM10^{B-/-} mice (**Figure 6B,C**).

ADAM10^{B-/-} mice have altered splenic and lymph node architecture

To better understand the relationship between decreased GC B cells and the defects in antibody production depicted in Figure 4, we assessed GC formation in immunized mice by immunohistochemistry. As depicted in **Figure 7A**, although several GCs could be detected in littermate controls, as determined by GL7⁺ cells, draining LNs of ADAM10^{B-/-} mice contained a paucity of GL7⁺ clusters. Interestingly, GL7⁺ cells were scattered throughout the LNs of ADAM10^{B-/-} mice (**Figure 7A**). Given the unusual pattern of GL7 expression, we then analyzed B and T cell localization within the LNs. Surprisingly, the distribution of B and T cells was aberrant, suggesting that B cell-

specific ADAM10 deletion leads to changes in LN structure (**Figure 7B**). In contrast, LN structure in non-draining nodes or unimmunized mice, were relatively normal with regard to B and T cell segregation, but B cell follicles appear thin, reminiscent of TNF α or LT β -deficient mice (**Figure 7D**)^{65,122}.

Given that FDCs play a crucial role in GC formation and lymphoid tissue structure^{123–125}, we stained draining LN sections for FDCs with CD21/CD35 (CR2). FDCs are known to up-regulate CD21/CD35 subsequent to activation¹²⁶. Consistent with the absence in GCs and disorganized lymphoid architecture, FDC networks were not detectable in LN and spleen from ADAM10^{B-/-} mice (**Figure 7C, 8D**). Unlike the draining LNs, GL7 staining was not detected in spleen of ADAM10^{B-/-} mice (**Figure 8A**). However, although normal in unimmunized mice, splenic architecture was also clearly altered post-immunization (**Figure 8B,C**).

Figure 3. ADAM10 expression on GC B cells

A and B, Expression of ADAM10 on gated GC $\text{PNA}^{\text{hi}}\text{IgD}^{\text{lo}}$ (blue) and naive $\text{PNA}^{\text{lo}}\text{IgD}^{\text{hi}}$ (red) B (CD19^+) cells isolated from PPs. Flow cytometry gates used to define the GC and naive B cell populations are indicated on the left. To demonstrate specificity of staining, we used isotype-matched monoclonal antibody (mAb) (isotype). A, Gating protocol is shown. B, Percentage of ADAM10^+ cells in naive and GC B cells. C, Frozen serial sections of PPs were stained to detect B cell follicles (B220^+ , blue), GCs (PNA^+ , green), and ADAM10 (red) (right panel). To demonstrate specificity of staining, we used isotype-matched mAb instead of mAb against ADAM10 (left panel). Original magnification $\times 20$. The mucosal epithelium (E) also reacts with PNA and anti-ADAM10. Figure courtesy of Joanna Cichy, from Jagiellonian University, Krakow, Poland.

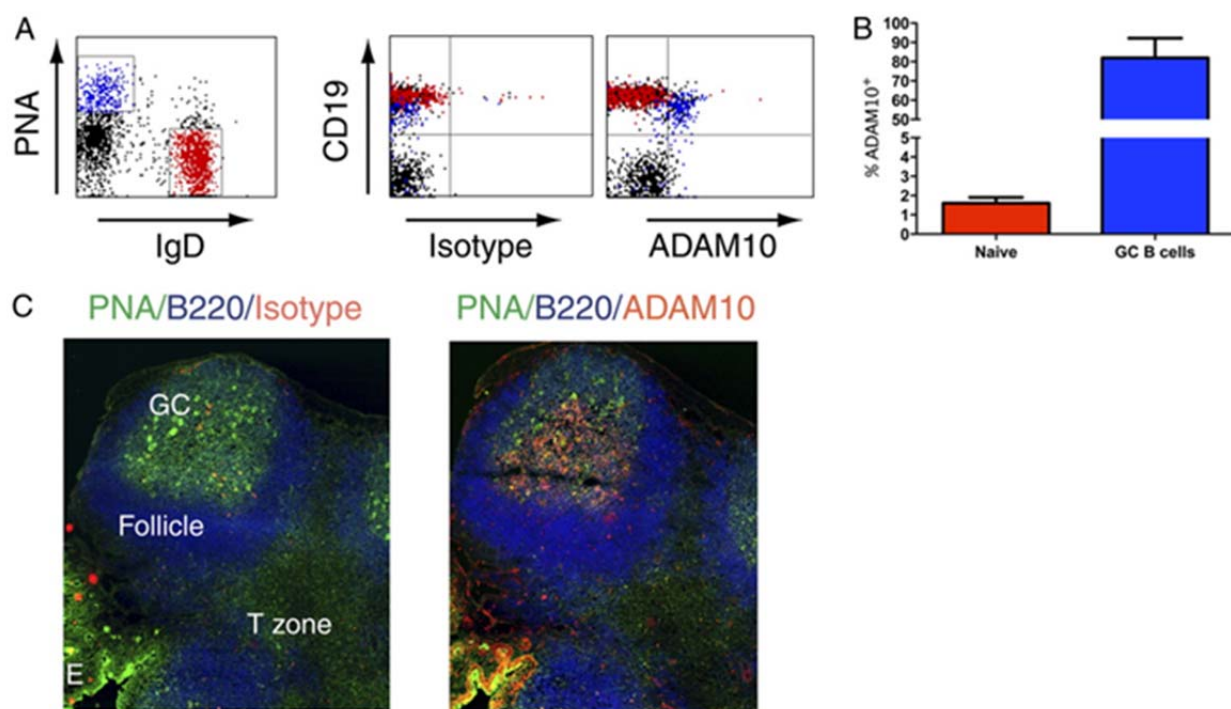


Figure 4. ADAM10^{B-/-} mice have impaired humoral responses.

A, Serum IgM, IgG1, IgG2a, and IgG2b were measured by capture ELISA from non-manipulated 8- to 12-wk-old mice. B, ADAM10^{B-/-} mice and WT littermate controls were immunized with 10µg NP-KLH emulsified in alum. At the indicated times, serum samples were collected and total NP-specific IgM, total IgG, and high-affinity IgG antibody titers were determined by ELISA, with NP-16–BSA as capture Ag for total and NP-4–BSA as capture Ag for high-affinity ELISA. C, Mice were immunized with NP-KLH emulsified in alum, rested for 42 d, and boosted with 10 µg NP-KLH for 5 d. Mice were bled weekly throughout the course of the experiment. Total and high-affinity Ag-specific IgG levels were measured by ELISA at each time point. The relative unit (RU) values for alum-injected mice were <0.001. ADAM10^{B-/-} (filled bars) and WT (open bars). Bars represent the mean ± SE of five to nine mice per group (*p < 0.05, **p < 0.01, ***p < 0.001). Data represent results obtained in at least two independent experiments.

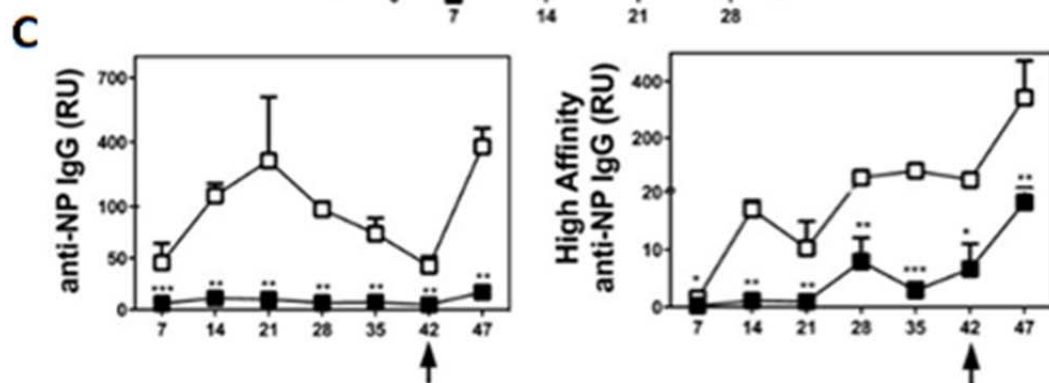
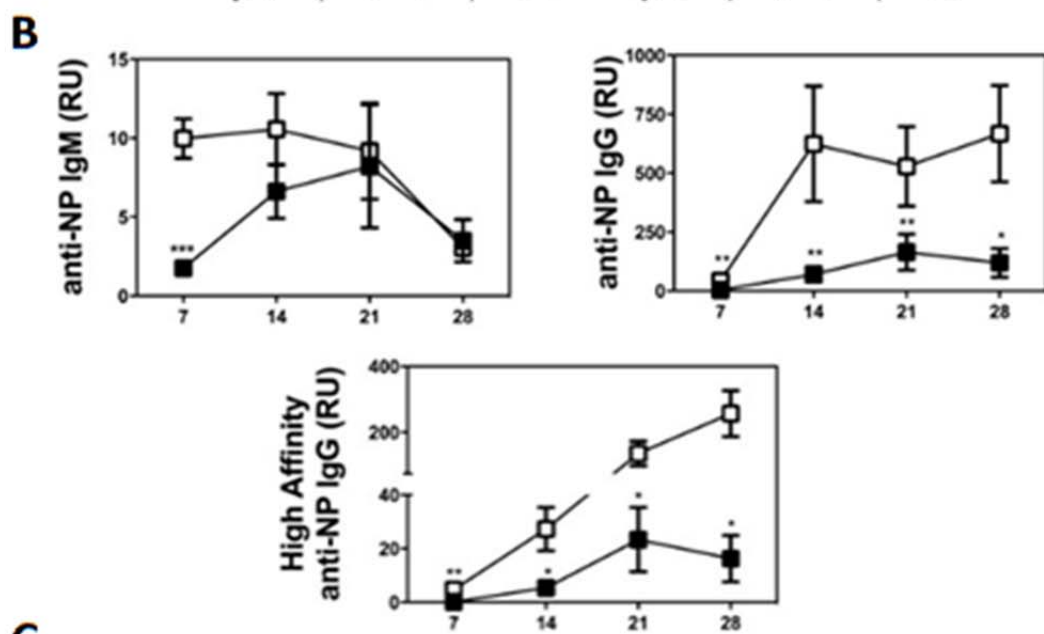
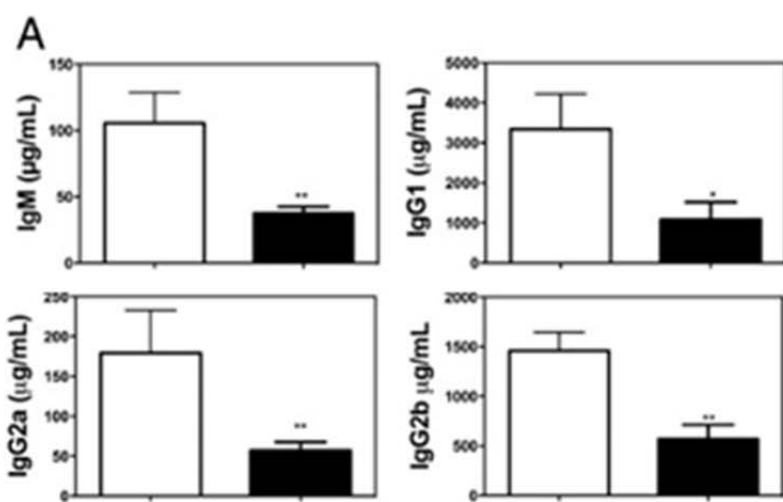


Figure 5. Decreased NP-specific IgG secretion is not IgG subset dependent and cannot be overcome by high antigen dose

A. ADAM10^{B/-} mice and WT controls were immunized with NP-KLH emulsified in alum. Twenty-eight days after primary immunization, samples were collected and NP-specific IgG1, IgG2a and IgG2b antibody titers were determined by ELISA with NP₁₄BSA as capture antigen. B. ADAM10^{B/-} and WT controls were immunized *i.p.* with 1mg of NP-KLH emulsified in alum. Samples were collected at the indicated time post immunization, and NP-specific antibodies were measured. The relative unit (RU) values for alum-injected mice were less than 0.001. Bars represent the mean \pm SEM of 5 mice per group. Data represents results obtained in two independent experiments. (*p<0.05, **p<0.01, ***p<0.001).

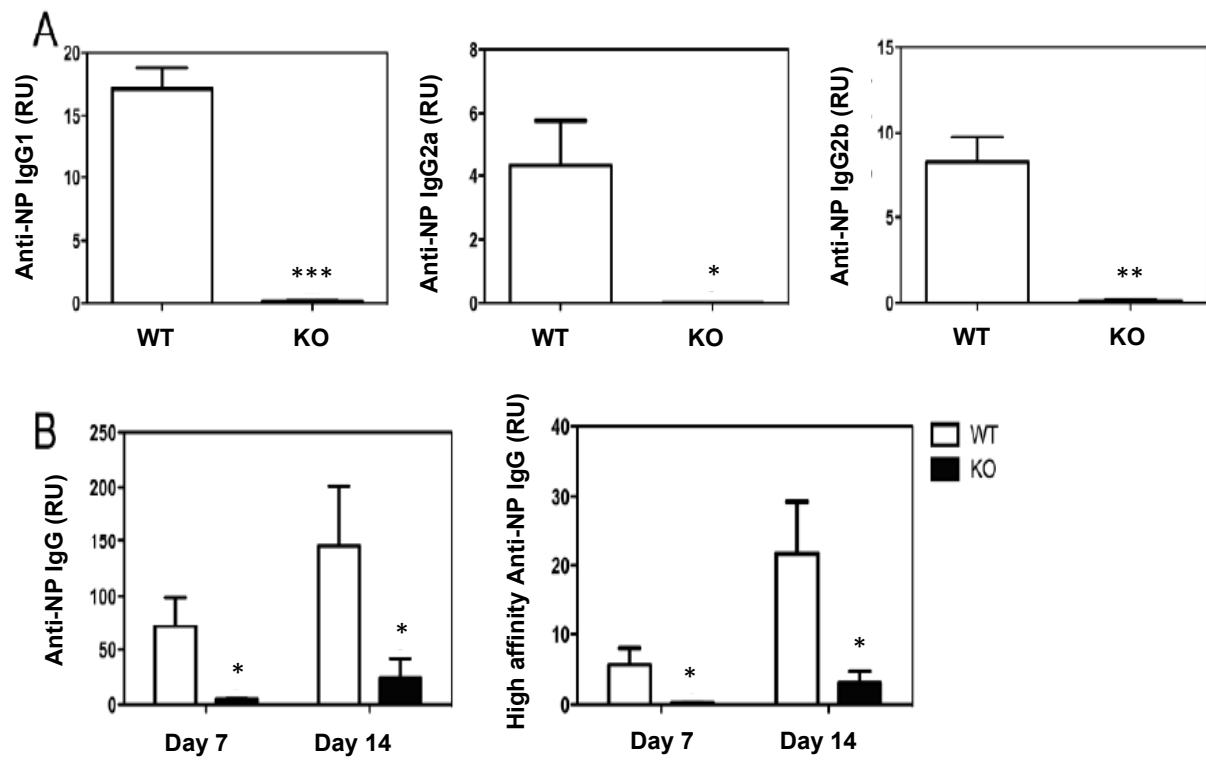


Figure 6. GC formation after T-dependent immunization

ADAM10^{B-/-} and WT mice were immunized with 10µg NP-KLH emulsified in alum.

Fourteen and 21 days post-immunization, flow cytometry was carried out and the

presence of GC B cells (IgM^{lo}IgD^{lo}B220⁺IgG1⁺CD38⁻) in the spleen of WT and

ADAM10^{B-/-} mice was assessed. Staining protocol is depicted (A). Both percentage (B)

and total number (C) of GCs were enumerated. ADAM10^{B-/-} (filled bars) and WT (open

bars). Bars represent the mean ± SE of eight mice per group. *p < 0.05, **p < 0.01.

Data are representative of three independent experiments.

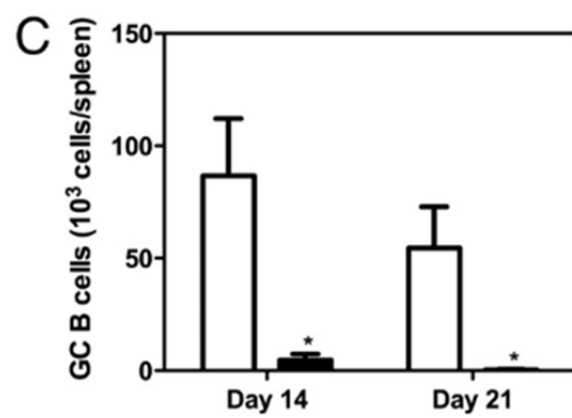
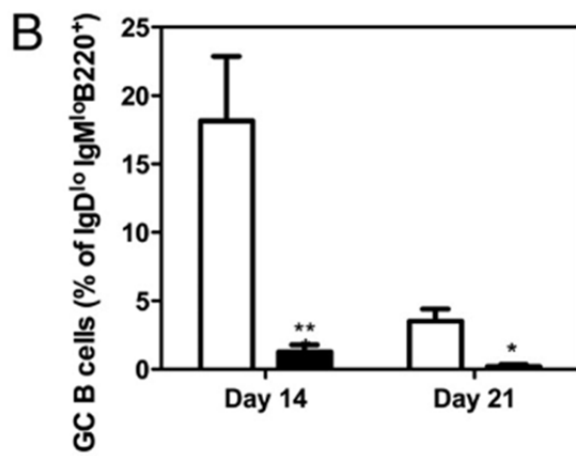
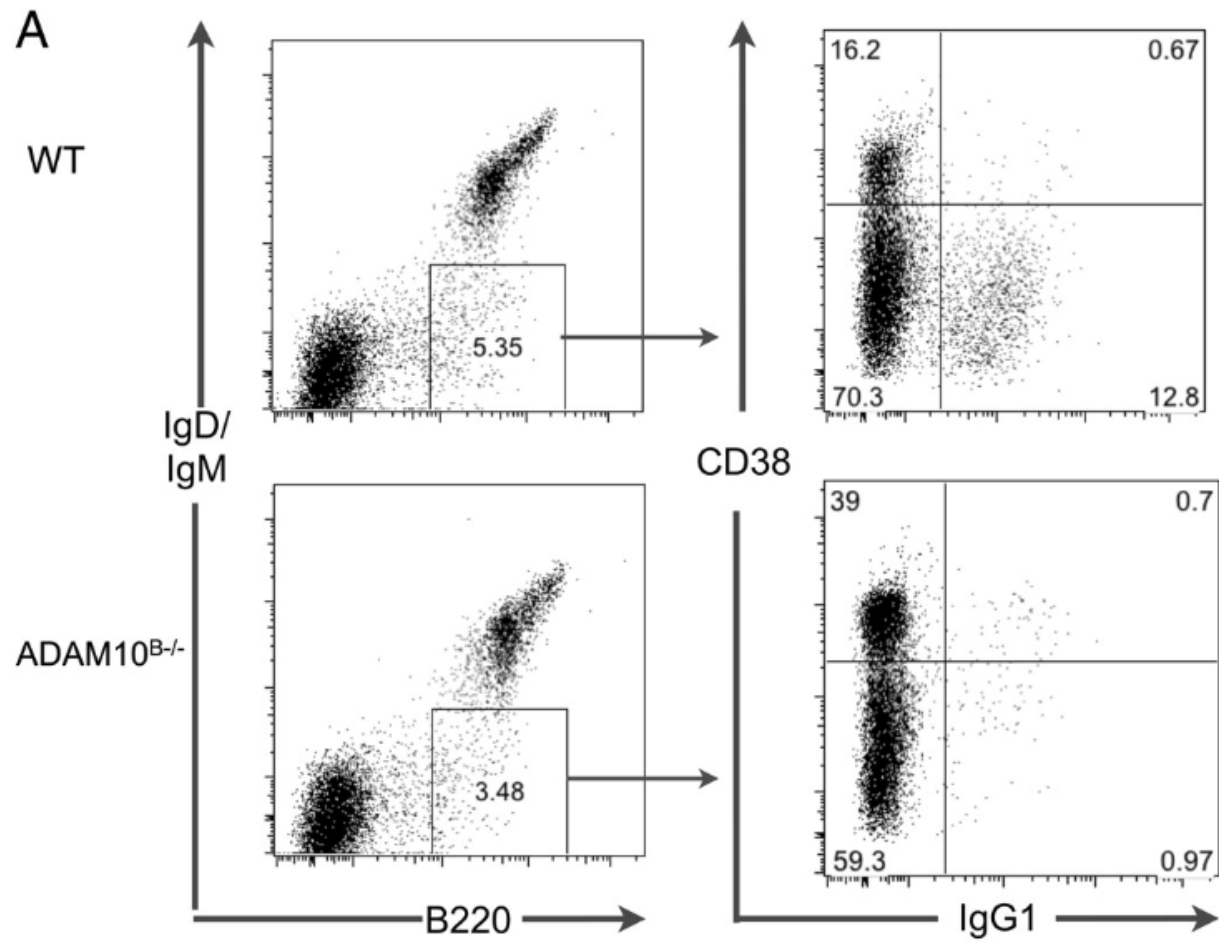


Figure 7. Immunohistochemistry analysis of GC formation and LN architecture after T-dependent immunization

ADAM10^{B-/-} and WT mice were immunized with 10µg NP-KLH emulsified in alum.

Fourteen days after immunization, draining LN sections were stained for (A) GL7 (green) and IgD (red); (B) Thy1.2 (green) and B220 (red); (C) CD21/35 (green) and B220 (red). D, Non-draining LNs were also stained with CD3 (green) and B220 (red).

Photomicrographs are representative of three independent experiments. Original magnification ×20.

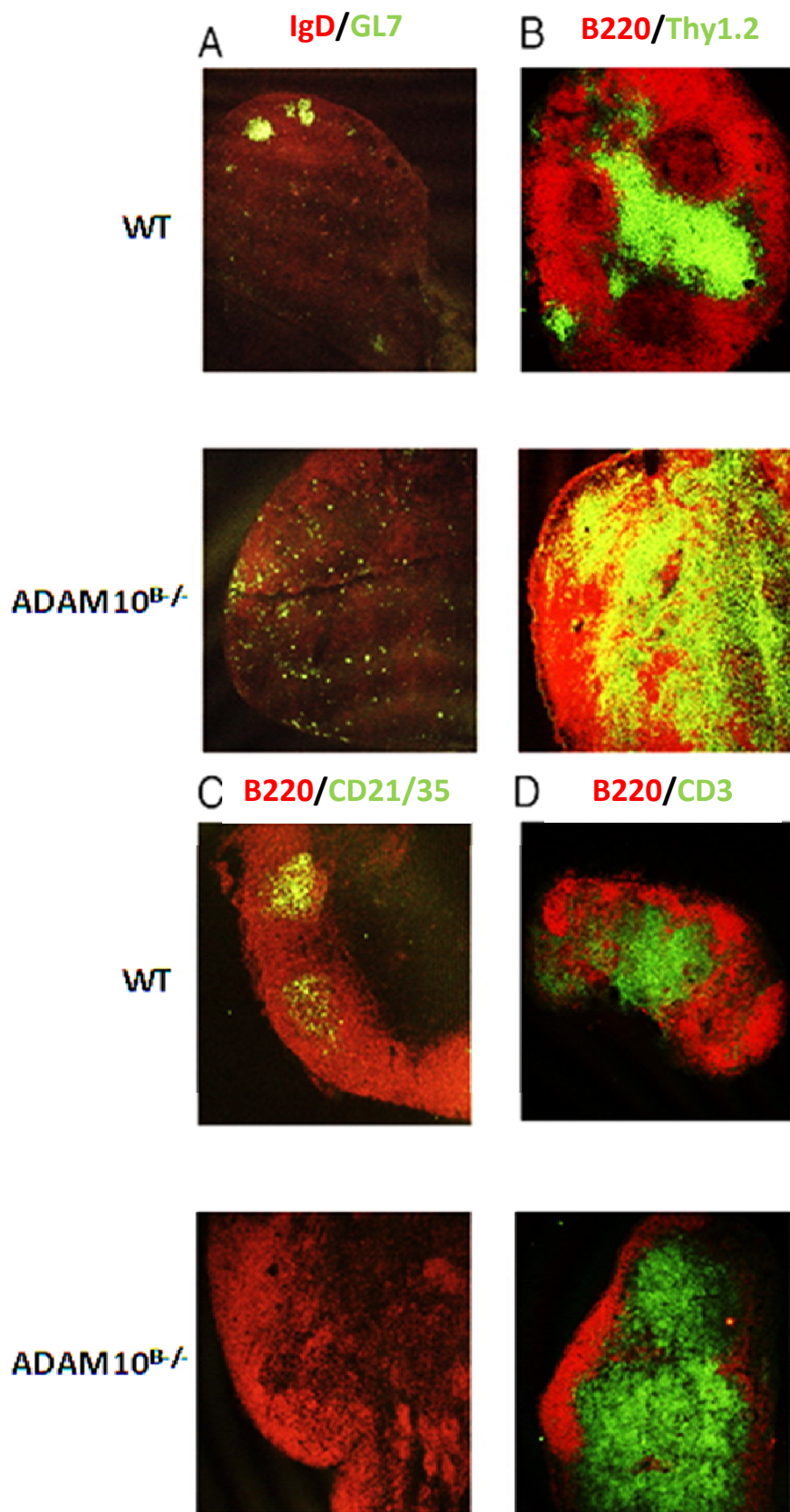


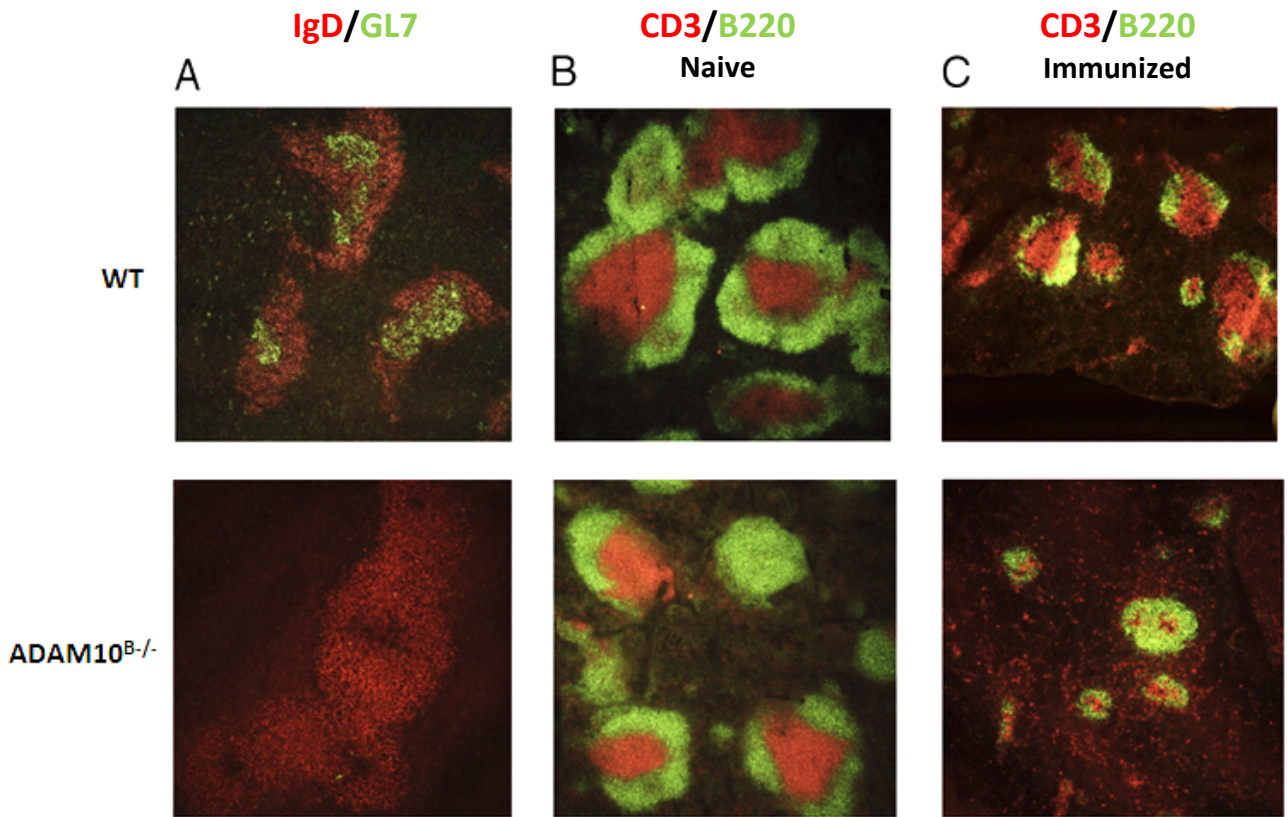
Figure 8. Immunohistochemistry analysis of GC formation and splenic architecture after T-dependent immunization

ADAM10^{B-/-} and WT mice were immunized with 10µg NP-KLH emulsified in alum.

Fourteen days after NP-KLH immunization, spleens were isolated and sectioned.

Sections were stained for (A) GL7 (green) and IgD (red). Photomicrographs are representative of three independent experiments. B, Spleens isolated from naive animals or (C) isolated 14 d post-immunization, were stained with CD3 (red) and B220 (green). Photomicrographs are representative of three independent experiments.

Original magnification ×20 (A, B); ×10 (C).



ADAM10^{B/-} mice have dysregulated chemokine expression following antigen challenge

Chemokine gradients maintain tight control over the organization of secondary lymphoid tissue. To determine if altered chemokine expression was contributing to the structural changes observed in the ADAM10^{B/-} mouse, we assessed draining and non-draining LN chemokine expression by quantitative PCR. As expected, non-draining LNs from control and ADAM10^{B/-} mice had similar CXCL13, CCL19, and CCL21 expression (**Figure 9A**). In sharp contrast, draining LNs isolated from ADAM10^{B/-} mice exhibited increased CCL21 expression, whereas CXCL13 levels were comparable. CCL19 levels trended higher, but the increase was not statistically significant (**Figure 9B**). Analysis of CCL21 expression by immunohistochemistry revealed diffuse staining in the ADAM10^{B/-} LNs consistent with the localization of T cells within draining LNs (**Figure 9B**). These results demonstrate that B cell-expressed ADAM10 is important for maintenance of lymphoid architecture by regulating chemokine expression during active immune responses.

Defect in humoral in ADAM10^{B/-} mice is Notch2 and CD23-independent

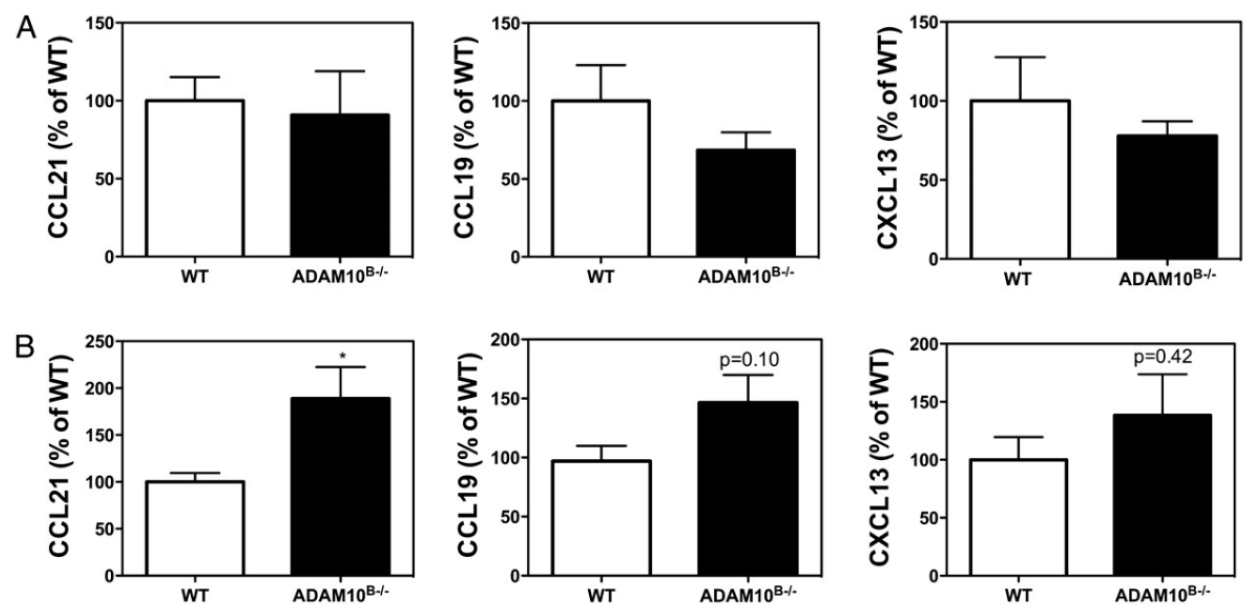
Recent studies have suggested that Notch signaling might be involved in antibody production and ASC differentiation^{50,57}. ADAM10 is critical for Notch signaling. ADAM10^{B/-} mice that have constitutively active Notch2 signaling in B cells (ADAM10^{B/-}-N2ICD-Tg^{B+}) were immunized, and antibody production, GC formation, and LN architecture were examined to determine whether the antibody production defects were due to impaired Notch signaling. As expected, expression of N2ICD recovered MZ B development in these mice, demonstrating that the transgene was indeed active (**Figure 10A**). Littermate controls, ADAM10^{B/-}, and ADAM10^{B/-}-N2ICD-Tg^{B+} mice were

immunized. Consistent with previous experiments, ADAM10^{B-/-} mice had significantly reduced levels of NP-specific antibodies. Importantly, introduction of N2ICD transgene failed to rescue the defect in antibody production and GC formation, and did not prevent changes in LN architecture (**Figure 10B,C**). These results demonstrate that increased Notch signaling cannot rescue the defects in humoral responses observed in ADAM10^{B-/-} mice.

Our lab reported that ADAM10 is responsible for the cleavage of the low-affinity IgE receptor, CD23¹¹⁹, and consequently, ADAM10^{B-/-} B cells have increased CD23 expression^{56,127}. Studies have revealed that CD23 overexpression leads to decreased IgG1 and IgE production^{112,128}. However, when CD23Tg mice were immunized with NP-KLH, analysis of NP-specific IgG indicated that CD23Tg mice had a normal antibody response to NP-KLH (**Figure 11**). Furthermore, it has been previously reported that CD23Tg mice form GCs post-immunization with T-dependent antigens. It should be noted that the GCs observed in CD23Tg mice had a more globular appearance than WT¹²⁹. These results suggest that the humoral defect observed in ADAM10^{B-/-} mice is not secondary to CD23 overexpression, however, this should be more carefully addressed.

Figure 9. Chemokine expression in draining LNs

Mice were immunized in the footpad with 10 μ g NP-KLH. Fourteen days post-immunization, draining and non-draining LNs were isolated and chemokine expression was analyzed by quantitative PCR for CCL19, CCL21, and CXCL13. Non-draining (A) and draining (B) LNs are shown. (C) Draining LNs were stained for CCL21 and CD3. Pictures are representative of three mice per group *p < 0.05. Bars represent the mean \pm SE of eight mice per group. Data are representative of two independent experiments.



C

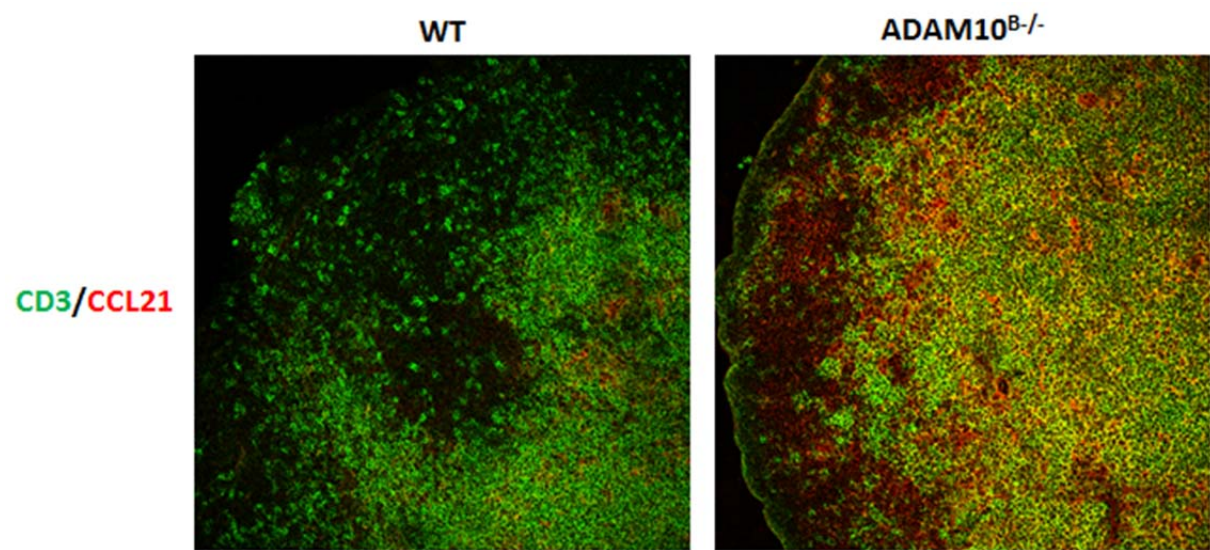


Figure 10. Defects in humoral responses in ADAM10^{B-/-} mice seem to be Notch2-independent

(A) Splenocytes isolated from ADAM10^{B-/-}, ADAM10^{B-/-N2ICD-TgB+} and WT mice were stained with B220, CD23, CD21/35 and IgM. MZ B cells were defined as B220⁺CD23⁻/loCD21/35^{hi}IgM⁺. (B) ADAM10^{B-/-}, ADAM10^{B-/-N2ICD-TgB+}, and WT mice were immunized *i.p.* with NP-KLH emulsified in alum. At the indicated times, serum samples were collected and total NP-specific IgG was determined by ELISA. Bars represent the mean \pm SE of 5 mice per group. (C) Mice were immunized in the footpad with NP-KLH, 14 days later draining LNs were isolated and stained for GL7 and IgD (top) and Thy1.2 and B220 (bottom). Data represents results obtained in two independent experiments. (*p<0.05, **p<0.01, ***p<0.001, One-way ANOVA with Tukey post-test). Significance refers to ADAM10^{B-/-} compared to WT and ADAM10^{B-/-N2ICD-TgB+} compared to WT. ADAM10^{B-/-} and ADAM10^{B-/-N2ICD-TgB+} were not different from each other at any time point.

Gated on B220⁺CD23^{-/lo}

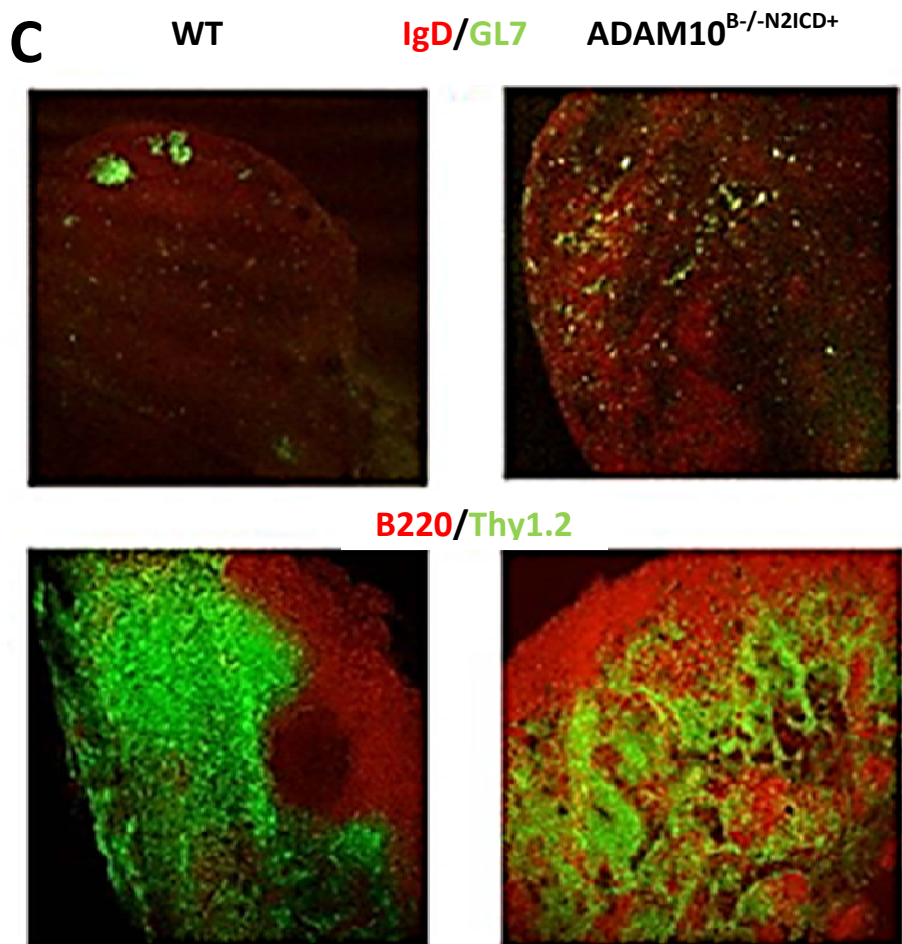
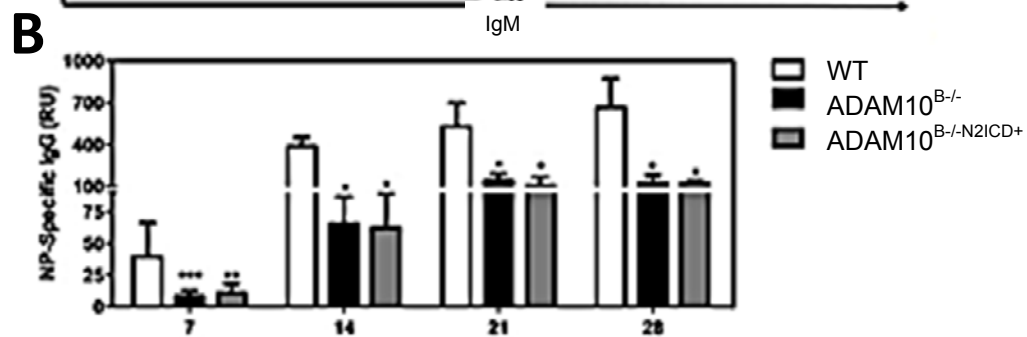
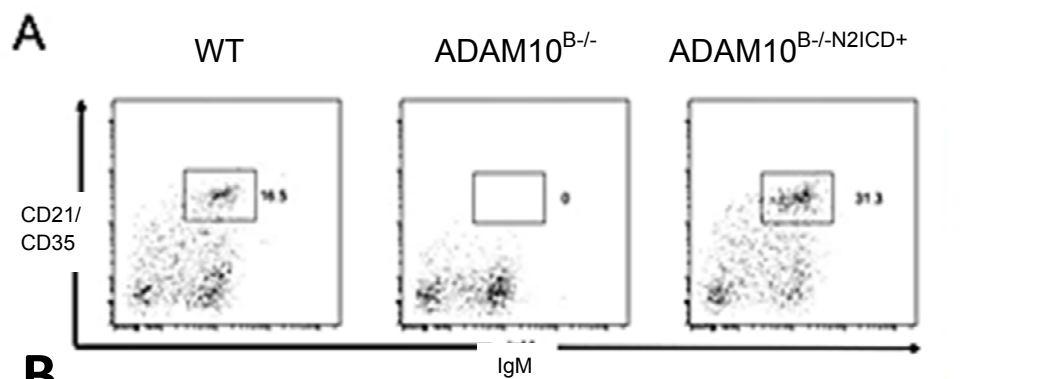
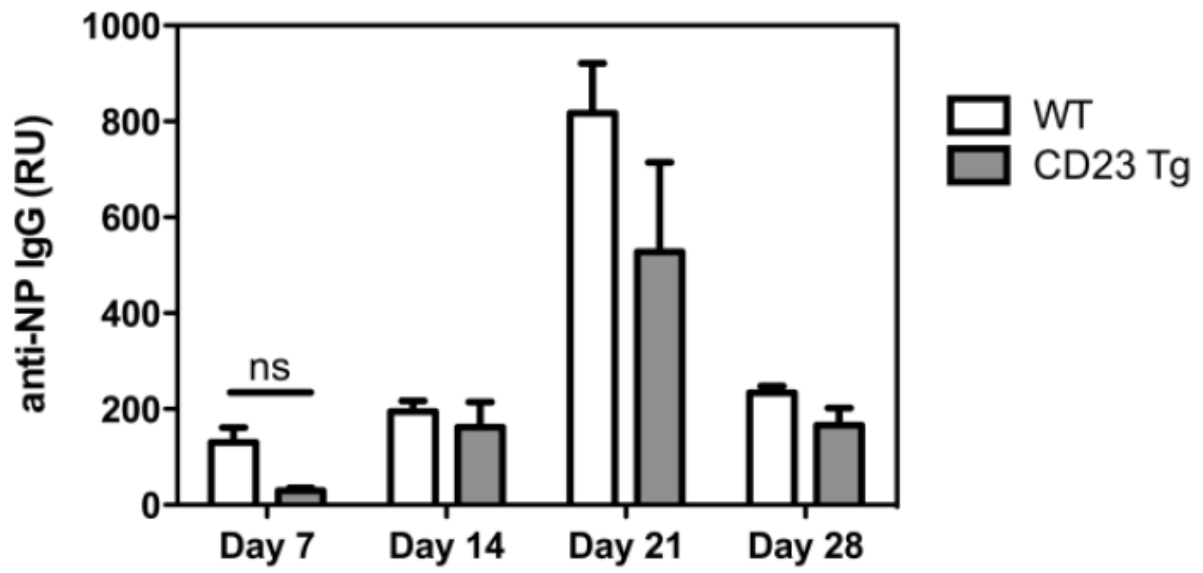


Figure 11. CD23Tg mice have a normal IgG response to NP-KLH

CD23Tg and WT mice were immunized with NP-KLH emulsified in alum. At the indicated times, serum samples were collected and total NP-specific IgG was determined by ELISA. Bars represent the mean \pm SE of 8 mice per group. Data represent results obtained in two independent experiments.



1.3.3 Discussion

Members of the ADAM family regulate a wide range of functions, including cell migration, proliferation, and adhesion¹³⁰. ADAM10, in particular, has been recently shown to be critical for lymphocyte development through initiation of the canonical Notch signaling pathway^{47,56}. We report that ADAM10 is essential for the maintenance of splenic and LN architecture during responses to T-dependent Ags. A decrease in Ag-specific IgG production is seen both with respect to serum levels and IgG ASCs, indicating that PC differentiation is influenced. Cells producing high-affinity antibodies were particularly affected, consistent with a defect in GC reactions and markedly repressed FDC-reticula. Moreover, ADAM10-deficient B cells are able to class switch normally when stimulated *in vitro*. Therefore, the defective humoral response in ADAM10^{B-/-} mice results from impaired B cell activation *in vivo*.

Impaired Notch signaling and increased CD23 expression, are not likely to contribute to the phenotype observed in ADAM10^{B-/-} mice

To determine the mechanism for the observed severely impaired humoral functions and lymphoid architecture disruption, we investigated the two clear substrates for ADAM10 in B cells: Notch and CD23^{47,56,119}. The role of notch signaling in mature B cell function is controversial. Although some studies have clearly shown a role for Notch in antibody production, others fail to identify such a role^{57,131}. To assess the role of Notch signaling in antibody production, we overexpressed N2ICD in a B cell-specific manner. In this study, we show that restoration of Notch2 signaling in ADAM10^{B-/-} mice is not sufficient to rescue antibody production or GC formation. Studies have shown that N2ICD and N1ICD have redundant functions. Our results, therefore, suggest that the

phenotype observed in ADAM10^{B-/-} mice is not dependent on Notch1 or Notch2 signaling¹³². However, the role of Notch1 in B cell biology should be more thoroughly studied. *In vitro* studies have demonstrated that Notch signaling enhances B cell activation¹³³ and support GC B cell survival¹³⁴. Although Notch signaling enhances humoral responses *in vitro*, decreased Notch signaling does not explain the phenotype observed in ADAM10^{B-/-} mice. Because Notch signaling also enhances CD21 expression, this finding also suggests that CD21 is not involved in the ADAM10^{B-/-} phenotype. In addition, unlike CD21/CD35^{-/-} mice, ADAM10^{B-/-} mice had impaired affinity maturation and failed to mount an antibody response comparable with controls even after immunization with large Ag dosages (i.e., 1 mg)¹³⁵.

CD23 is also known as the low affinity IgE receptor and is another B cell-expressed ADAM10 substrate is CD23¹¹⁹. We have recently demonstrated that CD23 surface expression is significantly enhanced after deletion of ADAM10 in B cells⁵⁶. Defects observed in ADAM10^{B-/-} could result from CD23 overexpression. Previous studies with CD23Tg mice, however, demonstrated that elevated CD23 levels resulted in inhibition of IgE and IgG1 production, whereas other classes were not significantly affected. Furthermore, the defect was evident only after boosting^{112,129}. In contrast, in ADAM10^{B-/-} mice, all classes of IgG were influenced, and this defect was observed after one injection. Moreover, when immunized with NP-KLH, CD23Tg mice had Ig levels comparable with that of WT. In contrast, ADAM10^{B-/-} mice showed diminished levels of both low- and high-affinity anti-NP antibodies. These results indicate that elevated CD23 levels do not explain the phenotype of ADAM10^{B-/-} mice. It is likely that

B cells express another ADAM10 substrate that is responsible for the observed phenotype in ADAM10^{B-/-} mice.

ADAM10 is important for B cell follicle formation and maintenance of lymphoid architecture

In lymphoid organs, the correct positioning of cells, such as B and T cells, is dictated by the local production of chemokines by stromal cells, as well as the coordinated expression of chemokine receptors by migrating cells¹²⁵. The positioning of these cells and the migration during an immune response are critical for adequate interaction between them¹³⁴. Our results demonstrate that although B cell-expressed ADAM10 is dispensable for proper cellular positioning during LN and spleen development, ADAM10 is critical for the maintenance of the correct position of cells after immune stimulation.

CCL21, CCL19, and CXCL13 have been shown to play a key role in inducing and maintaining normal cellular compartments¹. Draining LNs from ADAM10^{B-/-} mice showed increased CCL21 expression. This increase in CCL21 was also confirmed at the protein level by immunohistochemistry. Interestingly, ADAM10^{B-/-} mice had a larger area of CCL21 staining. The larger area of production is consistent with the aberrant T cell localization seen in draining LNs.

FDCs are important for GC development, CSR, SHR, and affinity maturation, as well as induction of recall responses^{136–139}. FDCs also secrete CXCL13 and are thus important for recruitment of CXCR5-expressing B cells and T cells into the follicle¹⁴⁰, and are important for the maintenance B and T cell zones¹³⁴. The loss of B and T cell

segregation and the lack of GCs in the draining secondary lymphoid tissues of ADAM10^{B-/-} mice is thus consistent with fewer activated FDC networks. TNF α is another ADAM10 substrate, and it has been implicated in the formation of primary B cell follicles and GCs. TNF α global knockout mice have severe defects in T-dependent immune response as well as have defective FDC networks, GC formation and B cell follicle maintenance¹⁴¹. Additionally studies done with mice expressing non-cleavable TNF α on B cells have defective secondary lymphoid tissue formation¹⁴². The primary sheddase for TNF α is ADAM17, the ADAM most closely related in structure to ADAM10^{12,143}. Recent work done by *Folgosa et al.* has shown that ADAM10 deletion results in up regulation of ADAM17 in a compensatory mechanism^{29,144}. This up regulation of ADAM17 increases the cleavage of membrane bound TNF α , converting its active soluble form¹⁴⁴. Additionally, these studies show that the compensatory increase in ADAM17 and thus increased cleavage of TNF α induces a feedback loop to further increase TNF α production²⁹. *Folgosa et al.* shows that ADAM10^{B-/-} mice express increased levels of ADAM17, decreased levels of ADAM10 and increased TNF α on B cells²⁹. This increase in TNF α is also seen within the immunized LNs of ADAM10^{B-/-} mice. This work implicates that increased TNF α in ADAM10^{B-/-} mice results in the observed defects seen in secondary lymphoid architecture²⁹.

Conclusions

In conclusion, examination of humoral responses in B cell-specific ADAM10-deficient mice has demonstrated that ADAM10 is critical for the maintenance of splenic and LN architecture during active immune responses. ADAM10^{B-/-} mice have impaired GC formation, affinity maturation, and CSR. Therefore, B cell-expressed ADAM10 is

required for proper humoral responses. Thus, B cell-expressed ADAM10 is essential for the maintenance of lymphoid structure after Ag challenge.

Chapter 4: B cell ADAM10 expression and activity is increased during active allergy

1.4.1 Introduction to CD23

The low affinity IgE receptor, (FcεRII) is also known as CD23. Through an unknown mechanism, when IgE is bound, signaling through this receptor shuts down IgE synthesis, creating a negative feedback loop^{145,146}. CD23 is a 45kDa (in humans), type II transmembrane protein and is a member of the calcium-dependent (C-type) lectin family. CD23, in its membrane bound form is a trimer^{145,146}. It has two isoforms, CD23a and CD23b, in mice the first being found on B cells and FDCs and the latter found mainly on gut epithelial cells and FDCs^{139,147,148}. In humans CD23a is found on B lymphocytes and CD23b is found on a variety of hematopoietic cells and others cell types including epithelial cells¹⁴⁹.

Murine models of CD23 expression have given insight into the in vivo effects of CD23 on IgE synthesis. CD23 deficient mice show increased antigen specific IgE when immunized with T-dependent antigens¹⁵⁰. They also show increased specific-IgE and airway hyper-responsiveness to murine asthma models¹⁵¹. CD23Tg mice created using the MHC class I promoter and IgH enhancer have decreased basal serum IgE levels as well as IgG1. These mice also have decreased IgE and IgG1 in response to ova/alum immunization and helminth infections¹¹². Both strains of mice show evidence, that CD23 is an important negative regulator of IgE synthesis. CD23 can be cleaved into a soluble form. Soluble CD23 (sCD23) can still bind IgE, but with much lower affinity than its membrane bound form^{146,152}. Soluble CD23 has also been shown to bind CD11b-CD18 on monocytes, leading to activation, differentiation into macrophages and release

of inflammatory mediators^{153,154}. Soluble CD23 has been shown to be increased in sera of allergic patients in active allergy season, correlative with increased IgE levels¹⁵⁵. Increased cleavage of CD23 leaves less membrane bound CD23 to negatively regulate IgE response as well as increased sCD23 to interact with other ligands to increase inflammation. This makes blocking cleavage of CD23 an important target in regulating IgE synthesis and allergic response. This has been demonstrated using an antibody against CD23 in a mouse model of human rheumatoid arthritis resulting in reduction of clinical symptoms that was dose dependent¹⁵⁶.

ADAM10 has been shown as the principal protein responsible for cleaving CD23¹¹⁹. ADAM10 is ubiquitously expressed on all cells types. ADAM10 has many other important substrates (previously described, see section 1.1.1). ADAM10^{B-/-} mice have decreased sCD23 and increased membrane bound CD23, but similar CD23 message levels⁵⁶. This supports the model of CD23 cleavage where CD23 is internalized by the B cell and moved into Multi-vesicular bodies (MVBs) where it then interacts with ADAM10 with increased binding¹⁵². ADAM10, being a major regulator of CD23 has potential to be an important therapeutic target in regulating IgE synthesis in allergic disease. ADAM10's importance in cleavage of many other essential proteins makes regulating it difficult, but local drug delivery systems could potentially allow local benefits without global negative side effects.

1.4.2 ADAM10 in allergic asthma models

In a previous study in our lab, *Mathews et al.* showed that when surface levels of CD23 are increased, the features of IgE-dependent experimental asthma are reduced. This was shown using CD23Tg mice and ADAM10^{B-/-} mice, which both have high levels

of surface CD23 as well as with WT mice treated intranasally with ADAM10 inhibitor¹⁵². It was also shown that when ADAM10 was blocked either genetically or with an inhibitor, there was a decrease in antigen-specific IgE, Th2 cytokines in the lung, lung AHR, lung inflammation, and infiltration of eosinophils¹⁵². Additionally, with the ADAM10 inhibitor, Th2 transcription factor, GATA3 expression was decreased, but Th1 transcription factor, Tbet, was not¹⁵². Overall, these results demonstrate that ADAM10 is important to the Th2 driven allergic response beyond control over IgE synthesis by CD23 cleavage.

1.4.2 ADAM10 in allergic patients

Previous studies have shown that increased serum IgE in allergic patients with seasonal allergic rhinitis correlate with increased sCD23¹⁵⁵. This argues that ADAM10 levels are responsible for this increase in sCD23 in active allergic patients. Moreover, given the data showing that B cell ADAM10 plays an important role in regulating Th2 immune responses in mouse models of asthma, we wanted to characterize the ADAM levels on patients in active allergic disease. Here, we show that symptomatic allergic patients have increased total ADAM10 expression on B cells, but not on T cells or monocytes. We additionally show that allergic patients have increased ADAM10 activity on B cells as measured by sCD23 output.

Chapter 5: Materials and Methods

1.5.1 Human studies

Allergic rhinitis (allergic) patients and non-allergic, control patients were recruited to the study by Dr. Anne-Marie Irani in pediatric allergy clinic at Virginia Commonwealth University. Patients were consented and completed an IRB approved survey before enrollment into the study was permitted. Twenty mLs of peripheral blood was obtained from either allergic or non-allergic controls. Peripheral blood mononuclear cells (PBMC) were separated using Ficoll-Paque Plus (GE Healthcare), then stained for flow cytometry or set up for *in vitro* cultures.

1.5.2 Flow cytometry

Staining protocol

Human PBMC were washed with PBS and 100,000 cells were resuspended in 50 μ L FACS Buffer (see section 1.2.6 for recipe). Samples were blocked on ice for 15 minutes with Human Fc Block (Miltenyi Biotec). Anti-human antibodies were then added at concentrations according to manufacturer's protocol. For intracellular total staining, cells were fixed with 500 μ L x for 15 mins on ice (add fixative name here). Samples were then washed with PBS and permeabilized with 1X Perm Wash (company) for 10 minutes on ice. Samples were washed in PBS and resuspended in 50 μ L PBS. Samples were then Fc blocked and stained as described above. Samples were run on the Canto (BD) with Diva software and data was analyzed with Flowjo v7.6.5 software (Tree Star).

Antibodies

All antibodies used for Allergic patient flow cytometry are listed in **Table 3**.

1.5.3 In vitro cultures

Allergic patient or control PBMC was counted and plated in cRPMI 1640 containing 10% FBS, 2mM L-glutamine, 50µM 2-mercaptoethanol, 100 U/mL penicillin, 100g/mL streptomycin, 1mM HEPES (Quality Biological), and 1mM sodium pyruvate (Cellgro). PBMC was cultured at set cell concentrations with 200ng/mL human IL-21 (American Type Culture Collection (ATCC)), anti-CD40 (Clone G28-5, ATCC), and 10ng/mL rhIL-4 (R&D). 10µM ADAM10 inhibitor or DMSO vehicle control were added where described. Cell-free Supernatants were harvested on Day 5 for sCD23 ELISA.

1.5.4 Enzyme Linked Immunosorbent Assay

sCD23 ELISA

Plates were coated with mouse anti-human CD23 (the Binding Site) at 2µg/mL in BBS (see previous section 1.2.5 for recipe) and incubated at 37°C for 1 hour. Plates were then washed three times with ELISA wash (section 1.2.5). Plates were blocked in PBS with 10%FBS for 1 hour at 37°C and were washed as above. Samples were added at various concentrations, diluted in media. EcCD23LZ (in house) standards started at 1µg/mL and were serially diluted in media. Plates were incubated and washed as previous. Sheep anti-human CD23 (the Binding Site) was added at 1:200 dilution in block. Plates were incubated as previous. Plates were then washed five times with ELISA wash and the detection antibody, Rabbit anti-Sheep IgG conjugated to horseradish peroxidase HRP (Southern Biotech) was added at 1:1000 diluted in block.

Plates were again incubated as previous and were then washed seven times with ELISA wash. TMB substrate was added at a 1:1 mixture and incubated for 15 minutes at room temperature in the dark. When plates were fully developed, STOP solution (0.18M H₂SO₄) was added to stop the reaction by denaturing the HRP enzyme. Plates were read at 450nm.

1.5.5 Reagents

The ADAM10 hydroxamate inhibitors, INC008765¹⁵⁷, were synthesized by the Incyte Corporation. These inhibitors are very selective for ADAM10 as shown by both cell free as well as cell-based assays requiring at least 5 fold higher concentrations to inhibit MMP12 and at least 20 fold to inhibit any other enzymes including ADAM17¹⁵⁷.

1.5.6 Statistical analyses

Data was analyzed as in section 1.2.8 except that when noted, error bars represent a 95% confidence interval.

Table 3. Antibodies for flow cytometry

Specificity	Clone	Conjugate	Company
Human-ADAM10	163003	FITC	R&D
Human-CD19	HIB19	PE	Biolegend
Human-CD3	HIT3A	PE	Biolegend
Human-CD14	HCD14	APC	Biolegend

Chapter 6: Characterizing ADAM10 in allergic patients PBMC

1.6.1 Allergic Patients B cells have increased ADAM10 levels and activity.

Allergic patients have increased total B cell ADAM10

Previous studies have shown that increased serum IgE in allergic patients with seasonal allergic rhinitis correlate with increased sCD23¹⁵⁵. This argues that ADAM10 levels are responsible for this increase in sCD23 in active allergic patients. Therefore, we examined total ADAM10 levels in allergic patients versus control. Allergic patients were identified by Dr. Anne-Marie Irani. Patients were consented and asked to fill out an IRB approved questionnaire. Twenty milliliters of blood was collected with venipuncture from each patient enrolled in our study, allergic or control.

Clinical diagnosis, Nasal cytology, symptom score and sensitization information such as skin-prick testing or RAS test are all standard of care at the clinic where our patients are recruited. The study clinicians, Dr. Anne-Marie Irani, MD and Dr. Neil Roberts, MD, have access to this information to better classify the patients, without patients having to undergo any additional procedures. Our patient questionnaire asks if the patient has had a positive skin test result and what they are allergic to. It confirms that the patients are having allergic symptoms at the time of blood draw and provides a checklist of symptoms for easy description. Symptoms listed are sneezing, itchy nose or eyes, runny nose, redness in the eyes, wheezing or coughing. It also asks what medications that the patients are currently taking. It specifically asks if the patient is on anti-histamines or steroids. This information helped us classify each patient as being in active allergy as well as to exclude medicated patients for this study. We recruited

patients with asthma and allergic rhinitis, both conditions known to have elevated serum IgE levels^{158–160}.

Total ADAM10 levels were measured on B cells and T cells. Membrane bound ADAM10 was traditionally thought to be involved in the cleavage of CD23. Though some plasma membrane bound ADAM10 may be cleaving CD23, we consider this to be a minimal contribution. Recent data has shown that the majority of cleavage takes place inside the cell³⁵. This makes it necessary to stain intracellular for ADAM10 as well as staining for membrane bound ADAM10. In **Figure 12A and B**, we show that total ADAM10 is significantly elevated in patients with allergic disease over control, whereas membrane ADAM10 levels alone are comparable.

ADAM10 is not elevated on T cells or monocytes of allergic patients

ADAM10 levels on T cells and monocytes were used as controls to show that this is a B cell specific phenomenon and that ADAM10 is not constitutively elevated in all peripheral leukocyte varieties in active allergy. Total ADAM10 levels were not different on CD3⁺ T cells or CD14⁺ monocytes from allergic vs. control PBMC (**Figure 13A,B**)

sCD23 is increased in culture supernatant of stimulated allergic patient PBMC over control in an ADAM10 dependent manner

ADAM10 was identified as the primary ‘shedase’ for CD23¹¹⁹. This makes the soluble product of ADAM10 cleavage of CD23 or sCD23, a good indicator of ADAM10 activity. PBMC from allergic patients or controls was plated with conditions to stimulate B cell proliferation. After five days of culture, sCD23 was analyzed from the supernatants. Allergic patient cultures were found to have higher levels of sCD23

(**Figure 14A**). To confirm this was from ADAM10, an ADAM10 inhibitor was added to the culture. Compared to vehicle, ADAM10 inhibition reduced both allergic and control sCD23 (**Figure 14B**). This shows that CD23 cleavage is due to ADAM10 activity.

Figure 12. Allergic patients have increased total B cell ADAM10

(A) Peripheral blood CD19⁺ B cells from 16 control (square) and 16 allergic (circle)

patients were fixed, permeabilized, and analyzed for total ADAM10 (A) Error bars

indicate 95% confidence interval. (B) Peripheral blood CD19⁺ B cells from control

(circle) and allergic (square) patients were analyzed for surface ADAM10 expression.

***p <0.0005.

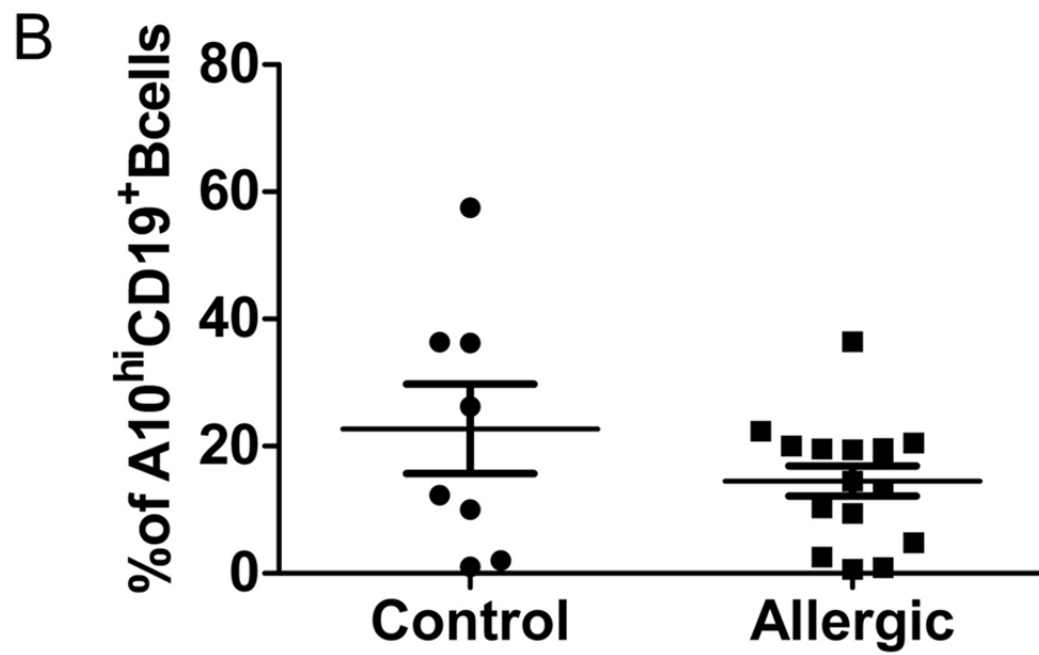
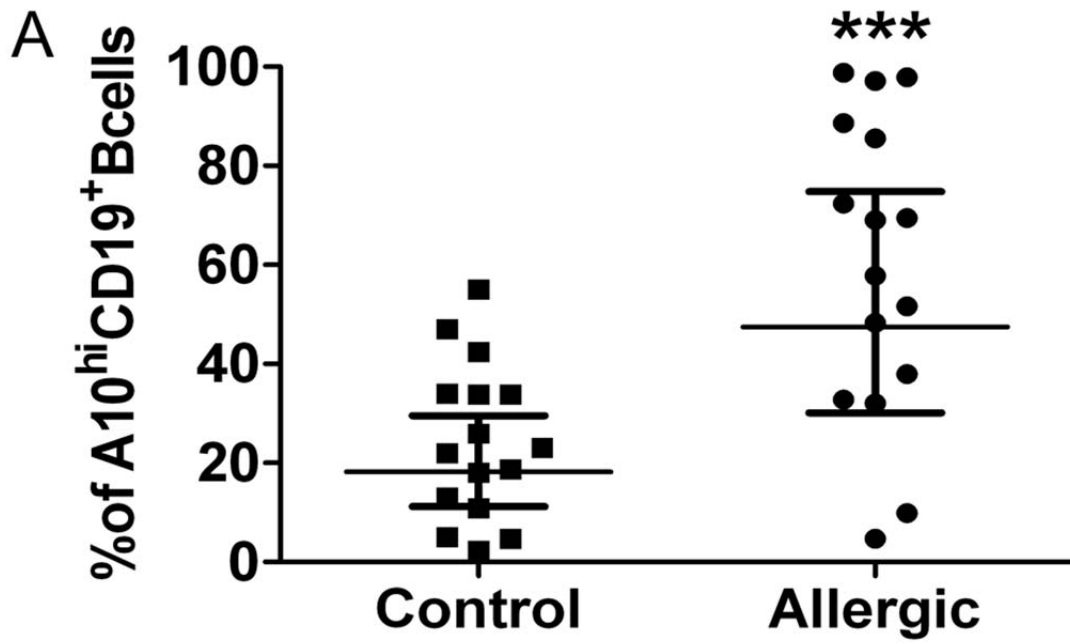
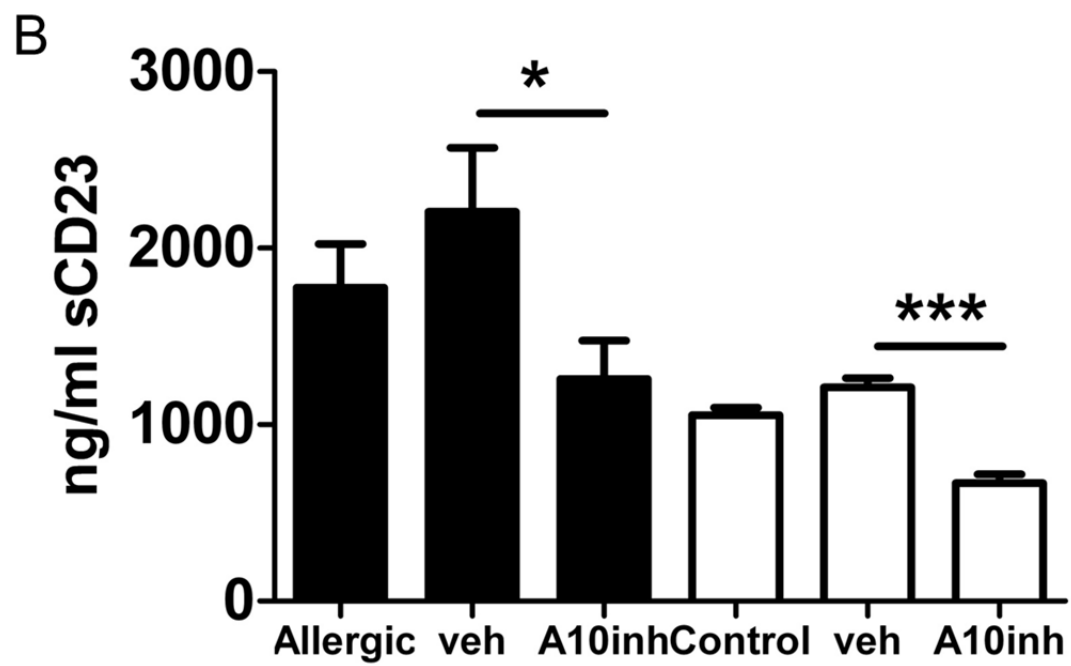
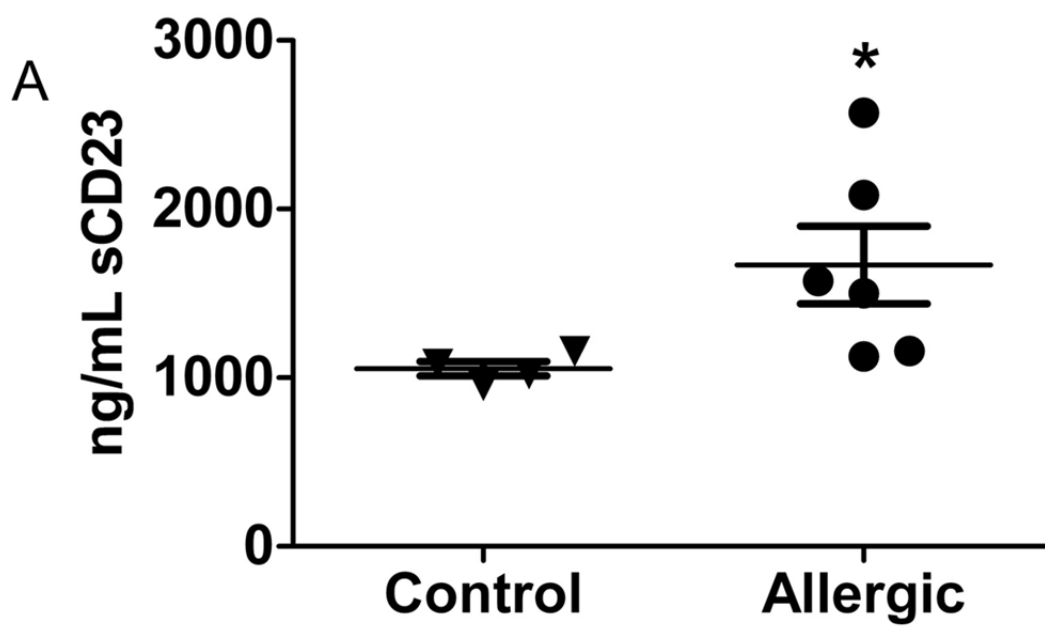


Figure 13. ADAM10 is not elevated on T cells or monocytes of allergic patients

Peripheral blood CD3⁺ T cells (A) and CD14⁺ monocytes (B) were fixed, permeabilized, and analyzed for total ADAM10 expression by flow cytometry. Gated off of live cells based on FSC and SSC. In A, Allergic are represented by (square) and control (circle). In B, Allergic are represented by (red circle) and control (black square). There is no significant difference between columns (A,B). Error bars represent \pm SEM.

Figure 14. sCD23 is increased in culture supernatant of stimulated allergic patient PBMC over control in an ADAM10 dependent manner

Cell-free culture supernatants were measured for sCD23 levels by ELISA. A. After five days of stimulation with IL-21, IL-4 and anti-CD40 sCD23 was measured of control (triangle) or allergic (circle) culture supernatants. B. 10 μ g ADAM10 inhibitor INC008765 was added to cultures of allergic (closed bar) or control (open bar) PBMC. ADAM10 inhibitor was dissolved in DMSO. Statistical analyses compare DMSO vehicle and inhibitor. Error bars represent \pm SEM. * $p < 0.05$, *** $p < 0.0005$.



Section 2

Chapter 1: ADAM10 in MDSC development and function

2.1.1 ADAM10 and myeloid cell development

In the classical model of hematopoiesis, hematopoietic stem cells (HSCs) differentiate to yield common myeloid progenitors (CMP) and CLP¹⁶¹. CMPs undergo further differentiation into mature myeloid cells, including myeloid-derived suppressor cells (MDSC). Due to the negative role of these suppressor cells in anti-tumor responses, myeloid differentiation has been the subject of many recent investigations¹⁶². As discussed further below, numerous hematopoietic pathways, including Notch signaling, have been implicated but remain controversial. Several investigators have reported that alterations in Notch signaling have minimal effects on the myeloid compartment^{48,163,164}. Yet, *Kawamata et al.* reported that constitutive Notch signaling promotes myeloid differentiation in a non-cell autonomous manner⁵². This is supported by a report of abrogated B cell and myeloid cell development in mice deficient in downstream targets of Notch¹⁶⁵. However, other studies have indicated that Notch signaling inhibits myeloid differentiation^{166,167}. *Qyang et al.* demonstrated that blockade of Notch signaling at the γ -secretase cleavage site induces myeloid accumulation¹⁶⁷.

Many of these alterations were observed in mice with altered lymphocyte development. This suggests that ADAM10 directed Notch signaling may modulate the differentiation pathway of CLPs and CMPs from a common upstream progenitor. Two groups have recently described common myelo-lymphoid progenitors (CMLPs) that are

indistinguishable from HSC^{161,168}. Although these multipotent cells often commit to the B or T cell lineage, they retain the potential for myeloid development. Therefore, alterations in Notch signaling during lymphocyte development could also affect myelopoiesis. Collectively, these findings indicate that myeloid differentiation may be regulated by the signal strength and temporal stage of Notch signaling. Therefore, examination of other Notch regulators, including ADAM10, could clarify the role of Notch signaling in myeloid differentiation.

2.1.2 Development of myeloid derived suppressor cells (MDSCs)

The hierarchal differentiation of multipotent progenitors into mature blood cells of various lineages is known as hematopoiesis. The microenvironment of the BM provides a complex network of cytokines, transcription factors, and intercellular signaling pathways that regulate this process¹⁶⁹. HSCs are characterized as lacking lineage markers. They express the receptor tyrosine kinase (RTK) c-kit and the surface protein Sca-1, together termed Lin⁻ Sca-1⁺c-kit⁺ (LSK)¹⁷⁰. The expression of Flt3 RTK and CD34 further subdivide the LSK compartment into self-renewing long and short-term HSC populations as well as a multipotent progenitor (MPP) population. This hierarchy descends deeper into lymphoid and myeloid compartments where the progenitors are again subdivided into three distinct populations based upon CD34 and low affinity IgG Fc receptors (FcγRII/RIII). These include CD34⁺FcγRII/III^{lo} common myeloid progenitors (CMP), CD34⁺FcγRII/III^{hi} granulocyte-macrophage progenitors (GMP), and CD34⁻FcγRII/III^{lo} megakaryocyte-erythroid progenitors (MEP)¹⁷¹. MPPs then give rise to either lineage restricted common myelo-erythroid progenitors (CMEP) or CLPs¹⁷². This process is dependent upon the expression of three proteins: c-kit, the IL-7 receptor and

recombination activation gene 1 (RAG1)¹⁷³. The relative expression of these act as a 'switch' that determines the ultimate hematopoietic destination. While RAG1 and IL-7R expressing CLPs become T and B cells, c-kit⁺ CMEPs generate myeloid and erythroid cells^{174,175}.

This classical model has been recently challenged by the idea that lineage restriction is not necessarily permanent. Several independent observations indicate that early thymocyte and B cell progenitors retain myeloid potential, leading to an alternative, 'myeloid-based' mechanism of hematopoiesis^{161,168}. In this model, CMLPs are observed give rise to either B cells, T cells, or myeloid cells. The myeloid-based mechanism excludes the existence of CLPs, stating that differentiation occurs from these CMLP and CMEP progenitors¹⁷⁶. This suggests that, although committed toward T or B lineage, progenitor cells retain the potential towards myeloid lineage. The existence of progenitor myeloid, B and T (p-MBT) cells which are committed B or T cells, yet retain the ability to revert back to myeloid cells further support this possibility¹⁷⁷. Additionally, the observation of several leukemic disease states containing cells of both myeloid and lymphoid origin indicate that a close relationship exists between p-MTB progenitors¹⁶¹. This process is heavily influenced by the microvasculature in terms of cytokines and signaling pathways it can provide to a developing HSC. Therefore, the cytokine profiles in any given pathologic state can also heavily impact hematopoiesis and thus the subsequent immune response.

During acute inflammatory reactions, the host enters a state of 'emergency' hematopoiesis characterized by increased recruitment of myeloid lineage cells such as neutrophils and macrophages¹⁷⁸. Unresolved inflammation increases myelopoiesis,

shifting the distribution of myeloid subpopulations¹⁷⁹. This results in the premature release from the BM, a heterogeneous population of mononuclear (CD11b⁺Gr-1^{int}Ly6G⁻Ly6C⁺) and polymorphonuclear (CD11b⁺Gr-1^{high}Ly6G⁺Ly6C⁻) MDSCs¹⁶². These cells accumulate in a spectrum of disease states including cancer, the natural aging process, solid organ transplantation, parasitic infections, sepsis, autoimmune disease, trauma, and burns^{180–183}. The phenotypic and functional characteristics of MDSCs strongly underscore their myeloid origin. Common cytokines involved in myeloid development have been implicated in the induction of MDSCs. These factors include macrophage-colony stimulating factor (M-CSF), granulocyte-macrophage colony stimulating factor (GM-CSF), IL-6, vascular endothelial growth factor (VEGF), and granulocyte-colony stimulating factor (G-CSF). Several transcription factors involved in myelopoiesis are interferon-regulatory factor 8 (IRF-8), CAAT/enhancer binding protein-beta (C/EBP-β), and PU.1. These have also been demonstrated to regulate MDSC development¹⁸⁴. In addition to myeloid differentiation antigen Gr-1 and CD11b, MDSCs also express various other markers that are traditionally used to define myeloid cells such as CX3CR1, CCR2, CXCL10, CD206, and IL-1β. Recent investigations demonstrate that, at the tumor site, MDSCs bear several classically activated (M1) and alternatively activated (M2) macrophage phenotypic and functional characteristics¹⁸⁵. MDSCs express IL-1β, TNFα, CXCL10, and inducible nitric oxide synthase (iNOS) that is characteristic to M1 macrophages as well as CD206, and arginase I (Arg I), which are M2 specific. Since MDSC development and proliferation occur in an asynchronous manner along the differentiation of CMPs and GMPs toward mature myeloid cells, it is not surprising that they retain a wide spectrum of myeloid cell characteristics.

2.1.3 Development of the ADAM10Tg mouse

ADAM10Tg mice that overexpress murine ADAM10 cDNA under control of the H-2Kb promoter and the IgH enhancer region were generated by our lab to study the role of ADAM10 in lymphocyte development. The H-2Kb vector allows expression in early lymphocyte progenitors^{112,186,187}. Inclusion of the IgH enhancer results in preferential expression on B lineage cells. This overexpression of ADAM10 was observed on BM cells and markedly reduced the numbers of pro, pre, and immature B cells in the BM and an almost complete loss of peripheral B2 B cells⁵⁶. The only B cell population unaltered by ADAM10 overexpression were peritoneal lavage fluid resident B1a (B220^{int}CD11b⁺CD5⁺) and B1b cells (B220^{int}CD11b⁺CD5⁻)⁵⁶. ADAM10 overexpression did not alter peripheral T cell levels⁵⁶.

ADAM10Tg animals also exhibited significant myeloid accumulation. In the BM of these mice, CD11b⁺Gr-1⁺ cells constitute over 90% of the BM cells. These cells leave the BM and migrate to all secondary lymphoid organs. Spleens of ADAM10Tg mice are increased at least 300% in size, filled with these cells. CD11b⁺Gr-1⁺ cells outside the BM are classified as MDSCs, consisting of monocytic (CD11b⁺Ly6C⁺Ly6G⁻) and granulocytic (CD11b⁺Ly6C^{int}Ly6G⁺) subsets¹⁸⁸. This heterogeneous population was observed within the MDSCs in the ADAM10Tg⁵⁶.

This expansion of myeloid cells and blockade of B2 cell development in ADAM10Tg mice indicates that ADAM10 regulates the commitment of BM progenitors to myeloid or lymphoid lineages. Investigations by *Gibb et al.* showed that hematopoietic alterations in ADAM10Tg mice occur prior to the commitment of CLPs to the B cells¹⁶⁹. Additionally, LSKs are unaffected in the ADAM10Tg but myeloid

progenitors are drastically altered. The profile of myeloid progenitors in ADAM10Tg mice shows an almost complete reduction in GMPs and MEPs, with a dramatic increase in CMPs, accounting for the overexpression of CD11b⁺Gr-1⁺ myeloid cells¹⁶⁹. This was confirmed to be a cell intrinsic result of overexpression of ADAM10 and not to be alterations in the stromal compartment of the BM⁵⁶.

As previously described, ADAM10 disruption and thus defunct Notch signaling dramatically effects embryonic, thymocyte, and MZB development^{22,47,56}. Studies done by *Gibb et al.* suggest that ADAM10 overexpression may cause myeloid development by dysregulating Notch signaling in the absence of sufficient ligand engagement. This is caused by generating excessive S2 product that is not processed in the absence of ligand-induced γ -secretase activity¹⁶⁹. They additionally found evidence that ADAM10 activity blocks B cell development¹⁶⁹.

Although MDSC accumulation is a byproduct of ADAM10 overexpression in early hematopoietic progenitors, ADAM10 expression is not altered in these cells. Here, we examined whether ADAM10Tg mice could be exploited to study MDSC-mediated immune regulation in an environment devoid of confounding tumor-derived factors.

2.1.4 Introduction to MDSC Function

Despite the ambiguity surrounding their origin, MDSCs are most prominently recognized for their role in the anti-tumor immune response. MDSCs are a heterogeneous population divided into two main subpopulations: monocytic and granulocytic. In mice, CD11b⁺Ly6G⁻Ly6C⁺ and CD11b⁺Ly6G⁺Ly6C^{lo} surface markers define these cells, respectively^{162,169,189}. Although human markers differ, both subsets

are represented. The heterogeneity of these cells allows for a broad range of cellular functions within the total population. MDSCs have been extensively studied in the context of cancer and exert their pro-neoplastic effects through the release of small soluble oxidizers, the impairment of T cell/antigen recognition, and the depletion of essential amino acids from the local extracellular environment resulting in T cell suppression¹⁹⁰. Both subpopulations of MDSCs have been shown to play integral roles in this suppression¹⁹⁰. The cumulative effect is increased tumor progression and diminished therapy results¹⁹¹. MDSCs additionally accumulate in and contribute to other disease states, such as parasitic infection where MDSCs have been shown to play an immunosupportive role^{183,192,193}.

MDSCs collectively represent a heterogeneous cell population with different patterns of surface protein expression. In the murine system are unified by expression of Gr-1 and CD11b. The Gr-1 epitope comprises of Ly6C and Ly6G molecules that are members of the Ly-6 family of low molecular weight phosphatidylinositol-anchored cell surface glycoproteins^{194–196}. Expression of the two distinct epitopes of Gr-1, allow the differentiation between the two major subpopulations of MDSCs. Ly6G⁺Ly6C^{lo} MDSCs are considered granulocytic and morphologically resemble polymorphonuclear (PMN) granulocytes while Ly6C⁺ MDSCs are considered monocytic and resemble mononuclear monocytes. In humans, MDSCs are defined as Lin⁻HLA-DR⁻CD34⁻CD33⁺ and further categorized into monocytic and granulocytic MDSCs by CD14⁺ and CD15⁺ expression, respectively¹⁹⁰. In mice, studies indicate that engagement of the Gr-1 epitope through Ly6G or Ly6C can differentially regulate myeloid cell activity and the

subsequent immune response^{194,197,198}. For example, ligation through Ly6G can induce cell death while Ly6C can lead to cellular expansion and differentiation^{194,198}.

Many groups have reported the utilization of other protein makers to further delineate monocytic MDSCs and granulocytic MDSCs. In humans, granulocytic MDSCs are defined as CD11b⁺CD33⁺CD14^{lo}CD15^{hi} and can be further characterized by expression of CD66b, a member of the carcinoembryonic antigen family that is commonly expressed on human neutrophils. Additionally, human granulocytic MDSCs have also been indicated to express VEGFR1 and low levels of CD62L^{199–201}. Although these surface proteins are often associated with neutrophils, the main differentiating factor between granulocytic MDSCs and neutrophils in humans is that in contrast to conventional neutrophils, granulocytic MDSCs are purified from the mononuclear cell fraction in density gradients of peripheral blood²⁰². Another marker, CD124 or IL-4R α , can be used to mark granulocytic MDSCs in patients with non-small cell lung cancer, but in melanoma and colorectal cancers it is found on both subpopulations^{203–205}. Granulocytic MDSCs, as demonstrated by *Trellakis et al.*, exhibit higher levels of the S100 protein, S100A8/A9 complex as compared to S100A9 on monocytic MDSCs in patients with head and neck squamous cell cancer (HNSCC)²⁰⁶. Human granulocytic MDSCs express IL-13R under suppressive conditions and lower levels of CD33 as compared to monocytic MDSCs^{190,202,206,207}. Work by *Duffy et al.* on sorting and storage of MDSC subsets from gastrointestinal (GI) tumors identifies that CD33 expression may not be a beneficial marker for MDSC isolation from human patients. They show that CD33⁺ and CD33⁻CD15⁺ MDSCs have equivalent CD8⁺ T cell suppression²⁰⁸.

Human monocytic MDSCs are mainly defined as CD11b⁺CD33⁺CD14^{hi}CD15^{lo}. The preferential markers to delineate human monocytic MDSCs from granulocytic MDSCs favor granulocytic MDSCs. But work done by *Mandruzzato et al.* shows that IL-4Rα found on both subpopulation of human MDSCs, is important as a suppressive marker only in the monocytic MDSC population²⁰⁵. A third subpopulation of MDSCs is often described. These MDSCs are considered immature MDSCs and are defined by Lin⁻HLA-DR^{lo/-}CD33⁺CD14⁻CD15⁻²⁰⁴. These MDSCs are thought by many groups to be the lineage precursors in humans to granulocytic and monocytic MDSCs^{188,205,209–214}.

Murine MDSCs have been studied extensively, thus markers identifying the two subpopulations are many. Granulocytic MDSCs in mice are defined as CD11b⁺Ly6C^{lo}Ly6G⁺. Researchers have also been known to separate these cells out by Gr-1 expression, as granulocytic MDSCs are Gr-1^{high}. Other groups also indicate that granulocytic MDSCs express SLAMF4 (CD244) and/ or CSF-R (CD115) in tumor bearing mice²⁰³. Furthermore, *Youn* and colleagues reported the expression of M-CSFR on granulocytic MDSCs and utilization of CD244 as a marker of granulocytic MDSC identification and T cell suppressing nature. The authors indicate that CD244⁺ granulocytic MDSCs are capable of inhibiting antigen specific T cell responses while CD244⁻ granulocytic MDSCs are unable to do so²¹⁵. Additionally, *Toh et al*, reports that granulocytic MDSCs express CXCR2 (IL-8Rβ), which binds CXCL1, CXCL2, and CXCL5. Granulocytic MDSCs also express CXCL1 and CXCL2 while tumors express CXCL5. The ligation of these particular molecules leads to the accumulation of granulocytic MDSCs and not monocytic MDSCs in the murine tumor microenvironment. In fact, inhibition of CXCR2 inhibited granulocytic MDSC trafficking to primary

melanoma tumor²¹⁶. This is supported by another finding in a murine model of traumatic spinal cord injury, indicating the expression of CXCR1 and CXCR2 on granulocytic MDSCs²¹⁷.

Murine monocytic MDSCs are defined by markers CD11b⁺Ly6G⁻Ly6C⁺. Monocytic MDSCs are additionally Gr-1 intermediate and can be differentiated from high Gr-1 expressing granulocytic MDSCs without the use of the Ly6G or Ly6C epitopes. In addition, monocytic MDSCs are also characterized by expression of CCR2, which is expressed mainly by monocytic MDSCs and not granulocytic MDSCs²¹⁸. In tumor conditions, CCR2 induces monocyte trafficking from the BM, limits entry of tumor specific T cells into the tumor microenvironment, and leads to T cell inhibition by MDSCs in contact-dependent manner. Murine monocytic MDSCs are further define by CD49d, CCR7, and CX3CR1 expression^{217,219,220}. Another group reported the presence of F4/80 and CD93 on monocytic MDSCs in Experimental Autoimmune Encephalomyelitis (EAE)²²¹.

In addition to Gr-1 and CD11b in the murine system, both populations are also identified by functional markers such as Dectin-1, a non-toll like pattern recognition receptor, death receptor FAS, and ADAM17^{47,198,200}. Both populations of MDSCs also express TNFR1 and TNFR2²²².

2.1.5 Survival and Proliferation

Like neutrophils, granulocytic MDSCs have a reduced life-span, similar to the 3.8 days reported for neutrophils and are more sensitive to cryopreservation as compared to monocytic MDSCs^{196,208,215}. However, granulocytic MDSCs are quickly repopulated

from the BM and exhibit up to 80% survival when exposed to tumor explant supernatant and GM-CSF^{177,196,201,223}. This has been attributed to delayed apoptosis by increased CXCL8²²⁴. Despite the prolonged life-span, these conditions did not induce granulocytic MDSC proliferation, just survival. This has led to the current notion that monocytic MDSCs are the only subset capable of proliferation. In fact, in the same study, *Youn et al.* demonstrates that splenic monocytic MDSCs incorporated more than two-fold BrdU as compared to granulocytic MDSCs in tumor bearing mice²⁰⁷.

2.1.6 Polarization and differentiation

In addition to a shorter life span, granulocytic MDSCs are also incapable of differentiation while monocytic MDSCs can give rise to mature myeloid cells²⁰⁷. In fact, CD11b⁺Gr-1⁺CCR2⁺CX3CR1^{low} monocytic MDSCs are capable of differentiating into DCs and macrophages under appropriate stimuli²¹⁹. A recent study indicates that monocytic MDSCs can also differentiate into granulocytic MDSCs via epigenetic silencing of the retinoblastoma gene. Interestingly, the same study also suggests that granulocytic MDSCs can lose their immunosuppressive characteristics and become phagocytic upon *ex vivo* exposure to tumor explant supernatants and GM-CSF²²⁵.

In addition to differentiating into mature cells, MDSCs can be polarized towards immunostimulatory type1 or immunoinhibitory type2 cells. Paired immunoglobulin-like receptors A and B (PIR-A and PIR-B) along with human PIR homologues belong to the immunoglobulin super family. These molecules have recently been demonstrated to differentially regulate MDSC polarization. PIR-A and PIR-B were first identified as homologues to the human Fc receptor for immunoglobulin A (IgA). It has recently been reported that PIR signaling can alter polarization of monocytic MDSCs between the

classically activated proinflammatory phenotype (M1) to an alternatively activated anti-inflammatory (M2) phenotype and vice versa. PIR-A delivers activation signals in complex with a homodimeric Fc common γ chain, which harbors an immunoreceptor tyrosine-based activation motif (ITAM), resulting in cytokine production in myeloid cells^{226–228}. In contrast, PIR-B engagement results in negative signal transduction upon phosphorylation of immunoreceptor tyrosine-based inhibitory motifs (ITIMs) and recruitment of SH2-homology-containing protein-tyrosine phosphatase-1 (SHP-1) and SHP-2. *Yan et al.* reports that PIR-A ligation induces immunostimulatory M1 like monocytic MDSCs while PIR-B inhibits this interaction, in favor of M2-like M-MDSCs. In fact, SHP1 inhibition can shift M2 monocytic MDSCs to M1-MDSCs. Furthermore, *Fridlender et al.* also demonstrate that granulocytic MDSCs can also be polarized between G1 and G2 phenotypes but this is dependent upon TGF- β signaling. MDSCs and tumor cells secrete large amounts of TGF- β that induces pro-tumor G2 granulocytic MDSCs. However, blockade of TGF- β signaling via TGF- β R antagonization reprogrammed G2 granulocytic MDSCs to tumoricidal G1 granulocytic MDSCs²²⁹.

2.1.7 Oxidative Metabolism of MDSCs

While both subpopulations of MDSCs express Arg1. Granulocytic MDSCs and Monocytic MDSCs specifically generate reactive oxygen species (ROS) and inducible nitric oxide (iNOS), respectively¹⁶². Arg1 is widely expressed in murine myeloid lineage cells, yet is limited to neutrophil lineage in humans²¹⁵. The expression of Arg1 allows granulocytic MDSCs to contribute to cancer progression via T cell suppression. Arg1 acts by consuming the essential amino acid L-arginine (L-Arg) and metabolizes it to L-ornithine and urea, both essential components of cellular proliferation and

detoxification²³⁰. This *in vitro* L-Arg depletion by MDSCs, inhibited antigen-specific T cell proliferation in OT-1 and OT-2 transgenic mice^{231,232}. Furthermore, in the absence of L-Arg, T cells exhibit decreased CD3 ζ expression, Jak-3, NF κ B-p65 translocation and IFN- γ production²³². CD3 ζ is an essential component of the TCR, as it is imperative for the intracellular signaling cascade and subsequent T cell activation²³³. Loss of L-Arg decreases cyclin D mRNA transcriptional rates as well as translation, thus arresting T cells in G0-G1 phase²³⁴. However the depletion of L-Arg does not result in apoptosis and both CD3 ζ expression and proliferative potential can be restored upon L-Arg administration²³⁵. Nonetheless, *Kusmartsev et al.* report that under limited L-Arg concentration, NOS produces peroxynitrites (ONOO₂), which are strong oxidizing agents that nitrate proteins and cause T cell apoptosis²³⁶. Arg1 production can be induced through IL-13/IL-4R α signaling and in a murine model of graft versus host disease (GVHD) limits disease through T cell suppression¹⁸².

In addition to Arg1, granulocytic MDSCs induce T cell suppression via the production of ROS. Although ROS can be produced by several mechanisms, NADPH oxidase (NOX2) is primarily responsible for ROS production in leukocytes²³⁷. The main consequence of MDSC-mediated ROS production is inhibition of T cells in an antigen-specific manner by inducing MHC class-I restricted T cell tolerance²³⁸. *Nagaraj et al.* report that ROS nitrates tyrosine residues on CD8 and the TCR to alter peptide recognition but does not induce T cell deletion²³⁹. Finally, Granulocytic MDSCs limit natural kill cell (NK) responses via H₂O₂ production²⁴⁰. However, additional experiments are required to further elucidate the mechanism of this interaction²¹⁵.

Monocytic MDSCs are more potent suppressors of the immune response¹⁸⁸. Perhaps one of the main contributions of monocytic MDSC in pathologic conditions is the up regulation of iNOS, which generates nitric oxide (NO). *Mazzoni et al.* report that NO production by MDSCs blocks peptide-specific T cell proliferation. Further analysis revealed this is due to the prevention of T cells from entering the cell cycle. Interestingly, this was reversible. When T cells were stimulated with Con A in the presence of MDSCs, they only regained their proliferative potential once the MDSCs were removed. Thus, it is plausible that although monocytic MDSCs prevent T cell proliferation, they do not induce apoptosis but transiently induce T cell suppression²⁴¹. The contribution of NO is further elucidated by the observation that MDSCs generated from iNOS deficient mice are not suppressive²⁴². Another consequence of iNOS is the consumption of L-arginine as discussed above.

2.1.8 Cytokine production

Although the cytokine expression profile of each subset is dependent on disease state, each subset has been identified with certain cytokines. For example, granulocytic MDSCs secrete TNF α upon exposure to LPS, IFN γ , and TGF- β . Monocytic MDSCs have been shown to secrete IL-6, IL-10, IL-23, TGF- β , and VEGF- α ^{219,220}. The concomitant secretion of IL-10 and TGF- β also allows monocytic MDSCs to be potent inducers of CD4⁺CD25⁺Foxp3⁺ T-regulatory cells^{219,220}.

2.1.9 Cell Signaling

STAT signaling

Both monocytic MDSCs and granulocytic MDSCs signal through Janus Kinase (Jak) / signal transducer and activator of transcription (STAT) pathways²⁴³. STAT proteins are latent cytoplasmic transcription factors activated by a variety of hematopoietic and immune-mediated cytokine receptors. Monocytic MDSCs utilize STAT1 to induce downstream T cell suppression¹⁸⁸. Of the STAT signaling pathways, STAT3 has been strongly linked with MDSC proliferation and survival^{162,183}. STAT3 additionally promotes the activity of MDSCs, particularly Arg1 in CD14⁺ monocytic MDSCs²⁴⁴. Using the receptor tyrosine kinase inhibitor, sunitinib, Ko and colleagues demonstrate differential STAT3 and STAT5 signaling in murine monocytic MDSCs and granulocytic MDSCs. The authors indicate that sunitinib down regulates STAT3, subsequently abrogating monocytic MDSC proliferation and impairing granulocytic MDSC survival. However, the addition of GM-CSF provides protection via STAT5 signaling²⁴⁵. Tumor derived factor induction of STAT3 and STAT5 signaling has also been implicated in MDSC accumulation through down-regulation of IRF-8 in tumor bearing mice as well as late stage breast cancer patients. Mice overexpressing IRF-8 have decreased MDSC accumulation and attenuated tumor progression²⁴⁶.

Notch signaling

Altered Notch signaling is implicated in MDSC accumulation in the ADAM10Tg mice²⁴⁷. Notch signaling was found to be severely decreased in granulocytic MDSCs from breast cancer patients and from tumor bearing mice²⁴⁸. Serine/Threonine casein kinase 2 (CK2) is ubiquitously expressed and implicated in Notch signaling²⁴⁸. Recent

work by Cheng et al. showed that in tumor bearing mice CK2 catalytic activity is increased in granulocytic MDSCs, but not monocytic MDSCs²⁴⁸. This enhanced catalytic activity of CK2 disrupts the interaction between Notch and transcriptional repression CSL, which is needed for normal Notch signaling and DC formation. Inhibition of CK2 decreased tumor conditioned media-induced proliferation of murine tumor generated granulocytic MDSCs, but had no effect on monocytic MDSCs²⁴⁸. This work implicates tumor derived factors as driving CK2 activity and thus altered Notch signaling and the accumulation of MDSCs in cancer.

2.1.10 Cytokine induced MDSC expansion

Granulocyte-macrophage colony stimulating factor (GM-CSF) and granulocyte-colony stimulating factor (G-CSF) are two cytokines predominately associated with *in vivo* MDSC accumulation and *in vitro* MDSC generation in humans and mice^{162,169,220}. GM-CSF is recognized as a critical hematopoietic cytokine, mediating the differentiation of myeloid progenitors into granulocytes, eosinophils, monocytes, megakaryocytes, and erythrocytes. G-CSF and its receptor are critical regulators of steady state and emergency granulopoiesis. G-CSF promotes the survival, mobilization, and proliferation of myeloid progenitor cells alongside neutrophil differentiation. Several studies indicate that each cytokine preferentially induces granulocytic or monocytic MDSCs. Exposure of GM-CSF alone induces immunosuppressive monocytic MDSCs while G-CSF induces granulocytic MDSCs^{249,250}. In fact, in human glioblastoma patients, they exhibit high levels of G-CSF concomitant with granulocytic MDSC accumulation²⁵¹. Under steady state conditions, G-CSF acts in concert with CXCR2 ligands, CXCL1 and CXCL8 to induce mobilization and recruitment of neutrophils, respectively. Therefore, it has been

proposed that G-CSF may induce expansion of granulocytic MDSCs via CXCL1 and mobilization via CXCL8¹⁹⁶. In terms of GM-CSF, *Dolcetti et al.* demonstrates that 4T1 mammary cancer cell line, deficient in GM-CSF but not G-CSF, is less immunosuppressive due to the differential expansion of G-MDSCs over M-MDSCs²⁵⁰. The reduced tumor growth is accompanied by an increase in antigen specific T cells lymphocytes in LNs of mice challenged with GM-CSF deficient 4T1. These mice also exhibited an accumulation of G-MDSCs that did not affect the generation of tumor specific T cells¹⁹⁷. Moreover, *Greten et al.* indicate that human CD14⁺ monocytes purified from healthy donors can be differentiated into suppressive M-MDSCs upon co-culture with IL-4 and GM-CSF²²⁰. Interestingly, the combination of GM-CSF and G-CSF induces monocytic MDSCs from BM cells after 4-days of co-culture. Additionally, IL-1 β has been indicated to inhibit NK cell differentiation in favor of granulocytic MDSCs in 4T1 mammary carcinoma^{208,216,252}. Recently, murine hepatic stellate cells were found to mediate MDSC induction via the complement factor C3 upon adoptive transfer²⁵³. In humans, activated hepatic stellate cells induced monocytic MDSCs in a contact dependent and CD44 dependent manner²⁰⁴. Lastly, Simpson and colleagues demonstrated that the inflammatory cytokine, macrophage inhibitory factor (MIF), induces monocytic MDSC differentiation rather than granulocytic MDSCs²⁵⁴.

2.1.11 Subset accumulation in pathological conditions

Neoplasia.

The expansion of MDSC phenotypes is dependent upon the immunoregulatory factors altered by a given tumor or tumor model in mice. In humans, monocytic MDSCs are mostly associated with melanoma, prostate, lung, gastrointestinal, and

hepatocellular carcinoma while G-MDSCs are associated with breast, colon, pancreatic, bladder, and HNSC carcinoma²²⁰. Granulocytic MDSCs are found to be the most abundant population in solid tumors while monocytic MDSCs are more frequent in leukemia²⁵⁵. A detailed list is summarized elsewhere, but the overall trend is the dominant accumulation of granulocytic MDSCs in human cancer^{196,225}. However, in patients with hepatocellular carcinoma, CD14⁺ monocytic MDSCs continue to be the most frequent population in the peripheral blood and tumor²²⁰. In humans with renal cell carcinoma (RCC) and HNSCC, granulocytic MDSC accumulation is associated with an increase in tumor and serum expression of CXCL8 (IL-8), a potent inducer of neutrophil motility to site of inflammation²²⁴.

In naïve mice, MDSCs comprise 2-4% of total nucleated splenocytes with a 3:1 ratio of granulocytic MDSC to monocytic MDSC²²⁰. However, MDSCs can increase up to 50% with a 5:1 granulocytic MDSC to monocytic MDSC ratio in tumor bearing mice²²⁵. The population of granulocytic MDSCs becomes consistently increased in all tumor models, whereas the frequency of monocytic MDSCs is only significantly increased in a few models such as EL-4 lymphoma and ANV mammary carcinoma. Only in Lewis Lung Carcinoma (LLC), granulocytic MDSCs and monocytic MDSCs are equally elevated²¹². Moreover, in a given host, granulocytic MDSCs tend to localize at the primary tumor site (24.5% vs 4.2%) while monocytic MDSCs are found in cutaneous tumors (3.9% vs. 2.8%)²¹⁸. In a mouse model of multiple myeloma (MM), monocytic MDSCs begin to accumulate within one week of tumor induction while granulocytic MDSCs accumulate weeks later. Despite the delay in kinetics, granulocytic MDSCs continue to be the dominant population both in the BM and peripheral blood²⁵⁶. In tumor

bearing mice, granulocytic MDSCs are recruited out of the BM in response to stromal cell derived factor 1 α (SDF-1 α), the ligand for CXCR4. This was also supported by a separate observation indicating the importance of CXCR2 ligand in the recruitment of granulocytic MDSCs to primary tumor site. In fact, granulocytic MDSCs were 5 times more abundant as monocytic MDSCs and CXCR2 inhibition significantly abrogated this observation²⁵⁶.

While most attention has been given to the pathogenic mechanism of monocytic MDSCs, granulocytic MDSCs are now beginning to be appreciated for their contribution to tumor progression. Using a model of spontaneous melanoma, *Toh* and colleagues indicate that granulocytic MDSCs are needed for the early stages of cancer dissemination, as late depletion did not alter metastasis to skin, LNs, or lung. Additionally, upon co-culture with granulocytic MDSCs, NBT-II bladder carcinoma cells acquired a mesenchymal morphology, consisting of actin microfilament redistribution and down regulation of E-Cadherin. This was attributed to the production of Hepatocyte Growth Factor (HGF) and TGF- β , known inducers of epithelial-mesenchymal transition (EMT). Moreover, the same study reported that granulocytic MDSCs promoted tumor cell proliferation in a contact-independent manner²¹⁸.

Infection

MDSCs, predominantly granulocytic MDSCs, have been shown to accumulate in infections with microorganisms. In this context, they can play a beneficial role in limiting unwanted inflammation as mice unable to expand MDSCs exhibit markedly higher mortalities to sepsis-associated inflammation^{183,256,257}. As mentioned earlier, bacterial infections can skew MDSCs towards antitumor properties. The administration of

attenuated *Salmonella enterica* serovar Typhimurium vaccine (RASV) results in an accumulation of MDSCs, particularly the granulocytic subset. These MDSCs were very sensitive to LPS stimulation, released large amounts of TNF α , and exhibited anti-tumor properties. RASV treatment reduced Her-2/neu expressing tumor growth, shifted MDSC differentiation towards granulocytic MDSCs, and enhanced CTL anti-tumor response. It is for this reason that Salmonella-based cancer immunotherapies has been pursued with promising preclinical results^{192,258}. Furthermore, by limiting immune activation MDSCs play a protective role in sepsis. *Delano et al.* demonstrated that polymicrobial sepsis induced significant MDSC accumulation. More reports are surfacing, indicating a protective role of MDSCs in microbial infections, especially *Pseudomonas aeruginosa* colonization in burn victims and *Staphylococcus aureus* biofilm formation post orthopedic joint surgery^{183,195}. More recently, it was reported that MDSCs express dectin -1, a non-Toll-like pattern recognition receptor for β -Glucans, which are the main components of numerous bacteria, fungi, and yeast cell wall¹⁹⁹. The authors report that whole β -Glucans particle (WPG) administration preferentially enhances the survival of granulocytic MDSCs but does not induce their differentiation. In contrast, WPG treatment reduced monocytic MDSC survival but promoted differentiation towards CD11c⁺F4/80⁺ non-immunosuppressive cells. Monocytic MDSCs were no longer able to suppress T cell proliferation in the presence of WPG¹⁹⁹. This could be contributed to the fact that WPG reduced NO and Arg1 expression in monocytic MDSCs while it did not alter ROS expression of granulocytic MDSCs.

The protozoan parasite, *Trypanosoma cruzi* is the causative agent of myocarditis that manifests into Chagas disease. MDSCs comprise the majority of the inflammatory

cell infiltrates in the heart. The most abundant subset in this case is monocytic MDSCs (70%) as compared to granulocytic MDSCs (20%)²⁵⁹. Authors of this finding indicate that this is mainly mediated via CCL2 chemokine. Interestingly, these infiltrating monocytic MDSCs in the heart are not migrating from the BM but rather being replenished from the spleen. Like those isolated from the tumor microenvironment, the infiltrating monocytic MDSCs also express high levels of Arg1 and iNOS, and inhibit T cell proliferation. Given another report indicating the accumulation of granulocytic MDSCs in the peripheral organs of *T. cruzi* infected mice, it is possible that granulocytic MDSCs and monocytic MDSCs preferentially migrate to specific anatomical sites in a given disease state^{259,260}.

While the accumulation of MDSCs in parasitic infection has been reported, the immunomodulatory potential of these cells remained unknown²⁶¹. However, here we report the beneficial role of MDSCs in this context in the Th2 helminth *Nippostrongylus brasiliensis*. We additionally investigate the mediators and other cell types that are involved.

2.1.12 Interaction with cells other than T cells

Macrophages

Macrophages are capable of fighting both intracellular and extracellular pathogens and are thus classified into two distinct subsets based upon the cytokines required for their activation and the pathogens they target²⁶². Classically activated M1 macrophages are normally activated by IFN- γ or in response to lipopolysaccharides (LPS) to release NO in targeting intracellular pathogens as well as IL-12 and IL-23²⁶³.

Type I macrophages are characterized as capable of antigen presentation and promoting T cell proliferation and activity. In contrast, type 2 macrophages are considered to have poor antigen presentation capability as well as inhibit T cell proliferation and activity. Upon stimulation by IL-4 or IL-13, alternatively activated (M2) macrophages secrete IL-10, TGF- β and Arg-1 in response to extracellular pathogens²⁶⁴. MDSCs have not only been shown to resemble M2-like macrophages but also interact with macrophages. MDSCs decrease IL-12 production by macrophages and skew their differentiation towards an M2 phenotype. Macrophages in turn promote MDSC IL-10 production²⁶⁵. Although the authors of this study did not differentiate the subset of MDSCs, it can be deduced based on morphology and cytokine production that this interaction is mainly within the monocytic MDSC fraction. In *Staphylococcal aureus* biofilm infections of orthopedic joints, M1 macrophages are essential for clearance of the bacteria. Recruitment of MDSCs into the joint causes the skewing of macrophages to the M2 phenotype. This MDSC induced M2 macrophage skewing severely limits the ability of the immune system to clear the infection, thus inducing a persistent, chronic infection²⁶⁶.

Dendritic Cells

Another cell known to interact with MDSCs is DCs. DCs are professional APCs that identify, process, and present antigens to naïve, resting T cells²⁶⁷. This is critical for the generation of an appropriate immune response. MDSCs secrete IL-10 that inhibits toll like receptor (TLR) ligation and subsequent IL-12 production by DCs. This in turn reduces DC mediated T cell activation²⁶⁸. While MDSCs as a group have been shown to limit DC maturation, a recent group indicates CD14⁺ human monocytic MDSCs impair

the quality of a DC vaccine. The authors indicate that monocytic MDSCs not only prevent DC maturation but also antigen presentation and migration²⁶⁹. Interestingly, MDSCs can be converted to DCs. Two studies have been done to this effect, one indicating the requirement of NKT Cells and α -galactosylceramide; and another suggesting interaction of iNKT with CD1d on MDSCs^{252,270}.

Mast Cells

Recent findings are beginning to suggest that mast cells (MCs) contribute to the recruitment and activity of MDSCs^{193,271,272}. While MCs have well been documented to mediate allergic inflammation, their demonstrated involvement with neoplastic disease is more recent. Here, we investigate the novel interaction between the MDSC and the MC.

2.1.13 Introduction to the Mast Cell

MCs are large, granular, long-lived cells that typically reside in sites that interface with the environment such as the skin and mucosa of the respiratory and GI tracts^{273,274}. MCs originate from the BM and terminally differentiate in the tissues²⁷⁴. MCs serve as important sentinel cells and accumulate in the tissues in response to inflammation²⁷⁵. MCs are induced by cytokines IL-3, SCF, IL-4 and IL-9²⁷⁵. MCs are critical regulators of innate and adaptive immunity. Mast cells express Fc ϵ RI, the high affinity receptor for IgE. Antigen-specific IgE binds to Fc ϵ RI and upon encounter with the antigen; IgE cross-links the receptor inducing MC activation and degranulation. This degranulation is responsible for a wide variety of allergic reaction such as life-threatening anaphylaxis²⁷⁵. They are key regulators of the anti-parasitic immune response^{276–278} through the production of cytokines, and effector cell recruitment, including MDSCs²⁶¹.

It has been long known that increased MC numbers at the tumor site correlates with negative prognosis^{278,279}. This was presumably thought due to their secretion of various pro-inflammatory cytokines, MCs have also been shown to secrete mediators such as 5-LO and IL-17 to recruit MDSCs to the tumor site^{272,279}.

Mast Cell secreted histamine on MDSC function

Activated MCs secrete histamine, proteases, and lipid-derived mediators. The biogenic amine, histamine, is considered a major mediator released by MCs. Histamine acts on a spectrum of cell types through GPCRs, known as HR1–4. The expression profile of the HRs determines the net effect on cell growth, motility, phenotypic alterations, and signaling mechanisms^{280–282}. Through effects on target cells, histamine induces vasodilation, vasopermeability, smooth muscle contraction, and mucus production²⁸³. Numerous studies have linked excessive histamine production to allergic reactions, infections, and tumor growth^{284,285}. Myeloid cells have been reported to express HRs and HDC, the enzyme required for histamine synthesis²⁸⁶. Histamine, in turn, protects myeloid cells against apoptosis and promotes cytokine production. In fact, co-culture of monocytes with histamine has been shown to increase IL-10 and inhibit IL-12, thus skewing toward Th2 immunity²⁸⁷. Thus, histamine can alter the cytokine milieu, transcription factors, and signaling pathways important for MDSC accumulation²⁸⁸.

Mast Cell secreted IL-13 on MDSC function

IL-13 is a cytokine made by many cell types including MCs^{289,290}. IL-4 and IL-13 are both Th2-polarizing cytokines with overlapping roles^{291,292}. IL-4 binds IL-4 receptor subunit alpha (IL-4R α) complexed to both the common gamma chain as well as IL-13 receptor subunit alpha (IL-13R α). IL-13 is only able to bind to IL-4R α with IL-13R α .

However the downstream signaling appears to be divergent dependent on which ligand is bound^{291,292}. IL-13 is primarily responsible for the “weep and sweep” associated with intestinal parasitic clearance^{289,290}. This includes enteric nerve stimulation and goblet cell hyperplasia^{289,290}. The role of IL-13 in the context of neoplasia has been a controversial one. Initial studies found beneficial roles for both IL-13 and IL-4 in tumor rejection^{292–295}. These effects were noticed mainly in tumor lines that were genetically engineered to overexpress the cytokine^{292,293}. Currently, the evidence demonstrating IL-13 as tumor promoting is becoming more and more abundant^{296–298}. Phase I/II clinical trials are even underway for use of IL-13-PE (Cintredekin besudotox) in patients with metastatic and locally advanced adrenocortical carcinoma (ACC) and other advanced solid tumors with high expression of IL13R α 2²⁹⁹. Human studies of pancreatic, esophageal, and gastric tumors show that increased IL-13 in plasma is directly correlated with MDSC levels and increased mortality²⁹⁶. IL4R α is expressed on MDSCs and is related to the suppressive nature of the cells³⁰⁰. IL-13 signaling through IL-4R α on MDSCs induces increased production of Arg1, thus, increasing T cell suppression³⁰⁰. Mice deficient in IL-4R α have decreased Arg1 expression in the tumor microenvironment and decreased tumor growth in a mouse model of glioma³⁰¹. Additionally, with blockade of IL-4R α and subsequent loss of IL-13 signaling, 4T1 tumor progression is delayed. MDSC apoptosis is increased as well as CD8⁺ T cell infiltration to the tumor site²⁹⁸. The source of IL-13 has been debated, until recently when MC-derived IL-13 was shown to play an important role in tumor-genesis of pancreatic ductal adenocarcinoma²⁹⁷. The function of IL-13 in tumor development seems to be closely related to the source, timing of expression, dosage, as well as the molecular and

cellular environments³⁰¹. Other than induction of Arg1, thus increasing suppressive capabilities of MDSCs, the role of IL-13 in MDSC function is largely unknown¹⁸².

Chapter 2: Methods and Materials

2.2.1 Mice

Mice were kept at Virginia Commonwealth University (VCU) in accordance with the humane treatment of laboratory animals set forth by the National Institutes of Health and the American Association for the Accreditation of Laboratory Animal Care. C57BL/6 ADAM10Tgs were generated by the VCU Transgenic Mouse Core, as previously described²⁴⁷. C57BL/6 WT mice, Pmel-1 and Kit^{Wsh/Wsh} mice were purchased from The Jackson Laboratory (Bar Harbor, ME, USA). Cpa3cre; Mcl-1^{fl/fl} mice³⁰² (C57BL/6 background) were generously provided by Dr. Stephen Galli (Stanford University, Stanford, CA, USA). All mouse protocols were approved by the VCU Institutional Animal Care and Use Committee.

2.2.2 Cell Lines

Mouse bone marrow-derived MCs (BMMCs) were derived from femurs of WT mice and cultured in cRPMI 1640 containing 10% FBS, 2mM L-glutamine, 100 U/mL penicillin, 100µg/mL streptomycin, 1mM HEPES (Quality Biological, Gaithersburg, MD, USA), and 1mM sodium pyruvate (Cellgro, Herndon, VA, USA). Cultures were supplemented with IL-3-containing supernatant from WEHI-3 cells (1ng/mL) and stem cell factor containing supernatant from BHK-MKL cells (10ng/mL). Mature BMMCs were used after 28 days of culture. The LLC cell line was obtained from the American Type Culture Collection. The B16-melanoma cell line was maintained in DMEM with 10% FBS, 1% penicillin, 1% streptomycin, and 1% L-glutamine. B16 melanoma and GM-CSF–B16 cells were provided by Harry D. Bear, MD, PhD and maintained as previously described³⁰³.

2.2.3 Isolation of MDSCs and AT, T cell depletion, and dye labeling.

Spleens were harvested from ADAM10Tg or LLC-bearing WT mice, depending upon the experimental protocol. They were then dispersed into single-cell suspensions and filtered through 70- μ m nylon mesh strainers (Invitrogen). Erythrocytes were lysed using an ammonium chloride potassium lysing buffer (Quality Biological). T cells were depleted using CD90.2 magnetic depletion (Miltenyi Biotec, Auburn, CA, USA), according to the manufacturer's protocol. Gr-1⁺, Ly6G⁺, or Ly6C⁺ cells were purified from ADAM10Tg spleens using the EasySep PE-Selection kit (Stemcell Technologies, Vancouver, BC, Canada), according to the manufacturer's protocol. For AT studies, 10×10^6 ADAM10Tg MDSCs were injected into the tail vein of each experimental group every 3 days. For T cell depletion, mice were injected i.p. with 200 μ g anti-CD4 (GK1.5) and anti-CD8 (2.43) antibodies on days -3, -2, -1, 0, 5, and 10. For AT of dye-labeled MDSCs, cells were stained with the PKH26GL dye-linker kit (Sigma-Aldrich, St. Louis, MO, USA), according to the manufacturer's protocol.

2.2.4 Arginase1 and iNOS detection

MDSC cytoplasmic extracts were prepared from isolated ADAM10Tg- and LLC-bearing hosts and tested for urea production (DARG-200; BioAssay Systems). NO was measured using Greiss Reagent (G7921; Molecular Probes).

2.2.5 T cell suppression assays

For polyclonal T cell activation, CD90.2⁺ T cells were sorted from spleen and activated with immobilized anti-CD3 (10 μ g/mL) and soluble anti-CD28 (1 μ g/mL) in 96-well plates. Sorted MDSCs (Ly6G⁺, Gr-1⁺, and Ly6G⁻) from ADAM10Tg or LLC tumor-bearing mice were then added at increasing T cell/MDSC ratios. For Ag-specific T cell suppression

assays, soluble gp100 (1µg/mL) was added to defined ratios of pmel-1 transgenic splenocytes and ADAM10Tg MDSCs. After 54 hours of culture, 1 mCi [³H] thymidine was added to each well for an additional 18 hours, and thymidine incorporation was measured.

2.2.6 BMMC co-culture with ADAM10Tg MDSCs

BMMCs were derived from femurs of WT naive mice cultured in complete RPMI 1640 containing 20% WEHI-3–conditioned medium over a 4-wk period. They were resuspended at 0.5×10^6 cells/mL, loaded with 0.5µg/ml mouse IgE, and cultured with MDSCs at a 1:1 ratio in 10ng/mL IL-3 and 10 ng/mL GM-CSF overnight. MCs were activated by DNP-human serum albumin (20–100 ng/mL), and supernatants were collected 6 or 18 hours after cross-linking for ELISA.

2.2.7 Migration Assays

B16 (2×10^5), BMMC, or media alone were loaded into the lower well of 8µm transwell plates (Corning, Herndon, VA, USA). MDSCs (2×10^5) were loaded into the upper well. Plates were incubated for 4 h at 37°C, and the lower well was harvested for flow cytometry.

2.2.8 Survival curve and proliferation assays

MDSCs were cultured in cRPMI with 1, 5, 10, or 100µM histamine (Calbiochem, San Diego, CA, USA). For survival curves, counts were made with trypan blue dead cell exclusion, and cell concentration was 1×10^6 /mL in 5mL. For proliferation, MDSCs were pre-cultured for 15 min with 10µM CT, CIM, or alone, before histamine addition. Cell concentrations were 50,000 cells/well in a 96-well plate. After 48 h, a 24-hour pulse of

[H3]-thymidine, 1 mCi/mL (Perkin Elmer, Waltham, MA, USA), was used. Plates were harvested using a Filtermate cell harvester onto GF/C plates and read using a TopCount plate counter (Perkin Elmer).

2.2.9 Adoptive immunotherapy of B16 melanoma

T cells were prepared for adoptive immunotherapy (AIT), as previously described³⁰³. Recipient mice were injected *i.v.* with 0.25×10^6 B16 cells. One day prior to AIT, mice were treated *i.p.* with 2 mg cyclophosphamide (CYP) and 1.2 mg gemcitabine (GEM) and were treated every 5 days with GEM only.

2.2.10 PCR and quantitative PCR

PCR

Genotyping and PCR were run as described in section 1.2.2. Primers are listed in **Table 4**.

qPCR

MDSCs were isolated, as described previously, and cultured with 100 μ M histamine for 24 hours. Total RNA was extracted using TRIzol reagent (Invitrogen Life Technologies, Grand Island, NY, USA). RNA (400 ng/l) was reverse-transcribed using the iScript cDNA synthesis kit (Bio-Rad, Hercules, CA, USA). Primers for running an iQ SYBR Green Supermix (Bio-Rad) qPCR assay were purchased from Integrated DNA Technologies (Coralville, IA, USA). Probes were purchased from Applied Biosystems (Life Technologies, Grand Island, NY, USA) Primers and Probes are as listed in **Table 4**. Results were analyzed with Bio-Rad iQ5 Real-Time PCR software (version 2.0). Fold variation was determined using $\Delta\Delta C_t$ method of analysis.

2.2.11 Flow cytometry

Sample preparation

Cell isolation and labeling were conducted as described previously in section 1.2.4 and 1.2.6.

Immunohistochemistry

Sample preparation and staining as in section 1.2.6

Antibodies

Antibodies are listed in **Table 5**.

Table 4. List of primers for PCR and qPCR

PCR	
ADAM10Tg Forward	5'-CCA ACA GTG TTA ATT CTG CTC C-3'
ADAM10Tg Reverse	5'-TTC TTT CAG CCA GAG TTG TGC G-3'
Cpa3-cre Forward	5'-CGA TGC AAC GAG TGA TGA GG-3'
Cpa3-cre Reverse	5'-GCA TTG CTG TCA CTT GGT CGT-3'
oIMR5147	5'-GCA GTA CAG GTT CAA GCC GAT G-3'
oIMR5148	5'-CTG AGA GTT GTA CCG GAC AA-3'
qPCR	
Arg1 Forward	5'-GAC CAC AGT CTG GCA GTT GG-3'
Arg1 Reverse	5'-TGG TTG TCA GGG GAG TGT TG-3'
iNOS Forward	5'-CAC CCC AAG TTC GAC TGG TT-3'
iNOS Reverse	5'-CTA AAG GGA CAG GCG CTG AA-3'
IL-13	Mm00434206
IL-4	Mm00445259
GAPDH	Mm99999915

Table 5. List of antibodies used for flow cytometry

Specificity	Clone	Label	Source
Mouse-Arg1	9819S	unlabeled	Cell Signaling
Mouse-HRH2	M-19	unlabeled	Santa Cruz
Mouse-HRH3	C-20	unlabeled	Santa Cruz
Mouse-HRH4	M-12	unlabeled	Santa Cruz
Mouse-Gr1	RB6-8C5	FITC, PE	Biolegend
Mouse-Ly6C	HK1.4	APC	Biolegend
Human-CD15	W6D3	PerCP/Cy5.5	Biolegend
Mouse-CD11b	M170	Pe/Cy7	Biolegend
Human-CD33	WM-53	Pe/Cy7	Biolegend
Mouse-HRH1	Polyclonal	Pe/Cy5	Bioss
Human-CD11b	ICRF44	APC	eBioscience
Human-CD14	61D3	PE	eBioscience
Mouse-Ly6G	1A8	FITC	BD Biosciences
Goat-IgG	Polyclonal	FITC	Santa Cruz
Rabbit-IgG	Poly 4064	Dylight 649	Biolegend
Human-CD34	561	FITC	Biolegend

2.2.12 *N. brasiliensis* infection, GEM treatment, CET treatment, CIM treatment, B16 melanoma or LLC injection, and AT of MDSCs

Eggs per gram of feces enumeration

N. brasiliensis larvae were generously provided by Joe Urban (Agriculture Research Station, Beltsville, MD) and were maintained as previously described³⁰⁴. Each experimental group of mice was infected with ~650 stage 3 larvae (L3) *N. brasiliensis*. Fecal egg burdens were enumerated on days 5–13. Fecal pellets were collected from mice and weighed. Fecal weight determined calculated amount of flotation solution (saturated sodium chloride solution in diH₂O) to be added. Feces were dissolved in 500μL diH₂O for approximately 30mins. Flotation solution was then added. [(Fecal weight (grams) x 60mLs)/1gram] - .5mL diH₂O = x mL flotation solution. Feces solution was then agitated by vortex for 5 seconds and 1mL was immediately removed and loaded in the chamber of a McMaster counting slide. Eggs within counting grid were enumerated three times per feces solution sample. Eggs per gram of feces (EPG) were calculated by averaging individual counts and multiplying by 400^{193,305}.

L4 and L5 enumeration

Groups of animals were euthanized on day 2 post-infection and lungs were removed. Lungs were cut with scissors into approximately 5mm pieces and immersed in 0.5% PBS agarose spread over cheesecloth and allowed to solidify. Cheesecloth bundles were hung in the top of 50mL conical tubes filled with 37°C PBS. Tubes were placed in a 37°C incubator for 4 hours. Lung worms were removed with a transfer pipette and enumerated from the bottom fraction of the PBS with a dissecting microscope.

Additional animals were euthanized on day 7 post-infection, and the proximal halves of

the small intestines were harvested. Intestinal pieces were cut into 1 cm sections, sliced longitudinally and opened to expose the inter lumen. Sections were placed lumen side down on cheese cloth. Cheese cloth bundles were suspended from tops of 50mL conical tubes filled with pre-warmed PBS. After incubation for four hours at 37°C, adult worms were removed from the bottom fraction of PBS and enumerated using a dissecting microscope.

Serum collection, drug administration, and AT of MDSCs

Serum was collected by tail vein nick, days 7 or 14 post-infection. Serum was collected by cardiac puncture at the termination of the experiment. For mice injected with GEM, 1.2 mg was injected *i.p.* starting on day 0 and repeated every 5 d throughout the experiment. For AT studies, WT mice were injected with $5\text{--}10 \times 10^6$ naive ADAM10Tg MDSCs via tail vein injection starting at day -1 of infection and repeated every 3 days thereafter. For mice treated with CT, 0.5 mg/kg was injected *i.p.*, starting on Day -1 and repeated daily. For mice injected with CIM, 20 mg/kg was injected *i.p.*, starting on Day -1 and repeated every 2 days.

B16 melanoma or LLC injection

For B16 melanoma or LLC, mice were injected *i.v.* with 250,000 cells, monitored daily, and killed after 3 weeks; lungs were harvested and weighed to determine degree of colonization. Or lung nodules were counted, as previously described^{303,306}; if too many to count, they were assigned a count of 250. For LLC, at the termination of the experiment, lungs were filled by tracheal perfusion with 5% India ink solution and then removed and fixed in Feketes buffer.

2.2.13 Human MDSCs

Human studies were conducted under appropriate Institutional Review Board-approved protocols. All patients gave informed consent for this research. Blood (20 mL) was collected in EDTA-coated vacuum tubes from allergic patients, identified as symptomatic or non-allergic controls, and PBMC were isolated using Ficoll-Paque separation medium (GE Healthcare, Buckinghamshire, UK).

2.2.14 Statistical analysis

P values were calculated using unpaired two-tailed Student's t-tests or unpaired Mann-Whitney analysis in GraphPad Prism v5. Error bars represent the SEM or SD between samples as noted in figure legends. $P < 0.05$ is considered statistically significant.

Chapter 3: Results

2.3.1 Mast Cells critically augment MDSC activity

MDSCs from ADAM10Tg mice are phenotypically and functionally analogous to tumor-induced MDSCs

Although MDSC accumulation is a byproduct of ADAM10 overexpression in early hematopoietic progenitors, ADAM10 expression is not altered in these cells²⁴⁷. To ascertain whether ADAM10Tg-derived MDSCs are functional, *ex vivo* T cell suppression assays were performed. ADAM10Tg MDSCs inhibited T cell proliferation of both ADAM10Tg and WT purified T cells under polyclonal (**Figure 15A,B**) and Ag-specific (**Figure 15C**) conditions in a manner parallel to tumor-derived MDSCs (**Figure 15D**). Tumor-derived MDSCs can be divided into granulocytic (CD11b⁺Ly6G^{high}) and more immunosuppressive monocytic (CD11b⁺Ly6C^{high}) subsets³⁰⁷. Accordingly, monocytic MDSCs possessed more suppressive potential. Furthermore, similar to T cells from tumor-bearing hosts, ADAM10Tg T cells exhibited reduced levels of L-selectin (CD-62L), a receptor required for homing of naive T cells to the LNs (**Figure 15E, F**)¹⁹⁸. MDSCs impair the T cell response through the activity of arginase 1 and inducible NO synthase. Accordingly, ADAM10Tg MDSCs had levels of these enzymes that were comparable to tumor-derived MDSCs (**Figure 15G,H**)¹⁹¹. These *ex vivo* observations indicate that MDSCs present in tumor-free ADAM10Tg animals behave similarly to tumor-derived MDSCs.

Monocytic MDSCs promote B16 metastasis

We used the B16 melanoma model to examine *in vivo* activities of MDSCs from ADAM10Tg mice. B16 was injected *i.v.*; although not a true metastasis, this allows comparison of tumor colonization into the lung with and without MDSCs and is commonly used to assess AIT³⁰³. When challenged with B16, ADAM10Tg animals were more susceptible to metastasis than were WT controls (**Figure 16A**). The ADAM10Tg animals had tumor nodules that were too numerous to count and were consequently assigned a count of 250. Parallel to the *ex vivo* assay, the suppressive activity of MDSCs was attributed to the monocytic population. When WT mice were challenged with B16 and AT of either monocytic or granulocytic MDSCs, melanoma metastasized more aggressively in mice given the monocytic subset, and granulocytic MDSCs had no effect (**Figure 17A**). AIT exerted a minimal effect on ADAM10Tg mice, suggesting that the presence of MDSCs diminished the activity of adoptively transferred T cells. Although AIT treatment did not completely abolish metastasis in WT lungs, it induced a significant decrease in metastatic lesions. Given that lympho-depleting chemotherapy is known to enhance AIT³⁰⁸, the protocol was modified to incorporate CYP and GEM. CYP lympho-depletes recipient mice, permitting homeostatic proliferation of transferred T cells; GEM preferentially decreases MDSC levels in tumor-bearing mice^{309,310}. CYP and GEM alone and in combination in WT mice did not significantly alter metastasis, indicating that they have minimal effects on tumor cells (**Figure 17C**). However, GEM selectively diminished the MDSC population in ADAM10Tg mice without affecting lymphocyte levels (**Figure 17B**). ADAM10Tg mice treated with GEM alone exhibited an antitumor response comparable to WT counterparts, demonstrating that T cell function

is restored upon MDSC depletion (**Figure 16B,C**). Additionally, the combination of GEM, CYP, and AIT (tri-therapy) resulted in complete regression of metastasis in both WT and ADAM10Tgs (**Fig. 16B, C**). **Figure 16D** illustrates the significant abrogation of metastasis arising from tri-therapy. Ideal AIT would use tumor-specific T cells and chemotherapy. Thus, the AIT protocol was adjusted to incorporate pmel-1 mice that are TCR transgenic for gp100 melanoma peptide³⁰³. Similar results were observed, in that successful AIT required MDSC depletion (**Figure 17C**). Thus, MDSCs in ADAM10Tg mice are functionally analogous to tumor-derived MDSCs, promote tumor metastasis, and compromise the efficacy of tumor immunotherapy.

Figure 15. MDSCs from ADAM10Tg mice are phenotypically and functionally analogous to tumor-derived MDSCs.

(A) Proliferation of WT and ADAM10Tg (B) T cells or (C) pmel-1 TCR transgenic splenocytes in the presence of increasing amounts of CD11b⁺ MDSCs (Ly6G⁺ (dotted line), Ly6G⁻ (dashed line), or Gr-1⁺ (solid line)); WT and ADAM10Tg T cells were stimulated with immobilized anti-CD3 and soluble anti-CD28. (D) Tumor-derived MDSCs were purified from LLC bearing mice and used in suppression assays with Pmel1 splenocytes at increasing ratios (T cells or splenocytes: MDSCs, *p<0.05). All Pmel-1 splenocytes were stimulated with soluble gp100. (E) Cell surface expression of L-selectin (CD62L) by CD4⁺ and CD8⁺ (Isotype control (grey filled), WT (solid line) and ADAM10Tg (dashed line) (F) gated T cells from peripheral LNs. Lysates of MDSCs derived from LLC bearing WT hosts and ADAM10Tg MDSCs were analyzed for the activity of (G) Arginase by urea production and (H) Nitric oxide by Greiss Reagent. The data is representative of at least three independent experiments with splenocytes from three or more mice.

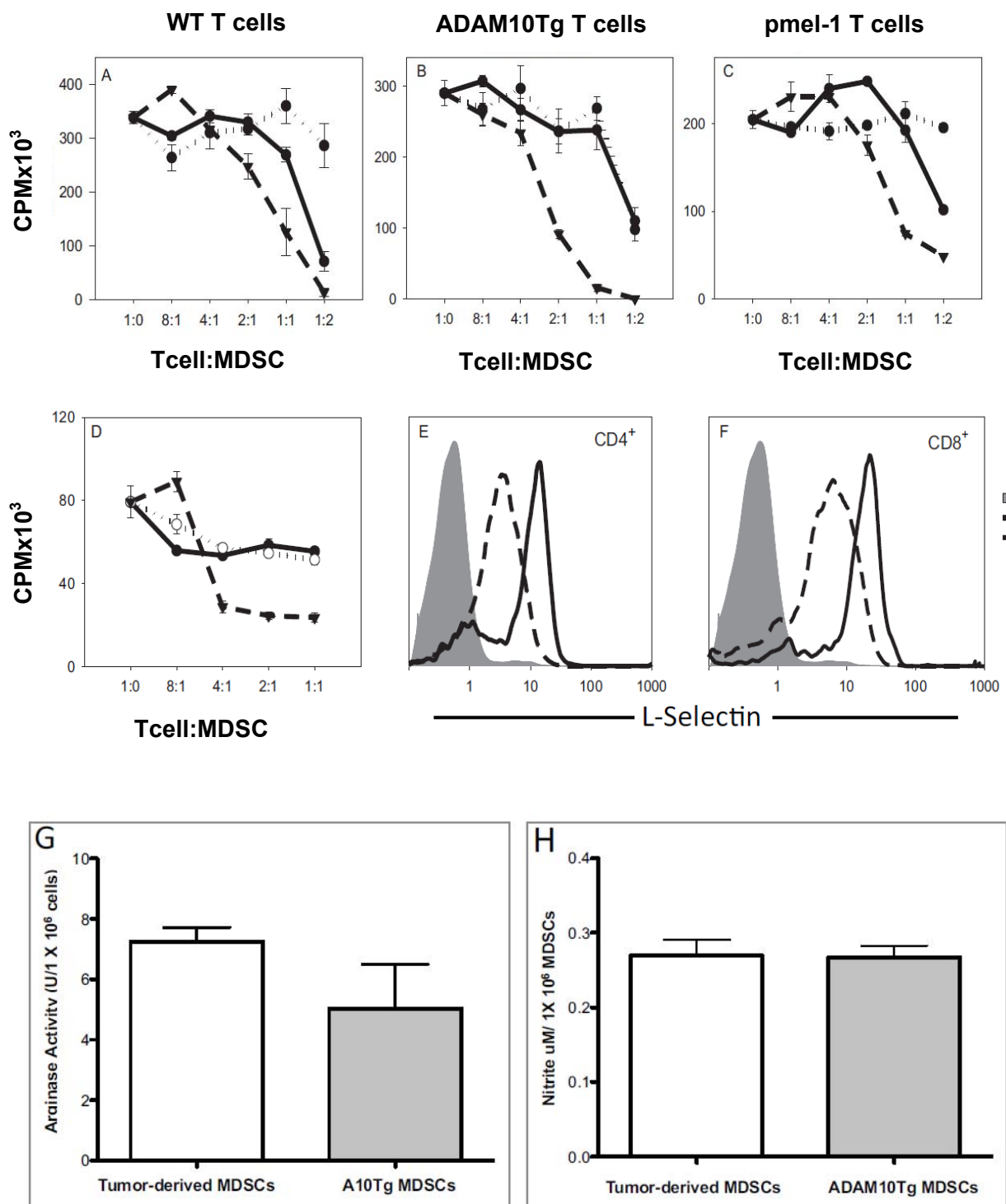


Figure 16. MDSC depletion restores the antitumor response and prevents metastatic progression of B16 melanoma in ADAM10Tg mice

(A) Number of lung metastases in WT and ADAM10Tg animals challenged with B16

melanoma with (filled bars) or without (open bars) AIT (A), as described in Materials and

Methods. Number of lung metastases of WT (B) or ADAM10Tg (C) mice challenged

with B16 and treated as in (A), with the addition of CYP (C) and GEM (G). (D)

Representative lungs of WT and ADAM10Tg mice with AIT, with and without CYP and

GEM. Data represent five mice/group. * $p < 0.05$ versus respective untreated controls.

ND, None detected.

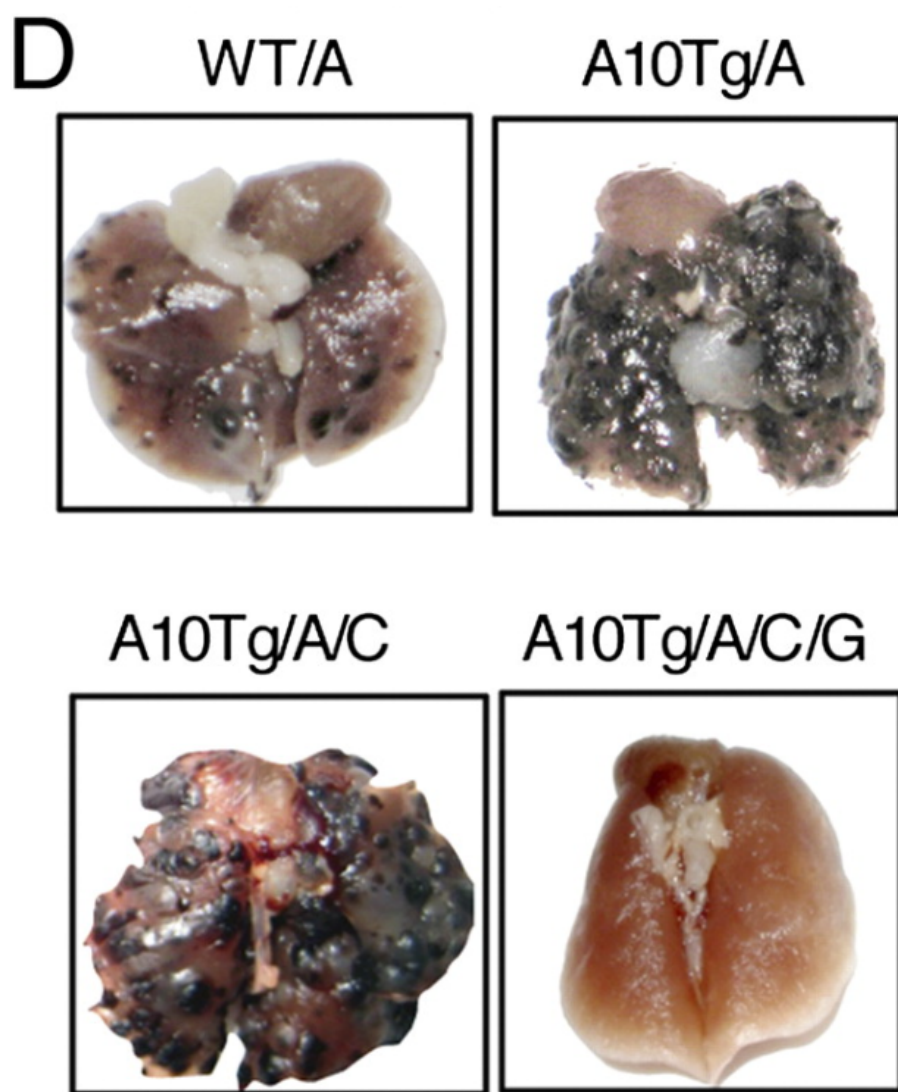
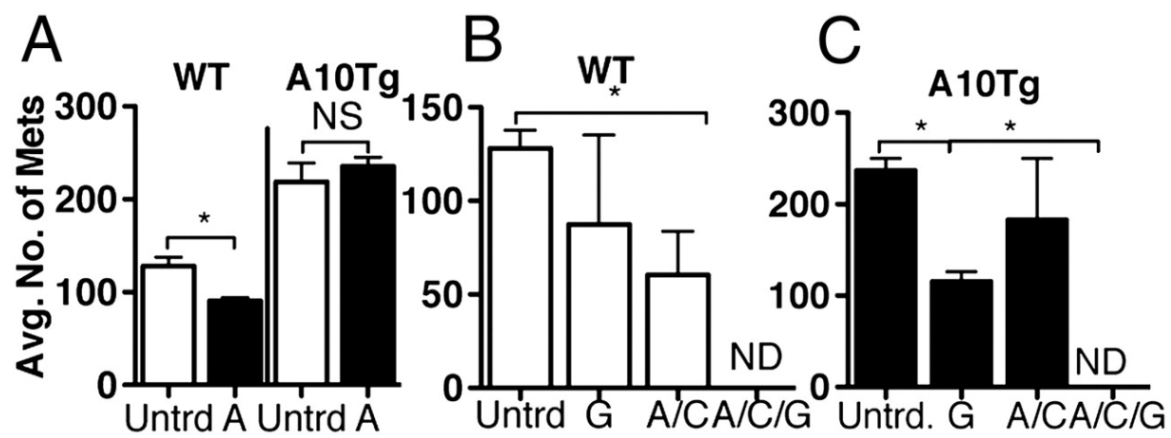
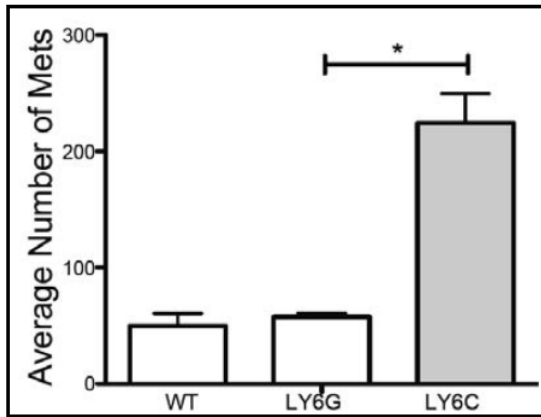


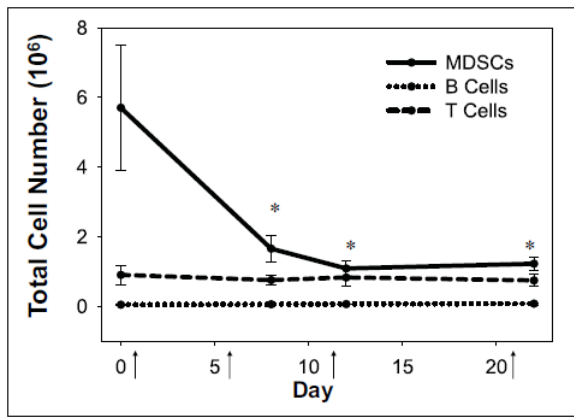
Figure 17. Gemcitabine selectively depletes MDSCs, which allows for effective AIT with tumor specific T cells

(A) Quantification of B16 lung metastasis in WTC57 with AT of either granulocytic (CD11b⁺Ly6G⁺) or monocytic (CD11b⁺Ly6C⁺) MDSCs. (B) Cytometric analysis of peripheral blood leukocyte levels in ADAM10Tg mice following *i.p.* injections with gemcitabine (upward arrow) every five days for three weeks, * $p < 0.05$. (C) Number of B16 lung metastases in mice treated with AIT comprised of pmel-1 transgenic T cells and chemotherapeutics as described in Methods. More than five mice were used per group in three independent experiments. * $p < 0.05$ in comparison to respective untreated controls and # $p < 0.05$ in comparison to respective AIT+ CYP treatment.

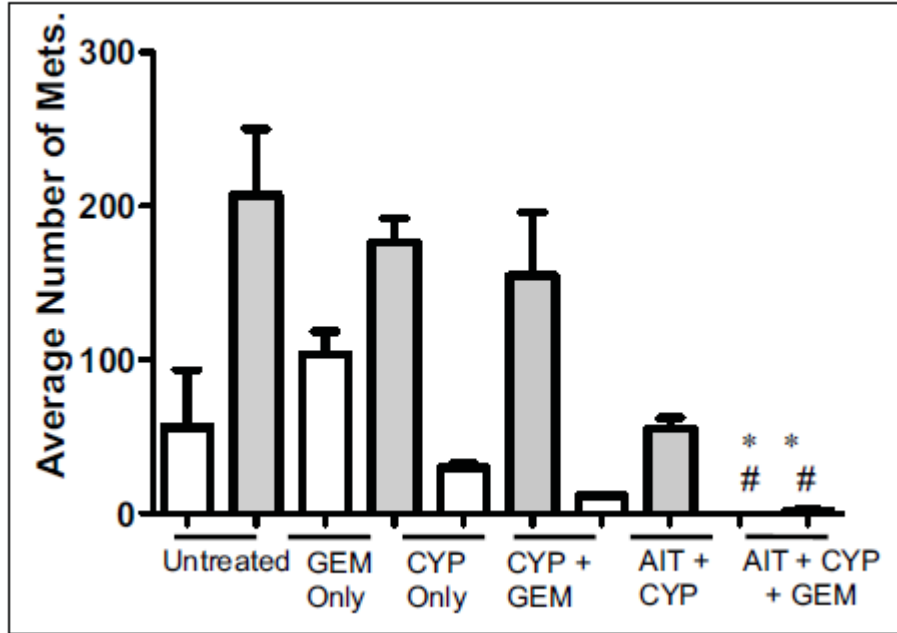
A



B



C



MDSCs enhance the immune response against N. brasiliensis

Next, we examined the effect of MDSCs on the immune response in anti-parasite immunity. Although MDSC accumulation following *N. brasiliensis* infection has been reported²⁶¹, the direct immunomodulatory role of MDSCs in anti-*N. brasiliensis* responses has not been examined. In *N. brasiliensis* infection, a WT response is characterized by production of Th2-associated cytokines that ultimately mediate adult worm clearance 10–12 d post-inoculation³¹¹. Following *N. brasiliensis* challenge, ADAM10Tg animals had significantly reduced fecal egg counts compared with WT controls (**Figure 18A**). This is highly correlated with 50% reduction in L5 adult worm burden in ADAM10Tgs (**Figure 18B**) and a 25% reduction in L4 stage worms in the lung (**Figure 18C**). This indicated that MDSCs may facilitate parasite clearance. To determine whether the increased worm clearance correlated with an increase in Th2 cytokines, we examined a panel of Th2 cytokines. Analysis of peak infection (day 7) serum levels of IL-4, IL-5, and IL-13 demonstrated significantly enhanced levels in *N. brasiliensis*-infected ADAM10Tg animals compared with infected littermates (**Figure 19**). Additionally, IL-17 and IL-33, which were reported to recruit MDSCs, were also elevated in serum of ADAM10Tg mice^{271,312}. On Day 14, mesenteric lymph nodes (MLN) were taken from *N. brasiliensis* infected ADAM10Tg mice and LM controls. These nodes were stained for Gr-1 to elucidate location of MDSCs (**Figure 20**).

To determine whether enhanced *N. brasiliensis* clearance is dependent on MDSC activity, MDSCs were depleted from ADAM10Tg mice. GEM treatment resulted in elevated egg counts in ADAM10Tg mice similar to WT levels (**Figure 21A**). Additionally, *N. brasiliensis* infection resulted in a modest 4–5-fold increase in MDSCs in

WT spleens from days 0 to 14. This level of WT MDSCs is sufficient to promote *N. brasiliensis* clearance and prevent a chronic infection (**Figure 21B**). However, GEM-mediated MDSC depletion in WT mice significantly exacerbated the peak level of *N. brasiliensis* infection (**Figure 21C**). We additionally examined the intestines of mice treated with GEM to confirm that off-target effects were not responsible for results seen. MCs are an important mediator of *N. brasiliensis* clearance and MCs per villus/crypt unit were not adversely affected with GEM treatment (**Figure 21D**). Taken together, the data indicate that the enhanced immune response in ADAM10Tg is a consequence of elevated MDSC levels.

Next, to eliminate off-target effects of GEM, ADAM10Tg MDSCs were purified and adoptively transferred to WT mice over the course of *N. brasiliensis* infection. Like the MDSCs that were observed accumulating following *N. brasiliensis* infection, the transferred MDSCs also contained both Ly-6G⁺ and Ly6C⁺ populations. AT of MDSCs resulted in significantly reduced egg counts, comparable to ADAM10Tgs (**Figure 22A**). Additionally L5 adult worms were reduced, but L4 lung worms were not (**Figure 22B,C**). This indicates that AT MDSCs do not reach the level needed to decrease lung worms by Day2. To confirm our findings with MDSCs were not only a result of ADAM10Tg MDSCs, MDSCs were harvested from spleens and tumors of LLC-bearing mice and injected *i.v.* into WT mice during *N. brasiliensis* infection. Tumor derived MDSCs were able to additionally mediate *N. brasiliensis* clearance confirming that ADAM10Tg MDSCs are analogous to tumor-derived MDSCs (**Figure 22D**).

Granulocytic MDSCs mediate N. brasiliensis clearance in a T cell-independent fashion

To determine which MDSC subset was responsible for this observation, MDSCs were purified based upon Ly6G and Ly6C expression and adoptively transferred into WT *N. brasiliensis*-infected mice. The Ly6G^{high} population had the same effect as did total Gr-1⁺-purified MDSCs, whereas the adoptively transferred Ly6C^{high} population had no effect. This indicates that the granulocytic population of MDSCs mediates the anti-*N. brasiliensis* immunity (**Figure 23A**). The direct role of MDSCs was further supported in WT mice that were T cell depleted. Flow cytometry confirmed T cell depletion (**Figure 24**). These mice exhibited the same rapid rate of clearance as WT adoptively transferred with MDSCs (**Figure 23B**). As expected, *N. brasiliensis* clearance was significantly slower in T cell-depleted WT mice without AT of MDSCs (**Figure 23B**) and chronic, unresolved infection was evident by L5 adult worms on Day 14 (**Figure 23C**).

Mast Cells are essential for MDSC-mediated parasitic clearance

Mucosal MC hyperplasia is a hallmark of gastrointestinal helminth infection that enhances the immune response, leading to parasite clearance^{277,313}. Mice deficient in MCs exhibit delayed clearance kinetics³¹⁴. Given that MCs mainly produce Th2-polarizing and proinflammatory cytokines and that MCs chemoattract MDSCs, we examined whether the interaction between the two cell types could be contributing to the enhanced *N. brasiliensis* expulsion. Surprisingly, AT of MDSCs into MC-deficient mice did not enhance *N. brasiliensis* expulsion, indicating that an MDSC/MC interaction is critical for MDSC-mediated anti-*N. brasiliensis* responses (**Figure 26A-C**). To confirm that this was not unique to Kit^{Wsh/Wsh} mice, which have other hematopoietic issues, two studies were done. Kit^{Wsh/Wsh} mice, which were reconstituted with WT BMDCs, responded to AT of MDSC with enhanced parasite clearance (**Figure 26C**). In

addition, another strain of MC-deficient mice, Cpa3cre; Mcl-1^{fl/fl} (C57BL/6 background) was tested. These mice express Cre recombinase under the control of the Cpa3 promoter. C57BL/6-Cpa3cre; Mcl-1^{fl/fl} mice are severely deficient in MCs and basophils with no other apparent hematologic changes³⁰². Similar to Kit^{Wsh/Wsh} mice, AT of MDSCs also failed to clear *N. brasiliensis* in the Cpa3cre; Mcl-1fl/fl mice. These studies further confirm that MCs are required for MDSC-mediated parasite clearance (**Figure 26D**). To assess this interaction *ex vivo*, MCs were co-cultured with MDSCs. This resulted in a synergistic increase in IL-6, IL-13, TNFα, and MIP-1α (**Figure 27**).

MCs also contribute to MDSC-mediated immune suppression in B16 melanoma

Given that MDSCs require MCs to enhance anti-*N. brasiliensis* immunity, the B16 metastasis study was re-evaluated in MC-deficient mice. Several groups demonstrated that MCs recruit MDSCs, which accumulate in the tumor microenvironment and correlate with poor prognosis. In addition, MC-deficient mice have decreased rates of tumor growth that increases to WT levels subsequent to MC reconstitution³¹⁵. Therefore, we anticipated that B16 melanoma cells would metastasize more slowly in Kit^{Wsh/Wsh} mice compared with WT controls, but it would be enhanced with MDSC AT. Kit^{Wsh/Wsh} and WT mice were injected with B16, with and without AT of MDSCs. WT mice were more susceptible to B16 metastasis compared with Kit^{Wsh/Wsh} mice. Upon MDSC AT, WT mice exhibited similar levels of tumor nodules as did B16 ADAM10Tgs, indicating the direct contribution of MDSCs to the immune response. However, much to our surprise, AT of MDSCs into Kit^{Wsh/Wsh} mice failed to increase B16 metastasis (**Figure 28**). Thus, these results demonstrate that MDSCs promote B16 melanoma

metastasis in an MC-dependent manner and indicate that MDSC/MC interactions significantly enhance the MDSC-mediated suppression of antitumor immunity.

MCs promote MDSC trafficking and parasite clearance

Given the literature highlighting MCs as attractants of MDSCs and the importance of MDSC recruitment in an immune response, the trafficking behavior of MDSCs was analyzed after AT in the presence or absence of MCs. MDSCs were labeled with the PKH26GL lipid dye and AT by *i.v.* injection into naïve mice. As shown in **Figure 29A and B**, 18 h post-AT, MDSCs preferentially trafficked to the liver; this agrees with other published results³¹⁶. To determine whether MDSCs exhibit similar trafficking patterns during the course of *N. brasiliensis* infection, MDSCs were labeled and infused concomitant with *N. brasiliensis* challenge in WT and MC-deficient Kit^{Wsh/Wsh} mice. As with naïve mice, MDSCs trafficked to liver in infected WT mice. However, the accumulation of MDSCs in the liver was reduced significantly in Kit^{Wsh/Wsh} mice, indicating the role of MCs in MDSC recruitment (**Figure 29C–E**). The PKH26GL dye used for labeling does not affect MDSC functionality, as labeled cells were fully capable of reducing parasite egg burden in the feces (**Figure 30**). Livers of Kit^{Wsh/Wsh} mice on Day7 post *N. brasiliensis* infection were sectioned and stained for Gr-1 expressing MDSCs. The immunohistochemistry reinforces finding of reduced migration MDSCs to the liver (**Figure 31**). These results were supported by *in vitro* migration assays, in which MDSCs exhibited a high degree of migration toward MCs (**Figure 32**). This is consistent with published literature, indicating that MDSCs traffic to the liver in tumor models and that MCs secrete mediators from the liver through the bile³¹⁷.

We next wanted to see if MDSC accumulation and migration to the liver are MC-dependent during tumor development. A model of B16 melanoma metastasis was used. In B16 melanoma, WT lung colonization is exacerbated with the AT of MDSCs. While in Cpa3cre; Mcl-1^{fl/fl} MC-deficient mice, AT of MDSCs did not cause increased lung colonization, confirming previous data published with the Kit^{Wsh/Wsh} mice (**Figure 33A**)¹⁹³. Additionally, MDSCs are reduced in liver but not in spleen over WT mice, with or without AT of MDSCs (**Figure 33B**).

MDSC interaction with MCs maintains the granulocytic population in vitro.

Since MCs are required for MDSC effects *in vivo*, we wanted to look at MC/MDSC co-cultures *in vitro*. We cultured MDSCs for five days in culture with and without MCs in media supplemented for MC growth, then looked at the subpopulations of MDSCs. Without MCs, the granulocytic MDSC population does not survive *in vitro*. However, in the presence of MCs, the granulocytic MDSC population is maintained *in vitro* (**Figure 34**).

Figure 18. ADAM10Tg mice are resistant to *N. brasiliensis* infection

(A) Eggs per gram of feces (EPG) were determined at the indicated times in WT and

ADAM10Tg mice upon infection with 650 *N. brasiliensis* L3 worms. (B) WT and

ADAM10Tg mice were examined on day seven for adult worm recovery and (C) on day

two for L4 lung larval stage as described in Materials and Methods. . * $p < 0.05$;

** $p < 0.005$. Error bars are \pm SEM. Data represents five mice per group.

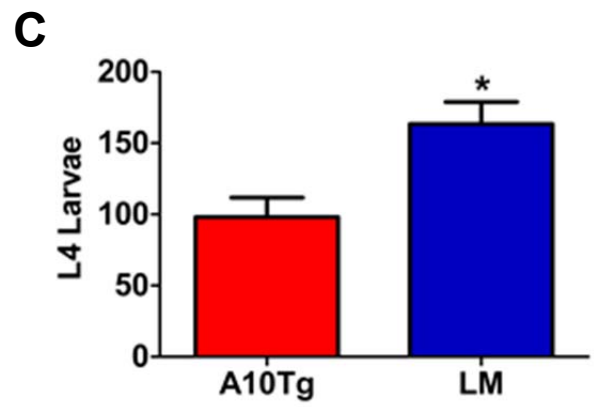
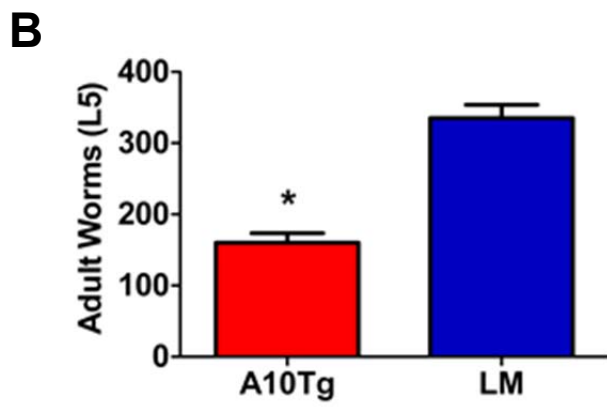
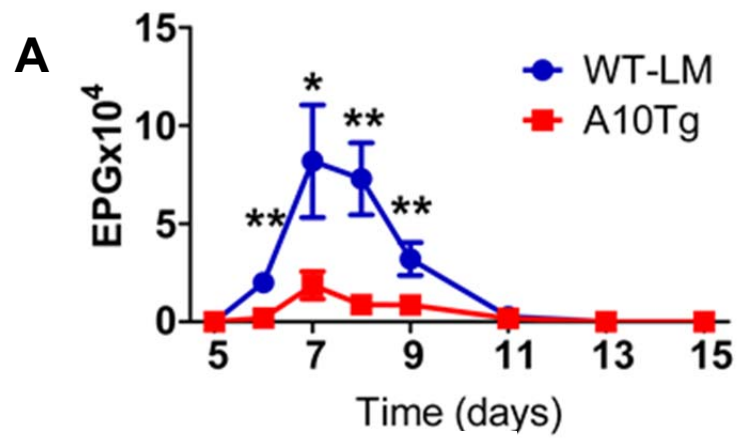


Figure 19. ADAM10Tg MDSCs have increased cytokine expression over WT during *N. brasiliensis* infection.

Day 7 serum from ADAM10Tg or WT mice infected with *N. brasiliensis*. Cytokine

analysis on serum was performed using a Milliplex Mouse Cytokine Kit. * $p < 0.05$. Error

bars are \pm SEM. Data represents five mice per group.

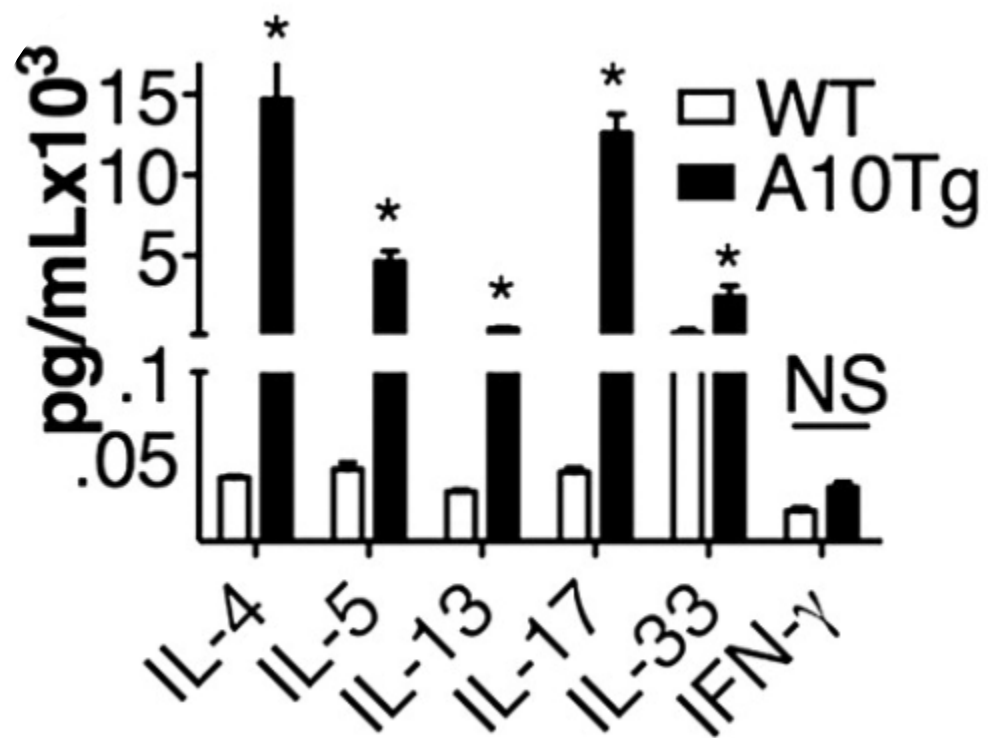


Figure 20. MDSCs accumulate in mesenteric lymph nodes in *N. brasiliensis* infection

MLNs were harvested from WT or ADAM10Tg mice on Day 14 post *N. brasiliensis* infection. MLNs were sectioned and stained with anti-Gr1 (blue) and anti-CD3 (red).

Pictures are representative of 5 mice per group.

WT

ADAM10Tg

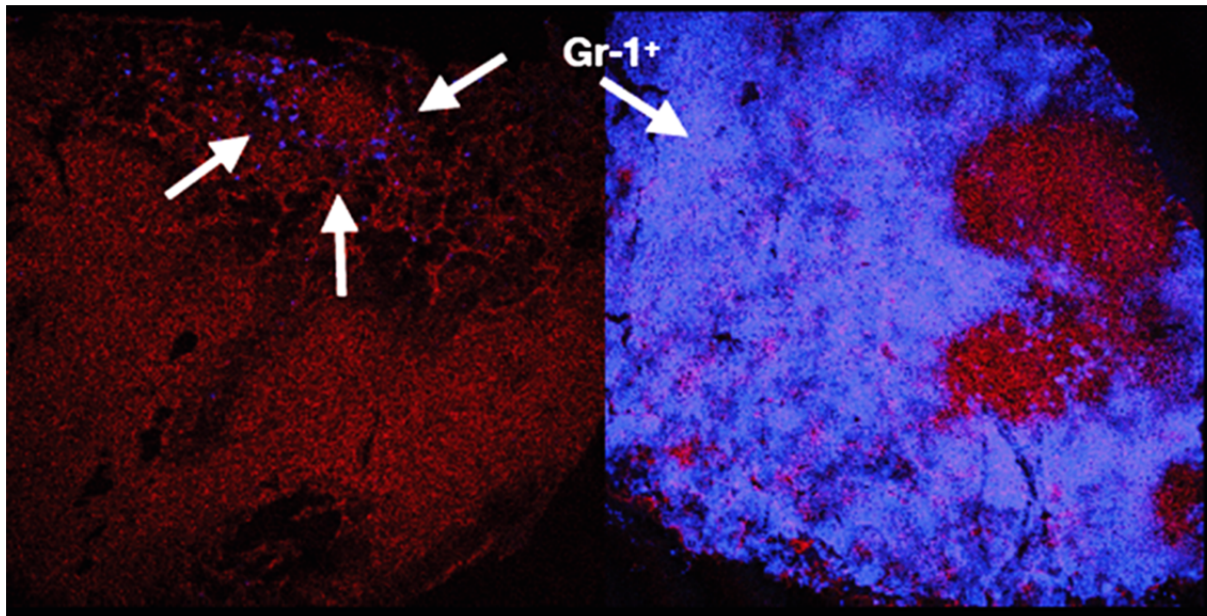


Figure 21. Gemcitabine depletion of MDSCs restores WT response to *N. brasiliensis* infection to ADAM10Tg mice.

(A) ADAM10Tg mice were treated with GEM during *N. brasiliensis* infection. EPG were enumerated. Data represents at least five mice per group and two independent experiments. (B) Spleens of mice were harvested at day 14 post *N. brasiliensis* infection and percent Gr-1+CD11b+ MDSCs were gated off of total live cells. Plots are representative of five mice per group. (C) WT mice were treated with GEM during *N. brasiliensis* infection. EPG were enumerated. (D) Day 15 post infection, *N. brasiliensis* infected ADAM10Tg mice with or without GEM. Proximal half of the small intestines were stained with toluidine blue to enumerate mast cells. Mast cells from ten villus/crypt units (VCU) were counted per mouse. Data represents at least five mice per group.

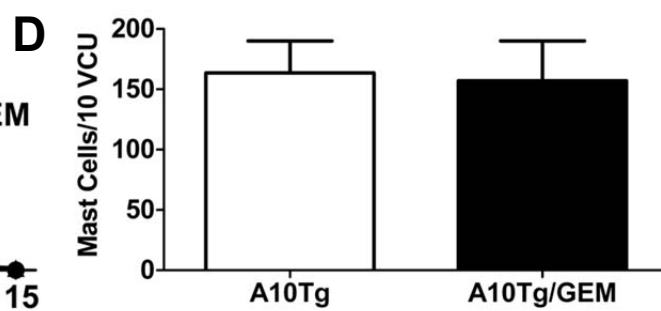
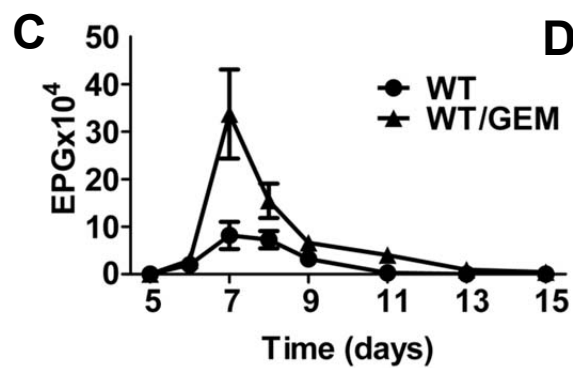
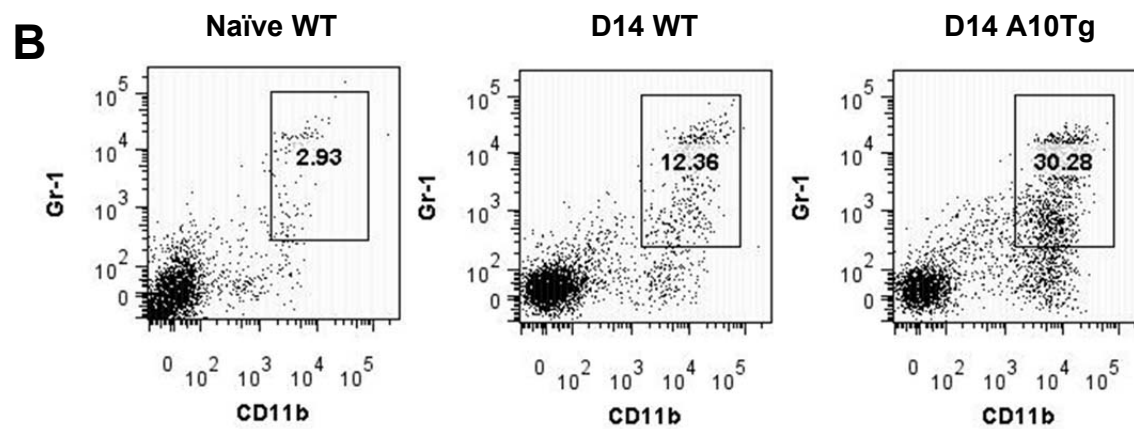
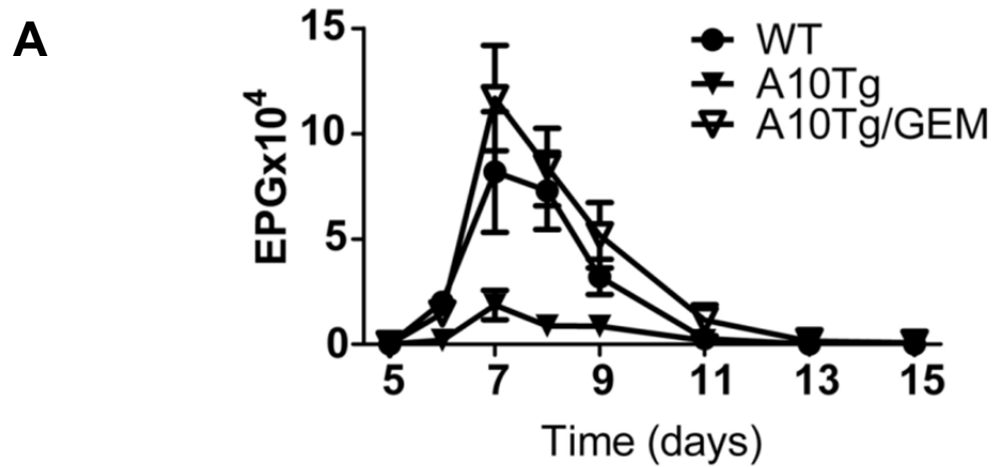


Figure 22. Adoptive transfer of MDSCs from ADAM10Tg mice or LLC-tumor bearing mice induce increased parasitic clearance of *N. brasiliensis*.

(A) EPG were determined at the indicated times in WT and WT mice with AT of

ADAM10Tg MDSCs upon infection with 650 *N. brasiliensis* L3 worms. (B) WT and WT

mice with AT of ADAM10Tg MDSCs examined on day seven for L5 adult worm recovery

or (C) L4 lung worm recovery. (D) EPG were determined at the indicated times in WT

and WT mice with AT MDSCs from LLC-tumor bearing mice. * $p < 0.05$, ** $p < 0.005$. Error

bars are representative of \pm SEM. Data represents at least five mice per group and at

least two independent experiments.

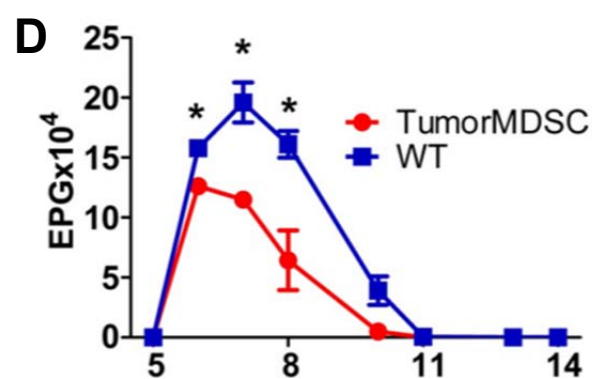
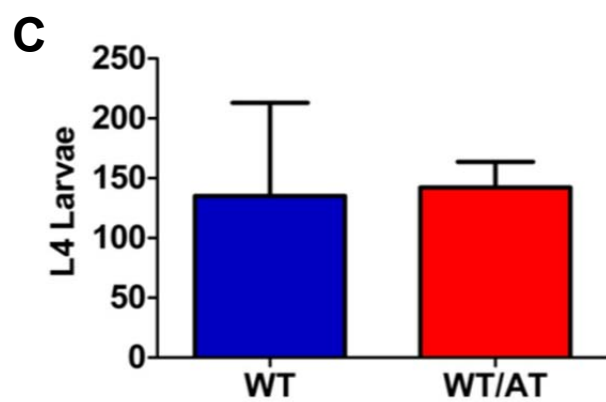
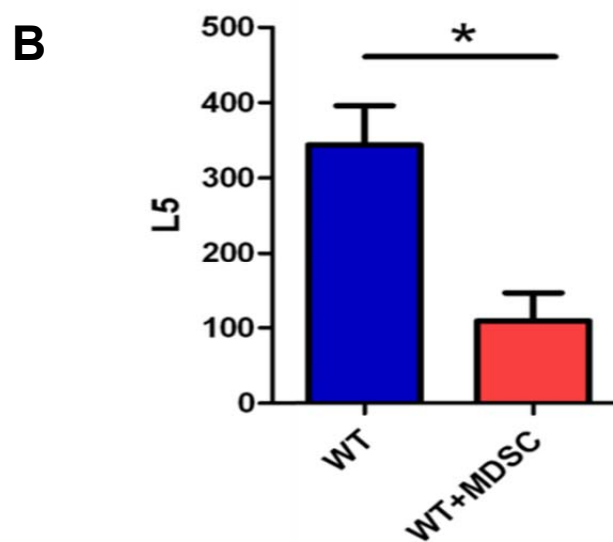
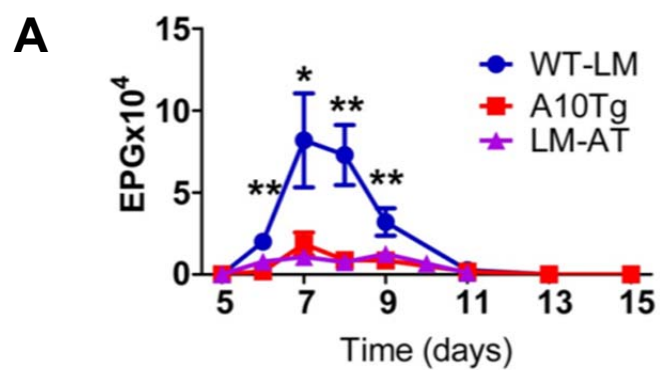


Figure 23. Granulocytic MDSCs are responsible for MDSC enhanced parasitic clearance in a T cell independent manner

(A) Enumerated EPG of infected WT mice with AT of either the CD11b⁺Ly6G^{high}Ly6C^{low} or CD11b⁺Ly6G^{low}Ly6C^{high} population of MDSCs. (B) EPG of WT mice, with or without MDSC AT, and with or without depletion of CD4 and CD8 T cells, as described in *Materials and Methods*. (C) In T cell depleted mice, L5 adult worms were enumerated on Day 14 to confirm clearance or chronic infection. . *p<0.05, **p<0.005. Error bars are representative of \pm SEM. Data represents at least five mice per group.

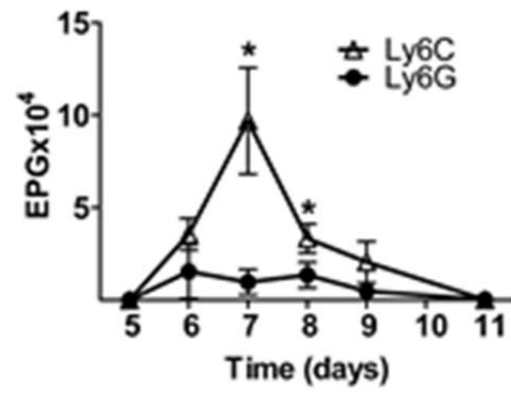
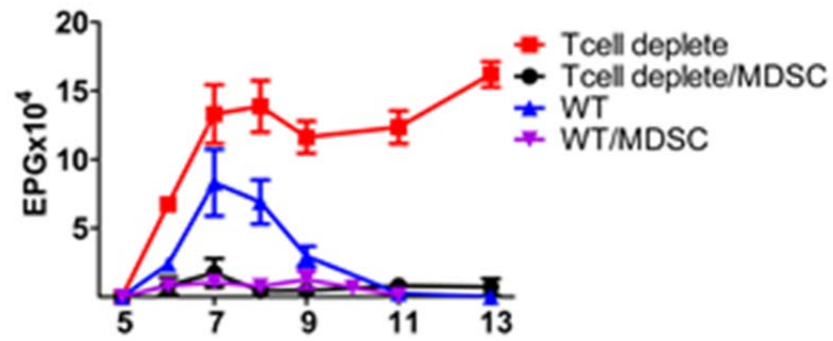
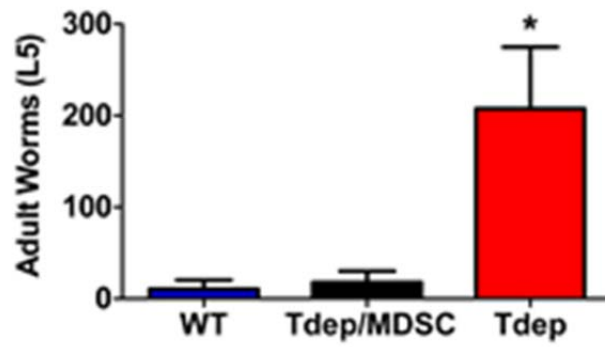
A**B****C**

Figure 24. T cell depleting antibodies completely deplete T cells.

Peripheral blood of WT and T cell depleted mice after injection with CD4 and CD8

depleting antibodies prior to *N. brasiliensis* infection for experiment in **Figure 23**. (A)

Percent positive for B220. (B) Percent positive for CD4. (C) Percent positive for CD8.

Flow cytometry plots are representative of at least five mice per group.

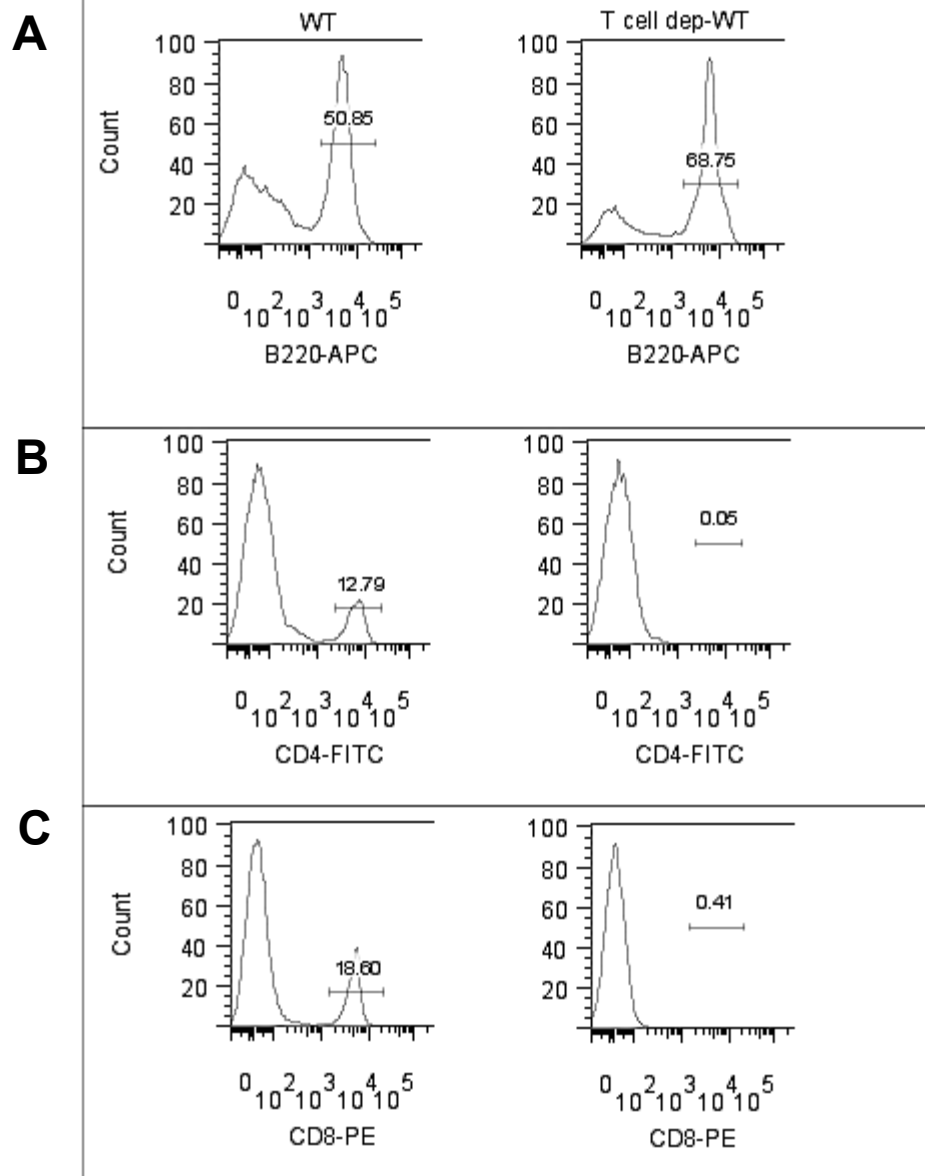


Figure 25. Monocytic MDSCs promote B16 melanoma colonization to the lungs. Quantification of B16 lung metastasis in WT/C57 with AT of either granulocytic MDSCs (CD11b⁺Ly6G⁺) or monocytic MDSCs (CD11b⁺Ly6C⁺), as described in *Methods*. More than five mice were used per group in three independent experiments. *p<0.05 in comparison to respective granulocytic MDSC group.

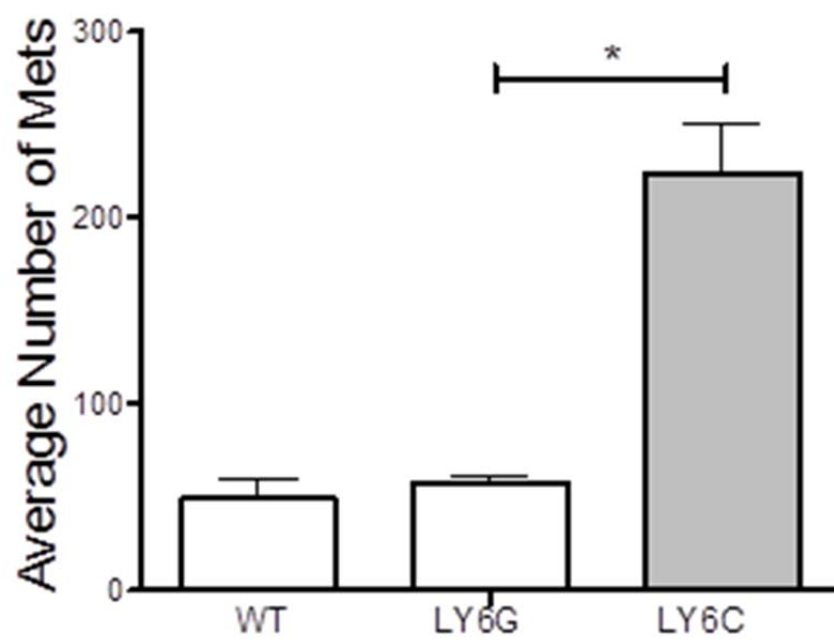


Figure 26. MCs are required for MDSC-mediated *N. brasiliensis* clearance

(A) Enumerated EPG on days noted of MC-deficient Kit^{Wsh/Wsh} mice, with or without MDSCs and infected with 650 *N. brasiliensis* L3 worms. (B) Adult worms enumerated on day 7. (C) Kit^{Wsh/Wsh} mice were reconstituted with BMDC as described in *Methods and Materials*. Reconstituted mice were AT with or without MDSCs and infected with *N. brasiliensis*. Significance refers to reconstituted Kit^{Wsh/Wsh} mice with AT of MDSCs as compared to Kit^{Wsh/Wsh} mice with AT of MDSCs. (D) MC-deficient Cpa3^{cre}, Mcl-1^{flox/flox} mice were infected with *N. brasiliensis*, with or without AT of MDSCs, and EPG were enumerated on noted days. The data represent at least five mice per group. *p< 0.05, **p< 0.005, ***p<0.005.

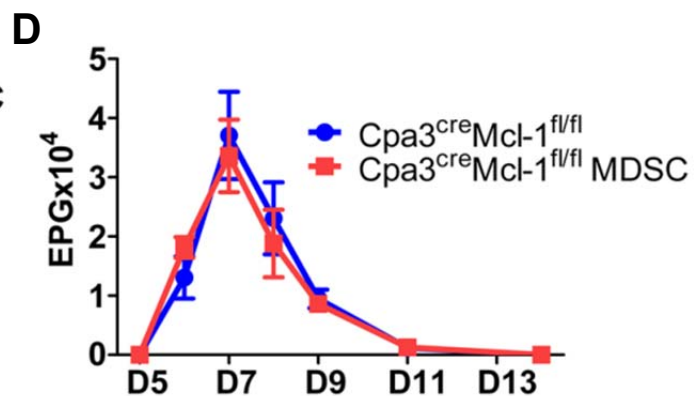
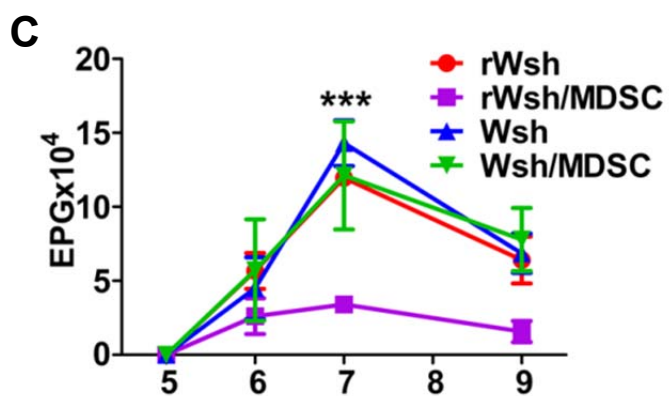
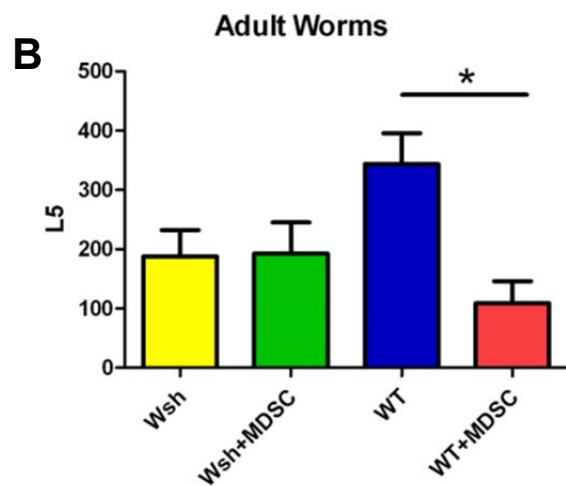
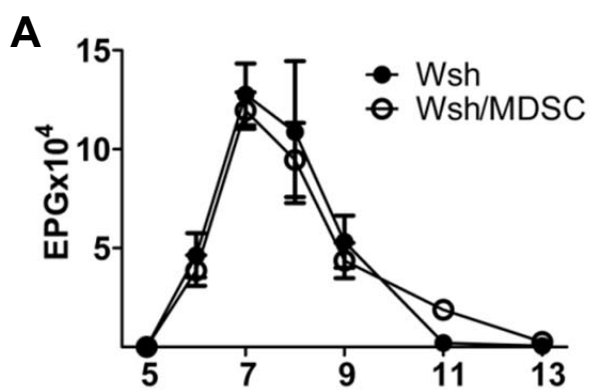


Figure 27. MC/MDSC interaction augments cytokine production.

BMMCs were co-cultured with ADAM10Tg MDSCs, as described in Materials and Methods. Supernatants were collected and analyzed for the production of IL-6 (A), IL-13 (B), MIP-1 α (C), and TNF α (D). The data represent pooled spleens of at least three mice/group. *p < 0.05 versus MCs alone. Figure courtesy of Johanna K. Morales and John J. Ryan, Virginia Commonwealth University, Richmond, VA, USA.

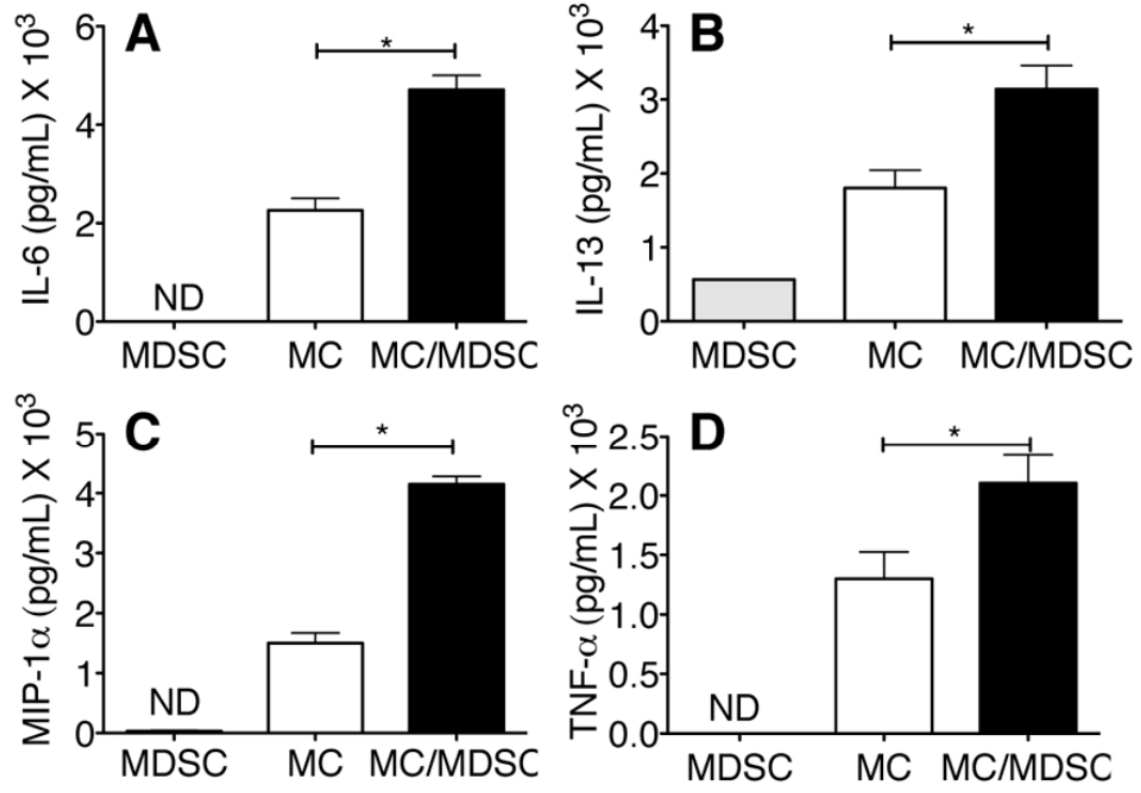


Figure 28. MC/MDSC interaction is required for MDSC-mediated immune suppression.

Photographic representation (A) and quantification (B) of B16 lung metastasis in control C57 and Kit^{Wsh/Wsh} mice, with and without AT of MDSCs. The data are representative of at least five mice/group. *p < 0.05 versus WT alone or Kit^{Wsh/Wsh} with MDSCs.

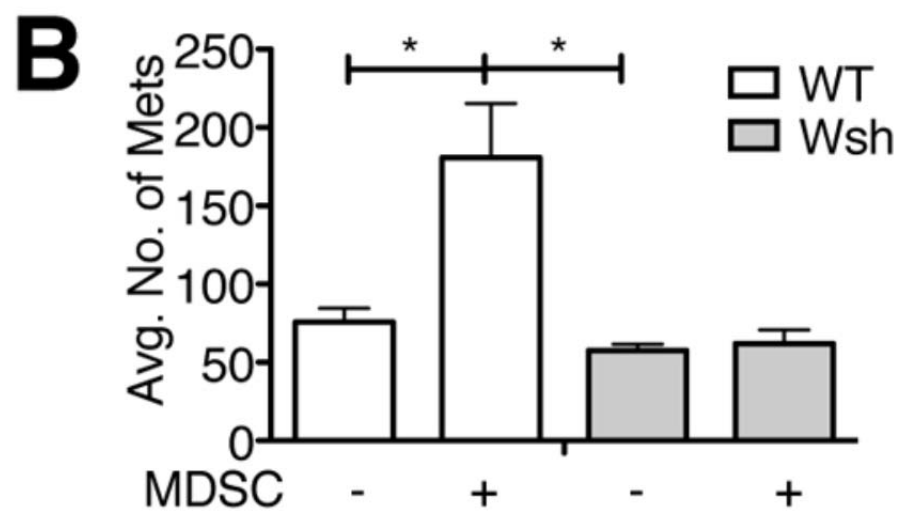
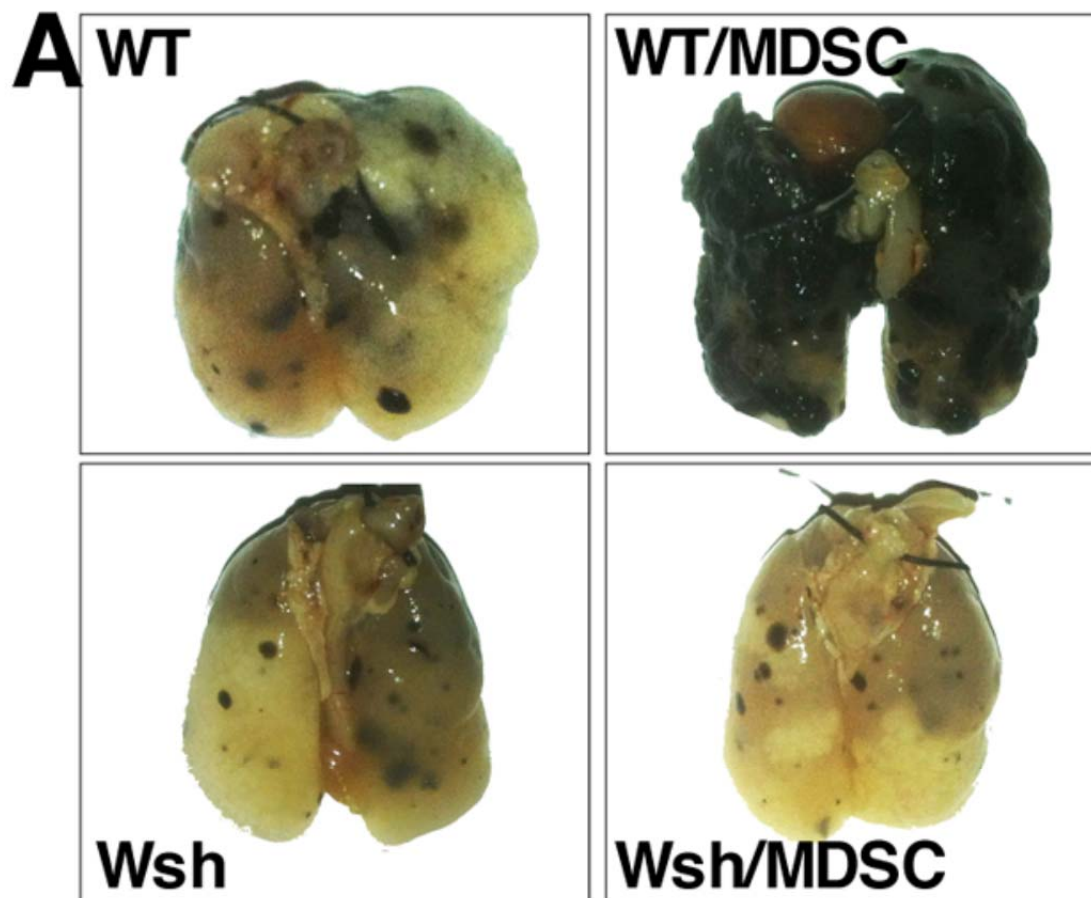


Figure 29. MDSCs preferentially migrate to the liver in a MC-dependent manner

(A) WT mice given labeled MDSCs, analyzed 18 hours later. MDSC in liver, peripheral blood (PB), spleen, and bone marrow (BM). Data compiled in B. (C) Wsh or WT was given labeled MDSCs, infected with *N. brasiliensis*, and examined for MDSC staining on Day 7. Cell percentage of PKH26GL⁺ cells out of total Gr1⁺CD11b⁺ cells (D) and number (E) from C. (F). MDSCs were given on Days -1, 2, and 5. *P<0.05;

***P<0.0005. Mean ± SD; n=5/group.

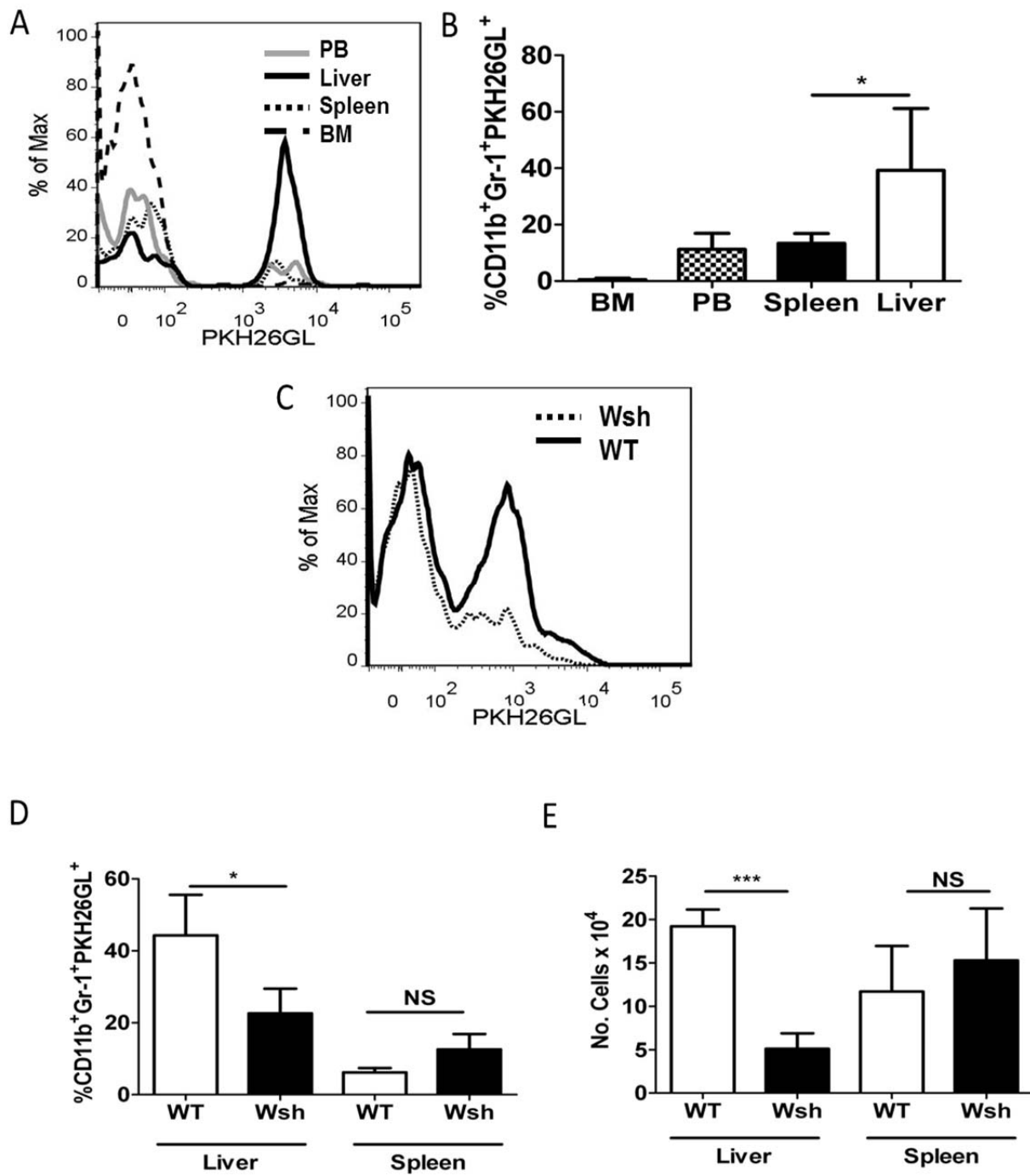


Figure 30. PKH26GL⁺ MDSCs are functional

WT mice with or without AT of labeled MDSCs on Days -1, 2 and 5. Mice infected with *N. brasiliensis* and examined for EPG on Day 7. *P<0.05. Mean \pm SD; n=5 mice/group.

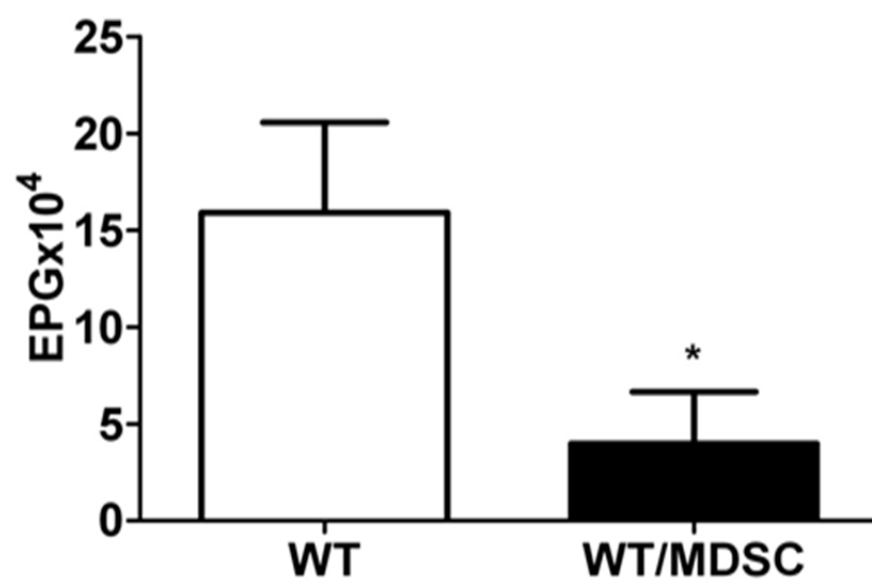


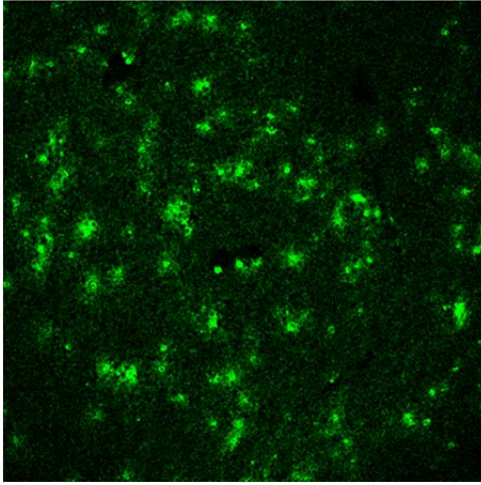
Figure 31. MDSCs do not traffic to livers of MC-deficient mice during *N. brasiliensis* infection

WT or Wsh mice with AT of MDSCs on Days -1, 2, and 5 were infected with *N.*

brasiliensis on Day 0. Livers were sectioned and stained with Gr-1⁺ (green) MDSCs.

Pictures are representative of five mice per group.

WT +MDSC



Wsh +MDSC

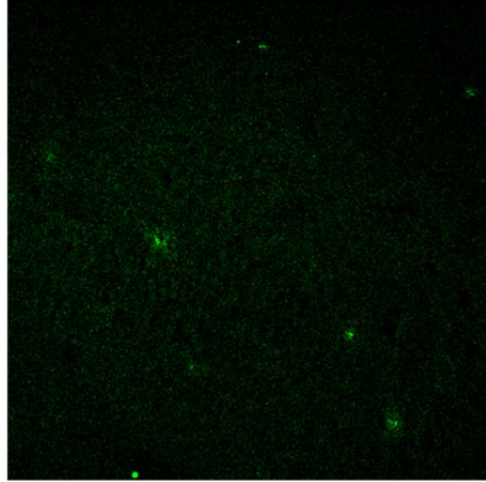


Figure 32. MDSCs migrate preferentially to mast cells

MDSCs placed in top well of 8µm transwell plate. B16 melanoma, MCs or media alone were placed in the bottom well. Four-hour MDSC migration was assessed by flow cytometry. *P<0.05. Mean ± SD; n=5/group.

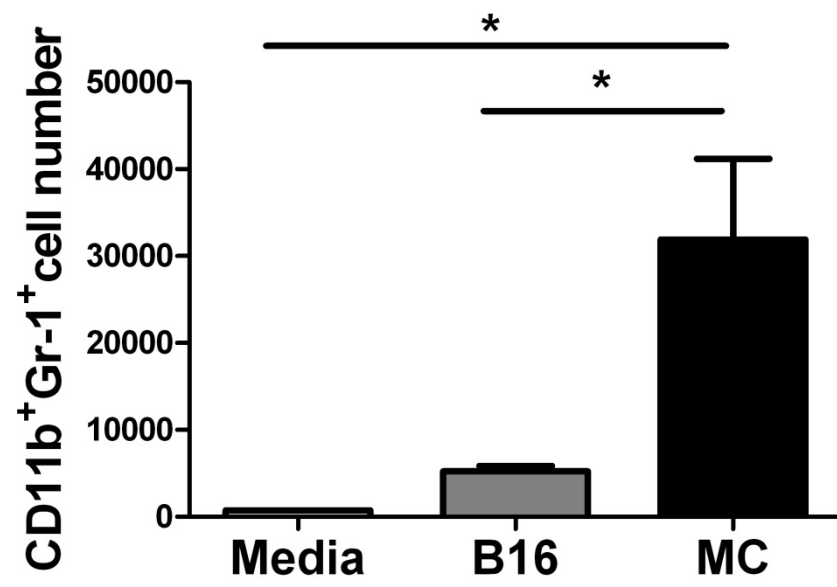


Figure 33. MCs are required for MDSC-mediated tumor progression

(A) Cpa3^{cre}Mcl-1^{fl/fl} (MC^{-/-}) or WT Mice were challenged with B16 melanoma concomitant with or without MDSCs. Mice were sacrificed and lung tumor colonies were enumerated. (B) Liver and spleen were examined for MDSC accumulation.

*P<0.05, n= at least four mice per group.

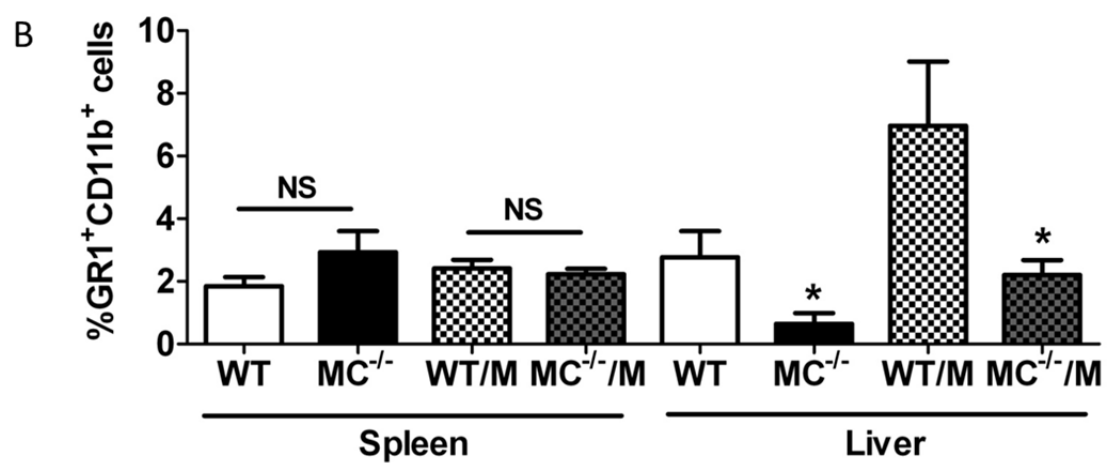
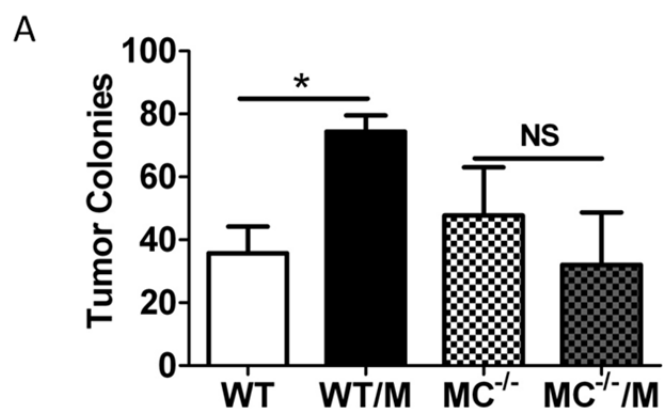


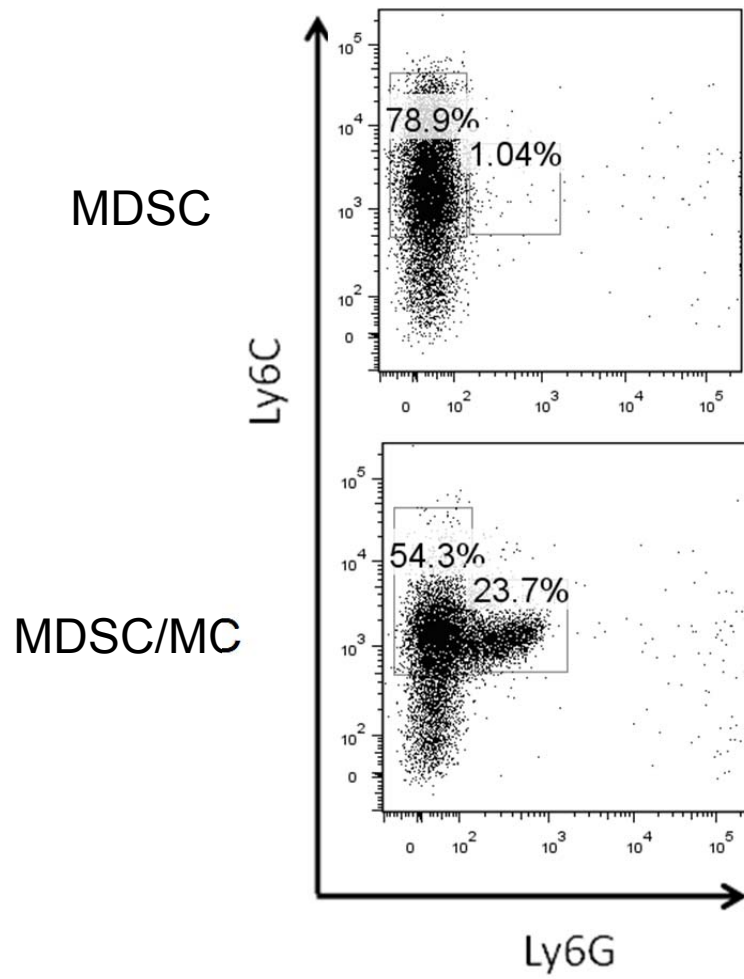
Figure 34. Mast cells help maintain the granulocytic population of MDSCs *in vitro*

MDSCs were cultured with and without MCs, in media containing IL-3 and SCF to

maintain MC survival. Culture was maintained for 5 days and then harvested for flow

cytometric analysis. Live cells were assessed for CD11b staining. CD11b⁺ cells were

gated to look at the Ly6G⁺ or Ly6C⁺ distribution.



2.3.2 Mast cell histamine promotes immunoregulatory activity of MDSCs

MDSCs express HR1 and HR2

Given the contribution of histamine to MDSC activity, cell proliferation, and Th2-skewed immune responses^{280,286}, we examined whether histamine could serve as a potential mediator in the MC/MDSC cross-communication. Liver MDSCs were examined, as they were the population most affected in MC-deficient mice. They express HR1–3 but not 4 (**Figure 35A**). Splenic MDSCs express high levels of HR1, as shown in **Figure 35B**. Additionally, purified MDSCs express detectable HR2 and 3 but not 4 (**Figure 35C**).

Histamine induces MDSC proliferation and differential gene expression in monocytic versus granulocytic MDSCs

As shown in **Figure 36A** and **B**, *in vitro* exposure to histamine promoted survival and proliferation of MDSCs in a dose-dependent manner. The contribution of histamine was confirmed using CT, CIM, HR1, and HR2 antagonists, respectively. As shown in **Figure 36C**, CT and CIM inhibited histamine-stimulated cell proliferation. Both subtypes of MDSCs are responsive to histamine; however, the monocytic subset is significantly more sensitive to the proliferative effects of histamine than are granulocytic MDSCs (**Figure 36D**).

Given the ability of histamine to induce MDSC proliferation *in vitro*, a logical step was to examine its role in modulating markers of MDSC activity. Accordingly, monocytic or granulocytic MDSCs were cultured with 100 μ M histamine, as in **Figure 36A**, and analyzed for expression of Arg1 and iNOS via qPCR. It has been documented that

MDSC immunosuppression largely results from impairment of T cell activity modulated by these enzymes^{162,318}. In the presence of histamine, we observed a fivefold increase ($\Delta\Delta\text{Ct}$ method)³¹⁹ in the expression of Arg1 and a twofold increase in the expression of iNOS in monocytic MDSCs over granulocytic MDSCs. However, the granulocytic MDSCs exhibit a fivefold decrease in the expression of Arg1 and a threefold decrease in the expression of iNOS, exhibiting striking differential gene expression between the two populations (**Figure 37A,B**). These data are reinforced by intracellular flow cytometry, showing increased protein expression of Arg1 by monocytic MDSCs when exposed to histamine *in vitro* but unchanged expression by the granulocytic MDSC (**Figure 38A, B**).

Arg1 and iNOS are essential for classical MDSC-mediated T cell suppression, whereas IL-13 and IL-4 are important Th2 cytokines involved in *N. brasiliensis* clearance. With addition of histamine, granulocytic MDSCs—the population important for augmented parasitic clearance—increased IL-4 expression fourfold and IL-13 expression over 200-fold compared with monocytic MDSCs (**Figure 37C**).

Histamine antagonist prevents MDSC-mediated N. brasiliensis expulsion and tumor progression

To confirm the effects of histamine on MDSC activity *in vivo*, mice were infected with 650 L3 *N. brasiliensis*, a Th2 helminth. MDSCs were AT *i.v.* in conjunction with CT, CIM, HR1, or HR2 antagonists, respectively. Administration of CT or CIM significantly abrogated the ability of MDSCs to increase the clearance of *N. brasiliensis* (**Fig. 39A, B**). This was correlated with reduced-infiltrating MDSCs in the liver (**Figure 39C**) and

diminished phenotypic conversion toward granulocytic MDSCs (**Figure 39D**), which is the important phenotype for *N. brasiliensis* clearance¹⁹³.

As histamine induces increased iNOS and Arg1 message (**Figure 37A, B**), both important for MDSC-induced T cell suppression, we analyzed whether histamine blockade affected MDSC-induced tumor progression. A mouse model of melanoma was used (B16). This model does not naturally accumulate large numbers of MDSCs, so AT of MDSCs was used to increase MDSC numbers. Mice receiving AT with MDSCs and treated with CIM had significantly reduced colonization to the lungs with B16 melanoma compared with mice that received MDSCs but no CIM, as determined by lung weight (**Figure 40**). CIM alone had no significant effect on tumor burden in the absence of AT of MDSCs. This is consistent with data showing similar results using a model of murine Lewis lung carcinoma, a model with natural accumulation of MDSCs, where CIM treatment resulted in reduced tumor size³²⁰.

MDSCs are increased in allergic patients

Allergy is a MC-mediated, Th2-dependent immune response. Allergic patients experiencing symptoms have increased levels of circulating MC-derived histamine³²¹. Additionally, *Deshane et al.*³²² describe MDSCs as being involved in Th2-driven airway hyper-responsiveness. To elucidate the translational relevance of our findings, we isolated PBMC from patients currently experiencing allergy symptoms and non-allergic controls, as determined by a patient questionnaire. Patients that reported taking antihistamines were excluded from the study. PBMC was examined by flow cytometry; human MDSCs are defined as CD34⁻ CD33⁺CD11b⁺ cells²²⁰. Monocytic MDSCs are defined as CD34⁻CD11b⁺CD14⁺ and granulocytic MDSCs as CD34⁻

CD11b⁺CD15⁺²²⁰(**Figure 42**). Allergic patients were found to exhibit 40% more circulating MDSCs than controls (**Figure 41A, B**). Interestingly the monocytic subset of MDSCs appeared to be the dominant subpopulation in the controls, but was not elevated significantly in allergic patients (**Figure 41C**). However, the granulocytic MDSCs, which are the population implicated to be more important in Th2 responses, such as helminth immunity, were increased significantly with 20% more in the allergic patients compared with controls (**Figure 41D**). MDSCs are elevated in the peripheral blood of patients with cancer. To elucidate the response of human MDSCs to histamine, MDSCs were sorted from the blood of cancer patients and stimulated with or without histamine. Histamine promotes increased survival of human MDSCs at 48 hours over media alone (**Figure 43**).

IL-13^{-/-} mice have reduced MDSC accumulation in the periphery

Given the striking trafficking data and the emerging role of MC-IL-13 in tumor, mice deficient in IL-13 (IL-13^{-/-}) were injected s.c. with LLC. In this model, MDSCs were generated by the BM, but they were unable to escape out of the blood and traffic to the liver as indicated by a higher percentage of MDSCs in the peripheral blood (PB) and fewer in the liver compared to tumor-bearing WT mice (**Figure 44A,B**). Interestingly, despite increased PB MDSCs, the IL-13^{-/-} mice had smaller tumor volume compared to WT. These findings introduce a novel hypothesis that MC-secreted IL-13 recruits MDSCs out of the circulation and into MC resident tissues, where they further increase their suppressive properties through IL-4R α signaling and enhance development of tumor metastasis. This hypothesis is reinforced by preliminary data using a LLC colonization model in which IL-13^{-/-} mice had dramatically fewer tumor colonies in the

lungs over WT (**Figure 44C**), and fewer MDSCs in the liver (**Figure 44D**). Interestingly, these IL-13^{-/-} mice had significantly increased PB MDSCs over WT (**Figure 44D**).

Backcrossing the IL-13^{-/-} mice to the ADAM10Tg has allowed us to generate IL-13^{-/-} MDSCs as well as observe the effects IL-13 has on MDSC development.

ADAM10TgIL-13^{-/-} mice have reduced MDSCs levels in the liver and spleen, as compared to ADAM10Tgs (**Figures 45 and 46**). Yet, BM precursors to CMPs are unaffected (**Figure 47**). This shows that MDSC development is unaffected and points to alterations in MDSC trafficking or survival.

Figure 35. MDSCs express HRs

A. HR expression on liver MDSCs as compared to secondary alone (shaded). B. H1 receptor expression on splenic ADAM10Tg MDSCs was determined by comparing HR1 staining on (line) MDSCs and comparing it to HR1 staining on GR1⁺CD11b⁻ cells (shaded). HR2 (C), HR3 (D) and HR4 (E) presence was determined by flow cytometry of isolated MDSCs after 12 hours of culture in cRPMI. (Shaded area represents secondary antibody alone) Three independent experiments.

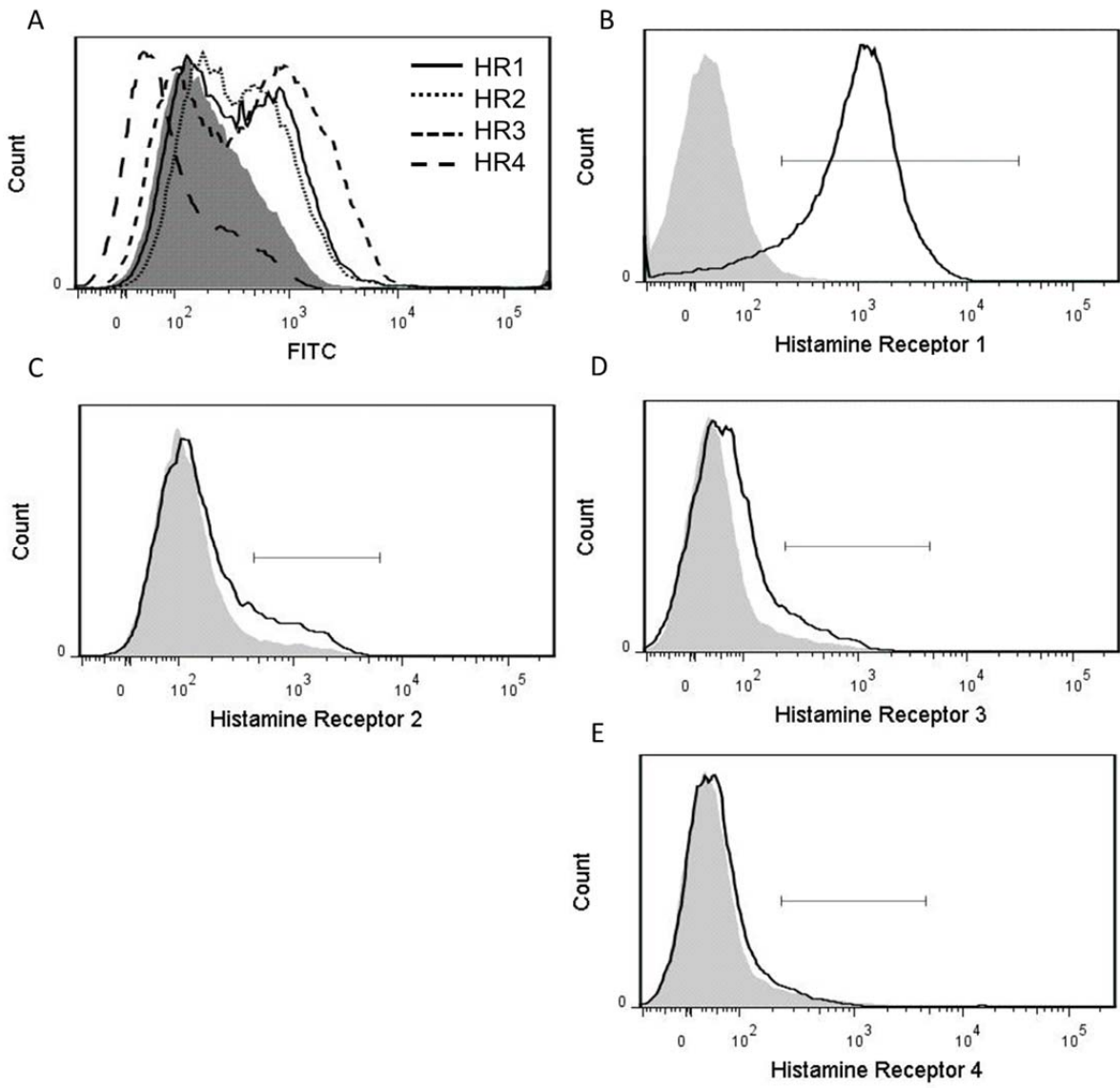


Figure 36. Histamine increases MDSC survival and proliferation

(A) Survival assessed by trypan blue exclusion over time course of MDSCs alone (circle) or with histamine (triangle). (B and C) Proliferation assays of MDSCs cultured alone, with histamine (H), or in combination with indicated agents, as measured by counts per minute (CPM). (D) MDSCs were cultured with histamine or media. * $P < 0.05$; ** $P < 0.005$; *** $P < 0.0005$. Mean \pm SD; $n = 10$ /group and at least two independent experiments.

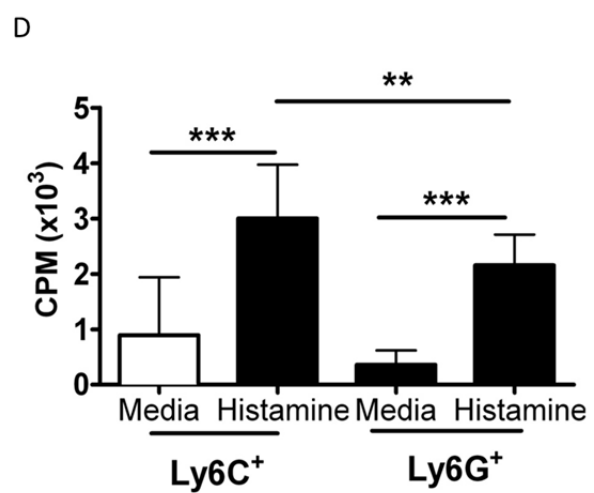
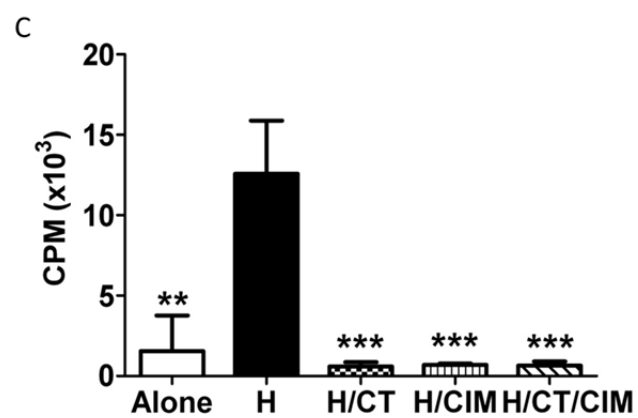
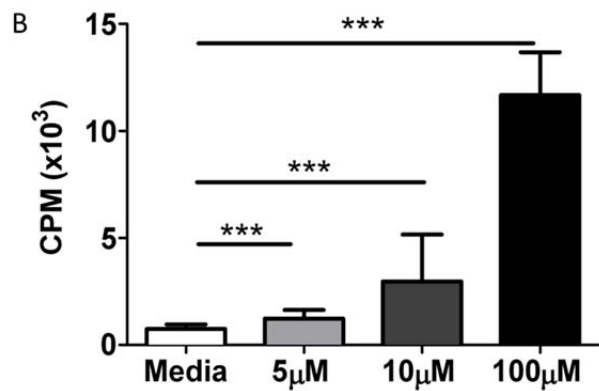
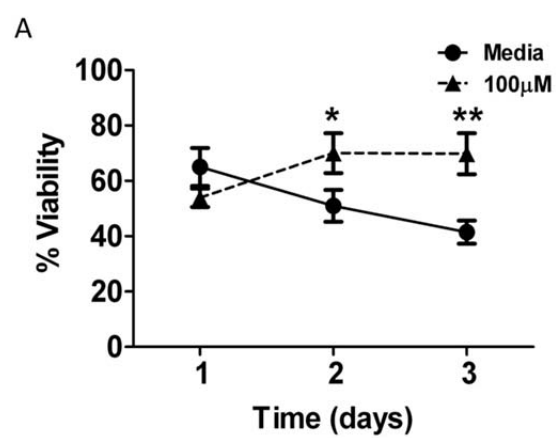


Figure 37. Histamine influences MDSC gene expression

Ly6C⁺ or Ly6G⁺ MDSCs were cultured \pm histamine and analyzed (48 h) for Arg1 (A) or iNOS (B) message. Fold change of histamine-treated/media alone (A and B). Fold change of IL-13 and IL-4 message from histamine treated Ly6G⁺/Ly6C⁺ cells (C). After normalization to GAPDH, data were analyzed using the $\Delta\Delta C_t$ method.***P<0.0005. Mean \pm SD; n=5 from two experiments.

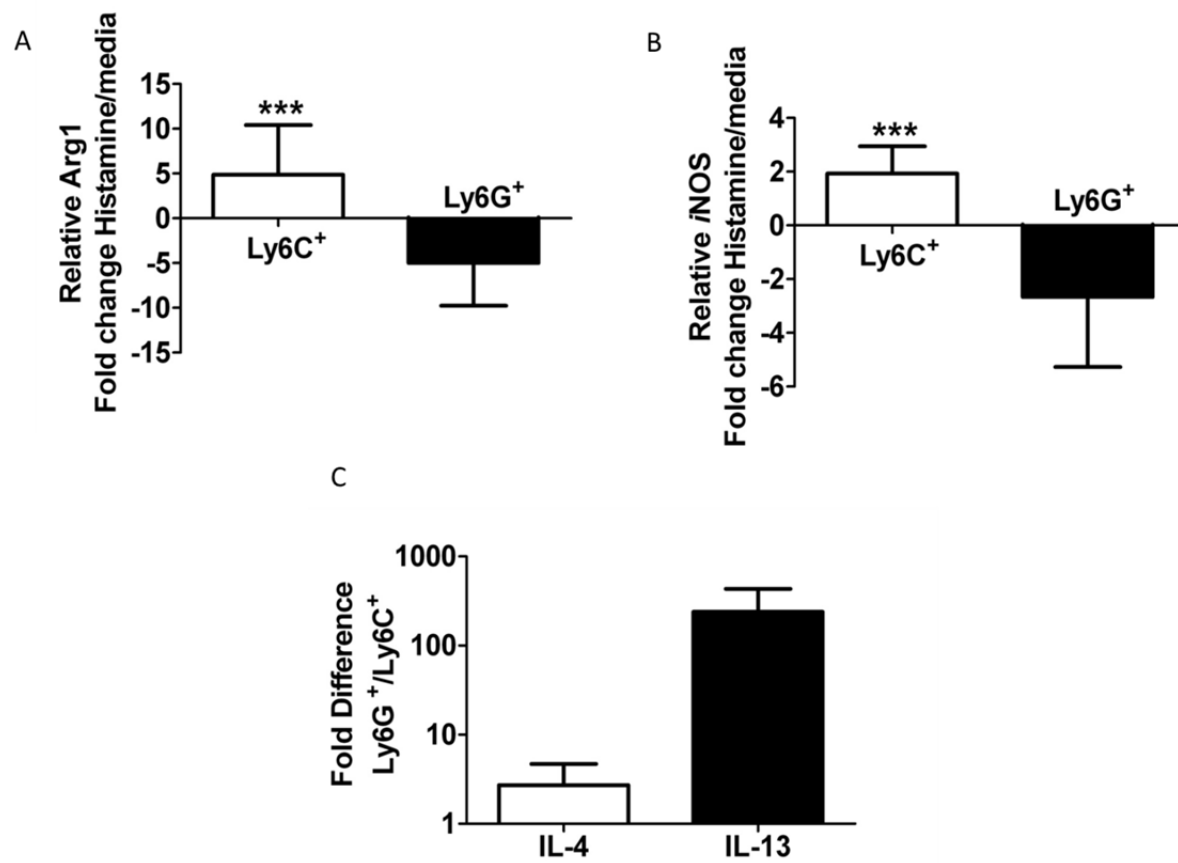


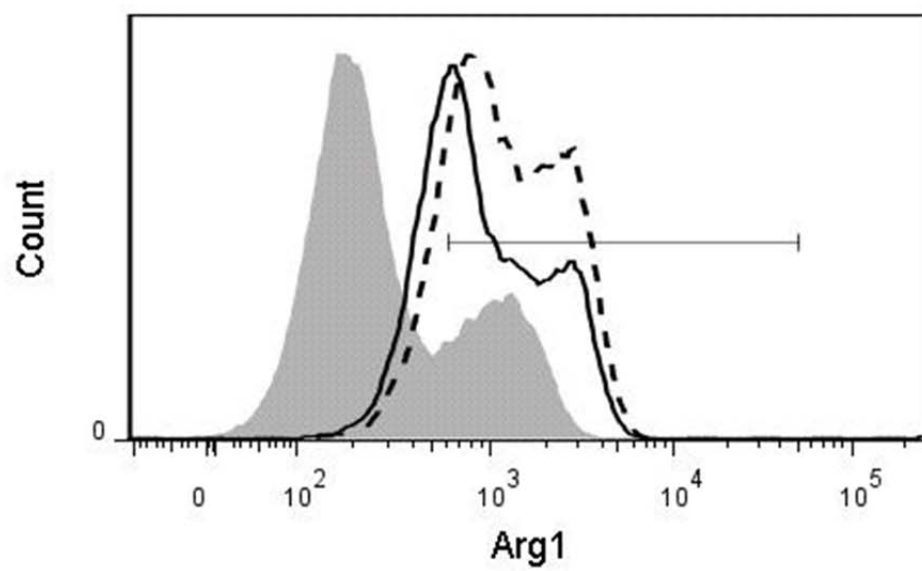
Figure 38. Ly6C⁺ MDSCs express increased Arg1 protein with Histamine

MDSCs were isolated from ADAM10Tg spleen and treated with histamine for 12 hours.

Arg1 expression was determined by utilizing intracellular flow cytometry. Ly6C⁺CD11b⁺

(A.) or Ly6G⁺CD11b⁺ (B.) MDSCs with histamine treatment (dashed line) or without (solid line), as compared to secondary alone (shaded).

A



B

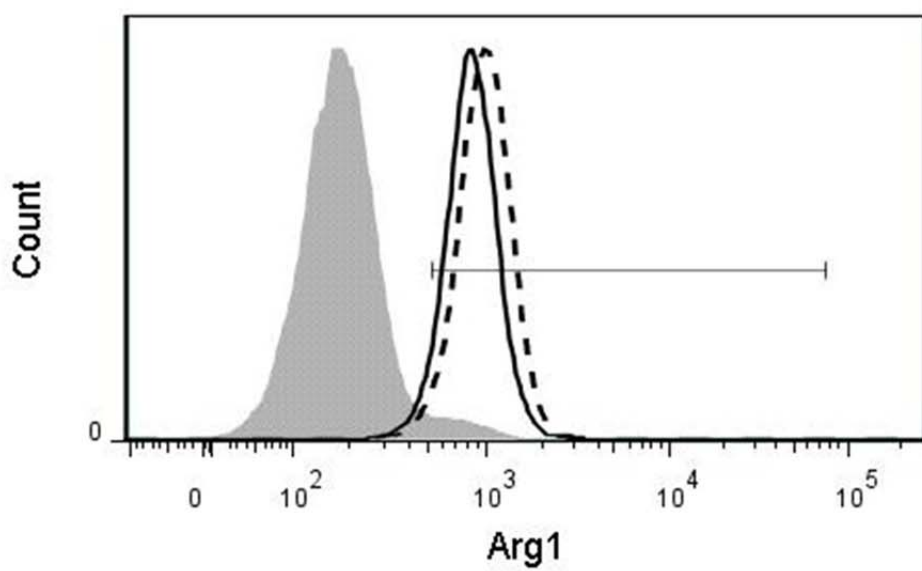
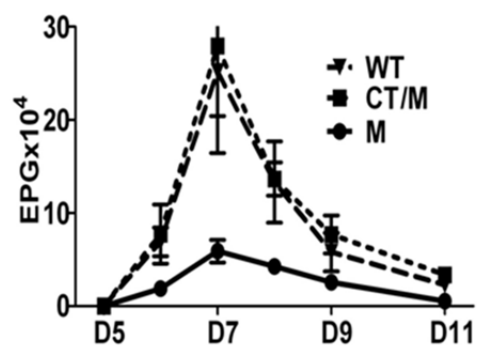


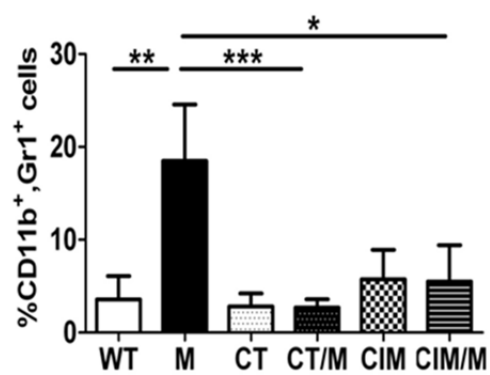
Figure 39. HR1 and HR2 antagonists blocks MDSC mediated *N. brasiliensis* clearance

A, B. Eggs/gm feces in *N. brasiliensis* infected, \pm MDSCs (M) on indicated days and \pm daily CT treatment (A) or every other day CIM treatment (B). C. Day 14 analysis of total MDSCs. D. Flow cytometric determination of liver monocytic or granulocytic populations. * $P < 0.05$, *** $P < 0.0005$. Mean \pm SD, $n \geq 5$ with two independent experiments.

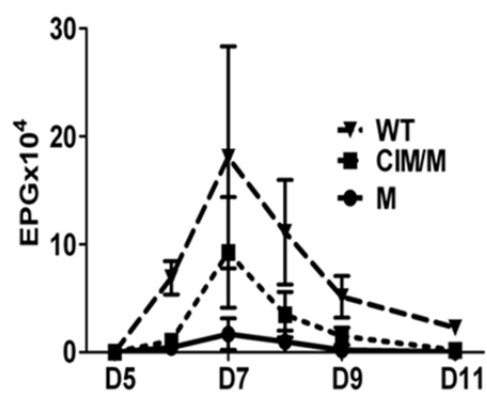
A



C



B



D

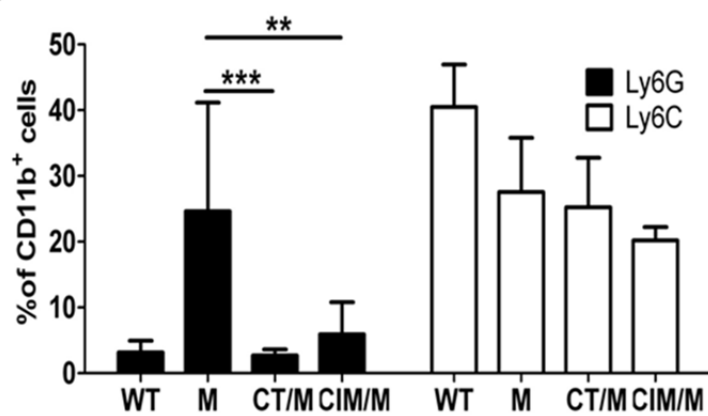


Figure 40. HR antagonization inhibits MDSC mediated tumor progression

Mice were challenged with B16 concomitant with MDSCs in the presence or absence of cimetidine (CIM), an HR2 antagonist. Mice were subsequently sacrificed and their lungs weighed for B16 colonization. Error bars represent Mean \pm SD. *P<0.05. n=at least five mice per group.

B16 melanoma

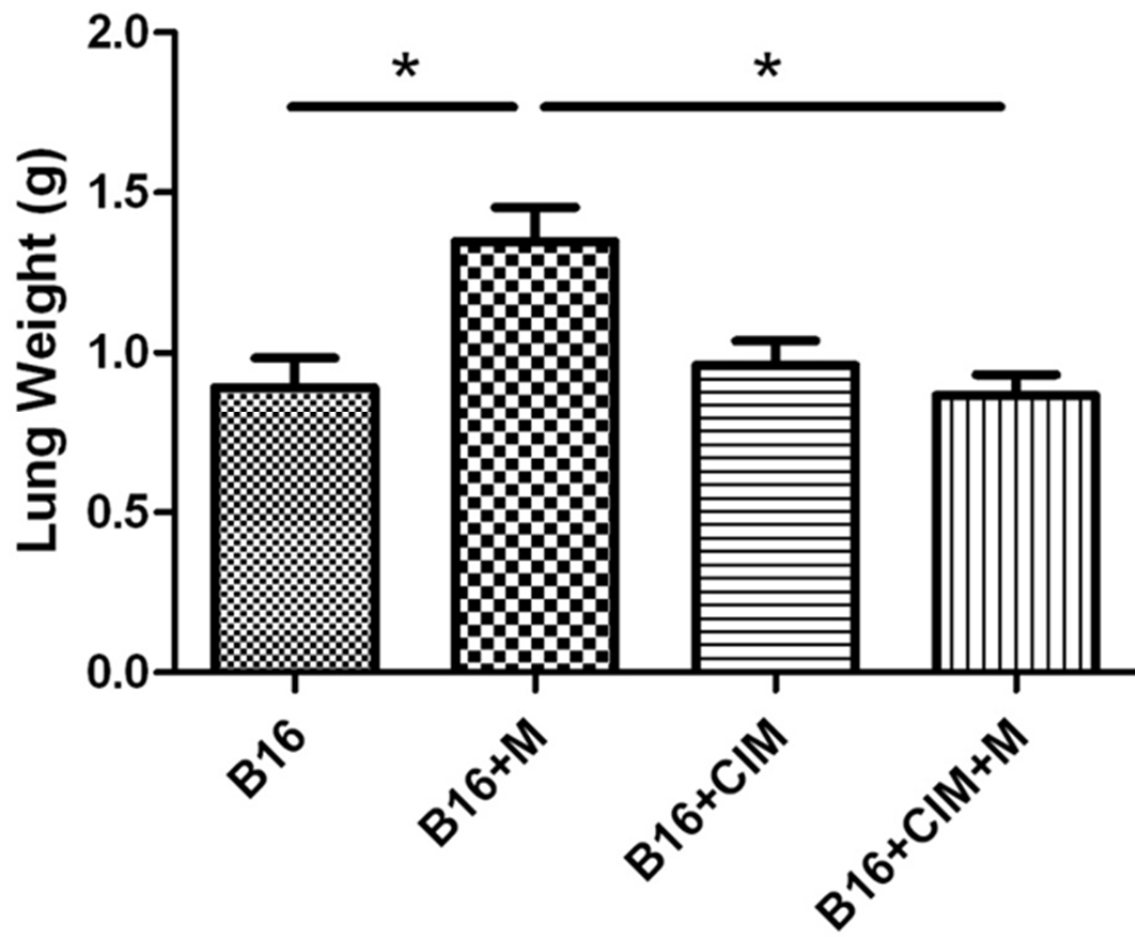
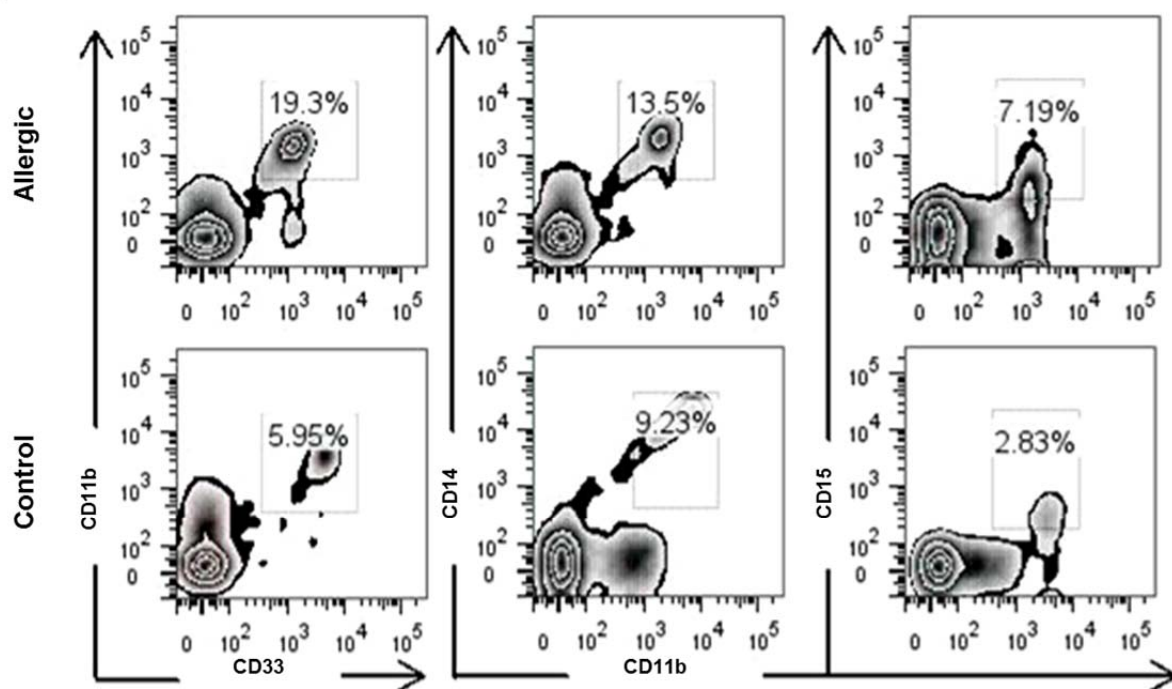


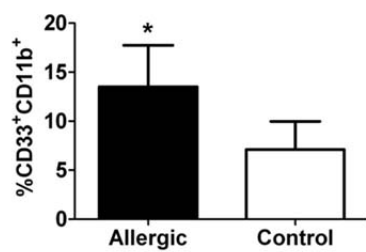
Figure 41. Allergic patients have increased circulating MDSCs. Symptomatic allergic patients were compared with non-allergic controls.

Cells were isolated from peripheral blood gating strategy (**Figure 41**). Percent total MDSCs (B) and subpopulations, CD14⁺ (C) or CD15⁺ (D), were determined by flow cytometry. (A) Representative allergic patient versus control and (B–D) compiled.*P < 0.05. Mean ± SD. Allergic patients, n=6; controls, n=6.

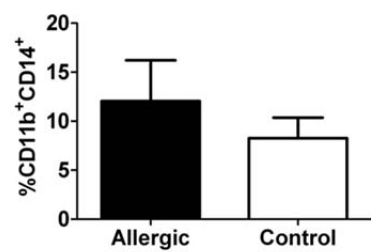
A



B



C



D

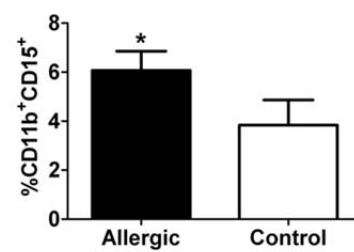


Figure 42. MDSC gating strategy for allergic patient study.

CD34⁻ cells were gated off of the live cell population and CD33⁺CD11b⁺ dual positive

MDSCs were analyzed (as shown in **Figure 40A,B**). For subpopulations, this was

further extrapolated by looking at the CD11b⁺ CD15⁺ or CD11b⁺CD14⁺ populations and analyzed (as shown in **Figure 40A,C,D**)

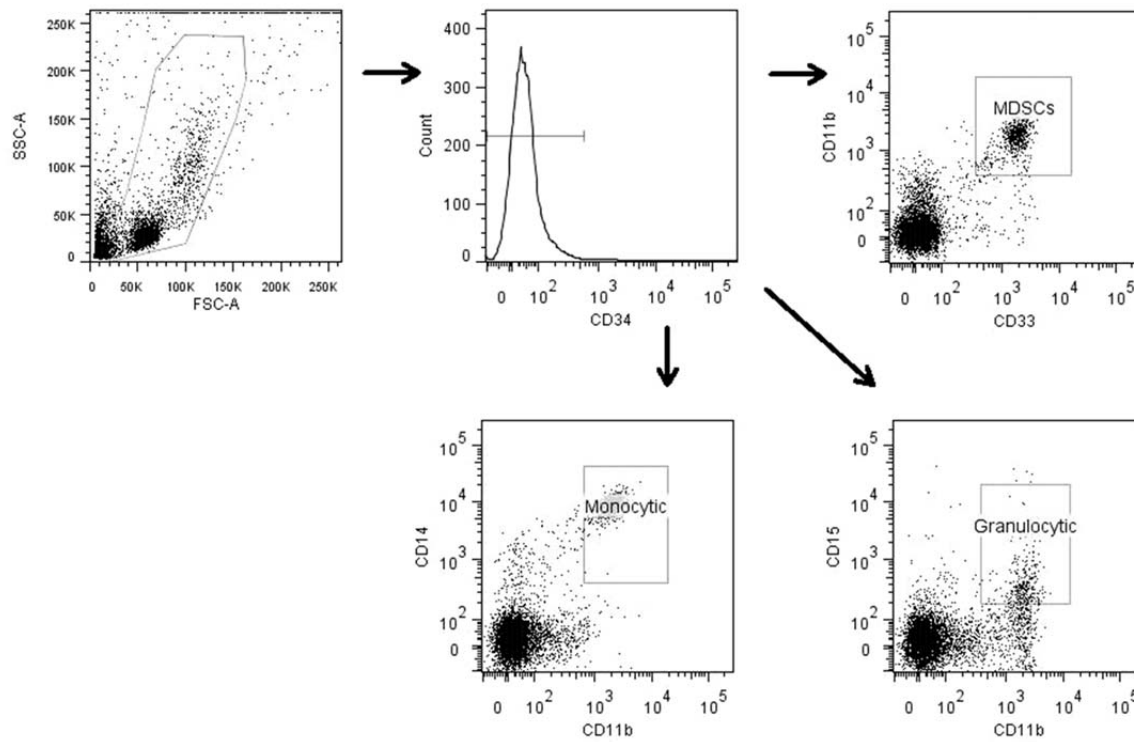


Figure 43. Human MDSCs have increased survival in the presence of histamine. MDSCs sorted as HLA-DR^{low}-CD11b⁺CD33⁺ from peripheral blood of a stage 1 breast cancer patient. Cells were stained for flow cytometry prior to culture and after 48 hours of culture with 100μM histamine or in media alone. Patient data is representative of two independent experiments. Data is courtesy of Kyle K. Payne and Masoud Manjilli, Ph.D. at Virginia Commonwealth University, Richmond, VA, USA.

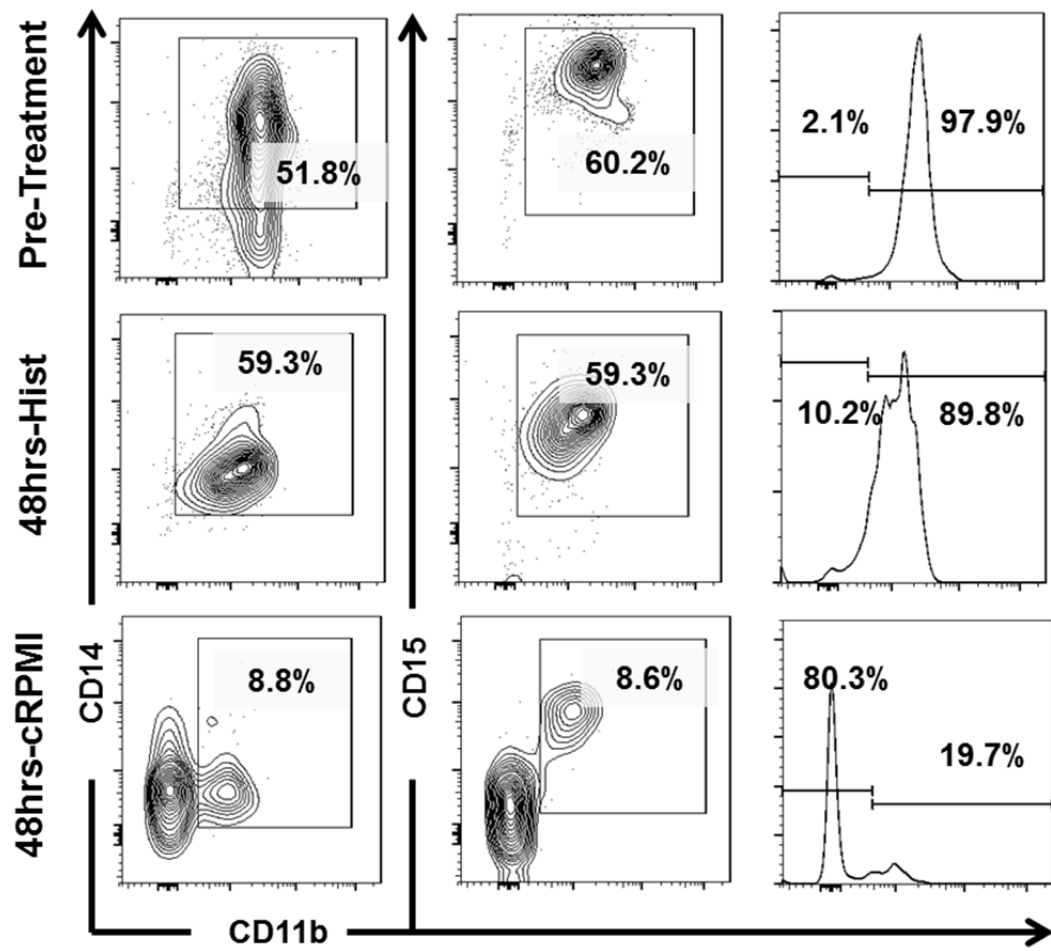


Figure 44. IL13 is important for MDSC-driven suppression of tumor immunity

A. IL13^{-/-} or WT Mice were challenged with LLC s.c. tumors. Tumor volume (A) and percent Gr1⁺CD11b⁺ cells in spleen/liver (B) were assessed. C. Mice were challenged with LLC *i.v.* and lungs were infused with India ink to visualize tumor, representative lungs. D. Percent Gr1⁺CD11b⁺ cells in spleen/lungs were analyzed by flow cytometry. Error bars represent Mean \pm SD. *P<0.05. n>5 mice/group.

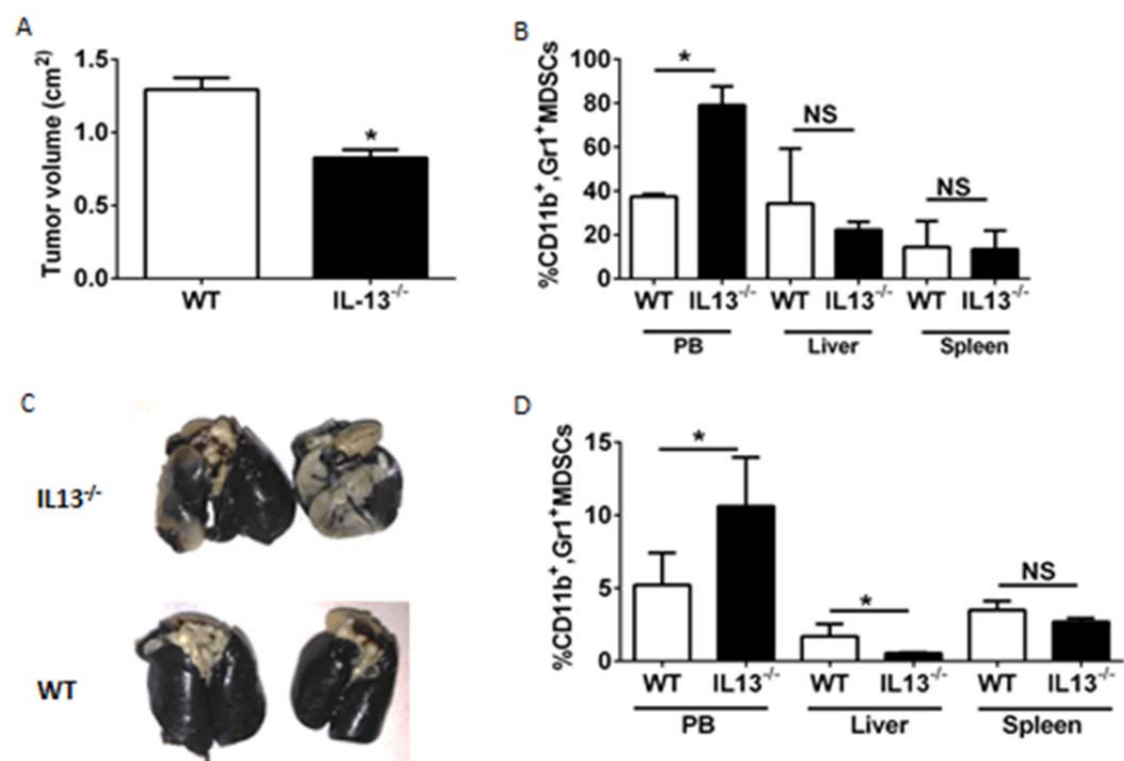


Figure 45. IL13 deficiency decreases MDSC accumulation in the liver

A,B. IL13^{-/-} or WT naïve mice liver by flow cytometry and C,D. IL-13^{-/-}ADAM10Tg or ADAM10Tg. Livers stained for Gr-1⁺CD11b⁺ of total live cells (A) and Ly6C⁺Ly6G⁺ of total CD11b⁺ cells (B). Representative flow cytometry plots.

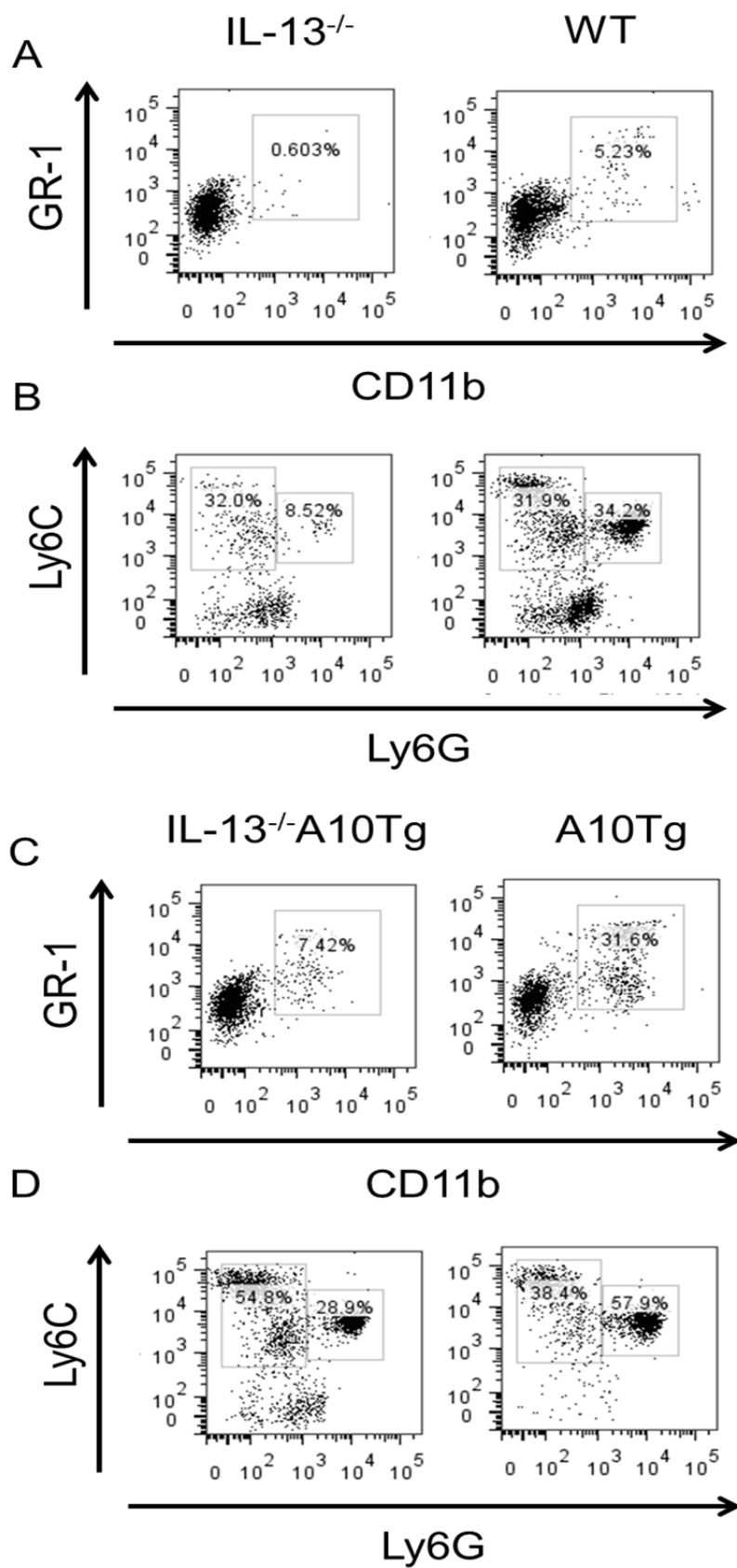


Figure 46. IL13 deficiency decreases MDSC accumulation in the spleen

A,B. IL13^{-/-} or WT naïve mice spleen by flow cytometry and C,D. IL-13^{-/-}ADAM10Tg or ADAM10Tg. Spleens stained for Gr-1⁺CD11b⁺ of total live cells (A) and Ly6C⁺Ly6G⁺ of total CD11b⁺ cells (B). Representative flow cytometry plots.

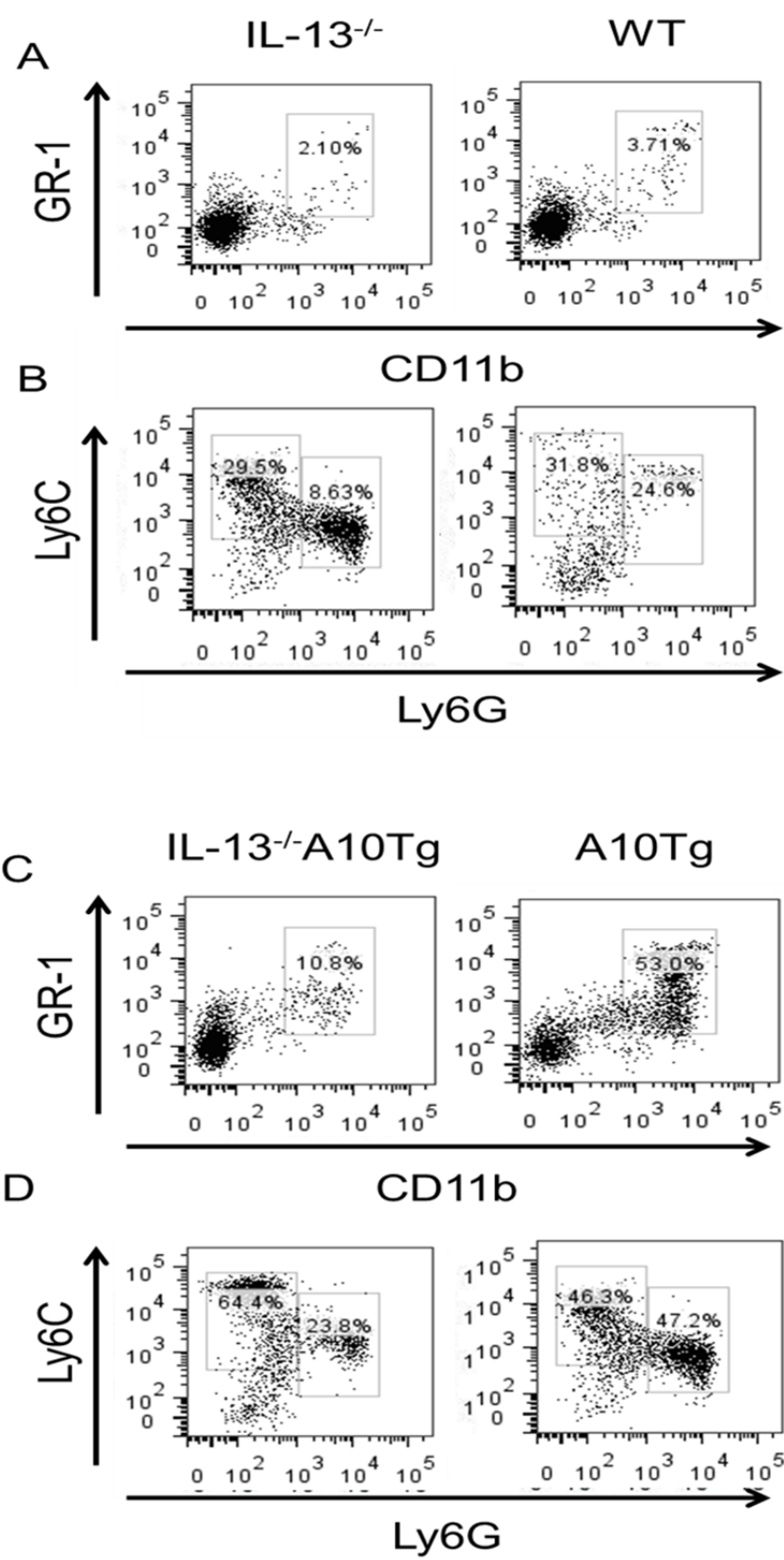
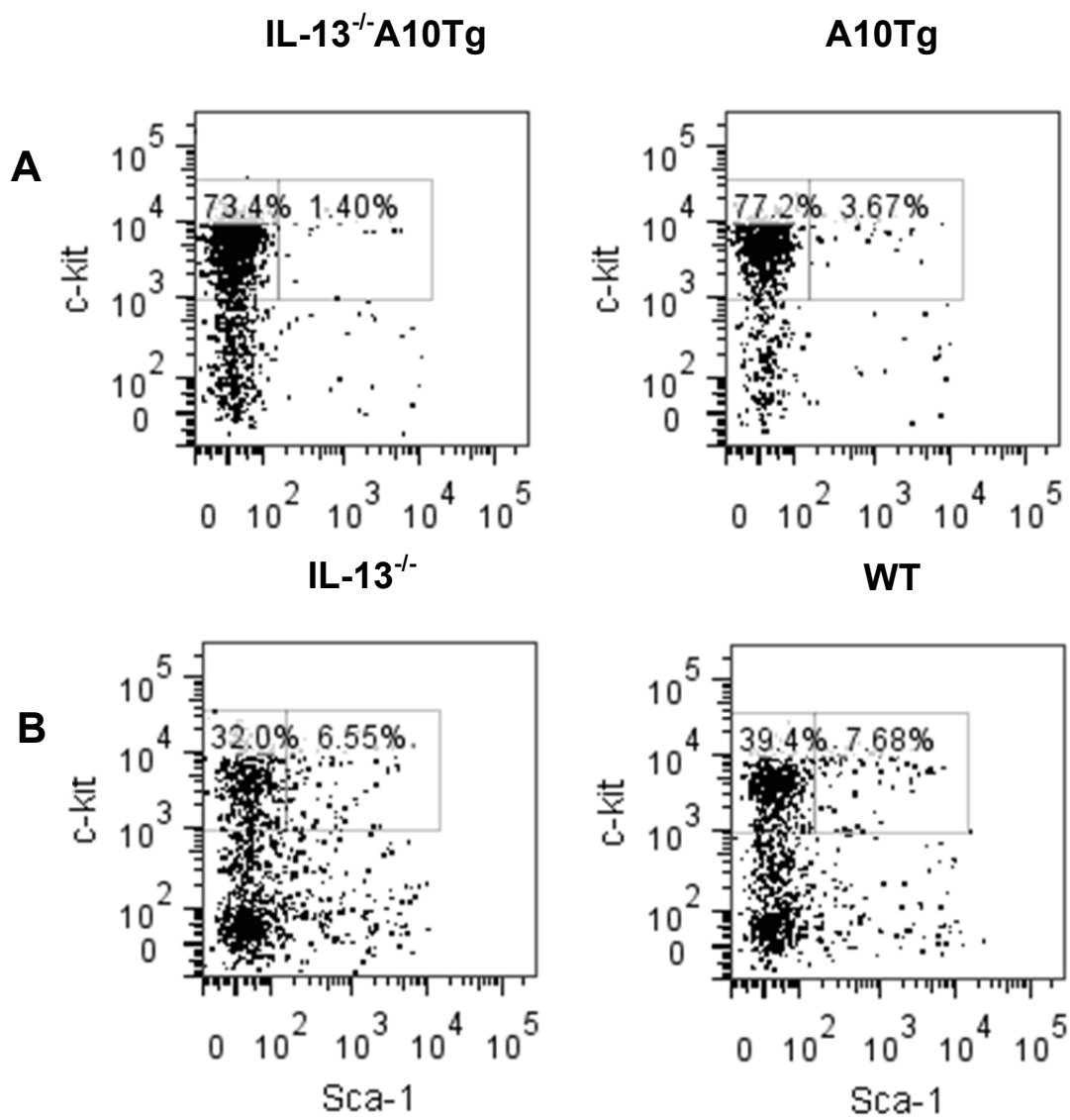


Figure 47. IL13 deficiency does not affect committed progenitor cells of the bone marrow

A. IL13^{-/-} or WT naïve mice BM by flow cytometry and B. IL-13^{-/-}ADAM10Tg or ADAM10Tg. BM from Lineage⁻ of total live cells and divided into c-kit and sca-1 staining. Representative flow cytometry plots.



2.3.3 Discussion

The ADAM10Tg mouse affords a unique tool to characterize the immunomodulatory potential of MDSCs in an environment free of established tumor. Because the ADAM10Tgs suffer no confounding pathology, this was an ideal system in which to elucidate the immunomodulatory roles of MDSCs. We used this system to investigate roles for MDSCs in both neoplasia and helminth infection. In B16 metastasis, monocytic MDSCs strongly suppressed the immune response, whereas granulocytic MDSCs failed to promote metastasis (**Figure 25**). However, in *N. brasiliensis* infection, the granulocytic MDSCs enhanced the anti-parasitic immune response, and the monocytic MDSCs had no effect (**Figure 23**). AT studies demonstrated that this differential immune regulation by MDSCs occurs in an MC-dependent manner. The *ex vivo* co-culture studies indicate that MDSC/MC interactions may modulate immune responses by increasing cytokine production. MDSCs traffic to MCs, affording a synergistic Th2-skewed immune response. Although undesirable in the context of neoplasia, the observed response is ideal in helminth infections. Overall, this data is indicative that inhibition of MC function may serve as a novel target to inhibit MDSC activity.

The use of AT of labeled MDSCs allowed examination of their trafficking pattern and migration during parasitic infection. Previous literature indicates that during tumor progression, MDSCs traffic and accumulate in the liver in addition to the tumor site, where they inhibit Kupffer cells and T cells to dampen anti-tumor immune responses^{316,323,324}. Similarly, in our *N. brasiliensis* infection model, MDSCs preferentially migrated to the liver (**Figure 29A, B**). Previous work has shown that liver-accumulated MDSCs produce an array of proinflammatory and regulatory cytokines and

chemokines in response to tumor challenge³¹⁶. This would argue that the liver is a critical site for MDSC function. In models of MC deficiency, where MDSCs do not traffic to the liver, MDSCs do not function as efficiently¹⁹³. MCs are seen in normal liver surrounding the vessels and the bile ducts in the portal tracts as well as to a lesser extent in the hepatic parenchyma³²⁵. It has been reported that hepatic MCs release histamine and other mediators through the portal bile ducts and into the bile³¹⁷. Therefore, we hypothesized that MDSCs may interact with hepatic MCs in the liver and become further activated. The attraction between these two cells may explain that in the absence of MCs, MDSC migration to the liver and parasite expulsion are reduced significantly (**Figure 29**).

MCs and histamine have been shown to play an important role in parasitic clearance. Increased numbers of MCs and concentrations of histamine are positively correlated with natural helminth resistance³²⁴. The role of histamine in parasitic infection has been ascribed to smooth muscle contraction to enhance the “sweep” portion of the “weep and sweep” method of parasitic clearance, acting in conjunction with IL-13/IL-4^{326,327}. Taken in conjunction with the positive correlation of histamine levels and parasitic resistance, this could imply that natural immunity in these animals may not only be a result of the effect of histamine on smooth muscle cells but also effects via MDSC activation and proliferation. Whereas potentially, this could be tested using mice deficient in HDC, the secondary increase in goblet cells seen in these mice would be a complicating issue³²⁸. To our knowledge, the response to helminth infection has not been reported in these mice.

The addition of histamine to MDSCs protected against cell death and increased cellular proliferation *in vitro* (**Figure 36A, B**). Furthermore, histamine enhanced expression of T cell suppression markers Arg1 and iNOS in monocytic MDSCs and decreased expression of these markers in granulocytic MDSCs (**Figure 37A, B**). As a result of these findings, T cell suppression by monocytic MDSCs should be increased after exposure to histamine or culture with MCs. These studies are currently underway. The granulocytic MDSCs increase IL-13 and IL-4 expression over monocytic MDSCs when exposed to histamine. IL-13 is essential in *N. brasiliensis* infection for worm expulsion responsible for increased mucus production and enteric nerve stimulation^{291,292}. This expression reinforces the differential roles that both subsets of MDSCs play^{193,329}. These studies are supported by a recent publication, in which histamine blockade with CIM increased MDSC apoptosis, reduced Arg1 and iNOS enzyme expression, and decreased MDSC accumulation in a mouse model of LLC³²⁰.

These results indicate that MCs enhance site-specific migration and as a result of histamine secretion, induce increased MDSC proliferation and differential gene expression. We hypothesize that in liver, as well as other sites of immune response, resident MCs attract MDSCs and activate them via histamine release. This affords the production of soluble mediators that can act locally and distally by secretion into the bile in our parasitic model. Given our findings and other published studies on MDSCs, the following model is suggested (**Figure 48**). MDSCs secrete Th2 cytokines, notably IL-4 and IL-13, which promote Th2 differentiation, along with IL-6 and TGF- β that chemoattract additional MCs. The T cells not only contribute to the pool of IL-4 and IL-13 but also increase IgE synthesis. IgE, in turn, further activates MCs. These events

afford a self-sustaining and synergistic cycle of MC/MDSC activation, resulting in increased survival and proliferation/activation of MDSCs, in addition to a Th2-skewed immune response. This Th2-skewed immune response is detrimental in the setting of allergic disease or neoplasia but beneficial for parasite clearance.

The importance of the histamine/MDSC interaction was demonstrated dramatically in that histamine blockade, with HR1 and HR2 antagonists, reversed *in vitro* the proliferative effects of histamine (**Figure 36C**) and reversed *in vivo* MDSC-mediated clearance of parasites, similar to the deficit in MDSC functions found in MC-deficient mouse models (**Figure 39A, D**). Impressively, HR2 blockade also decreased lung tumor burden in a B16 melanoma model (**Figure 40**) and other tumor models³²⁰. In addition to having the same effect on parasite clearance, HR1 and HR2 blockade decreased liver MDSC accumulation significantly (**Figure 39B**). This suggests that HR1 and HR2 have overlapping roles in the MDSC/MC interaction and when blocked, result in reduced total MDSC function. The HR1 antagonist, CT, has been shown previously to affect migration of other cells of myeloid lineage, such as monocytes, *in vitro* and could be responsible for the reduced trafficking when the drug is used^{330,331}. HR2 antagonists have been shown to affect production in T cells of IL-13, IL-4, and IL-5, all cytokines important in *N. brasiliensis* infection^{291,292}. In this manuscript, we show that granulocytic MDSCs are producing IL-4 and IL-13 message after histamine addition (**Figure 37C**), and this finding suggests that CIM may work by reducing MDSC IL-4 and IL-13 production. Whereas the MC/MDSC interaction is multifaceted, we propose that MC-derived histamine drives distinct MDSC subpopulations to differential gene expression, inducing phenotypic activation that further directs the activity of the MDSC.

Up-regulation of MDSCs in patient peripheral blood has been detected in many cancers^{332–334} and suggested as a marker of poor prognosis³³⁵. The link between inflammation and cancer has been studied heavily in the last decade. MC and MDSC interactions can potentially serve as a bridge between allergic inflammation and tumorigenic host responses^{279,336,337}. This is the first report that patients with allergic inflammation have increased circulating MDSCs (**Figure 41A, B**). Taken together, our results have important implications for regulation of MDSC survival, trafficking, and activity via antihistamines for disease states, in which the accumulation of MDSCs is detrimental to the host.

IL-13, as mentioned earlier, is a Th2 cytokine that is functionally redundant with IL-4³³⁸. Both IL-4 and IL-13 bind IL-4R α , a subunit that complexes with either common γ chain, IL-13R α 1 or IL-13R α 2. IL-4 can bind IL-4R α complexed with either common γ chain or IL-13R α 1. But, when complexed with IL-13R α 2, only IL-13 will bind it, thus inducing IL-13 specific effects³³⁸. The bulk source of IL-13 in the body is made by Th cells, but IL-13 is also secreted by mast cells^{339,340}. Interestingly, in a model of peanut-induced allergy in the gut, it was uncovered that IgE mediated MC-degranulation through Fc ϵ RI induced IL-13 production by the MC and that this IL-13 production was essential for the development of the intestinal allergic responses to peanut³⁴⁰. Interestingly, IL-13 from the MC drove primarily CCL2 (MCP-1) production. Most importantly, in a model where MC-deficient mice were reconstituted with IL-13^{-/-} MCs, so that only MC-IL-13 was absent, mice completely failed to develop allergic diarrhea³⁴⁰. In other studies, IL-13 has emerged as a key driver of CCL2 expression^{339–342}. IL-13

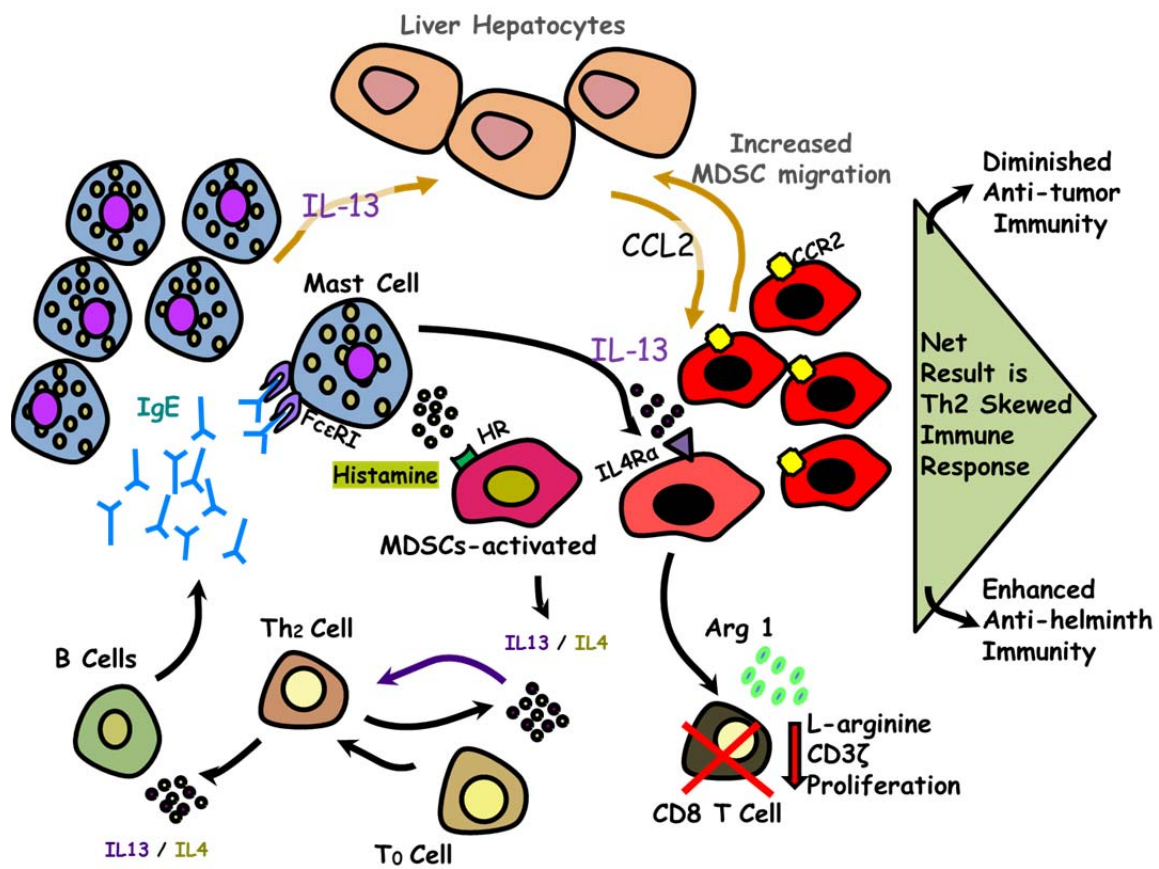
drives CCL2 expression in the human endothelium *in vitro*, as well as the bronchiolar and intestinal epithelium in mouse models of allergic disease *in vivo*^{341,342}.

The liver is emerging as a protective niche for MDSCs^{343,344}. MDSC depletion by anti-Gr-1 administration fails to eliminate them from the liver in tumor-bearing mice³⁴³. The accumulation of MDSCs in the livers of these mice seems to be CCL2/CCR2 dependent³⁴³. CCL2 is a chemokine that binds to CCR2. MDSCs have been shown to express CCR2³⁴⁵. Elevated levels of CCL2 in the circulation of breast cancer patients is been correlated with poor prognosis³⁴⁵. CCR2^{-/-} or CCL2^{-/-} mice both have reduced tumor burden and reduced trafficking of MDSCs³⁴⁵. In mouse models of hepatocellular carcinoma, CCR2⁺ MDSCs migrate *in vivo* in response to the ligand CCL2^{346,347}. CCR2^{-/-} mice additionally exhibit deficiencies in MDSC migration to hepatocellular carcinoma tumor sites³⁴⁷. Hepatocytes have been shown to make CCL2 and recruit myeloid cells in humans with obesity and murine models of this disease. This recruitment promotes hepatic steatosis³⁴⁸. This CCL2/CCR2 dependent accumulation in the liver is additionally seen in mouse models of colitis³⁴³.

Data from **Figure 44** shows that IL-13^{-/-} mice have reduced tumor burden in primary and metastatic models. Interestingly, these mice have increased MDSC levels in the circulation. We hypothesize that this reduction in MDSC numbers in the tissues, but increase in circulation is a result of a disrupted CCL2 chemokine gradient. This disruption results in excess MDSCs stuck in the circulation, where they eventually perish. Further study is underway to confirm this theory, as well as to determine if MC-IL-13 is the driving source for the CCL2 dysregulation.

Figure 48. Model of MDSC/MC interaction

MCs are required for MDSC activity. MCs in the liver release IL-13, which induces production of CCL2 by hepatocytes. This creates a chemokine gradient that increases migration of CCR2 expressing MDSCs, resulting in accumulation in the liver. MCs release mediators, such as histamine, that induce MDSC activation, proliferation, and Th2 cytokine production. This enhanced cytokine production culminates in Th2-skewed immune responses that promote allergy and parasitic clearance and diminish antitumor responses.



Section 3

Chapter 1: B1 B cell IgE production in helminth infection

3.1.1 Introduction to B1 cells

B cells are divided into multiple lineages. There are four mature B cell lineages in the mouse: FO B cells (B2 cells), MZ B cells, B regulatory cells (B reg), and B1 cells³⁴⁹. MZ B cells and B1 cells are both termed innate-like B cells. B1 cells are distinct from B2 cells in the fact that B1 cells can self-replenish and are long lived. Murine B1 cells are found mainly in the pleural and peritoneal cavities^{350,351}. They are derived from the fetal liver and exist in a self-replenishing B1 cell pool. B1 cells have also been shown to transport and present antigen^{352,353}. They are delineated from B2 cells by expression of CD23 and CD11b. B1 cells are CD23⁻, CD11b⁺, B220^{int}, CD19⁺, IgM^{high} and IgD^{lo}³⁵⁴. CD5 is a marker that subdivides the two distinct B1 populations. B1a cells are CD5⁺, while B1b cells are CD5⁻.

In these cells the BCR repertoire is enriched for highly poly-specific receptors with low-affinities to a broad range of antigens³⁵⁵. Antibody generation in these cells generally occurs without T-cell help, SHM, or affinity maturation, and class switching was thought to be limited³⁴⁹. These cells produce low affinity or 'natural' antibody important in immediate response to pathogens^{356–359}. *In vitro* studies with B1 cells have mainly linked them with IgM antibody production, but *in vivo* studies hint that B1 cells can generate other isotypes. *In vivo* B1a cells and B1b cells seem to both be linked to antibody production, but each cell tends to lean towards promotion of certain classes of

antibody. B1a cells are linked to *in vivo* production of IgG2a, IgG2b and IgG3, while B1b cells were previously linked to *in vivo* production of IgG1 and IgE^{360,361}.

B1 cells were first described in 1983³⁶². Since then, B1 cells have been described in resistance to intestinal flora, defense from viral pathogens, generating autoimmune responses and responding to parasites^{363–366}. B1 cells are well known secretors of IgM and gut IgA, but direct evidence of IgG or IgE production is only hinted at in a few papers³⁶⁷. Balb/c *Xid* mice carry an X-linked mutation that prevents B1 cell development. When these mice are infected with *T. cruzi*, they display significantly lower levels of specific and non-specific antibody³⁶⁸. Additionally, in a mouse model of *Schistosomiasis*, which is a Th2 infection characterized by high IL-4, IL-5, and non-specific IgE, B1b cells have been shown to stain positive for IgE and thus be capable of IgE production³⁶⁹. Next, Mice injected with Natterins, a protease that induces a strong antibody driven-Th2 response similar to DerP1, B1b cells are dramatically increased in the peritoneal lavage. In this model B1b cells stimulate ASCs to make increased IgE³⁷⁰. Lastly, ES-62 is a phosphoryl choline (PC)-containing glycoprotein that is secreted by filarial nematodes. ES-62 induces B2 cell hypo-responsiveness. Interestingly, ES-62 activates B1 cells to proliferate and mice treated with this glycoprotein still have high IgE³⁷¹. These cases argue that B1 cells may play an important role in producing immunoglobulin, but don't definitively show that B1 immunoglobulin production is accounting for the increases seen.

B1 cells are described as being activated to produce antibody in a few different ways. Cytokine IL-5 paired with IL-6 induces B1 cells to make *in vivo* IgA in the gut^{350,370}. IL-5 alone stimulates B1 cell proliferation in both B1a and B1b subsets, *in*

vivo, as they both express IL-5 receptor³⁵⁰. IL-5 in conjunction with IL-4 or IL-4 in conjunction with CD40L stimulation by T cells was shown to induce B1 cells to make IgG1 or IgE *in vitro*³⁷². *Kaneko et al.* claimed that anti-CD40 and IL-4 stimulation on B1 cells has the potential to produce more IgE than B2 cells³⁷². Unfortunately, B1 cells were sorted out the peritoneal cavity based only upon CD5^{lo}B220^{int} expression³⁷². *Hastings et al.* in 2006 showed that a population of B2 cells exists in the peritoneal cavity that expresses both CD5^{lo} and B220^{int} expression. They are segregated from B1 cells by CD11b expression. These peritoneal B2 cells survive *in vitro* culture and produce antibody³⁷³. This indicates that B2 cells cannot be ruled out of the population sorted by *Kaneko et al.* due to the fact that they did not sort based on CD11b staining. Both subsets of B1 cells additionally express IL-9 receptor, and IL-9 transgenic mice have been shown to have dramatically increased B1 cells. These mice additionally make increased antibody in response to antigen stimulation. But, *in vitro* B1 proliferation or antibody production was unsuccessful³⁶¹. Excitingly, a new study was just released by *Ghosh et al.*, which showed that during a model of fungal asthma, B1 cells in the pleural cavity secreted IgE into the BALF. μ MT mice have a disruption in the μ heavy chain causing a block in B cell development at the pre-B cell stage³⁷⁴. But surprisingly develop a population of CD19⁺CD9⁺IgD⁺CD23⁻ B1 cells³⁷⁵. Since these mice lack evidence of any B2 cells, IgG and IgE production can be contributed to the B1 cells *in vivo*³⁷⁵. In all, *in vivo* models hint that B1 cells may be able to produce IgG and even IgE, but more extensive evidence is needed, as well as successful *in vitro* culture.

3.1.2 Introduction to IgE

IgE is the first line of defense against intestinal helminths. IgE levels are tightly regulated, being the Ig with the lowest levels *in vivo*³⁷⁶. Interestingly, only very small amounts of antigen are detected by IgE, making it a “gatekeeper” of sorts, being the first to detect foreign particles in areas of interface with the environment. When these foreign particles are innocuous, such as pollen, cat dander or peanut proteins, IgE moves from beneficial to potentially life threatening. IgE mediates allergic responses from mild reactions to severe, such as allergic rhinitis, atopic dermatitis, urticaria, asthma, and anaphylactic shock³⁷⁷.

IgE controls the immune system in one of three ways described here. First, antigen specific IgE is loaded onto MCs or basophils, FcεRI, where it can stay for up to 21 days waiting to bind to antigen, cross-link the FcεRI and degranulate the cell³⁷⁸. This releases mediators such as histamine, lipid mediators, and other biologically active products immediately, while additionally activating the MC or basophil to induce late stage cytokine production³⁷⁷. All of this induces the symptoms of various allergic diseases depending upon the location of the reaction. Second, circulating IgE can bind to its antigen creating an IgE-immune complex. IgE immune complexes are then picked up by circulating FO B cells via CD23, the low affinity IgE receptor (FcεRII). These CD23⁺ B cells then traffic to the splenic follicles, where antigen transfer ensues (described further in section 4) and subsequent rapid increases in specific CD4⁺ T cell proliferation and antigen-specific IgG responses occurs³⁷⁹. Third, circulating IgE can bind to CD23 on B cells, inducing a negative regulatory response to shut down and control excessive IgE synthesis¹⁴⁵.

There are two ways for a B cells to class switch to IgE. The first and more traditional route is through the intermediate γ heavy chain (μ to γ to ϵ)³⁸⁰. This route of CSR is mediated in the GC and induces high-affinity antibodies³⁸⁰. The high levels of IgE production seen in helminth infections is not always high-affinity. A considerable amount of the IgE is considered to be low-affinity. This low-affinity IgE is thought to be mediated from a direct μ to ϵ switch³⁸⁰. We hypothesize that B1 cells generate IgE through this mechanism.

3.1.3 Correlation between allergy and helminth infections

One in five children in industrialized countries suffers from allergic diseases such as asthma, allergic rhinitis and eczema³⁸¹. In these industrialized countries, helminth infection is greatly reduced and when observed it is commonly associated with a reduced parasite burden³⁸². One billion individuals are heavily infected with helminth worldwide and are rarely affected by allergic disease¹⁷². Many epidemiological studies have proven this correlation^{382,383}. Allergic diseases share many factors with helminth infections, including a similar cytokine milieu and most importantly up-regulation of IgE^{382,383}. These factors induce the symptomology of allergic disease, yet in helminth infected individuals, are protective against this symptomology^{382,383}. This is despite helminth being the strongest natural promoter of IgE synthesis³⁸⁴. It is well established that parasite-specific IgE is important for anti-helminth immunity, but helminthes are also known to elicit large amounts of polyclonal or non-specific IgE in the serum of infected individuals. This has been thought to be a protective response³⁸⁴. Helminth evolution has selected this trait that benefits parasite life and reproduction, assisting the helminth in immune evasion³⁸⁴.

Utilizing the intestinal helminth *N. brasiliensis* we show that B1 cells sorted from peritoneal lavage of WT infected mice produce high levels of IgE in culture, whereas B1 cells from uninfected mice do not. We additionally show that this phenomenon is augmented with the addition of myeloid derived suppressor cells (MDSCs). MDSCs have been shown to accumulate in parasitic infection. Extensive myeloid cell infiltration and proliferation has also been associated with B1 cell accumulation in a mouse model of *Schistosomiasis*³⁶⁹. These cells are most commonly associated with immunosuppressive activity. But, we have shown that these cells play an immunosupportive role in the clearance of intestinal helminthes.

Chapter 2: Methods and Materials

3.2.1 Mice

Mice were kept at Virginia Commonwealth University (VCU) in accordance with the humane treatment of laboratory animals set forth by the National Institutes of Health and the American Association for the Accreditation of Laboratory Animal Care. C57BL/6 ADAM10Tg mice were generated by the VCU Transgenic Mouse Core, as previously described²⁴⁷. C57BL/6 WT mice were purchased from The Jackson Laboratory (Bar Harbor, ME, USA). All mouse protocols were approved by the VCU Institutional Animal Care and Use Committee.

3.2.2 Isolation of MDSCs and AT, T cell depletion, and dye labeling

Spleens were harvested from ADAM10Tg. They were then dispersed into single-cell suspensions and filtered through 70- μ m nylon mesh strainers (Invitrogen). Erythrocytes were lysed using an ammonium chloride potassium lysing buffer (Quality Biological). T cells were depleted using CD90.2 magnetic depletion (Miltenyi Biotec, Auburn, CA, USA), according to the manufacturer's protocol. Gr-1⁺ cells were purified from ADAM10Tg spleens using the EasySep PE-Selection kit (Stemcell Technologies, Vancouver, BC, Canada), according to the manufacturer's protocol. For AT studies, 10×10^6 ADAM10Tg MDSCs were injected into the tail vein of each experimental group every 3 days.

3.2.3 ELISA

Total IgE ELISA

Plates were coated with mouse anti-mouse IgE (B1E3; in house) at 5µg/mL in BBS (see previous section 1.2.5 for recipe) and incubated at 37°C for 1 hour. Plates were then washed three times with ELISA wash (section 1.2.5). Plates were blocked (section 1.2.5) for 1 hour at 37°C and were washed as above. Samples were added at various concentrations, diluted in block. Mouse IgE anti-DNP (in house) standards started at 1µg/mL and were serially diluted in block. Plates were incubated and washed as previous. Biotinylated rat anti-mouse IgE (R1E4; in house) was added at 1:2000 dilution in block. Plates were incubated as previous. Plates were then washed five times with ELISA wash and the detection antibody, streptavidin conjugated to alkaline phosphatase (AP) (Southern Biotech) was added at 1:400 diluted in block. Plates were again incubated as previous and were then washed five times with ELISA wash. Substrate buffer (section 1.2.5) was added at 100µL/well and incubated for 15 minutes at room temperature in the dark. When plates were fully developed, they were read at 405nm-650nm.

Total IgG1 ELISA

Plates were coated with mouse anti-mouse IgG (Southern Biotech) at 5µg/mL in BBS (see previous section 1.2.5 for recipe) and incubated at 37°C for 1 hour. Plates were then washed three times with ELISA wash (section 1.2.5). Plates were blocked (section 1.2.5) for 1 hour at 37°C and were washed as above. Samples were added at various concentrations, diluted in block. For standard curve, normal mouse IgG1 (Southern Biotech) was used. Plates were then incubated as previous. Plates were washed three

times with ELISA wash and goat-anti IgG1-AP was diluted in block (1:400 dilution) (Southern Biotech). After 1 hour incubation at 37°C, plates were washed and developed with phosphate tablets (Sigma-Aldrich) dissolved in substrate buffer (section 1.2.5). Absorbance at 405nm-650nm was measured.

3.2.4 Flow cytometry, cell sorting and immunohistochemistry

Flow cytometry

Cell isolation was conducted as previously described in section 1.2.4 and stained as in section 1.2.6.

Cell sorting

Cells were isolated from peritoneal lavage (PL) fluid. RBC lysis was done as in section 1.2.4. PL cells were stained as described in 1.2.6 and sorted on the Aria II (BD Biosciences) into FBS coated 15mL conical tubes.

Immunohistochemistry

Organs were harvested, prepared and stained as described in section 1.2.6.

Antibodies

Antibodies used are listed in **Table 6**.

Table 6. Antibodies used in section 3

Specificity	Clone	Conjugate	Company
Flow Cytometry and Cell Sorting			
Mouse-IgE	23G3	FITC	Southern Biotech
Mouse-CD5	53-7.3	PE	Biolegend
Mouse-B220/CD45R	RA3-6B2	APC	Biolegend
Mouse-CD11b	M170	PE/Cy7	Biolegend
Mouse IgM	R-MM1	PerCP/Cy5.5	
Immunofluorescence			
Mouse-GL7(B and T cell activation antigen)	GL7	FITC	Biolegend
Mouse-CD3	1445-2C11	PE	Biolegend
Mouse-B220/CD45R	RA3-6B2	PE	Biolegend

3.2.5 B1 cell culture

Sorted B1 cells, B1a, B1b or B2 cells were set up in 96 well cell culture plates at 50,000cells/well. Cells were incubated in cRPMI 1640 containing 10% FBS, 2mM L-glutamine, 100 U/mL penicillin, 100µg/mL streptomycin, 1mM HEPES (Quality Biological, Gaithersburg, MD,USA), and 1mM sodium pyruvate (Cellgro, Herndon, VA, USA) Cell cultures were supplemented with either CD40L-transfected Chinese hamster ovary (CHO) cells as a B cell stimulant (6×10^4 cells/well) or with 2µL/mL of stimulating anti-CD40 antibody (Invitrogen) and when noted, IL-4 (10,000U/mL; NIH) for nine days. Cell-free supernatants were then harvested and analyzed for IgE production by ELISA.

CHAPTER 3: Th2 helminth infected mice induce a strong B1 cell IgE response that is augmented by MDSCs.

3.3.1 ADAM10Tg mice lack B2 cell development, but elicit a strong IgE response during *N. brasiliensis* infection

ADAM10Tg mice lack B2 cells but have an intact B1 cell compartment

ADAM10Tg mice lack B2 cells due to a defect in hematopoiesis (discussed in section 2). In **Figure 49**, overexpression of the transgene markedly reduced the levels of pro/pre B cells and immature B cells ($B220^{hi}IgM^{+}$) in BM. This led to a near complete loss of peripheral B cells in secondary lymphoid organs (**Figure 49**). Analysis of B cells from peritoneal fluid revealed that levels of B1a ($B220^{int}CD11b^{+}CD5^{+}$) and B1b cells ($B220^{int}CD11b^{+}CD5^{-}$) in ADAM10Tg mice were not significantly altered compared to littermate (LM) controls, whereas B2 cells ($B220^{hi}CD11b^{-}CD5^{-}$) were nearly absent (**Figure 50**). Thus, the block in B cell development was specific to BM-derived B2 cells.

Figure 49. ADAM10 Overexpression blocks B2 B cell development

(A) Flow cytometric analysis of pro/pre B cells ($B220^{+}IgM^{+}$) and immature B cells

($B220^{hi}IgM^{+}$) in BM of littermate (LM) and ADAM10Tg progeny. (B) Flow cytometric

analysis of $CD3^{+}$ T cells and $B220^{+}$ B2 cells in the spleen of ADAM10Tgs or LMs. Data representative of three independent experiments.

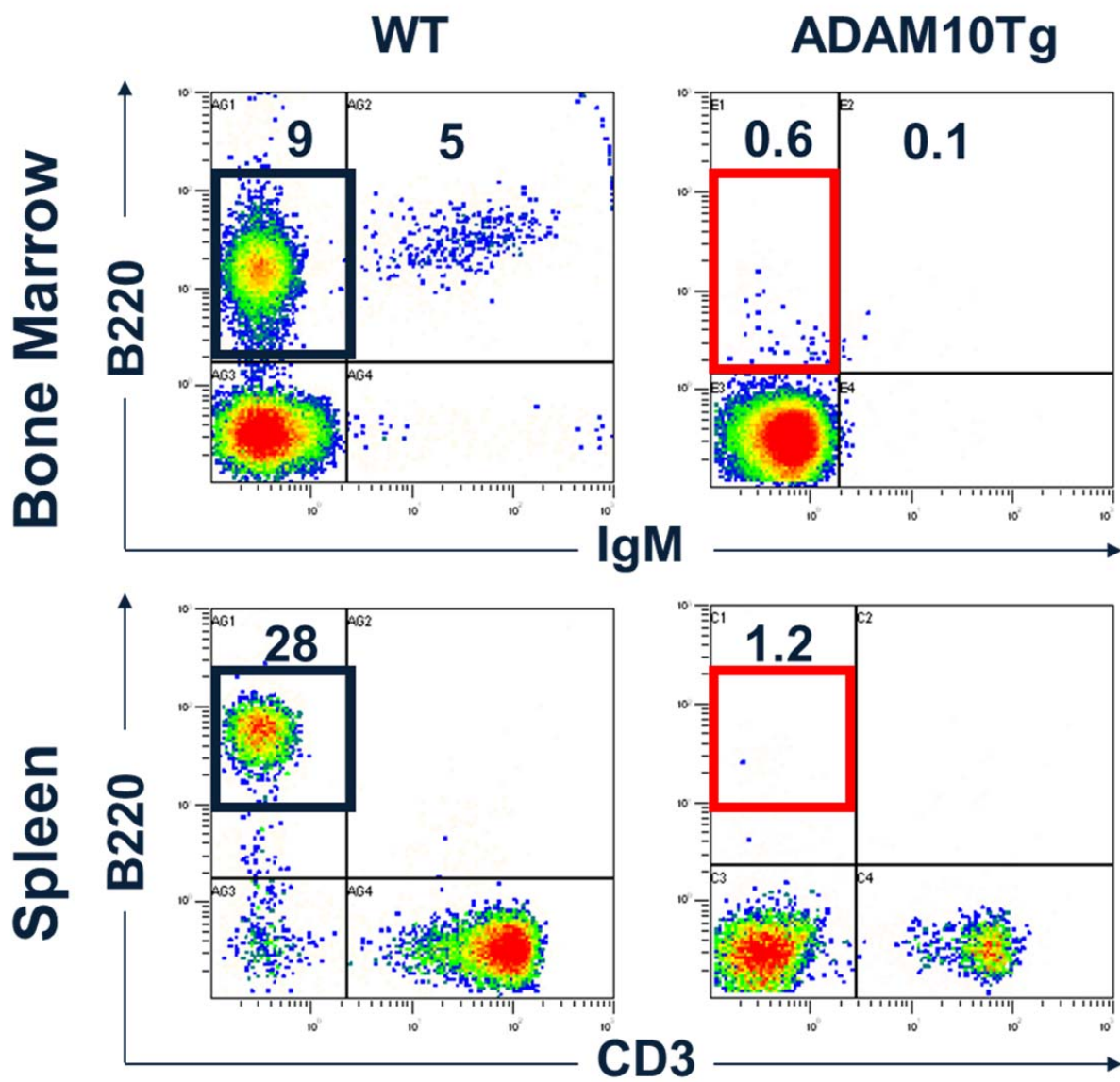
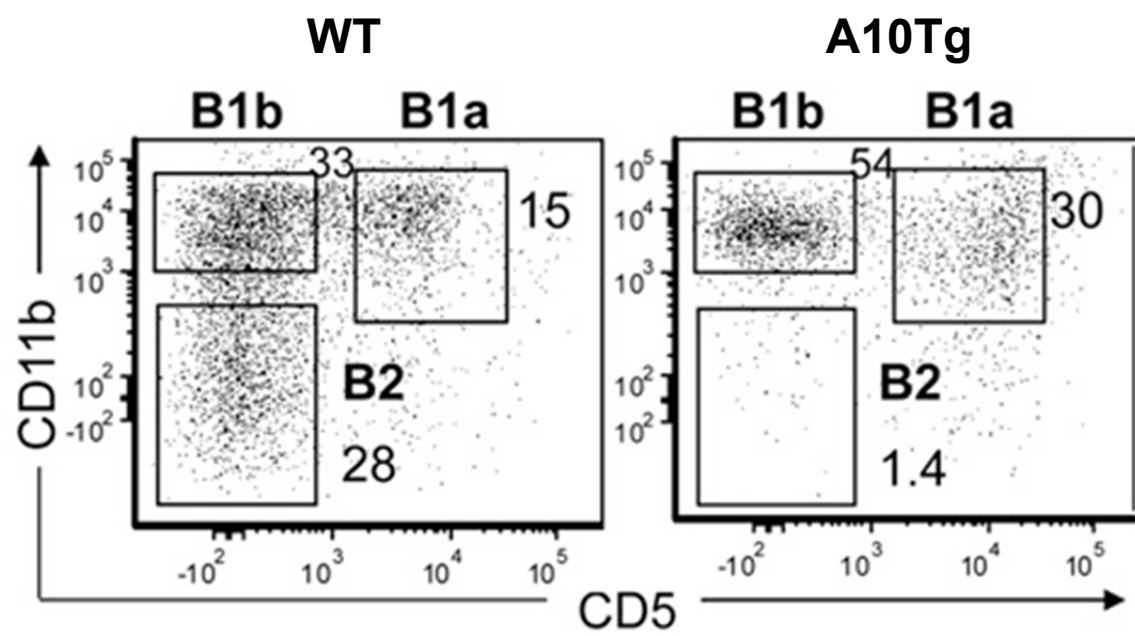


Figure 50. ADAM10 overexpression does not affect B1 cell development

Flow cytometry on B cell subsets in peritoneal lavage fluid. Panels are gated on B220⁺

cells. B2 cells: B220^{hi}CD11b⁺ CD5⁺, B1a cells: B220^{int}CD11b⁺CD5⁺, B1b cells:

B220^{int}CD11b⁺CD5⁺. This is representative of at least three experiments.



ADAM10Tg mice have increased B1 IgE production

As described in section 2, the ADAM10Tg mouse has an over accumulation of MDSCs *in vivo*. Mice were infected with *N. brasiliensis* to ascertain the role of MDSCs in Th2 helminth infection (section 2). A hallmark of *N. brasiliensis* infection is high IgE levels. Helminth infections are some of the most potent natural inducers of IgE synthesis. Knowing that the ADAM10Tg mouse lacked BM-derived B2 cells, all antibody production in the mouse is attributed to B1 cells. Throughout the infection, IgE levels were measured in the serum of ADAM10Tg mice versus WT mice with intact B2 cell development. Surprisingly, in the absence of B2 cells, the ADAM10Tg mouse has equivalent and at some time points, significantly increased total IgE (**Figure 51**). These mice additionally had augmented parasitic clearance with decreased worm burdens at L4 in the lung, L5 adult worm in the intestine and egg production in the feces (**Figure 18**). This indicates that amplified IgE levels were not due to elevated worm burden.

ADAM10Tg mice lack GC development

To confirm that CSR is occurring outside of GCs to produce IgE, *N. brasiliensis* infected ADAM10Tg mice were euthanized on day 14 post-infection and MLNs were harvested. MLNs are the principle draining LNs during the intestinal helminth infection. MLNs were examined for GL7, an activation antigen expressed on GC B and T cells. In ADAM10Tg mice, no GC cells were found (**Figure 52**). This confirms the hypothesis that B1 IgE production is occurring outside of normal GC development. MLNs were additionally examined for B220 and CD3 to look at LN structure (**Figure 53**). B220 staining was evident in small pockets of the ADAM10Tg node, representing fetal liver derived B1 B cells colonizing the MLNs (**Figure 53**). CD3⁺ T cells form pocket-like

structures behind the B1 cells. ADAM10Tg MLNs are also filled with Gr-1⁺ MDSCs as evident in **Figure 20**.

*B1 cells from WT *N. brasiliensis* infected mice stain positive for IgE*

To further understand if this B1 IgE production was specific to ADAM10Tg mice, we infected C57B/6 WT mice with *N. brasiliensis*. On day 7 post-infection, peritoneal lavage (PL) fluid and spleens were examined for B cell distribution (**Figure 54**) and each population was further assessed for IgE staining to help delineate the major population responsible for IgE production (**Figure 55**). Since, SHM, CSR and GC response usually take longer we were unable to detect B2 IgE staining. Interestingly, B1a cells stained positive for IgE, confirming that in WT mice, B1 cells are capable of IgE production. This early IgE is majorly attributed to B1a cells, but B1b cells additionally stained positive for IgE. Interestingly, the populations of B1 cells in the spleen had a higher percentage of IgE positive staining within the small populations of B1 cells (**Figure 55**). This IgE staining cannot be cytophilic IgE, as B1 cells are CD23 negative³⁵⁴.

*B1 cells from *N. brasiliensis* infected mice make IgE in vitro after stimulation with IL-4 and anti-CD40*

We next wanted to isolate B1 cells to see if we could induce IgE production *in vitro*. B1 cells were sorted from PL fluid of *N. brasiliensis* infected C57B/6 WT mice. Both B1 cell populations were sorted, B1a (B220^{int} CD11b⁺ CD5⁺) and B1b (B220^{int} CD11b⁺ CD5⁺). Cells were plated in vitro with anti-CD40 alone or anti-CD40 and IL-4. After nine days, cell-free supernatants were assessed for total IgE production by ELISA. Extremely large amounts of IgE were detected in supernatants from B1a cells and B1b

cells. Although both B1 populations made IgE, B1a cells, by far, made the highest IgE (**Figure 56**). Moreover, without addition of IL-4, B1 cells did not make any detectable IgE. To confirm that B1 IgE production is dependent on signals first experienced in helminth infection, we sorted B1 cells from naïve C57B/6 WT mice. B1a and B1b cell populations made significantly less IgE from naïve mice than when sorted from *N. brasiliensis* infected mice (**Figure 57**). This leads us to believe that possible cytokine signals, such as IL-5 or IL-4, induced in parasite infection are required for the B1 switch to IgE production.

Figure 51. ADAM10Tg mice make increased IgE during *N. brasiliensis* infection

Serum was collected from ADAM10Tg (open square) or WT (closed circle) mice on days indicated over the course of *N. brasiliensis* infection and assessed for total IgE by ELISA. IgE was assessed on days indicated by ELISA. * $p > 0.05$; n= at least five mice per group.

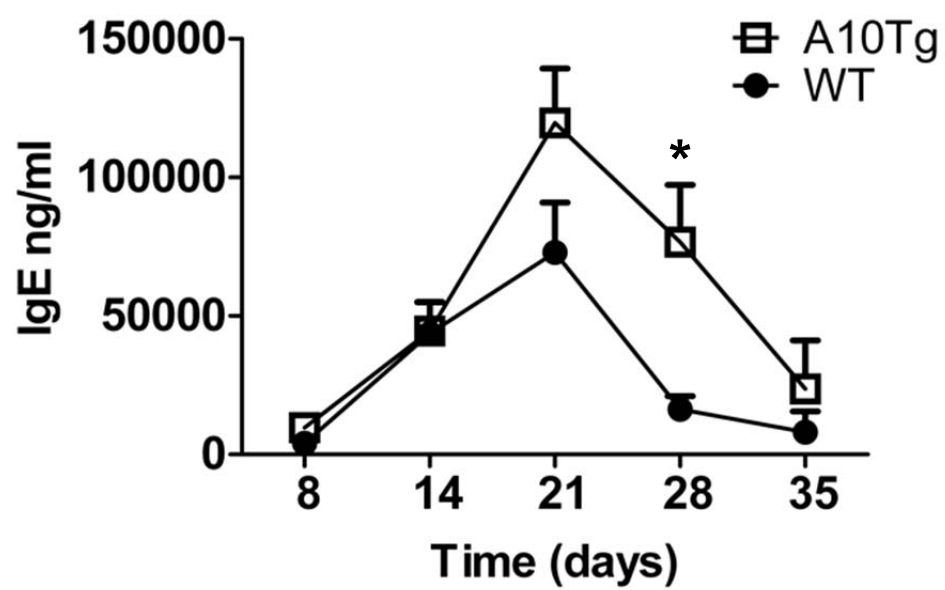


Figure 52. ADAM10Tg mice lack GCs

MLNs were harvested on day 14 post *N. brasiliensis* infection. MLNs were sectioned and stained with GL7 (green). Pictures were taken with a 10x objective and are representative of at least three independent experiments.

WT MLN

GL7

A10TgMLN

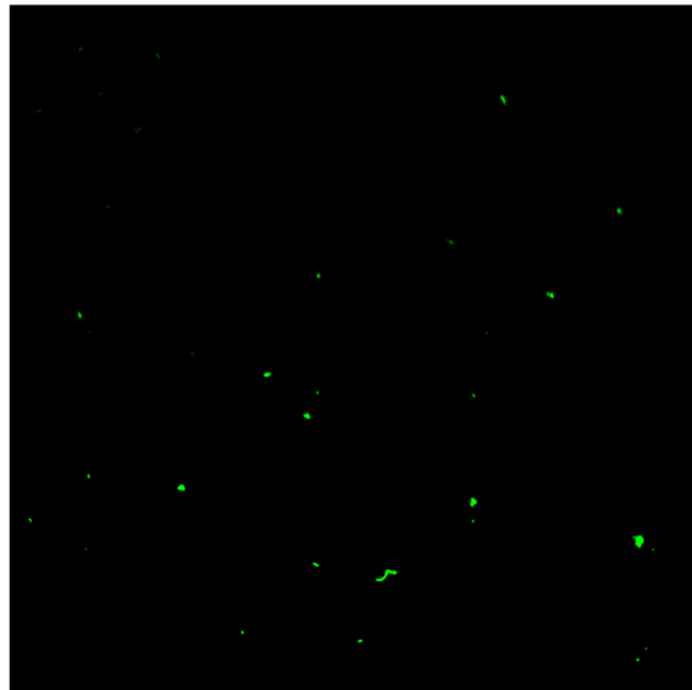
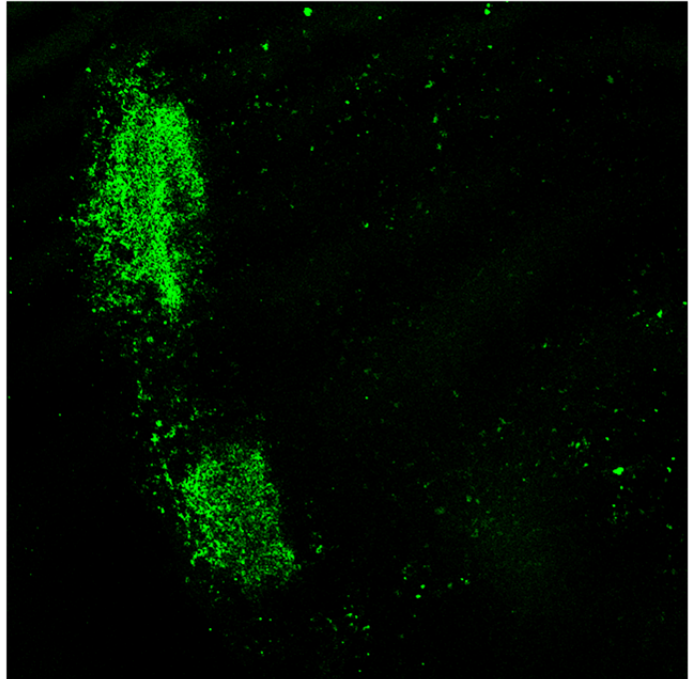


Figure 53. ADAM10Tg mice lack normal secondary lymphoid architecture

MLNs were harvested on day 14 post *N. brasiliensis* infection. MLNs were sectioned and stained with B220 (red) or CD3 (green). Pictures were taken with a 10x objective and are representative of at least three independent experiments.

WT MLN

B220/CD3

A10TgMLN

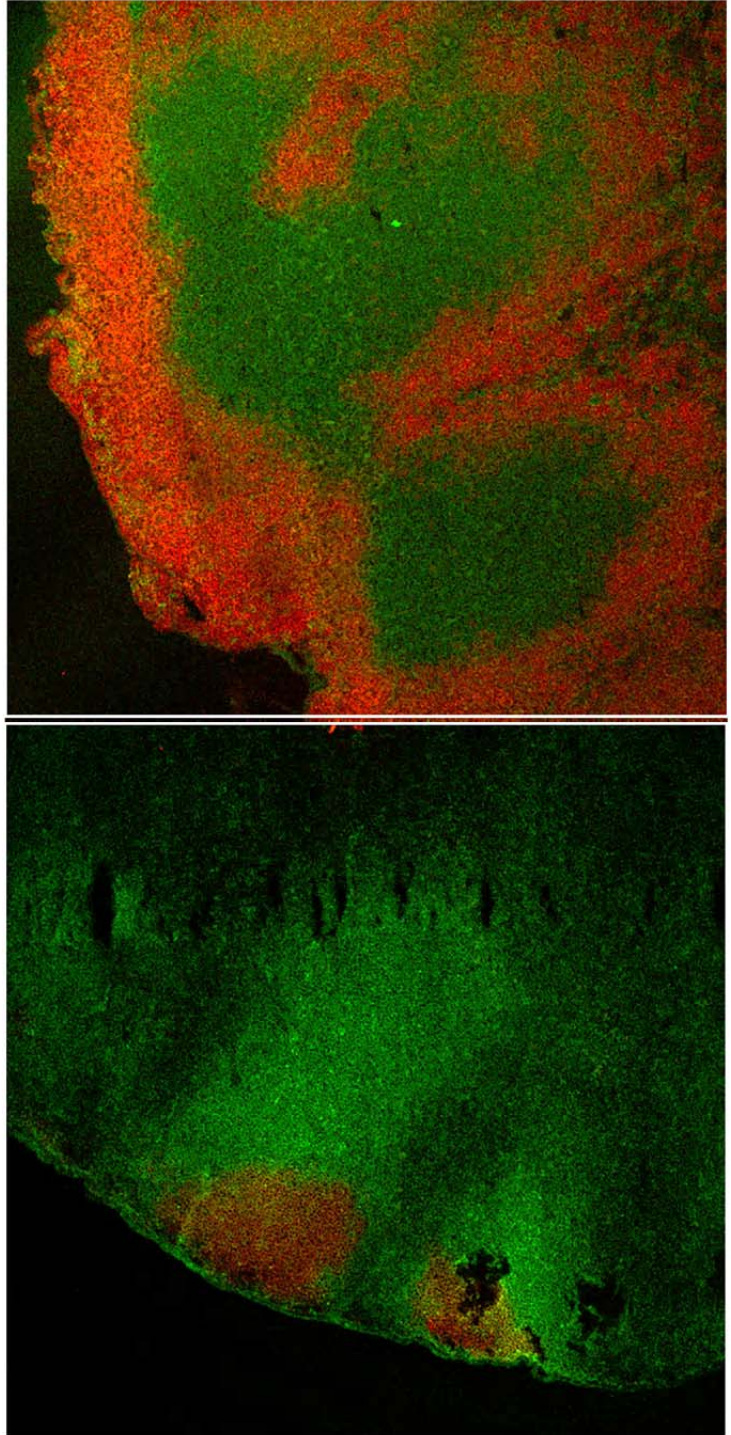


Figure 54. Peritoneal lavage and spleens from *N. brasiliensis* infected mice contain B1a, B1b and B2 cells

PL fluid and spleens were harvested from *N. brasiliensis* infected mice on day 7 post-infection. A. Flow cytometry plots of four mice showing PL fluid B1 and B2 cell populations from total live cells (top), PL distribution of B2, B1a and B1b cells gated from B220⁺ population (middle) and splenic distribution of B2 and B1 cell populations from total live cells (bottom). B. PL and spleen B1 and B2 cell percentages compiled. C. PL B2, B1a, and B1b cells percentages compiled. n= four mice per group.

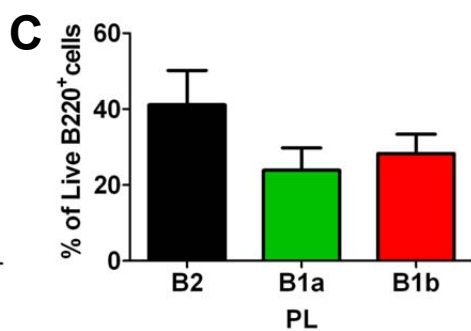
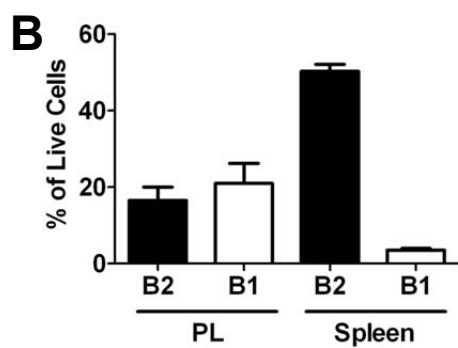
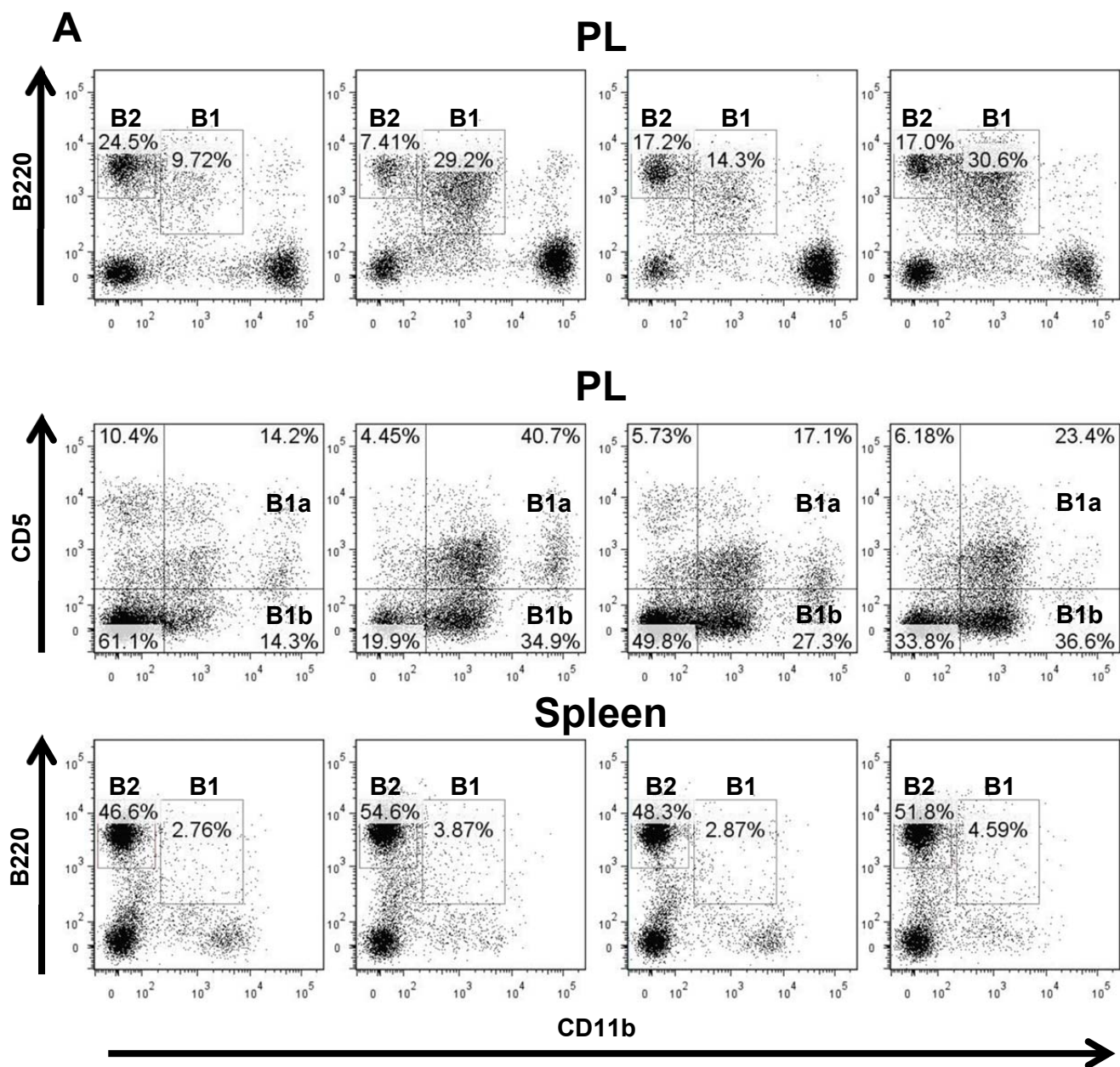


Figure 55. B1a cells from peritoneal lavage and spleens of *N. brasiliensis* infected WT mice stain for IgE

PL fluid and spleens were harvested from *N. brasiliensis* infected mice on day 7 post-infection. PL (A) or spleen (B) is shown in histograms representing IgE staining. B2 cells (black filled) are gated from **Figure 54A** (top for PL and bottom for spleens). B1a cells (green) and B1b cells (red) were gated as in **Figure 54A** (middle) for spleens and PL. C. Compiled percentages of IgE^{high} staining cells, as represented by black bars in (A) and (B). * $p > 0.05$, *** $p > 0.0005$; n=four mice per group. Statistics compare B1a vs B1b bars in both PL and spleen.

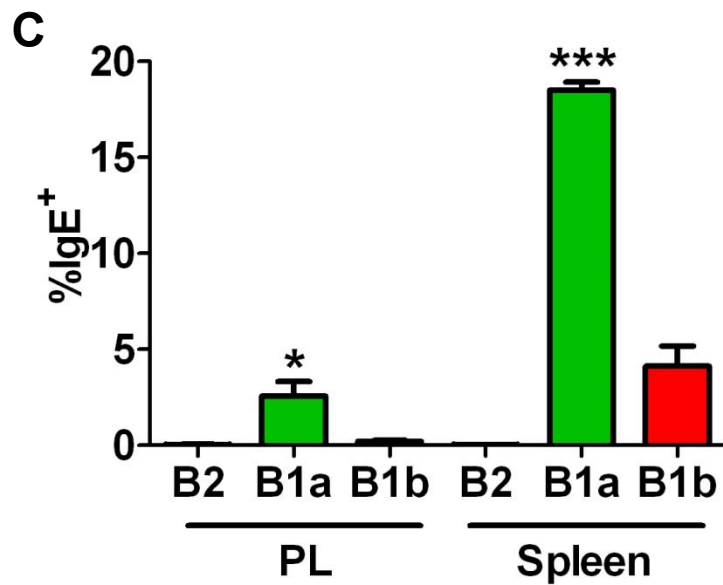
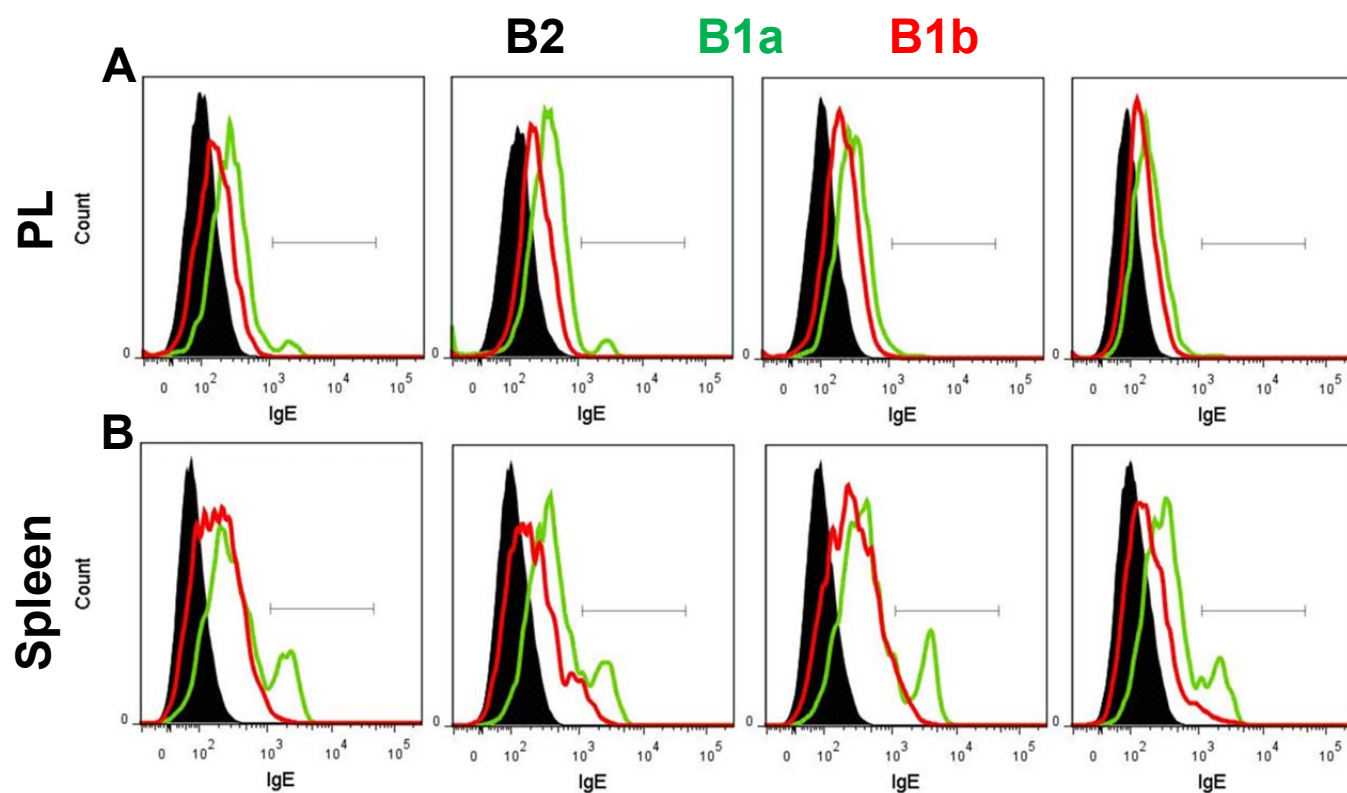


Figure 56. B1 cells sorted from peritoneal lavage fluid of *N. brasiliensis* infected mice make IgE *in vitro* after stimulation

PL fluid was sorted on day 7 post infection with *N. brasiliensis*. B1a cells were sorted as B220^{int}CD11b⁺CD5⁺ cells. B1b cells were sorted as B220^{int}CD11b⁺CD5⁻ cells.

Sorting was accomplished with 95% accuracy. Cells were plated at 50 thousand/well and stimulated with anti-CD40 and with IL-4 (red) or without IL-4 (blue) for 9 days as described in *Methods and Materials*. Total IgE was assessed from cell-free

supernatants by ELISA.***p>0.0005; n= three replicates per group. nd=none detected.

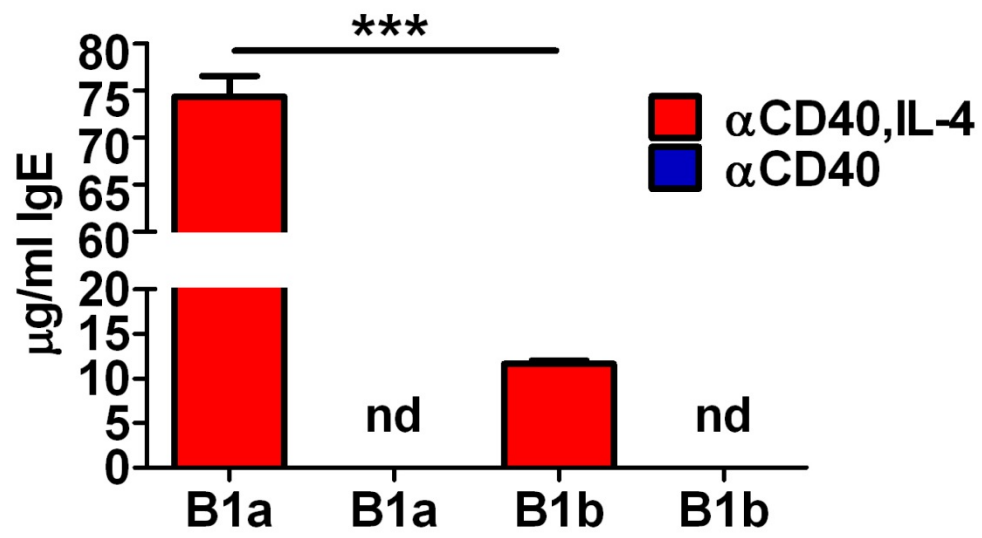
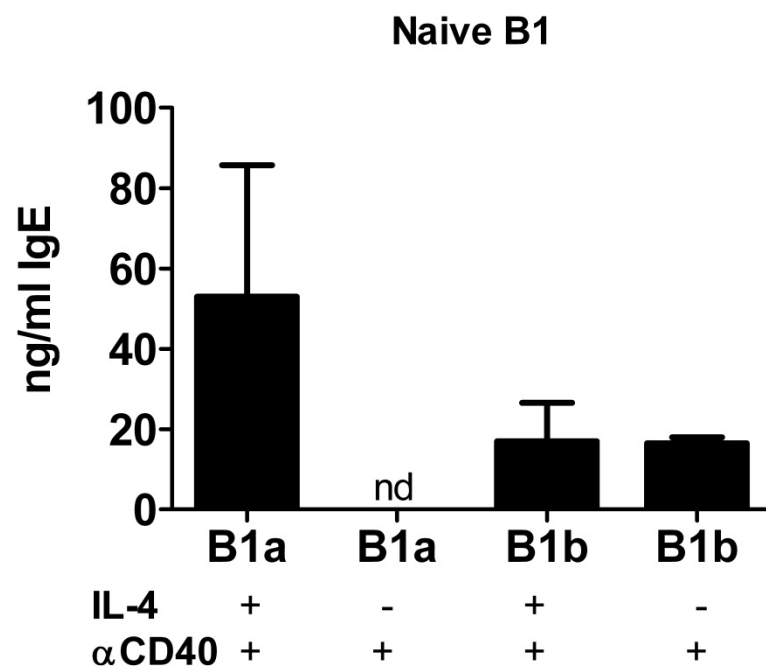


Figure 57. Naïve B1 cells secrete very little IgE without *N. brasiliensis* infection

PL fluid was sorted. B1a cells were sorted as B220^{int}CD11b⁺CD5⁺ cells. B1b cells were sorted as B220^{int}CD11b⁺CD5⁻ cells. Sorting was accomplished with 95% accuracy. Cells were plated at 50 thousand/well and stimulated with anti-CD40 and with or without IL-4 for 9 days as described in *Methods and Materials*. Total IgE was assessed from cell-free supernatants by ELISA. n= three replicates per group. nd=none detected



MDSCs enhance B1 IgE production in WT mice

To investigate whether MDSC accumulation during parasitic infection correlated with increased IgE, we administered GEM. GEM selectively depletes MDSCs without affecting lymphocyte levels^{309,310}. With GEM administration through the course of *N. brasiliensis* infection, IgE levels were significantly decreased (**Figure 58**). This lead to the hypothesis that B1 cells make IgE during helminth infection and this is augmented by the accumulation of MDSCs.

B1 cells have augmented IgE production that is independent of IgG1 and GCs

Next we examined IgG1 levels, as they are usually correlated with the increase in IgE. CSR occurs in the GC from μ to γ and then to ϵ . High affinity IgE antibodies are made this way³⁸⁰. CSR outside of the GC results in low affinity, polyclonal antibodies. It can occur with a direct switch from μ to ϵ ³⁸⁰. It is thought that B1 cells would switch to IgE in this manner. IgG1 levels in the ADAM10Tg mouse infected with *N. brasiliensis* are significantly decreased as compared to WT (**Figure 59**). GEM treatment does not alter this (**Figure 59**). This indicates that B1 cells during helminth infection do not undergo CSR through the intermediate γ heavy chain.

MDSC AT into naïve mice increases IgE production by B1 cells

Furthermore, since *N. brasiliensis* infection induced enhanced myelopoiesis and MDSC accumulation in WT mice (**Figure 21**), we established the hypothesis that artificial MDSC accumulation could additionally augment B1 IgE production. To test this, we injected MDSCs *i.p.* into C57B/6 WT mice 5 days and 1 day prior to sorting of B1 B cells from the PL fluid. In **Figure 60**, we show that MDSC accumulation indeed increases B1 IgE production

Figure 58. ADAM10Tg mice make increased IgE during *N. brasiliensis* infection that is reduced upon GEM treatment

ADAM10Tg mice were treated with GEM (closed square) as described in Methods and Materials. IgE was assessed on days indicated by ELISA. * $p < 0.05$; $n =$ at least five mice per group. Significance in indicates difference between ADAM10Tg and ADAM10Tg treated with GEM at time points indicated.

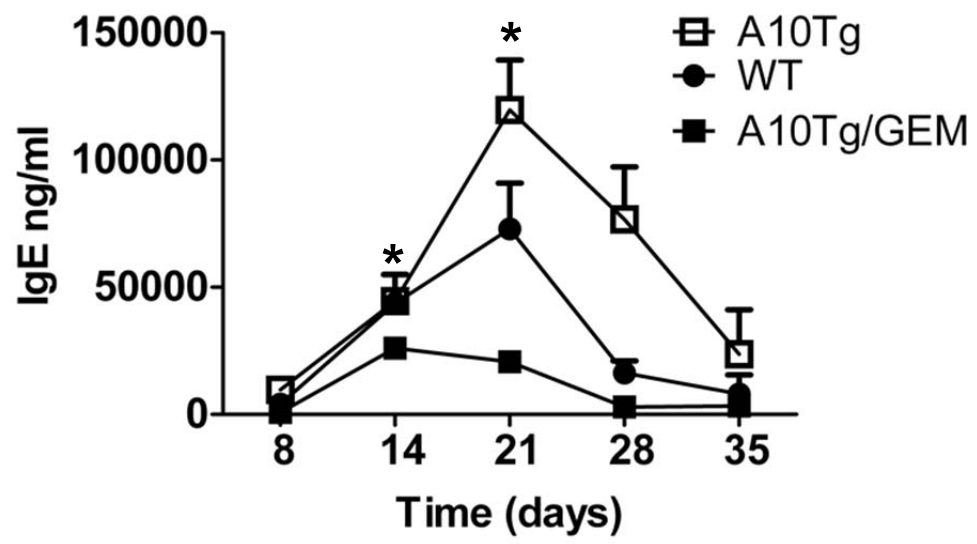


Figure 59. ADAM10Tg mice do not make increased IgG1 and GEM does not affect total IgG1 levels in *N. brasiliensis* infection

Total IgG1 levels were assessed by ELISA on days indicated. WT (blue), ADAM10Tg (red), and ADAM10Tg mice treated with GEM (purple) as described in *Materials and Methods*. * $p > 0.05$; n= at least five mice per group. Significance indicates difference between WT and ADAM10Tg at time point indicated.

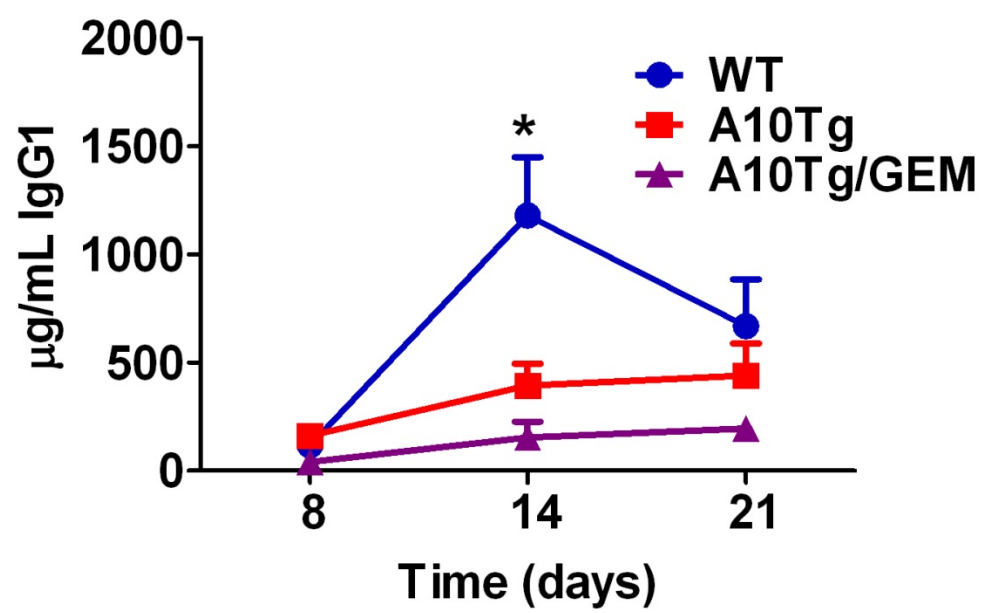
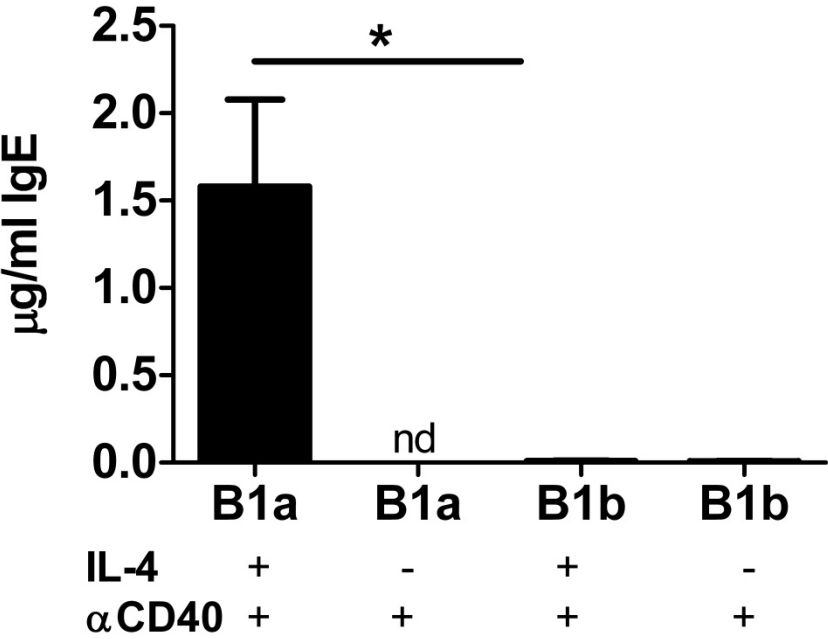


Figure 60. Adoptive transfer of MDSCs into Naïve WT mice induces B1 IgE production

PL fluid was sorted after AT of MDSCs, days -4 and -1 pre-sort. B1a cells were sorted as B220^{int}CD11b⁺CD5⁺ cells. B1b cells were sorted as B220^{int}CD11b⁺CD5⁻ cells.

Sorting was accomplished with 95% accuracy. Cells were plated at 50 thousand/well and stimulated with anti-CD40 and with IL-4 for 9 days as described in *Methods and Materials*. Total IgE was assessed from cell-free supernatants by ELISA. *p>0.05; n= three replicates per group. nd =none detected.

Naive B1+MDSCs



3.3.2 Discussion

The relationship between helminth infection and high IgE is a strong one. Over the years, this has been linked to the absence of allergic disease in countries with widespread parasite infection^{382,383}. Th2 helminthes are strong inducers of IgE³⁸⁴. IgE made in response to these infections are a mix of non-specific, low affinity IgE and high affinity, parasite-specific IgE³⁸⁵. Studies show that this ratio of high affinity to low affinity IgE changes depending on how infected the individual is. Individuals with high parasite burdens have mostly low-affinity, non-specific IgE. Individuals with a low parasite burden have increased parasite-specific IgE³⁸⁵.

N. brasiliensis is a Th2 helminth, similar to the human hookworm. In WT animals, IgE production is not necessary to clear the parasite, as IgE^{-/-} mice clear it effectively³⁸⁶. It is thought that the induction of the IgE response is an evolutionary characteristic of the helminth and that induction of large amounts of non-specific and low-affinity IgE protects it from high-affinity IgE³⁸⁴. Studies with the human hookworm show the opposite, that a high level of non-specific IgE is associated with decreased fecundity and reduced growth of adult worms³⁸⁷.

The source of this low-affinity IgE was always thought to be FO B cell in origin. Until recently, B1 cells have only been hinted at having the ability to class switch to IgE. Here, we show that ADAM10Tg mice lacking FO B cells induce high levels of IgE in response to infection with *N. brasiliensis* (**Figure 51**). This IgE production correlates with the increased MDSCs seen in these ADAM10Tg (**Figure 51**). Additionally, low-affinity antibody is thought to be mediated through a direct μ to ϵ -heavy chain switch³⁸⁰. In our mice we show that IgG1 levels remain unchanged, reinforcing that B1 cells direct

switch to IgE (**Figure 59**). This switch additionally occurs outside of the GC response (**Figure 52**). We also show that this occurs in WT *N. brasiliensis* infected mice and can reproduce it *in vitro* (**Figures 56,60**).

In vitro B1 production of IgE required that the mouse be infected with the parasite before sorting the cells out of the peritoneal cavity. *N. brasiliensis* infection up-regulates many cytokines associated with Th2 allergy³⁸³. IL-13, IL-4, IL-5, IL-9, IL-33 and IL-25 are all associated with parasitic infection³⁸³. Many of these have been previously associated with B1 cell antibody production or proliferation^{350,372}.

An unknown signal is first needed to activate the B1 to make IgE that is associated with parasitic infection. MDSCs accumulate naturally in response to parasitic infection (**Figure 21**). We hypothesize that MDSCs that accumulate in helminth infection are the natural source of this signal. ADAM10Tg mice have an over-accumulation of MDSCs and have increased B1 IgE production (**Figure 51**). In the absence of parasitic infection, AT of MDSCs directly into the peritoneal cavity of mice increased sorted B1 IgE production *in vitro* (**Figure 60**). This reinforces that MDSCs may be providing this activation for the B1 cell. In our ADAM10Tg mouse we find elevated levels of IL-4, IL-5, IL-13, IL-1, and IL-33 (**Figure 19**). Post-sort, IL-4 is required for B1 IgE production, but it is not enough to induce B1 IgE in naïve mice (**Figure 56 and 57**). Additionally, anti-CD40 is required (**Figure 56**). This alludes to the need for CD40 ligand stimulation. Traditionally, the CD4⁺ Th cell would have been thought to provide this signal, but many other cells express CD40L, including: mast cells, DCs, basophils, macrophages, and eosinophils³⁸⁸. So, this signal could come from many different sources.

With flow cytometry and *in vitro* cultures, we show that B1a cells are producing more IgE than B1b cells (**Figures 55 and 56**). In previous studies, the B1b cell has been eluded to as being capable of IgE production^{360,361}. We do not dispute this, as we additionally see B1b IgE production (**Figures 55 and 56**). But, our data indicates that B1a cells may be the source for the majority of B1 IgE. Overall, we definitively show that B1 cells can switch to IgE during helminth infection and that these cells may be responsible for the high levels of non-specific IgE found in parasitic infection. We additionally reveal a novel role for the MDSC as a potent inducer of B1 IgE synthesis.

Section 4

Chapter 1: CD23⁺ B cell-derived exosomes mediate IgE-antigen complex mediated immune stimulation

4.1.1 Introduction

Antibody, in complex with its antigen, provides the immune system with a feedback response against the complexed antigen. This feedback mechanism results in immune stimulation or suppression depending upon the antibody class (reviewed in³⁸⁹). IgE, complexed with antigen, has long been shown to induce a significantly increased immune response over antigen alone. This response results in increased antigen specific T cell proliferation and antigen specific IgG *in vivo*³⁹⁰. The low affinity receptor for IgE (CD23) is traditionally known for its role in the negative regulation of IgE synthesis. But, CD23 has additionally been known to internalize IgE antigen complexes and promote antigen presentation. Extensive studies using CD23^{-/-} animals proved CD23 to be essential to the immunostimulatory properties of IgE antigen complexes³⁹⁰. Combining antigen presentation properties of CD23 with the observed immunostimulation led to the hypothesis that antigen presentation by CD23⁺ B cells was responsible for these activities. This hypothesis was challenged by the recent finding that B cells rapidly transfer the antigen to the spleen³⁹¹ and were dispensable after 4 hours post IgE antigen complex injection. After that period, DCs were required³⁹². These intriguing findings suggested that IgE antigen complexes or fragments thereof were being carried to the secondary lymphoid system, in this case the spleen, by CD23⁺ B cells and then were being transferred to DCs. This led to the obvious question, what

is the mechanism of this transfer? *Henningson et al*³⁹² suggested two possibilities; trogocytosis by DCs or exosomal mediated transfer from B cells to DCs.

Exosomes are defined as tiny membrane bound particles ranging from 30-150nm. Although originally discovered in the 1980s and thought to be primarily for cellular waste²⁰⁹, exosomal research has undergone a resurgence given the protein and micro-RNA cargo that is packed into these particles (reviewed in³⁹³). In a previous publication, we demonstrated that CD23 and its protease, ADAM10 were found in B cell derived exosomes (bexosomes) from both mouse and human B cells³⁵. Additionally, β_2 -adrenergic stimulation of B cells further increased both CD23 and ADAM10 levels in bexosomes³⁹⁴. In this study we show that B cells stimulated with anti-CD40 and IL-4, in the presence of IgE antigen complexes, release bexosomes that contain both CD23 and IgE. In agreement with earlier studies³⁹⁵, these bexosomes were capable of directly stimulating antigen specific T cells *in vitro*, presumably via the MHC peptide complexes found on these bexosomes. Intriguingly, this stimulation was greatly enhanced if the bexosomes were isolated from B cells stimulated in the presence of IgE antigen complexes, and this enhanced stimulation was CD23 dependent. This data supports earlier *in vitro* studies where B cells were shown to directly present IgE antigen complexes, taken up via CD23, to T cells³⁹⁶. Yet, *in vivo*, direct injection of bexosomes did not cause increased T cell proliferation, which agrees with the requirement of DCs³⁹². In contrast, culture of bexosomes with bone marrow derived DCs (BMDC), followed by isolation and injection of DCs did directly enhance *in vivo* antigen specific T cell proliferation. Overall, this supports the hypothesis that bexosomes are responsible for antigen transfer from B cells to DCs, thus, providing a mechanism and suggesting a

model to explain the importance of DCs in the immunostimulatory activity of IgE complexes.

Chapter 2: Materials and Methods

4.2.1 Mice

Mice were maintained in the Virginia Commonwealth University animal facility in accordance to guidelines for the humane treatment of laboratory animals set forth by the National Institutes of Health and the American Association for the Accreditation of Laboratory Animal Care. C57BL/6 and BALB/C mice were purchased from Jackson Labs; DO11.10 and OTII mice were progeny from breeding pairs purchased from Jackson Laboratory. CD23 knockout (BALB/C)³⁹⁷ or B cell specific ADAM10 deficient mice (ADAM10^{B/-})(BALB/C backcross at least s6 generations)²⁴⁷ were bred in house. All mouse protocols were approved by the Virginia Commonwealth University Institutional Animal Care and Use Committee.

4.2.2 Exosomal Cell Cultures

All fetal bovine serum (FBS) used in exosome cultures was first centrifuged at 100,000xg for 1 hour to deplete bovine exosomes. Splenic B cells were isolated using B220 positive magnetic bead selection as per manufacturer protocol (Miltenyi Macs system) and cultured for 3 days in 6 well plates at 1×10^6 cells/mL in cRPMI 1640²⁹ containing 1 µg/mL anti-CD40 (HM40-3) (Biolegend) and 10,000 U/mL IL-4 (gift from Bill Paul NIH). When indicated, 10 µg/ml of anti-TNP- IgE (IGELb4)³⁹⁸ was present. When larger amounts of exosomes were needed, B lymphoma line M12.4.5 (M12)³⁹⁹ was used. M12 cells (1×10^6 cells/mL – total cell number $3-5 \times 10^8$) were cultured for 24 hrs in cRPMI 1640/10% FCS containing anti-CD40, IL-4, and anti-TNP (IGELb4) or anti-DNP IgE (10 µg/mL)^{398,400}.

4.2.3 Exosomal Isolation

Exosomes were isolated as previously described³⁴. Briefly, apoptotic bodies in cell free supernatants were removed by centrifugation at 27,000 x g for 20 minutes. Finally, exosomes were harvested by spinning at 100,000 x g for 1 hour; the exosome pellet was resuspended in 5 mL of HBS plus 2mM Ca²⁺ and pelleted again at 100,000 x g for 1 hour. Final exosome pellet were resuspended in HBS plus 2mM Ca²⁺ and then passed through a 0.2µm filter to remove particles larger than 200 nm and to assure sterility. Bradford Assay exosome yields were approximately 1.0-1.62 µg/µL, from B cell cultures and about 10-fold higher with M12 cultures depending upon original cell number.

4.2.4 Western Blotting

Western Blots were performed using 10% Bis-Tris gels and a mini gel system (Life Technologies). Equal amounts of exosome protein (20 µg) were loaded. NuPage MES SDS Running Buffer and NuPAGE MES Transfer Buffer were used according to manufacturer's instructions. After electrophoresis and transfer to nitrocellulose paper, blocking was performed using 5% powdered milk solution /0.05% v/v Tween-20 (two hours) followed by the primary antibody incubation (1 hour minimum) followed by HRP secondary antibody. Detection was observed by appropriate film exposure. Antibodies used were as follows: Mouse anti-mouse MHCII H2-I/Adβ (5K43) (Santa Cruz); Rabbit anti-mouse IgE (Fc specific) (Acris); goat anti-rabbit HRP (Southern Biotech); Rabbit anti-mouse CD23 as described⁴⁰¹.

4.2.5 Specific T cell proliferation:

In vitro

DO11.10 T cells were isolated using magnetic bead selection (Miltenyi Macs)B220⁺, CD11b⁺ and CD11c⁺ cells were depleted and then CD4 positive T cells were isolated using L3T4, non-activating selection. Bexosomes (15-20 µg /100 µL) were added to 1 x 10⁵ DO11.10 T cells in a final volume of 200 µL cRPMI/well in 96 well plates; TNP or DNP-OVA was added in indicated amounts. After 96 hours, cells were pulsed with 1 µCi/well of [H3]-thymidine for 24 hours (Perkin Elmer). Plates were then harvested using a Filtermate cell harvester onto GFC plates. Assays were read using a Topcount Plate Counter (Perkin Elmer, Waltham, MA).

In vivo

(B cell specific ADAM10 deficient) ADAM10^{B-/-}BALB/C or WT BALB/C mice were injected with IgE immune complexes (20 µg TNP-OVA + 50 µg anti-TNP-IgE³⁹². For bexosome or BMDC derived dexosome experiments, bexosomes were added to the DC cultures for 24 hours. After washing, LPS was added and cultures were continued for 72 hours and dexosomes were then isolated by centrifugation. Dexosomes, BMDCs or bexosomes or were i.v. injected into BALB/C mice that had been adoptively transferred (AT) with DO11.10 total splenocytes 24 hours previous. After 3 days, DO11.10 cell numbers in the spleen were determined either by flow cytometry or immunohistochemistry as described³⁹².

4.2.6 Flow Cytometry/Immunohistochemistry

Single cell suspensions were labeled with antibodies for cytometric analysis. Antibodies included unlabeled anti-mouse FcγR (2.4G2), FITC-conjugated anti-mouse DO11.10 (KJ1-26) (Biolegend), and PE-conjugated anti-mouse CD4 (145-2C11) (Biolegend). Flow cytometric analysis was performed using the Canto (BD Biosciences). Data analysis was conducted using FlowJo software v7.6.5 (Tree Star). Sections were prepared from frozen tissue and fixed with cold Acetone. Sections were blocked using 5% normal horse serum plus 1.5% BSA. Sections were stained using Biotinylated anti-DO11.10 (KJ1-26) followed by Streptavidin-APC and anti-B220-PE (RA3-6B2) (Biolegend). Slides were cover slipped utilizing Vectashield Hardset (Vector Labs) and imaged on the Leica TCS-SP2 AOBS CLSM Confocal laser-scanning microscope.

4.2.7 BMDC culture

Mouse bone marrow-derived dendritic cells (BMDC's) were derived from femurs of WT mice and cultured in complete RPMI (cRPMI) 1640 containing 10% FBS, 2mM L-glutamine, 100 U/mL penicillin, 100µg/mL streptomycin, 1mM HEPES (Quality Biological, Inc.), and 1mM sodium pyruvate (Cellgro). Cultures were supplemented with IL-4 1ng/mL (Peprotech) and GM-CSF 50ng/mL (Peprotech). Mature BMDC were harvested after 6 days of culture³⁹⁵.

4.2.8 Statistical Analysis

Analyzed as in section 1.2.8.

Chapter 3: IgE/Antigen Complexes stimulate OVA specific T cell proliferation

4.3.1 Results and Discussion

IgE is associated with bexosomes in a CD23 dependent manner.

As mentioned, CD23 and ADAM10 are both found associated with bexosomes³⁵. In order to determine if IgE is additionally associated, B cells were stimulated with anti-CD40 \pm IL-4 in the presence of IgE/Ag ICs. After 48 hours of culture, bexosomes were isolated by centrifugation. Equal amounts of protein were analyzed by Western blotting. **Figure 61A** shows that IL-4 stimulated B cells increases bexosomal CD23 levels. The blot indicated equal MHC class II expression. Interestingly, MHC class II levels were not increased by IL-4, in contrast to the well-known cell surface increase induced by this cytokine. In an earlier study using LPS as the activator³⁵, we found that ADAM10 was needed for bexosomal CD23 expression. With anti-CD40, CD23 is present even if ADAM10^{-/-} B cells are used; although the CD23 expression level is lower (data not shown). This indicates that CD40 activation is more efficient in allowing CD23 incorporation into bexosomes. In **Figure 61B**, the blot is examined using an ϵ -specific anti-IgE antibody, and lane 1 shows a strong 85Kd band indicates the presence of IgE. The amount of IgE was additionally increased in the presence of IL-4 (lane 2). This band was not present when B cells lacking CD23 were used (lanes 3 and 4) regardless of IL-4 stimulation. Thus, CD40-mediated CD23⁺ B cell activation results in release of bexosomes that contains CD23 and bound IgE. To examine if bexosomes additionally expressed co-stimulatory molecules in addition to MHCII, Bexosomes were blotted for CD80 and CD86 expression (**Figure 62**).

Increased in vivo antigen specific T cell proliferation is seen with bexosomes from anti-CD40/IL4 activated B cells when IgE/antigen complexes are present in the culture.

As mentioned above, bexosomes are known to induce antigen specific T cell proliferation if isolated from B cells cultured in the presence of the specific antigen³⁹⁵. The finding (**Figure 61**) that CD23 and IgE are present in bexosomes suggests that MHC class II peptide loading should be enhanced when IgE complexes are included in the culture. That this is indeed true is shown in **Figure 64A** where the initial B cells were cultured with increasing amounts of antigen (TNP-OVA) alone or the same plus anti-TNP-IgE. With B cells from either BALB/C or C57BL/6 mice and the corresponding strains of OVA-specific T cells, DO11.10 (**Figure 64A**) or OTII (**Figure 65**), increased specific T cell proliferation is seen when antigen specific IgE is present in the cultures. This data looks quite similar to the studies that initially demonstrated the enhanced antigen-presentation by IgE complexes with CD23⁺ B cells³⁹⁶ and relates to enhanced MHC class II loading due to the increased antigen found in the endosomal compartments. Confirmation that both IgE and CD23 are necessary for the bexosomal induced T cell proliferation is shown in **Figure 64A** where increased T proliferation is only seen when both are present. To determine whether ADAM10 was also needed for the enhancement of presentation, we turned to *in vivo* studies. WT or B cell-specific ADAM10 deficient (ADAM10^{B-/-}) BALB/C mice were *i.v.* injected on day -1 with 30 million DO11.10 total splenocytes. On day 0, they were *i.v.* injected with anti-TNP IgE/TNP-OVA complexes (Methods). Three days later, OVA-specific T-cell proliferation was determined by flow cytometry and immunohistochemistry. WT mice injected with IgE/Antigen complexes had increased DO11.10 proliferation, as indicated by the

number of antigen specific T cells in the spleen, as compared to WT OVA injected (**Figure 64B**). This was as expected. But, the ADAM10^{B-/-} mice had significantly more DO11.10 proliferation than did the WT. This finding was further confirmed by immunohistochemistry, where proliferation differences generally look more pronounced. The enhanced OVA-specific DO11.10 cell number in the T cell region of the spleen of the ADAM10^{B-/-} was clearly evident (**Figure 64C**). Thus, B cell ADAM10 is clearly not necessary for IgE antigen complex stimulation since this enhancement is seen. As the ADAM10^{B-/-} mice have been shown to have enhanced CD23 expression⁵⁶, we hypothesize that the increased CD23 leads to still further IgE-antigen incorporation with enhanced MHC class II loading in the endosomal compartment, leading to the results shown in **Figure 64B** and **C**. These studies also indicate that MZB are not necessary for IgE-antigen complex immunostimulation, since MZB are absent in ADAM10^{B-/-} mice⁵⁶. It also agrees with the observation that IgE complexes were found bound to mainly FO B cells and not to MZ B cells³⁹².

Bexosomes must first go through DCs in order to stimulate T cells in vivo.

To directly test if bexosomes from B cells activated with anti-CD40 and IL-4 would stimulate T cells *in vivo*, bexosomes were isolated from B cells activated as in **Figure 64A** with IgE/OVA complexes. They were injected into BALB/C mice AT with OVA-specific DO11.10 cells. This was ineffectual, so to increase the level of bexosomes for injection, 3 x 10⁸ M12.4.5 cells were activated instead of primary B cells. Bexosomes were isolated and injected into the OVA-specific T cell AT mice. In neither situation did we observe increased levels of OVA-specific T cell proliferation when the spleen was examined 3 days post bexosome injection (data not shown). We

considered that the most likely reason for this failure was that the bexosomes were not efficiently crossing the HEV to enter the peri-arteriolar lymphoid sheath (PALs) tissue. To increase chance for HEV crossing, bexosomes were cultured with LPS activated BMDCs, and DC were isolated 3 days post culture with bexosomes. In contrast to directly injected bexosomes, passage of the bexosomes through DCs, with injection of the DCs did cause a small but significant increase in OVA-specific proliferation, as determined by flow cytometry (**Figure 66**). This increase was significantly higher than what was seen by control DCs isolated from LPS activated cultured with the same amount of TNP-OVA alone or increased amounts. While the increase in T cell proliferation was not as dramatic as seen when directly injecting IgE immune complexes (**Figure 64B and Figure 66**), the results are clearly compatible with exosomes being responsible for the transfer of antigen to DCs as described by *Henningsson et al*³⁹². Thus, we propose the following model (**Figure 67**): IgE immune complexes are picked up by CD23⁺ B cells and this allows efficient transfer into the spleen. Once there, bexosomes are released and picked up by DCs which then activate antigen specific T cells and subsequently give the enhanced humoral response that is seen in IgE antigen complex injected animals³⁹⁶. Future studies could examine ways to increase transfer of the bexosome incorporated MHC class II cargo to DCs. If successful, this would allow immunization strategies that take advantage of the IgE immune complex stimulation that would bypass any difficulties seen by FcεRI interaction with IgE and antigen, and still allow efficient sensitization with low amounts of antigen.

Figure 61. IgE and CD23 are associated with bexosomes

(A) Bexosomes were isolated from B cell cultures stimulated with anti-CD40 \pm IL-4 or IgE as indicated. Equal bexosome protein was loaded on each lane and the blot was probed with polyclonal anti-CD23. Blot was stripped and probed with anti-MHC class II and the result is shown at the bottom of (A). (B) Exosomes from B cell cultures stimulated with anti-CD40 and IgE (All lanes). IL-4 stimulation is as indicated. Lanes 1 and 2 are bexosomes from WT mice, Lanes, 3 and 4 are bexosomes from CD23^{-/-} mice.

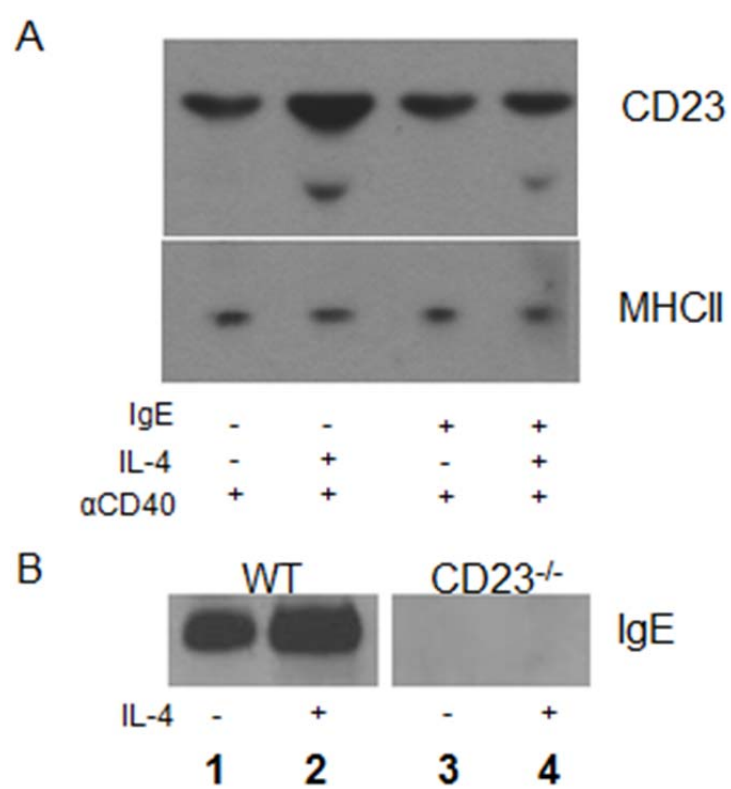


Figure 62. Bexosomes express co-stimulatory molecules CD80 and CD86

B cells were cultured in exo-free cRPMI under stimulation conditions with anti-CD40 and IL-4. Exosomes were isolated after several centrifugation steps. Western blotting was performed on (1) whole B cell lysates or (2) B cell derived exosomes lysates.

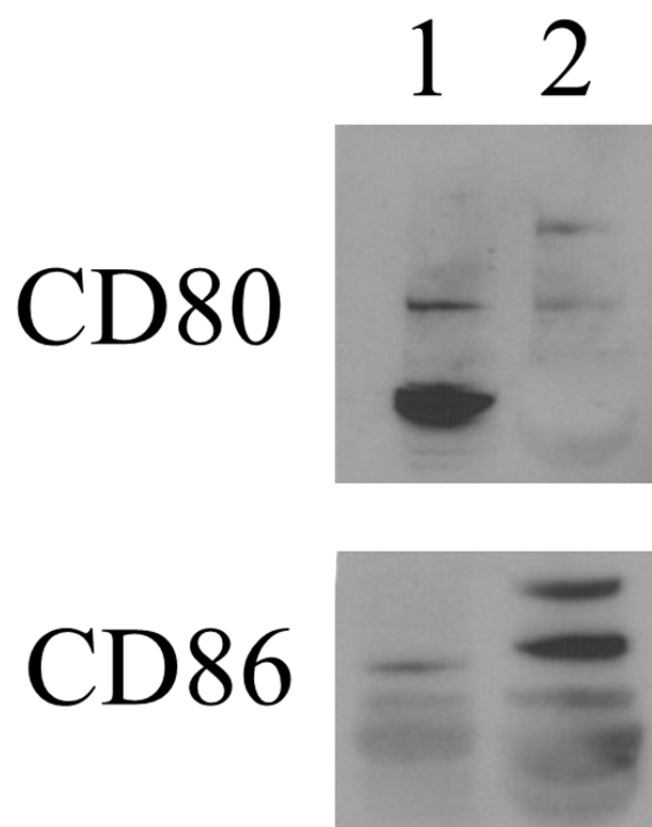


Figure 63. B cell derived exosomes by electron micrograph

For the negative staining, exosomes were placed on formvar-coated 150-mesh copper grids. The grid, formvar side to the sample, was then placed on top of the drop of sample and allowed to rest for 1 minute. Next a drop of the stain was placed on the parafilm and the grid was put on top of it for 1 minute. After 1 minute, the grid was picked up, and the excess stain was wicked off. The grid was then allowed to dry completely before scoping. Final developing solutions were tested: 1% Uranyl acetate, which gave a grainy image, and 1% Phosphotungstic acid at pH 7.0.

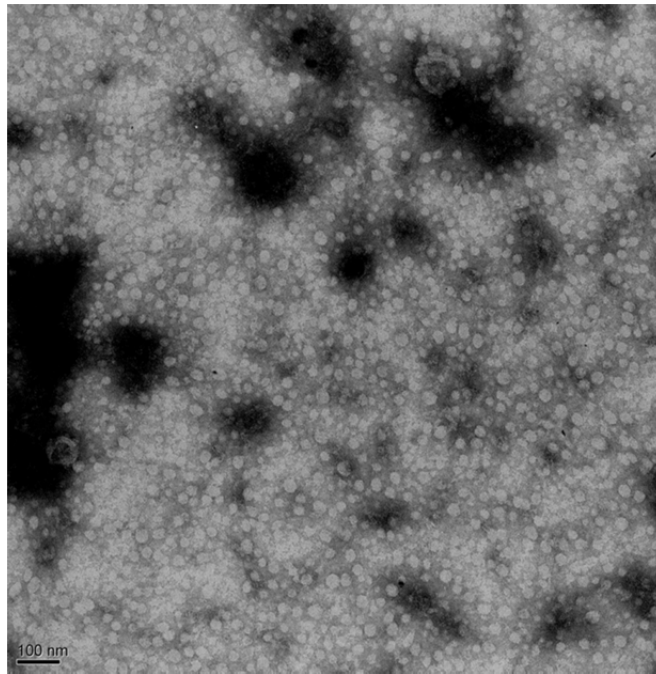


Figure 64. Bexosome-induced antigen specific T cell proliferation is enhanced by IgE, only when CD23 is present and *in vivo* IgE immune complex T proliferation is enhanced in ADAM10B^{-/-} mice

(A) B cell cultures stimulated as in *Methods*. B cells were incubated with or without IgE for 24 hours and then IgE/Ag ICs were added. Bexosomes were isolated. B cells were from either WT or CD23^{-/-} mice. Bexosomes and purified Ag-specific DO11 T cells were cultured for 3 days and proliferation determined using a [3H]-thymidine pulse (*Methods*). (B,C) On day -1 WT or ADAM10B^{-/-} mice were given Ag-specific DO11 T cells and on day 0 immunized with IgE/Ag ICs (*Methods*); on day 3, spleens were removed and examined for expanded Ag specific DO11⁺ CD4⁺ T cells by flow cytometry (B) or immunohistochemistry (C). *p>0.05, ***p>0.0005; n=at least five per group

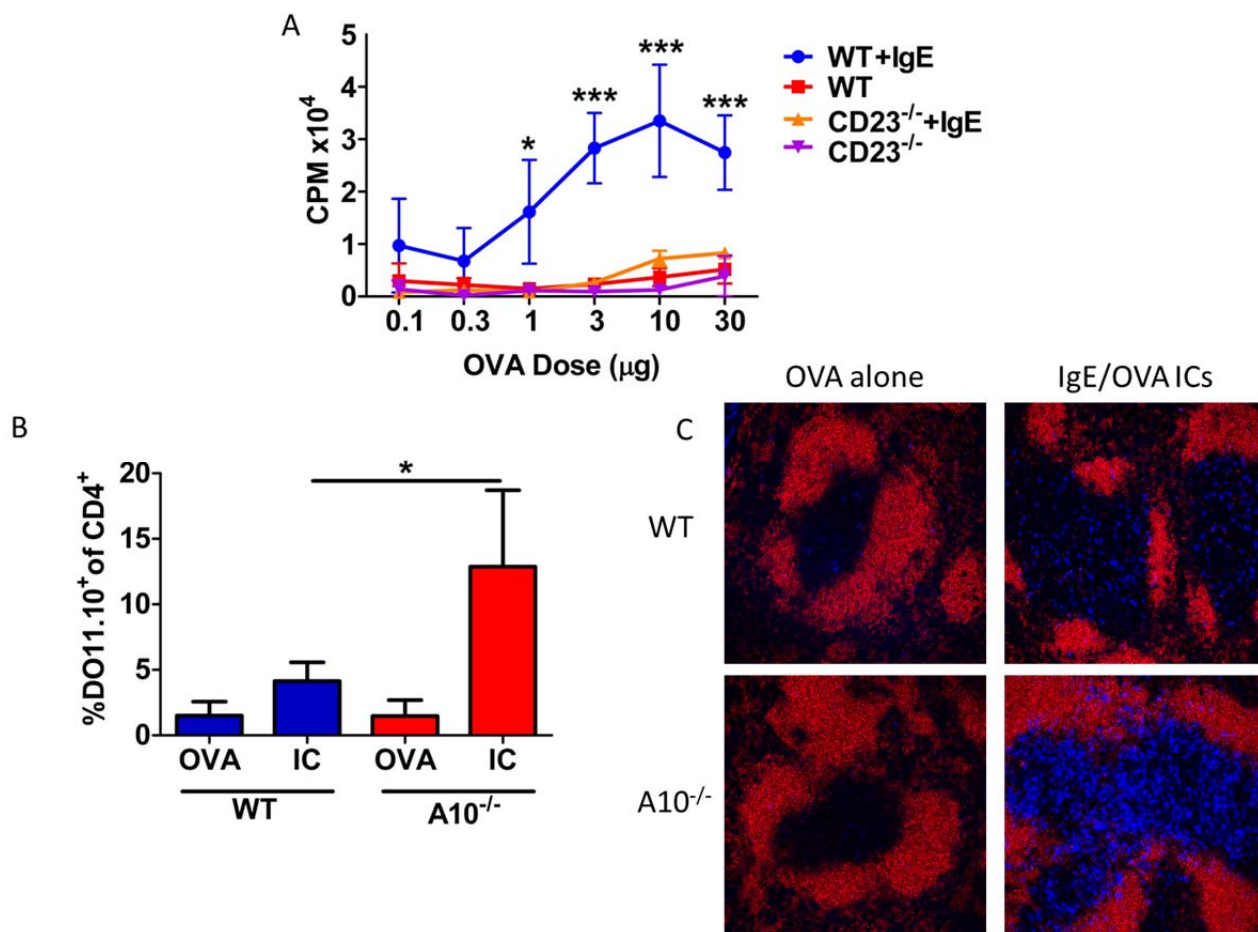


Figure 65. Bexosome-induced antigen specific T cell proliferation is enhanced by IgE in C57BL/6 model of OVA-specific T cell proliferation

B cell cultures stimulated as in *Methods*. B cells were incubated with IgE for 24 hours and then IgE/Ag ICs were added. Bexosomes were isolated. B cells were from WT C57BL/6 mice. Bexosomes and purified Ag-specific OTII T cells were cultured for 3 days and proliferation determined using a [3H]-thymidine pulse (*Methods*).

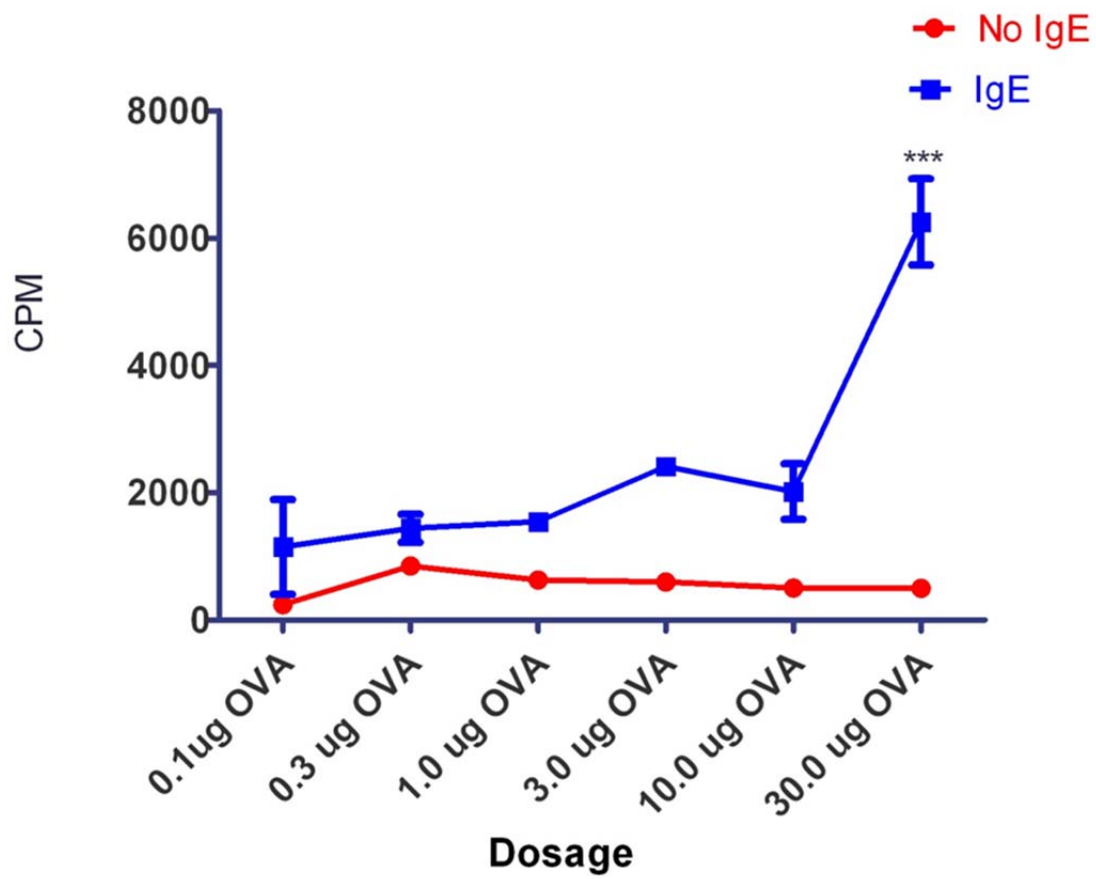


Figure 66. Increased *in vivo* T proliferation with *i.v.* injected DCs incubated with bexosomes

In vitro differentiated LPS activated DCs were incubated with bexosomes stimulated with IgE/Ag ICs plus 10µgOVA, 10µgOVA or 300µg OVA for three days. DCs were harvested and equivalent cells were injected into mice AT with DO11 cells. Spleens were assessed by flow cytometry on Day 3. Percent DO11TgTCR+ cells out of total CD4+ T cells were plotted. *p>0.05; n=5 per group

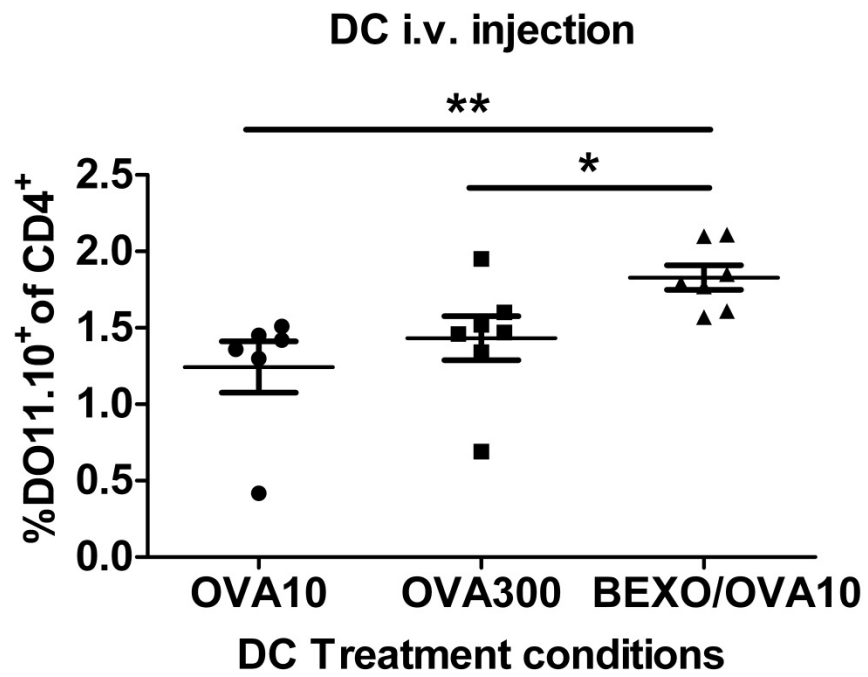
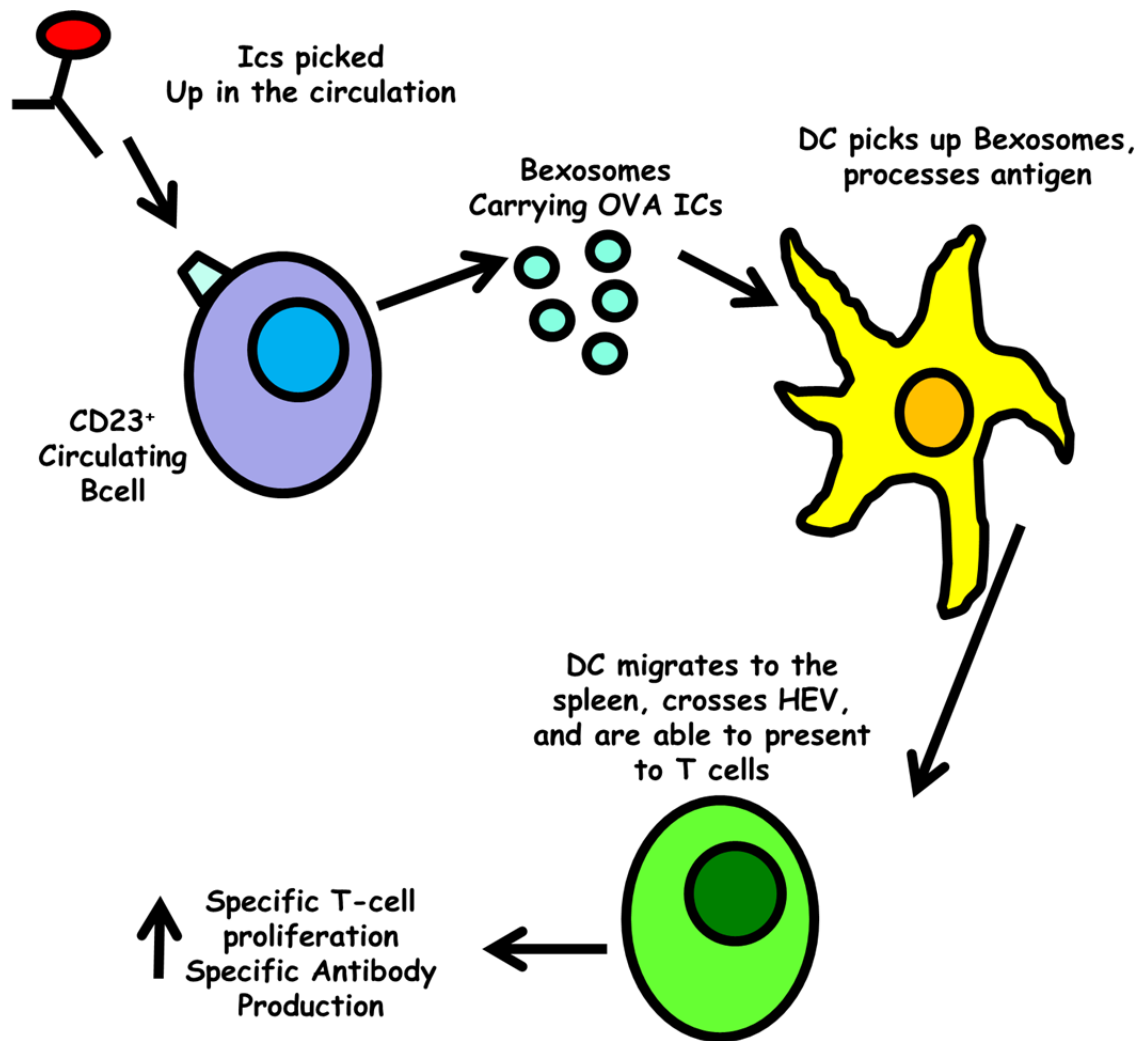


Figure 67. Model for the mechanism of IgE immune complex mediated humoral immunity enhancement



References

1. Weber, S. & Saftig, P. Ectodomain shedding and ADAMs in development. *Development* **139**, 3693–709 (2012).
2. Reiss, K. *et al.* Regulated ADAM10-dependent ectodomain shedding of gamma-protocadherin C3 modulates cell-cell adhesion. *J. Biol. Chem.* **281**, 21735–44 (2006).
3. Crawford, H. C., Dempsey, P. J., Brown, G., Adam, L. & Moss, M. L. ADAM10 as a therapeutic target for cancer and inflammation. *Curr. Pharm. Des.* **15**, 2288–99 (2009).
4. Becherer, J. D. & Blobel, C. P. Biochemical properties and functions of membrane-anchored metalloprotease-disintegrin proteins (ADAMs). *Curr. Top. Dev. Biol.* **54**, 101–23 (2003).
5. Matsumoto, M. *et al.* Affinity maturation without germinal centres in lymphotoxin-alpha-deficient mice. *Nature* **382**, 462–6 (1996).
6. Seals, D. F. & Courtneidge, S. A. The ADAMs family of metalloproteases: multidomain proteins with multiple functions. *Genes Dev.* **17**, 7–30 (2003).
7. Blobel, C. P. *et al.* A potential fusion peptide and an integrin ligand domain in a protein active in sperm-egg fusion. *Nature* **356**, 248–52 (1992).
8. Alfandari, D., Wolfsberg, T. G., White, J. M. & DeSimone, D. W. ADAM 13: a novel ADAM expressed in somitic mesoderm and neural crest cells during *Xenopus laevis* development. *Dev. Biol.* **182**, 314–30 (1997).
9. Nakamura, T., Abe, H., Hirata, A. & Shimoda, C. ADAM family protein Mde10 is essential for development of spore envelopes in the fission yeast *Schizosaccharomyces pombe*. *Eukaryot. Cell* **3**, 27–39 (2004).
10. Iida, A. *et al.* Metalloprotease-dependent onset of blood circulation in zebrafish. *Curr. Biol.* **20**, 1110–6 (2010).
11. Puente, X. S. & López-Otín, C. A genomic analysis of rat proteases and protease inhibitors. *Genome Res.* **14**, 609–22 (2004).
12. Edwards, D. R., Handsley, M. M. & Pennington, C. J. The ADAM metalloproteinases. *Mol. Aspects Med.* **29**, 258–89 (2008).

13. Wolfsberg, T. G. *et al.* The precursor region of a protein active in sperm-egg fusion contains a metalloprotease and a disintegrin domain: structural, functional, and evolutionary implications. *Proc. Natl. Acad. Sci. U. S. A.* **90**, 10783–7 (1993).
14. Huxley-Jones, J. *et al.* The evolution of the vertebrate metzincins; insights from *Ciona intestinalis* and *Danio rerio*. *BMC Evol. Biol.* **7**, 63 (2007).
15. Bode, W., Gomis-Rüth, F. X. & Stöckler, W. Astacins, serralytins, snake venom and matrix metalloproteinases exhibit identical zinc-binding environments (HEXXHXXGXXH and Met-turn) and topologies and should be grouped into a common family, the “metzincins”. *FEBS Lett.* **331**, 134–40 (1993).
16. Rooke, J., Pan, D., Xu, T. & Rubin, G. M. KUZ, a conserved metalloprotease-disintegrin protein with two roles in *Drosophila* neurogenesis. *Science* **273**, 1227–31 (1996).
17. Amour, A. *et al.* The in vitro activity of ADAM-10 is inhibited by TIMP-1 and TIMP-3. *FEBS Lett.* **473**, 275–9 (2000).
18. Pan, D. & Rubin, G. M. Kuzbanian controls proteolytic processing of Notch and mediates lateral inhibition during *Drosophila* and vertebrate neurogenesis. *Cell* **90**, 271–80 (1997).
19. Liu, M. *et al.* Two levels of protection for the B cell genome during somatic hypermutation. *Nature* **451**, 841–5 (2008).
20. Wolfsberg, T. G., Primakoff, P., Myles, D. G. & White, J. M. ADAM, a novel family of membrane proteins containing A Disintegrin And Metalloprotease domain: multipotential functions in cell-cell and cell-matrix interactions. *J. Cell Biol.* **131**, 275–8 (1995).
21. Kopan, R. & Ilagan, M. X. G. The canonical Notch signaling pathway: unfolding the activation mechanism. *Cell* **137**, 216–33 (2009).
22. Hartmann, D. *et al.* The disintegrin/metalloprotease ADAM 10 is essential for Notch signalling but not for alpha-secretase activity in fibroblasts. *Hum. Mol. Genet.* **11**, 2615–24 (2002).
23. Mumm, J. S. *et al.* A ligand-induced extracellular cleavage regulates gamma-secretase-like proteolytic activation of Notch1. *Mol. Cell* **5**, 197–206 (2000).
24. Brou, C. *et al.* A novel proteolytic cleavage involved in Notch signaling: the role of the disintegrin-metalloprotease TACE. *Mol. Cell* **5**, 207–16 (2000).

25. Saito, T. *et al.* Notch2 is preferentially expressed in mature B cells and indispensable for marginal zone B lineage development. *Immunity* **18**, 675–85 (2003).
26. Radtke, F., Wilson, A., Mancini, S. J. C. & MacDonald, H. R. Notch regulation of lymphocyte development and function. *Nat. Immunol.* **5**, 247–53 (2004).
27. Van Tetering, G. *et al.* Metalloprotease ADAM10 is required for Notch1 site 2 cleavage. *J. Biol. Chem.* **284**, 31018–27 (2009).
28. Le Gall, S. M. *et al.* ADAMs 10 and 17 represent differentially regulated components of a general shedding machinery for membrane proteins such as transforming growth factor alpha, L-selectin, and tumor necrosis factor alpha. *Mol. Biol. Cell* **20**, 1785–94 (2009).
29. Folgosa, L., Zellner, H. B., El Shikh, M. E. & Conrad, D. H. Disturbed follicular architecture in B cell A disintegrin and metalloproteinase (ADAM)10 knockouts is mediated by compensatory increases in ADAM17 and TNF- α shedding. *J. Immunol.* **191**, 5951–8 (2013).
30. Swiatek, P. J., Lindsell, C. E., del Amo, F. F., Weinmaster, G. & Gridley, T. Notch1 is essential for postimplantation development in mice. *Genes Dev.* **8**, 707–19 (1994).
31. Peschon, J. J. *et al.* An essential role for ectodomain shedding in mammalian development. *Science* **282**, 1281–4 (1998).
32. Bozkulak, E. C. & Weinmaster, G. Selective use of ADAM10 and ADAM17 in activation of Notch1 signaling. *Mol. Cell. Biol.* **29**, 5679–95 (2009).
33. Yuan, J. S., Kousis, P. C., Suliman, S., Visan, I. & Guidos, C. J. Functions of notch signaling in the immune system: consensus and controversies. *Annu. Rev. Immunol.* **28**, 343–65 (2010).
34. Stoeck, A. *et al.* A role for exosomes in the constitutive and stimulus-induced ectodomain cleavage of L1 and CD44. *Biochem. J.* **393**, 609–18 (2006).
35. Mathews, J. A., Gibb, D. R., Chen, B.-H., Scherle, P. & Conrad, D. H. CD23 Sheddase A disintegrin and metalloproteinase 10 (ADAM10) is also required for CD23 sorting into B cell-derived exosomes. *J. Biol. Chem.* **285**, 37531–41 (2010).
36. Marcello, E., Gardoni, F., Di Luca, M. & Pérez-Otaño, I. An arginine stretch limits ADAM10 exit from the endoplasmic reticulum. *J. Biol. Chem.* **285**, 10376–84 (2010).

37. Janes, P. W. *et al.* Adam meets Eph: an ADAM substrate recognition module acts as a molecular switch for ephrin cleavage in trans. *Cell* **123**, 291–304 (2005).
38. Kitano, M. *et al.* Bcl6 protein expression shapes pre-germinal center B cell dynamics and follicular helper T cell heterogeneity. *Immunity* **34**, 961–72 (2011).
39. Hwang, E. M. *et al.* Furin is an endogenous regulator of alpha-secretase associated APP processing. *Biochem. Biophys. Res. Commun.* **349**, 654–9 (2006).
40. Vikstrom, I. & Tarlinton, D. M. B cell memory and the role of apoptosis in its formation. *Mol. Immunol.* **48**, 1301–6 (2011).
41. Skovronsky, D. M., Moore, D. B., Milla, M. E., Doms, R. W. & Lee, V. M. Protein kinase C-dependent alpha-secretase competes with beta-secretase for cleavage of amyloid-beta precursor protein in the trans-golgi network. *J. Biol. Chem.* **275**, 2568–75 (2000).
42. Escrevente, C. *et al.* Functional role of N-glycosylation from ADAM10 in processing, localization and activity of the enzyme. *Biochim. Biophys. Acta* **1780**, 905–13 (2008).
43. Tippmann, F., Hundt, J., Schneider, A., Endres, K. & Fahrenholz, F. Up-regulation of the alpha-secretase ADAM10 by retinoic acid receptors and acitretin. *FASEB J.* **23**, 1643–54 (2009).
44. Kojro, E., Gimpl, G., Lammich, S., Marz, W. & Fahrenholz, F. Low cholesterol stimulates the nonamyloidogenic pathway by its effect on the alpha -secretase ADAM 10. *Proc. Natl. Acad. Sci. U. S. A.* **98**, 5815–20 (2001).
45. Sanderson, M. P. *et al.* ADAM10 mediates ectodomain shedding of the betacellulin precursor activated by p-aminophenylmercuric acetate and extracellular calcium influx. *J. Biol. Chem.* **280**, 1826–37 (2005).
46. Sturgill, J. L., Mathews, J., Scherle, P. & Conrad, D. H. Glutamate signaling through the kainate receptor enhances human immunoglobulin production. *J. Neuroimmunol.* **233**, 80–9 (2011).
47. Tian, L. *et al.* ADAM10 is essential for proteolytic activation of Notch during thymocyte development. *Int. Immunol.* **20**, 1181–7 (2008).
48. Pui, J. C. *et al.* Notch1 expression in early lymphopoiesis influences B versus T lineage determination. *Immunity* **11**, 299–308 (1999).
49. Tanigaki, K. & Honjo, T. Regulation of lymphocyte development by Notch signaling. *Nat. Immunol.* **8**, 451–6 (2007).

50. Santos, M. A. *et al.* Notch1 engagement by Delta-like-1 promotes differentiation of B lymphocytes to antibody-secreting cells. *Proc. Natl. Acad. Sci. U. S. A.* **104**, 15454–9 (2007).
51. Moriyama, Y. *et al.* Delta-like 1 is essential for the maintenance of marginal zone B cells in normal mice but not in autoimmune mice. *Int. Immunol.* **20**, 763–73 (2008).
52. Kawamata, S., Du, C., Li, K. & Lavau, C. Notch1 perturbation of hemopoiesis involves non-cell- autonomous modifications. *J. Immunol.* **168**, 1738–45 (2002).
53. Pillai, S., Cariappa, A. & Moran, S. T. Marginal zone B cells. *Annu. Rev. Immunol.* **23**, 161–96 (2005).
54. Zhang, P., Zhao, Y. & Sun, X.-H. Notch-regulated periphery B cell differentiation involves suppression of E protein function. *J. Immunol.* **191**, 726–36 (2013).
55. Quong, M. W. *et al.* Receptor editing and marginal zone B cell development are regulated by the helix-loop-helix protein, E2A. *J. Exp. Med.* **199**, 1101–12 (2004).
56. Gibb, D. R. *et al.* ADAM10 is essential for Notch2-dependent marginal zone B cell development and CD23 cleavage in vivo. *J. Exp. Med.* **207**, 623–35 (2010).
57. Thomas, M. *et al.* Notch activity synergizes with B-cell-receptor and CD40 signaling to enhance B-cell activation. *Blood* **109**, 3342–50 (2007).
58. Yoon, S.-O., Zhang, X., Berner, P., Blom, B. & Choi, Y. S. Notch ligands expressed by follicular dendritic cells protect germinal center B cells from apoptosis. *J. Immunol.* **183**, 352–8 (2009).
59. Auderset, F. *et al.* Notch signaling regulates follicular helper T cell differentiation. *J. Immunol.* **191**, 2344–50 (2013).
60. Wolniak, K. L., Shinall, S. M. & Waldschmidt, T. J. The Germinal Center Response. **24**, 39–66 (2004).
61. Chaplin, D. D. DEVELOPMENT AND MATURATION OF SECONDARY LYMPHOID TISSUES. 399–433 (1999).
62. Van de Pavert, S. a & Mebius, R. E. New insights into the development of lymphoid tissues. *Nat. Rev. Immunol.* **10**, 664–74 (2010).
63. Fu, Y. X. *et al.* Lymphotoxin-alpha (LTalpha) supports development of splenic follicular structure that is required for IgG responses. *J. Exp. Med.* **185**, 2111–20 (1997).

64. De Togni, P. *et al.* Abnormal development of peripheral lymphoid organs in mice deficient in lymphotoxin. *Science* **264**, 703–7 (1994).
65. Pasparakis, M., Alexopoulou, L., Episkopou, V. & Kollias, G. Immune and inflammatory responses in TNF alpha-deficient mice: a critical requirement for TNF alpha in the formation of primary B cell follicles, follicular dendritic cell networks and germinal centers, and in the maturation of the humoral immune response. *J. Exp. Med.* **184**, 1397–411 (1996).
66. Roozendaal, R. & Mebius, R. E. Stromal cell-immune cell interactions. *Annu. Rev. Immunol.* **29**, 23–43 (2011).
67. Goodnow, C. C. Chance encounters and organized rendezvous. *Immunol. Rev.* **156**, 5–10 (1997).
68. MacLennan, I. C. *et al.* The changing preference of T and B cells for partners as T-dependent antibody responses develop. *Immunol. Rev.* **156**, 53–66 (1997).
69. Castenholz, A. Architecture of the lymph node with regard to its function. *Curr. Top. Pathol.* **84 (Pt 1)**, 1–32 (1990).
70. Butcher, E. C. & Picker, L. J. Lymphocyte homing and homeostasis. *Science* **272**, 60–6 (1996).
71. Harwood, N. E. & Batista, F. D. Antigen presentation to B cells. *F1000 Biol. Rep.* **2**, 87 (2010).
72. Cyster, J. G. Chemokines and cell migration in secondary lymphoid organs. *Science* **286**, 2098–102 (1999).
73. Cyster, J. G. Chemokines and the homing of dendritic cells to the T cell areas of lymphoid organs. *J. Exp. Med.* **189**, 447–50 (1999).
74. Allen, C. D. C., Okada, T. & Cyster, J. G. Germinal-center organization and cellular dynamics. *Immunity* **27**, 190–202 (2007).
75. MacLennan, I. C. Germinal centers. *Annu. Rev. Immunol.* **12**, 117–39 (1994).
76. Ouyang, W., Kolls, J. K. & Zheng, Y. The biological functions of T helper 17 cell effector cytokines in inflammation. *Immunity* **28**, 454–67 (2008).
77. Heinzl, F. P., Sadick, M. D., Holaday, B. J., Coffman, R. L. & Locksley, R. M. Reciprocal expression of interferon gamma or interleukin 4 during the resolution or progression of murine leishmaniasis. Evidence for expansion of distinct helper T cell subsets. *J. Exp. Med.* **169**, 59–72 (1989).

78. Djuretic, I. M. *et al.* Transcription factors T-bet and Runx3 cooperate to activate Ifng and silence Il4 in T helper type 1 cells. *Nat. Immunol.* **8**, 145–53 (2007).
79. Mullen, A. C. *et al.* Hlx is induced by and genetically interacts with T-bet to promote heritable T(H)1 gene induction. *Nat. Immunol.* **3**, 652–8 (2002).
80. Schoenborn, J. R. & Wilson, C. B. Regulation of interferon-gamma during innate and adaptive immune responses. *Adv. Immunol.* **96**, 41–101 (2007).
81. Townsend, M. J. *et al.* T-bet regulates the terminal maturation and homeostasis of NK and Valpha14i NKT cells. *Immunity* **20**, 477–94 (2004).
82. Hwang, E. S., Szabo, S. J., Schwartzberg, P. L. & Glimcher, L. H. T helper cell fate specified by kinase-mediated interaction of T-bet with GATA-3. *Science* **307**, 430–3 (2005).
83. Usui, T. *et al.* T-bet regulates Th1 responses through essential effects on GATA-3 function rather than on IFNG gene acetylation and transcription. *J. Exp. Med.* **203**, 755–66 (2006).
84. Ansel, K. M., Djuretic, I., Tanasa, B. & Rao, A. Regulation of Th2 differentiation and Il4 locus accessibility. *Annu. Rev. Immunol.* **24**, 607–56 (2006).
85. Amsen, D. *et al.* Direct regulation of Gata3 expression determines the T helper differentiation potential of Notch. *Immunity* **27**, 89–99 (2007).
86. Van Panhuys, N. *et al.* In vivo studies fail to reveal a role for IL-4 or STAT6 signaling in Th2 lymphocyte differentiation. *Proc. Natl. Acad. Sci. U. S. A.* **105**, 12423–8 (2008).
87. McGeachy, M. J. & Cua, D. J. Th17 cell differentiation: the long and winding road. *Immunity* **28**, 445–53 (2008).
88. Korn, T. *et al.* IL-21 initiates an alternative pathway to induce proinflammatory T(H)17 cells. *Nature* **448**, 484–7 (2007).
89. Nurieva, R. *et al.* Essential autocrine regulation by IL-21 in the generation of inflammatory T cells. *Nature* **448**, 480–3 (2007).
90. Onoda, T. *et al.* Human CD4⁺ central and effector memory T cells produce IL-21: effect on cytokine-driven proliferation of CD4⁺ T cell subsets. *Int. Immunol.* **19**, 1191–9 (2007).
91. Zhou, L. *et al.* IL-6 programs T(H)-17 cell differentiation by promoting sequential engagement of the IL-21 and IL-23 pathways. *Nat. Immunol.* **8**, 967–74 (2007).

92. Garside, P. *et al.* Visualization of specific B and T lymphocyte interactions in the lymph node. *Science* **281**, 96–9 (1998).
93. Haynes, N. M. *et al.* Role of CXCR5 and CCR7 in follicular Th cell positioning and appearance of a programmed cell death gene-1high germinal center-associated subpopulation. *J. Immunol.* **179**, 5099–108 (2007).
94. Van den Eertwegh, A. J. *et al.* In vivo CD40-gp39 interactions are essential for thymus-dependent humoral immunity. I. In vivo expression of CD40 ligand, cytokines, and antibody production delineates sites of cognate T-B cell interactions. *J. Exp. Med.* **178**, 1555–65 (1993).
95. Damdinsuren, B. *et al.* Single round of antigen receptor signaling programs naive B cells to receive T cell help. *Immunity* **32**, 355–66 (2010).
96. Ramiscal, R. R. & Vinuesa, C. G. T-cell subsets in the germinal center. *Immunol. Rev.* **252**, 146–55 (2013).
97. TORO, I. & ROHLICH, P. [The problem of the structure of the lymph node; data obtained by electron microscopy]. *Magy. Radiol.* **13**, 331–9 (1961).
98. Hauser, A. E. *et al.* Definition of germinal-center B cell migration in vivo reveals predominant intrazonal circulation patterns. *Immunity* **26**, 655–67 (2007).
99. Victora, G. D. *et al.* Germinal center dynamics revealed by multiphoton microscopy with a photoactivatable fluorescent reporter. *Cell* **143**, 592–605 (2010).
100. Stavnezer, J., Guikema, J. E. J. & Schrader, C. E. Mechanism and regulation of class switch recombination. *Annu. Rev. Immunol.* **26**, 261–92 (2008).
101. Fazilleau, N., Mark, L., McHeyzer-Williams, L. J. & McHeyzer-Williams, M. G. Follicular helper T cells: lineage and location. *Immunity* **30**, 324–35 (2009).
102. Tarlinton, D. M. & Smith, K. G. Dissecting affinity maturation: a model explaining selection of antibody-forming cells and memory B cells in the germinal centre. *Immunol. Today* **21**, 436–41 (2000).
103. Tew, J. G. *et al.* Follicular dendritic cells and presentation of antigen and costimulatory signals to B cells. *Immunol. Rev.* **156**, 39–52 (1997).
104. Shokat, K. M. & Goodnow, C. C. Antigen-induced B-cell death and elimination during germinal-centre immune responses. *Nature* **375**, 334–8 (1995).

105. Pulendran, B., Kannourakis, G., Nouri, S., Smith, K. G. & Nossal, G. J. Soluble antigen can cause enhanced apoptosis of germinal-centre B cells. *Nature* **375**, 331–4 (1995).
106. Han, S., Zheng, B., Dal Porto, J. & Kelsoe, G. In situ studies of the primary immune response to (4-hydroxy-3-nitrophenyl)acetyl. IV. Affinity-dependent, antigen-driven B cell apoptosis in germinal centers as a mechanism for maintaining self-tolerance. *J. Exp. Med.* **182**, 1635–44 (1995).
107. Kelsoe, G. The germinal center: a crucible for lymphocyte selection. *Semin. Immunol.* **8**, 179–84 (1996).
108. Tarlinton, D. M. Evolution in miniature: selection, survival and distribution of antigen reactive cells in the germinal centre. *Immunol. Cell Biol.* **86**, 133–8 (2008).
109. You, Y., Zhao, H., Wang, Y. & Carter, R. H. Cutting edge: Primary and secondary effects of CD19 deficiency on cells of the marginal zone. *J. Immunol.* **182**, 7343–7 (2009).
110. Chaimowitz, N. S. *et al.* A disintegrin and metalloproteinase 10 regulates antibody production and maintenance of lymphoid architecture. *J. Immunol.* **187**, 5114–22 (2011).
111. Varadkar, P. A., Kraman, M. & McCright, B. Generation of mice that conditionally express the activation domain of Notch2. *Genesis* **47**, 573–8 (2009).
112. Payet, M. E., Woodward, E. C. & Conrad, D. H. Humoral response suppression observed with CD23 transgenics. *J. Immunol.* **163**, 217–23 (1999).
113. Rangel-Moreno, J. *et al.* Role of CXC chemokine ligand 13, CC chemokine ligand (CCL) 19, and CCL21 in the organization and function of nasal-associated lymphoid tissue. *J. Immunol.* **175**, 4904–13 (2005).
114. Khuda, S. E., Loo, W. M., Janz, S., Van Ness, B. & Erickson, L. D. Deregulation of c-Myc Confers distinct survival requirements for memory B cells, plasma cells, and their progenitors. *J. Immunol.* **181**, 7537–49 (2008).
115. Rickert, R. C., Roes, J. & Rajewsky, K. B lymphocyte-specific, Cre-mediated mutagenesis in mice. *Nucleic Acids Res.* **25**, 1317–8 (1997).
116. Otero, D. C. & Rickert, R. C. CD19 function in early and late B cell development. II. CD19 facilitates the pro-B/pre-B transition. *J. Immunol.* **171**, 5921–30 (2003).
117. Hobeika, E. *et al.* Testing gene function early in the B cell lineage in mb1-cre mice. *Proc. Natl. Acad. Sci. U. S. A.* **103**, 13789–94 (2006).

118. Chaimowitz, N. S., Kang, D.-J., Dean, L. M. & Conrad, D. H. ADAM10 regulates transcription factor expression required for plasma cell function. *PLoS One* **7**, e42694 (2012).
119. Weskamp, G. *et al.* ADAM10 is a principal “shedase” of the low-affinity immunoglobulin E receptor CD23. *Nat. Immunol.* **7**, 1293–8 (2006).
120. Oracki, S. A., Walker, J. A., Hibbs, M. L., Corcoran, L. M. & Tarlinton, D. M. Plasma cell development and survival. *Immunol. Rev.* **237**, 140–59 (2010).
121. Ridderstad, A. & Tarlinton, D. M. Kinetics of establishing the memory B cell population as revealed by CD38 expression. *J. Immunol.* **160**, 4688–95 (1998).
122. Alimzhanov, M. B. *et al.* Abnormal development of secondary lymphoid tissues in lymphotoxin beta-deficient mice. *Proc. Natl. Acad. Sci. U. S. A.* **94**, 9302–7 (1997).
123. Cupedo, T. *et al.* Initiation of cellular organization in lymph nodes is regulated by non-B cell-derived signals and is not dependent on CXC chemokine ligand 13. *J. Immunol.* **173**, 4889–96 (2004).
124. Tew, J. G., Wu, J., Fakher, M., Szakal, A. K. & Qin, D. Follicular dendritic cells: beyond the necessity of T-cell help. *Trends Immunol.* **22**, 361–7 (2001).
125. Ansel, K. M. *et al.* A chemokine-driven positive feedback loop organizes lymphoid follicles. *Nature* **406**, 309–14 (2000).
126. Ahearn, J. M. *et al.* Disruption of the Cr2 locus results in a reduction in B-1a cells and in an impaired B cell response to T-dependent antigen. *Immunity* **4**, 251–62 (1996).
127. Haaheim, L. R. Original antigenic sin. A confounding issue? *Dev. Biol. (Basel)*. **115**, 49–53 (2003).
128. Nutt, S. L., Eberhard, D., Horcher, M., Rolink, A. G. & Busslinger, M. Pax5 determines the identity of B cells from the beginning to the end of B-lymphopoiesis. *Int. Rev. Immunol.* **20**, 65–82 (2001).
129. Payet-Jamroz, M. *et al.* Suppression of IgE responses in CD23-transgenic animals is due to expression of CD23 on nonlymphoid cells. *J. Immunol.* **166**, 4863–9 (2001).
130. Overall, C. M. & Blobel, C. P. In search of partners: linking extracellular proteases to substrates. *Nat. Rev. Mol. Cell Biol.* **8**, 245–57 (2007).

131. Tanigaki, K. *et al.* Notch-RBP-J signaling is involved in cell fate determination of marginal zone B cells. *Nat. Immunol.* **3**, 443–50 (2002).
132. Kraman, M. & McCright, B. Functional conservation of Notch1 and Notch2 intracellular domains. *FASEB J.* **19**, 1311–3 (2005).
133. Thomas, M. *et al.* Notch activity synergizes with B-cell-receptor and CD40 signaling to enhance B-cell activation. *Blood* **109**, 3342–50 (2007).
134. Santos, M. A. *et al.* Notch1 engagement by Delta-like-1 promotes differentiation of B lymphocytes to antibody-secreting cells. *Proc. Natl. Acad. Sci. U. S. A.* **104**, 15454–9 (2007).
135. Chen, Z., Koralov, S. B., Gendelman, M., Carroll, M. C. & Kelsoe, G. Humoral immune responses in Cr2^{-/-} mice: enhanced affinity maturation but impaired antibody persistence. *J. Immunol.* **164**, 4522–32 (2000).
136. Wu, Y. *et al.* IL-6 produced by immune complex-activated follicular dendritic cells promotes germinal center reactions, IgG responses and somatic hypermutation. *Int. Immunol.* **21**, 745–56 (2009).
137. Tew, J. G., Kosco, M. H., Burton, G. F. & Szakal, A. K. Follicular dendritic cells as accessory cells. *Immunol. Rev.* **117**, 185–211 (1990).
138. Tew, J. G., Phipps, R. P. & Mandel, T. E. The maintenance and regulation of the humoral immune response: persisting antigen and the role of follicular antigen-binding dendritic cells as accessory cells. *Immunol. Rev.* **53**, 175–201 (1980).
139. Sukumar, S., Conrad, D. H., Szakal, A. K. & Tew, J. G. Differential T cell-mediated regulation of CD23 (Fc epsilonRII) in B cells and follicular dendritic cells. *J. Immunol.* **176**, 4811–7 (2006).
140. Mackay, C. R. Follicular homing T helper (Th) cells and the Th1/Th2 paradigm. *J. Exp. Med.* **192**, F31–4 (2000).
141. Pasparakis, M. Immune and inflammatory responses in TNF alpha-deficient mice: a critical requirement for TNF alpha in the formation of primary B cell follicles, follicular dendritic cell networks and germinal centers, and in the maturation of the humoral immune response. *J. Exp. Med.* **184**, 1397–1411 (1996).
142. Tumanov, A. V *et al.* Cellular source and molecular form of TNF specify its distinct functions in organization of secondary lymphoid organs. *Blood* **116**, 3456–64 (2010).
143. Le Gall, S. M. *et al.* ADAMs 10 and 17 represent differentially regulated components of a general shedding machinery for membrane proteins such as

- transforming growth factor alpha, L-selectin, and tumor necrosis factor alpha. *Mol. Biol. Cell* **20**, 1785–94 (2009).
144. Mezyk-Kopeć, R. *et al.* Identification of ADAM10 as a major TNF sheddase in ADAM17-deficient fibroblasts. *Cytokine* **46**, 309–15 (2009).
 145. Conrad, D. H., Ford, J. W., Sturgill, J. L. & Gibb, D. R. CD23: an overlooked regulator of allergic disease. *Curr. Allergy Asthma Rep.* **7**, 331–7 (2007).
 146. Acharya, M. *et al.* CD23/FcεRII: molecular multi-tasking. *Clin. Exp. Immunol.* **162**, 12–23 (2010).
 147. Montagnac, G. *et al.* Intracellular trafficking of CD23: differential regulation in humans and mice by both extracellular and intracellular exons. *J. Immunol.* **174**, 5562–72 (2005).
 148. Yu, L. C. H. *et al.* Intestinal epithelial CD23 mediates enhanced antigen transport in allergy: evidence for novel splice forms. *Am. J. Physiol. Gastrointest. Liver Physiol.* **285**, G223–34 (2003).
 149. Yokota, A. *et al.* Two species of human Fc epsilon receptor II (Fc epsilon RII/CD23): tissue-specific and IL-4-specific regulation of gene expression. *Cell* **55**, 611–8 (1988).
 150. Yu, P., Kosco-Vilbois, M., Richards, M., Köhler, G. & Lamers, M. C. Negative feedback regulation of IgE synthesis by murine CD23. *Nature* **369**, 753–6 (1994).
 151. Haczku, A. *et al.* CD23 deficient mice develop allergic airway hyperresponsiveness following sensitization with ovalbumin. *Am. J. Respir. Crit. Care Med.* **156**, 1945–55 (1997).
 152. Mathews, J. a *et al.* A potential new target for asthma therapy: a disintegrin and metalloprotease 10 (ADAM10) involvement in murine experimental asthma. *Allergy* **66**, 1193–200 (2011).
 153. Lecoanet-Henchoz, S. *et al.* CD23 regulates monocyte activation through a novel interaction with the adhesion molecules CD11b-CD18 and CD11c-CD18. *Immunity* **3**, 119–25 (1995).
 154. Lecoanet-Henchoz, S. *et al.* Mouse CD23 regulates monocyte activation through an interaction with the adhesion molecule CD11b/CD18. *Eur. J. Immunol.* **27**, 2290–4 (1997).
 155. Di Lorenzo, G. *et al.* Serum levels of soluble CD23 in patients with asthma or rhinitis monosensitive to *Parietaria*. Its relation to total serum IgE levels and

- eosinophil cationic protein during and out of the pollen season. *Allergy Asthma Proc.* **20**, 119–25
156. Plater-Zyberk, C. & Bonnefoy, J. Y. Marked amelioration of established collagen-induced arthritis by treatment with antibodies to CD23 in vivo. *Nat. Med.* **1**, 781–5 (1995).
 157. Zhou, B.-B. S. *et al.* Targeting ADAM-mediated ligand cleavage to inhibit HER3 and EGFR pathways in non-small cell lung cancer. *Cancer Cell* **10**, 39–50 (2006).
 158. Bernstein, D. I. ABCs of Asthma. *Clin. Cornerstone* **8**, 9–25 (2008).
 159. Agache, I. & Ciobanu, C. Risk factors and asthma phenotypes in children and adults with seasonal allergic rhinitis. *Phys. Sportsmed.* **38**, 81–6 (2010).
 160. Nauta, A. J. *et al.* Mechanisms of allergy and asthma. *Eur. J. Pharmacol.* **585**, 354–60 (2008).
 161. Kawamoto, H. & Katsura, Y. A new paradigm for hematopoietic cell lineages: revision of the classical concept of the myeloid-lymphoid dichotomy. *Trends Immunol.* **30**, 193–200 (2009).
 162. Gabrilovich, D. I. & Nagaraj, S. Myeloid-derived suppressor cells as regulators of the immune system. *Nat. Rev. Immunol.* **9**, 162–74 (2009).
 163. Stier, S., Cheng, T., Dombkowski, D., Carlesso, N. & Scadden, D. T. Notch1 activation increases hematopoietic stem cell self-renewal in vivo and favors lymphoid over myeloid lineage outcome. *Blood* **99**, 2369–78 (2002).
 164. Carlesso, N., Aster, J. C., Sklar, J. & Scadden, D. T. Notch1-induced delay of human hematopoietic progenitor cell differentiation is associated with altered cell cycle kinetics. *Blood* **93**, 838–48 (1999).
 165. Schroeder, T., Kohlhof, H., Rieber, N. & Just, U. Notch signaling induces multilineage myeloid differentiation and up-regulates PU.1 expression. *J. Immunol.* **170**, 5538–48 (2003).
 166. Bigas, A., Martin, D. I. & Milner, L. A. Notch1 and Notch2 inhibit myeloid differentiation in response to different cytokines. *Mol. Cell. Biol.* **18**, 2324–33 (1998).
 167. Qyang, Y. *et al.* Myeloproliferative disease in mice with reduced presenilin gene dosage: effect of gamma-secretase blockage. *Biochemistry* **43**, 5352–9 (2004).
 168. Chi, A. W., Bell, J. J., Zlotoff, D. A. & Bhandoola, A. Untangling the T branch of the hematopoiesis tree. *Curr. Opin. Immunol.* **21**, 121–6 (2009).

169. Saleem, S. J. & Conrad, D. H. Hematopoietic cytokine-induced transcriptional regulation and Notch signaling as modulators of MDSC expansion. *Int. Immunopharmacol.* **11**, 808–15 (2011).
170. Rosnet, O. *et al.* Human FLT3/FLK2 gene: cDNA cloning and expression in hematopoietic cells. *Blood* **82**, 1110–9 (1993).
171. Pronk, C. J. H. *et al.* Elucidation of the phenotypic, functional, and molecular topography of a myeloerythroid progenitor cell hierarchy. *Cell Stem Cell* **1**, 428–42 (2007).
172. Weissman, I. L., Anderson, D. J. & Gage, F. Stem and progenitor cells: origins, phenotypes, lineage commitments, and transdifferentiations. *Annu. Rev. Cell Dev. Biol.* **17**, 387–403 (2001).
173. Maeda, K. *et al.* Interleukin-6 aborts lymphopoiesis and elevates production of myeloid cells in systemic lupus erythematosus-prone B6.Sle1.Yaa animals. *Blood* **113**, 4534–40 (2009).
174. Karsunky, H., Inlay, M. A., Serwold, T., Bhattacharya, D. & Weissman, I. L. Flk2+ common lymphoid progenitors possess equivalent differentiation potential for the B and T lineages. *Blood* **111**, 5562–70 (2008).
175. Forsberg, E. C., Bhattacharya, D. & Weissman, I. L. Hematopoietic stem cells: expression profiling and beyond. *Stem Cell Rev.* **2**, 23–30 (2006).
176. Kawamoto, H., Wada, H. & Katsura, Y. A revised scheme for developmental pathways of hematopoietic cells: the myeloid-based model. *Int. Immunol.* **22**, 65–70 (2010).
177. Lu, T. *et al.* Tumor-infiltrating myeloid cells induce tumor cell resistance to cytotoxic T cells in mice. *J. Clin. Invest.* **121**, 4015–29 (2011).
178. Hirai, H. *et al.* C/EBPbeta is required for “emergency” granulopoiesis. *Nat. Immunol.* **7**, 732–9 (2006).
179. Sonda, N., Chioda, M., Zilio, S., Simonato, F. & Bronte, V. Transcription factors in myeloid-derived suppressor cell recruitment and function. *Curr. Opin. Immunol.* **23**, 279–85 (2011).
180. Dilek, N., van Rompaey, N., Le Moine, A. & Vanhove, B. Myeloid-derived suppressor cells in transplantation. *Curr. Opin. Organ Transplant.* **15**, 765–8 (2010).
181. Gomez, C. R., Boehmer, E. D. & Kovacs, E. J. The aging innate immune system. *Curr. Opin. Immunol.* **17**, 457–62 (2005).

182. Highfill, S. L. *et al.* Bone marrow myeloid-derived suppressor cells (MDSCs) inhibit graft-versus-host disease (GVHD) via an arginase-1-dependent mechanism that is up-regulated by interleukin-13. *Blood* **116**, 5738–47 (2010).
183. Cuenca, A. G. *et al.* A paradoxical role for myeloid-derived suppressor cells in sepsis and trauma. *Mol. Med.* **17**, 281–92
184. Auffray, C., Sieweke, M. H. & Geissmann, F. Blood monocytes: development, heterogeneity, and relationship with dendritic cells. *Annu. Rev. Immunol.* **27**, 669–92 (2009).
185. Geissmann, F., Jung, S. & Littman, D. R. Blood monocytes consist of two principal subsets with distinct migratory properties. *Immunity* **19**, 71–82 (2003).
186. Pircher, H. *et al.* T cell tolerance to Mlsa encoded antigens in T cell receptor V beta 8.1 chain transgenic mice. *EMBO J.* **8**, 719–27 (1989).
187. Malek, S. N., Dordai, D. I., Reim, J., Dintzis, H. & Desiderio, S. Malignant transformation of early lymphoid progenitors in mice expressing an activated Blk tyrosine kinase. *Proc. Natl. Acad. Sci. U. S. A.* **95**, 7351–6 (1998).
188. Movahedi, K. *et al.* Identification of discrete tumor-induced myeloid-derived suppressor cell subpopulations with distinct T cell-suppressive activity. *Blood* **111**, 4233–44 (2008).
189. McIlroy, A. *et al.* Histamine and prostaglandin E up-regulate the production of Th2-attracting chemokines (CCL17 and CCL22) and down-regulate IFN-gamma-induced CXCL10 production by immature human dendritic cells. *Immunology* **117**, 507–16 (2006).
190. Gabrilovich, D. I., Ostrand-Rosenberg, S. & Bronte, V. Coordinated regulation of myeloid cells by tumours. *Nat. Rev. Immunol.* **12**, 253–68 (2012).
191. Ostrand-Rosenberg, S. Myeloid-derived suppressor cells: more mechanisms for inhibiting antitumor immunity. *Cancer Immunol. Immunother.* **59**, 1593–600 (2010).
192. Pastuła, A. & Marcinkiewicz, J. Myeloid-derived suppressor cells: a double-edged sword? *Int. J. Exp. Pathol.* **92**, 73–8 (2011).
193. Saleem, S. J. *et al.* Cutting edge: mast cells critically augment myeloid-derived suppressor cell activity. *J. Immunol.* **189**, 511–5 (2012).
194. Gumley, T. P., McKenzie, I. F. & Sandrin, M. S. Tissue expression, structure and function of the murine Ly-6 family of molecules. *Immunol. Cell Biol.* **73**, 277–96 (1995).

195. Ribechini, E., Leenen, P. J. M. & Lutz, M. B. Gr-1 antibody induces STAT signaling, macrophage marker expression and abrogation of myeloid-derived suppressor cell activity in BM cells. *Eur. J. Immunol.* **39**, 3538–51 (2009).
196. Trellakis, S. *et al.* Granulocytic myeloid-derived suppressor cells are cryosensitive and their frequency does not correlate with serum concentrations of colony-stimulating factors in head and neck cancer. *Innate Immun.* **19**, 328–36 (2013).
197. Abrams, S. I. & Waight, J. D. Identification of a G-CSF-Granulocytic MDSC axis that promotes tumor progression. *Oncoimmunology* **1**, 550–551 (2012).
198. Hanson, E. M., Clements, V. K., Sinha, P., Ilkovitch, D. & Ostrand-Rosenberg, S. Myeloid-derived suppressor cells down-regulate L-selectin expression on CD4+ and CD8+ T cells. *J. Immunol.* **183**, 937–44 (2009).
199. Tian, J. *et al.* β -Glucan enhances antitumor immune responses by regulating differentiation and function of monocytic myeloid-derived suppressor cells. *Eur. J. Immunol.* **43**, 1220–30 (2013).
200. Sinha, P. *et al.* Myeloid-derived suppressor cells express the death receptor Fas and apoptose in response to T cell-expressed FasL. *Blood* **117**, 5381–90 (2011).
201. Brandau, S. *et al.* Myeloid-derived suppressor cells in the peripheral blood of cancer patients contain a subset of immature neutrophils with impaired migratory properties. *J. Leukoc. Biol.* **89**, 311–7 (2011).
202. Rodriguez, P. C. *et al.* Arginase I-producing myeloid-derived suppressor cells in renal cell carcinoma are a subpopulation of activated granulocytes. *Cancer Res.* **69**, 1553–60 (2009).
203. Tadmor, T., Attias, D. & Polliack, A. Myeloid-derived suppressor cells--their role in haemato-oncological malignancies and other cancers and possible implications for therapy. *Br. J. Haematol.* **153**, 557–67 (2011).
204. Höchst, B. *et al.* Activated human hepatic stellate cells induce myeloid derived suppressor cells from peripheral blood monocytes in a CD44-dependent fashion. *J. Hepatol.* **59**, 528–35 (2013).
205. Mandruzzato, S. *et al.* IL4Ralpha+ myeloid-derived suppressor cell expansion in cancer patients. *J. Immunol.* **182**, 6562–8 (2009).
206. Brandau, S., Moses, K. & Lang, S. The kinship of neutrophils and granulocytic myeloid-derived suppressor cells in cancer: cousins, siblings or twins? *Semin. Cancer Biol.* **23**, 171–82 (2013).

207. Youn, J.-I., Collazo, M., Shalova, I. N., Biswas, S. K. & Gabrilovich, D. I. Characterization of the nature of granulocytic myeloid-derived suppressor cells in tumor-bearing mice. *J. Leukoc. Biol.* **91**, 167–81 (2012).
208. Duffy, A. *et al.* Comparative analysis of monocytic and granulocytic myeloid-derived suppressor cell subsets in patients with gastrointestinal malignancies. *Cancer Immunol. Immunother.* **62**, 299–307 (2013).
209. Trams, E. G., Lauter, C. J., Salem, N. & Heine, U. Exfoliation of membrane ectoenzymes in the form of micro-vesicles. *Biochim. Biophys. Acta* **645**, 63–70 (1981).
210. Maeda, A., Kawamura, T., Ueno, T., Usui, N. & Miyagawa, S. Monocytic suppressor cells derived from human peripheral blood suppress xenogenic immune reactions. *Xenotransplantation* (2013). doi:10.1111/xen.12067
211. Bronte, V. *et al.* Identification of a CD11b(+)/Gr-1(+)/CD31(+) myeloid progenitor capable of activating or suppressing CD8(+) T cells. *Blood* **96**, 3838–46 (2000).
212. Youn, J.-I., Nagaraj, S., Collazo, M. & Gabrilovich, D. I. Subsets of myeloid-derived suppressor cells in tumor-bearing mice. *J. Immunol.* **181**, 5791–802 (2008).
213. Dugast, A.-S. *et al.* Myeloid-derived suppressor cells accumulate in kidney allograft tolerance and specifically suppress effector T cell expansion. *J. Immunol.* **180**, 7898–906 (2008).
214. Ghansah, T. *et al.* Expansion of myeloid suppressor cells in SHIP-deficient mice represses allogeneic T cell responses. *J. Immunol.* **173**, 7324–30 (2004).
215. Pillay, J., Tak, T., Kamp, V. M. & Koenderman, L. Immune suppression by neutrophils and granulocytic myeloid-derived suppressor cells: similarities and differences. *Cell. Mol. Life Sci.* **70**, 3813–27 (2013).
216. Zhao, F. *et al.* S100A9 a new marker for monocytic human myeloid-derived suppressor cells. *Immunology* **136**, 176–83 (2012).
217. Saiwai, H. *et al.* Ly6C⁺ Ly6G⁺ Myeloid-derived suppressor cells play a critical role in the resolution of acute inflammation and the subsequent tissue repair process after spinal cord injury. *J. Neurochem.* **125**, 74–88 (2013).
218. Toh, B. *et al.* Mesenchymal transition and dissemination of cancer cells is driven by myeloid-derived suppressor cells infiltrating the primary tumor. *PLoS Biol.* **9**, e1001162 (2011).

219. Zigmond, E. *et al.* Ly6C hi monocytes in the inflamed colon give rise to proinflammatory effector cells and migratory antigen-presenting cells. *Immunity* **37**, 1076–90 (2012).
220. Greten, T. F., Manns, M. P. & Korangy, F. Myeloid derived suppressor cells in human diseases. *Int. Immunopharmacol.* **11**, 802–7 (2011).
221. Zhu, B. *et al.* CD11b+Ly-6C(hi) suppressive monocytes in experimental autoimmune encephalomyelitis. *J. Immunol.* **179**, 5228–37 (2007).
222. Hu, X. *et al.* Transmembrane TNF- α promotes suppressive activities of myeloid-derived suppressor cells via TNFR2. *J. Immunol.* **192**, 1320–31 (2014).
223. Trellakis, S. *et al.* Peripheral blood neutrophil granulocytes from patients with head and neck squamous cell carcinoma functionally differ from their counterparts in healthy donors. *Int. J. Immunopathol. Pharmacol.* **24**, 683–93
224. Cohen-Hillel, E., Mintz, R., Meshel, T., Garty, B.-Z. & Ben-Baruch, A. Cell migration to the chemokine CXCL8: paxillin is activated and regulates adhesion and cell motility. *Cell. Mol. Life Sci.* **66**, 884–99 (2009).
225. Youn, J.-I. *et al.* Epigenetic silencing of retinoblastoma gene regulates pathologic differentiation of myeloid cells in cancer. *Nat. Immunol.* **14**, 211–20 (2013).
226. Yang, W.-C., Ma, G., Chen, S.-H. & Pan, P.-Y. Polarization and reprogramming of myeloid-derived suppressor cells. *J. Mol. Cell Biol.* **5**, 207–9 (2013).
227. Munitz, A., McBride, M. L., Bernstein, J. S. & Rothenberg, M. E. A dual activation and inhibition role for the paired immunoglobulin-like receptor B in eosinophils. *Blood* **111**, 5694–703 (2008).
228. Takai, T., Li, M., Sylvestre, D., Clynes, R. & Ravetch, J. V. FcR gamma chain deletion results in pleiotrophic effector cell defects. *Cell* **76**, 519–29 (1994).
229. Fridlender, Z. G. *et al.* Polarization of tumor-associated neutrophil phenotype by TGF-beta: “N1” versus “N2” TAN. *Cancer Cell* **16**, 183–94 (2009).
230. Morris, S. M. Regulation of enzymes of the urea cycle and arginine metabolism. *Annu. Rev. Nutr.* **22**, 87–105 (2002).
231. Rodriguez, P. C. *et al.* Arginase I in myeloid suppressor cells is induced by COX-2 in lung carcinoma. *J. Exp. Med.* **202**, 931–9 (2005).
232. Rodriguez, P. C. *et al.* L-arginine consumption by macrophages modulates the expression of CD3 zeta chain in T lymphocytes. *J. Immunol.* **171**, 1232–9 (2003).

233. Taheri, F. *et al.* L-Arginine regulates the expression of the T-cell receptor zeta chain (CD3zeta) in Jurkat cells. *Clin. Cancer Res.* **7**, 958s–965s (2001).
234. Rodriguez, P. C., Quiceno, D. G. & Ochoa, A. C. L-arginine availability regulates T-lymphocyte cell-cycle progression. *Blood* **109**, 1568–73 (2007).
235. Zea, A. H. *et al.* L-Arginine modulates CD3zeta expression and T cell function in activated human T lymphocytes. *Cell. Immunol.* **232**, 21–31
236. Kusmartsev, S. & Gabrilovich, D. I. STAT1 signaling regulates tumor-associated macrophage-mediated T cell deletion. *J. Immunol.* **174**, 4880–91 (2005).
237. Groemping, Y. & Rittinger, K. Activation and assembly of the NADPH oxidase: a structural perspective. *Biochem. J.* **386**, 401–16 (2005).
238. Kusmartsev, S., Nefedova, Y., Yoder, D. & Gabrilovich, D. I. Antigen-specific inhibition of CD8⁺ T cell response by immature myeloid cells in cancer is mediated by reactive oxygen species. *J. Immunol.* **172**, 989–99 (2004).
239. Nagaraj, S. *et al.* Altered recognition of antigen is a mechanism of CD8⁺ T cell tolerance in cancer. *Nat. Med.* **13**, 828–35 (2007).
240. Fortin, C., Huang, X. & Yang, Y. NK cell response to vaccinia virus is regulated by myeloid-derived suppressor cells. *J. Immunol.* **189**, 1843–9 (2012).
241. Mazzone, A. *et al.* Myeloid suppressor lines inhibit T cell responses by an NO-dependent mechanism. *J. Immunol.* **168**, 689–95 (2002).
242. Bronte, V., Serafini, P., Mazzone, A., Segal, D. M. & Zanovello, P. L-arginine metabolism in myeloid cells controls T-lymphocyte functions. *Trends Immunol.* **24**, 302–6 (2003).
243. Panopoulos, A. D. & Watowich, S. S. Granulocyte colony-stimulating factor: molecular mechanisms of action during steady state and “emergency” hematopoiesis. *Cytokine* **42**, 277–88 (2008).
244. Vasquez-Dunddel, D. *et al.* STAT3 regulates arginase-I in myeloid-derived suppressor cells from cancer patients. *J. Clin. Invest.* **123**, 1580–9 (2013).
245. Ko, J. S. *et al.* Direct and differential suppression of myeloid-derived suppressor cell subsets by sunitinib is compartmentally constrained. *Cancer Res.* **70**, 3526–36 (2010).
246. Waight, J. D. *et al.* Myeloid-derived suppressor cell development is regulated by a STAT / IRF-8 axis. **123**, (2013).

247. Gibb, D. R., Saleem, S. J., Kang, D.-J., Subler, M. A. & Conrad, D. H. ADAM10 overexpression shifts lympho- and myelopoiesis by dysregulating site 2/site 3 cleavage products of Notch. *J. Immunol.* **186**, 4244–52 (2011).
248. Cheng, P. *et al.* Effects of notch signaling on regulation of myeloid cell differentiation in cancer. *Cancer Res.* **74**, 141–52 (2014).
249. Luyckx, A. *et al.* G-CSF stem cell mobilization in human donors induces polymorphonuclear and mononuclear myeloid-derived suppressor cells. *Clin. Immunol.* **143**, 83–7 (2012).
250. Dolcetti, L. *et al.* Hierarchy of immunosuppressive strength among myeloid-derived suppressor cell subsets is determined by GM-CSF. *Eur. J. Immunol.* **40**, 22–35 (2010).
251. Raychaudhuri, B. *et al.* Myeloid-derived suppressor cell accumulation and function in patients with newly diagnosed glioblastoma. *Neuro. Oncol.* **13**, 591–9 (2011).
252. Manjili, M. H. Phenotypic plasticity of MDSC in cancers. *Immunol. Invest.* **41**, 711–21 (2012).
253. Hsieh, C.-C. *et al.* The role of complement component 3 (C3) in differentiation of myeloid-derived suppressor cells. *Blood* **121**, 1760–8 (2013).
254. Simpson, K. D., Templeton, D. J. & Cross, J. V. Macrophage migration inhibitory factor promotes tumor growth and metastasis by inducing myeloid-derived suppressor cells in the tumor microenvironment. *J. Immunol.* **189**, 5533–40 (2012).
255. Mougiakakos, D. *et al.* Immunosuppressive CD14+HLA-DRI^{low}/neg IDO⁺ myeloid cells in patients following allogeneic hematopoietic stem cell transplantation. *Leukemia* **27**, 377–88 (2013).
256. Ramachandran, I. R. *et al.* Myeloid-derived suppressor cells regulate growth of multiple myeloma by inhibiting T cells in bone marrow. *J. Immunol.* **190**, 3815–23 (2013).
257. Sander, L. E. *et al.* Hepatic acute-phase proteins control innate immune responses during infection by promoting myeloid-derived suppressor cell function. *J. Exp. Med.* **207**, 1453–64 (2010).
258. Chen, G. *et al.* Oral delivery of tumor-targeting Salmonella exhibits promising therapeutic efficacy and low toxicity. *Cancer Sci.* **100**, 2437–43 (2009).

259. Cuervo, H. *et al.* Myeloid-derived suppressor cells infiltrate the heart in acute *Trypanosoma cruzi* infection. *J. Immunol.* **187**, 2656–65 (2011).
260. Goñi, O., Alcaide, P. & Fresno, M. Immunosuppression during acute *Trypanosoma cruzi* infection: involvement of Ly6G (Gr1(+))CD11b(+) immature myeloid suppressor cells. *Int. Immunol.* **14**, 1125–34 (2002).
261. Van Ginderachter, J. A., Beschin, A., De Baetselier, P. & Raes, G. Myeloid-derived suppressor cells in parasitic infections. *Eur. J. Immunol.* **40**, 2976–85 (2010).
262. Fairweather, D. & Cihakova, D. Alternatively activated macrophages in infection and autoimmunity. *J. Autoimmun.* **33**, 222–30
263. Verreck, F. A. W. *et al.* Human IL-23-producing type 1 macrophages promote but IL-10-producing type 2 macrophages subvert immunity to (myco)bacteria. *Proc. Natl. Acad. Sci. U. S. A.* **101**, 4560–5 (2004).
264. Martinez, F. O., Helming, L. & Gordon, S. Alternative activation of macrophages: an immunologic functional perspective. *Annu. Rev. Immunol.* **27**, 451–83 (2009).
265. Sinha, P., Clements, V. K., Bunt, S. K., Albelda, S. M. & Ostrand-Rosenberg, S. Cross-talk between myeloid-derived suppressor cells and macrophages subverts tumor immunity toward a type 2 response. *J. Immunol.* **179**, 977–83 (2007).
266. Heim, C. E. *et al.* Myeloid-Derived Suppressor Cells Contribute to *Staphylococcus aureus* Orthopedic Biofilm Infection. *J. Immunol.* (2014). doi:10.4049/jimmunol.1303408
267. Gabrilovich, D. Mechanisms and functional significance of tumour-induced dendritic-cell defects. *Nat. Rev. Immunol.* **4**, 941–52 (2004).
268. Hu, C.-E., Gan, J., Zhang, R.-D., Cheng, Y.-R. & Huang, G.-J. Up-regulated myeloid-derived suppressor cell contributes to hepatocellular carcinoma development by impairing dendritic cell function. *Scand. J. Gastroenterol.* **46**, 156–64 (2011).
269. Poschke, I. *et al.* Myeloid-derived suppressor cells impair the quality of dendritic cell vaccines. *Cancer Immunol. Immunother.* **61**, 827–38 (2012).
270. Ko, H.-J. *et al.* Immunosuppressive myeloid-derived suppressor cells can be converted into immunogenic APCs with the help of activated NKT cells: an alternative cell-based antitumor vaccine. *J. Immunol.* **182**, 1818–28 (2009).

271. Yang, Z. *et al.* Mast cells mobilize myeloid-derived suppressor cells and Treg cells in tumor microenvironment via IL-17 pathway in murine hepatocarcinoma model. *PLoS One* **5**, e8922 (2010).
272. Cheon, E. C. *et al.* Mast cell 5-lipoxygenase activity promotes intestinal polyposis in APCDelta468 mice. *Cancer Res.* **71**, 1627–36 (2011).
273. Galli, S. J., Nakae, S. & Tsai, M. Mast cells in the development of adaptive immune responses. *Nat. Immunol.* **6**, 135–42 (2005).
274. Metcalfe, D. D., Baram, D. & Mekori, Y. A. Mast cells. *Physiol. Rev.* **77**, 1033–79 (1997).
275. Hepworth, M. R., Maurer, M. & Hartmann, S. Regulation of type 2 immunity to helminths by mast cells. *Gut Microbes* **3**, 476–481 (2012).
276. Huang, B. *et al.* SCF-mediated mast cell infiltration and activation exacerbate the inflammation and immunosuppression in tumor microenvironment. *Blood* **112**, 1269–79 (2008).
277. Miller, H. R. Mucosal mast cells and the allergic response against nematode parasites. *Vet. Immunol. Immunopathol.* **54**, 331–6 (1996).
278. Oldford, S. A. *et al.* A critical role for mast cells and mast cell-derived IL-6 in TLR2-mediated inhibition of tumor growth. *J. Immunol.* **185**, 7067–76 (2010).
279. Hanahan, D. & Coussens, L. M. Accessories to the crime: functions of cells recruited to the tumor microenvironment. *Cancer Cell* **21**, 309–22 (2012).
280. Elenkov, I. J. *et al.* Histamine potently suppresses human IL-12 and stimulates IL-10 production via H2 receptors. *J. Immunol.* **161**, 2586–93 (1998).
281. Hsu, C.-L. & Bryce, P. J. Inducible IL-33 expression by mast cells is regulated by a calcium-dependent pathway. *J. Immunol.* **189**, 3421–9 (2012).
282. Suzukawa, M. *et al.* Epithelial cell-derived IL-25, but not Th17 cell-derived IL-17 or IL-17F, is crucial for murine asthma. *J. Immunol.* **189**, 3641–52 (2012).
283. Galli, S. J., Tsai, M. & Piliponsky, A. M. The development of allergic inflammation. *Nature* **454**, 445–54 (2008).
284. Packard, K. A. & Khan, M. M. Effects of histamine on Th1/Th2 cytokine balance. *Int. Immunopharmacol.* **3**, 909–20 (2003).

285. Skokos, D. *et al.* Mast cell-derived exosomes induce phenotypic and functional maturation of dendritic cells and elicit specific immune responses in vivo. *J. Immunol.* **170**, 3037–45 (2003).
286. Yang, X. D. *et al.* Histamine deficiency promotes inflammation-associated carcinogenesis through reduced myeloid maturation and accumulation of CD11b+Ly6G+ immature myeloid cells. *Nat. Med.* **17**, 87–95 (2011).
287. Van der Pouw Kraan, T. C. *et al.* Histamine inhibits the production of interleukin-12 through interaction with H2 receptors. *J. Clin. Invest.* **102**, 1866–73 (1998).
288. Ishikawa, T., Kanda, N., Hau, C. S., Tada, Y. & Watanabe, S. Histamine induces human beta-defensin-3 production in human keratinocytes. *J. Dermatol. Sci.* **56**, 121–7 (2009).
289. Adams, W. J., Lawson, J. A. & Morris, D. L. Cimetidine inhibits in vivo growth of human colon cancer and reverses histamine stimulated in vitro and in vivo growth. *Gut* **35**, 1632–6 (1994).
290. Prizment, A. E. *et al.* History of allergy and reduced incidence of colorectal cancer, Iowa Women's Health Study. *Cancer Epidemiol. Biomarkers Prev.* **16**, 2357–62 (2007).
291. Elliott, K. A., Osna, N. A., Scofield, M. A. & Khan, M. M. Regulation of IL-13 production by histamine in cloned murine T helper type 2 cells. *Int. Immunopharmacol.* **1**, 1923–37 (2001).
292. Finkelman, F. D. *et al.* Interleukin-4- and interleukin-13-mediated host protection against intestinal nematode parasites. *Immunol. Rev.* **201**, 139–55 (2004).
293. Bhattacharjee, A. *et al.* IL-4 and IL-13 employ discrete signaling pathways for target gene expression in alternatively activated monocytes/macrophages. *Free Radic. Biol. Med.* **54**, 1–16 (2013).
294. Hallett, M. A., Venmar, K. T. & Fingleton, B. Cytokine stimulation of epithelial cancer cells: the similar and divergent functions of IL-4 and IL-13. *Cancer Res.* **72**, 6338–43 (2012).
295. Lebel-Binay, S. *et al.* Experimental gene therapy of cancer using tumor cells engineered to secrete interleukin-13. *Eur. J. Immunol.* **25**, 2340–8 (1995).
296. Rothe, M. *et al.* IL-13 but not IL-4 signaling via IL-4R α protects mice from papilloma formation during DMBA/TPA two-step skin carcinogenesis. *Cancer Med.* **2**, 815–25 (2013).

297. Sinha, P., Parker, K. H., Horn, L. & Ostrand-Rosenberg, S. Tumor-induced myeloid-derived suppressor cell function is independent of IFN- γ and IL-4R α . *Eur. J. Immunol.* **42**, 2052–9 (2012).
298. Gabitass, R. F., Annels, N. E., Stocken, D. D., Pandha, H. A. & Middleton, G. W. Elevated myeloid-derived suppressor cells in pancreatic, esophageal and gastric cancer are an independent prognostic factor and are associated with significant elevation of the Th2 cytokine interleukin-13. *Cancer Immunol. Immunother.* **60**, 1419–30 (2011).
299. Jain, M. *et al.* Interleukin-13 receptor alpha2 is a novel therapeutic target for human adrenocortical carcinoma. *Cancer* **118**, 5698–708 (2012).
300. Ma, Y., Hwang, R. F., Logsdon, C. D. & Ullrich, S. E. Dynamic mast cell-stromal cell interactions promote growth of pancreatic cancer. *Cancer Res.* **73**, 3927–37 (2013).
301. Roth, F. *et al.* Aptamer-mediated blockade of IL4R α triggers apoptosis of MDSCs and limits tumor progression. *Cancer Res.* **72**, 1373–83 (2012).
302. Lilla, J. N. *et al.* Reduced mast cell and basophil numbers and function in Cpa3-Cre; Mcl-1f/f mice. *Blood* **118**, 6930–8 (2011).
303. Le, H. K. *et al.* Incubation of antigen-sensitized T lymphocytes activated with bryostatin 1 + ionomycin in IL-7 + IL-15 increases yield of cells capable of inducing regression of melanoma metastases compared to culture in IL-2. *Cancer Immunol. Immunother.* **58**, 1565–76 (2009).
304. Camberis, M., Le Gros, G. & Urban, J. Animal model of *Nippostrongylus brasiliensis* and *Heligmosomoides polygyrus*. *Curr. Protoc. Immunol.* **Chapter 19**, Unit 19.12 (2003).
305. Martin, R. K. *et al.* Mast cell histamine promotes the immunoregulatory activity of myeloid-derived suppressor cells. *J. Leukoc. Biol.* (2014). doi:10.1189/jlb.5A1213-644R
306. Lipsky, K. A. *et al.* Sensitizing T-lymphocytes for adoptive immunotherapy by vaccination with wild-type or cytokine gene-transduced melanoma. *Ann. Surg. Oncol.* **4**, 334–341 (1997).
307. Peranzoni, E. *et al.* Myeloid-derived suppressor cell heterogeneity and subset definition. *Curr. Opin. Immunol.* **22**, 238–44 (2010).
308. Bracci, L. *et al.* Cyclophosphamide enhances the antitumor efficacy of adoptively transferred immune cells through the induction of cytokine expression, B-cell and

- T-cell homeostatic proliferation, and specific tumor infiltration. *Clin. Cancer Res.* **13**, 644–53 (2007).
309. Teitz-Tennenbaum, S. *et al.* Radiotherapy combined with intratumoral dendritic cell vaccination enhances the therapeutic efficacy of adoptive T-cell transfer. *J. Immunother.* **32**, 602–12
 310. Le, H. K. *et al.* Gemcitabine directly inhibits myeloid derived suppressor cells in BALB/c mice bearing 4T1 mammary carcinoma and augments expansion of T cells from tumor-bearing mice. *Int. Immunopharmacol.* **9**, 900–9 (2009).
 311. Else, K. J. & Finkelman, F. D. Intestinal nematode parasites, cytokines and effector mechanisms. *Int. J. Parasitol.* **28**, 1145–58 (1998).
 312. Perrigoue, J. G., Marshall, F. A. & Artis, D. On the hunt for helminths: innate immune cells in the recognition and response to helminth parasites. *Cell. Microbiol.* **10**, 1757–64 (2008).
 313. Turnquist, H. R. *et al.* IL-33 expands suppressive CD11b⁺ Gr-1(int) and regulatory T cells, including ST2L⁺ Foxp3⁺ cells, and mediates regulatory T cell-dependent promotion of cardiac allograft survival. *J. Immunol.* **187**, 4598–610 (2011).
 314. Mitchell, L. A., Wescott, R. B. & Perryman, L. E. Kinetics of expulsion of the nematode, *Nippostrongylus brasiliensis*, in mast-cell deficient W/W^v mice. *Parasite Immunol.* **5**, 1–12 (1983).
 315. Starkey, J. R., Crowle, P. K. & Taubenberger, S. Mast-cell-deficient W/W^v mice exhibit a decreased rate of tumor angiogenesis. *Int. J. Cancer* **42**, 48–52 (1988).
 316. Connolly, M. K. *et al.* Distinct populations of metastases-enabling myeloid cells expand in the liver of mice harboring invasive and preinvasive intra-abdominal tumor. *J. Leukoc. Biol.* **87**, 713–25 (2010).
 317. Collins, A. M. *et al.* A role for the hepatobiliary system in IgE-mediated intestinal inflammation in the rat. *Clin. Exp. Allergy* **29**, 262–70 (1999).
 318. Condamine, T. & Gabrilovich, D. I. Molecular mechanisms regulating myeloid-derived suppressor cell differentiation and function. *Trends Immunol.* **32**, 19–25 (2011).
 319. Dussault, A.-A. & Pouliot, M. Rapid and simple comparison of messenger RNA levels using real-time PCR. *Biol. Proced. Online* **8**, 1–10 (2006).
 320. Zheng, Y. *et al.* Cimetidine suppresses lung tumor growth in mice through proapoptosis of myeloid-derived suppressor cells. *Mol. Immunol.* **54**, 74–83 (2013).

321. Bush, R. K. Etiopathogenesis and management of perennial allergic rhinitis: a state-of-the-art review. *Treat. Respir. Med.* **3**, 45–57 (2004).
322. Deshane, J. *et al.* Free radical-producing myeloid-derived regulatory cells: potent activators and suppressors of lung inflammation and airway hyperresponsiveness. *Mucosal Immunol.* **4**, 503–18 (2011).
323. Chan, T., Wiltrout, R. H. & Weiss, J. M. Immunotherapeutic modulation of the suppressive liver and tumor microenvironments. *Int. Immunopharmacol.* **11**, 879–89 (2011).
324. Saddiqi, H. A., Sarwar, M., Iqbal, Z., Nisa, M. & Shahzad, M. A. Markers/parameters for the evaluation of natural resistance status of small ruminants against gastrointestinal nematodes. *Animal* **6**, 994–1004 (2012).
325. Farrell, D. J. *et al.* Intrahepatic mast cells in chronic liver diseases. *Hepatology* **22**, 1175–81 (1995).
326. Nawa, Y. *et al.* Selective effector mechanisms for the expulsion of intestinal helminths. *Parasite Immunol.* **16**, 333–8 (1994).
327. Shin, E.-H. *et al.* Effects of anti-allergic drugs on intestinal mastocytosis and worm expulsion of rats infected with *Neodiplostomum seoulense*. *Korean J. Parasitol.* **41**, 81–7 (2003).
328. Yamauchi, K. *et al.* Enhanced goblet cell hyperplasia in HDC knockout mice with allergic airway inflammation. *Allergol. Int.* **58**, 125–34 (2009).
329. Schmidt, J., Fleissner, S., Heimann-Weitschat, I., Lindstaedt, R. & Szelenyi, I. Histamine increases anti-CD3 induced IL-5 production of TH2-type T cells via histamine H2-receptors. *Agents Actions* **42**, 81–5 (1994).
330. Jinqun, T. *et al.* Cetirizine inhibits the in vitro and ex vivo chemotactic response of T lymphocytes and monocytes. *J. Allergy Clin. Immunol.* **95**, 979–86 (1995).
331. Walsh, G. M., Moqbel, R., Hartnell, A. & Kay, A. B. Effects of cetirizine on human eosinophil and neutrophil activation in vitro. *Int. Arch. Allergy Appl. Immunol.* **95**, 158–62 (1991).
332. Basso, D. *et al.* Pancreatic tumors and immature immunosuppressive myeloid cells in blood and spleen: role of inhibitory co-stimulatory molecules PDL1 and CTLA4. An in vivo and in vitro study. *PLoS One* **8**, e54824 (2013).
333. Jiao, Z.-J. *et al.* Correlation between circulating myeloid-derived suppressor cells and Th17 cells in esophageal cancer. *World J. Gastroenterol.* **18**, 5454–61 (2012).

334. Sun, H.-L. *et al.* Increased frequency and clinical significance of myeloid-derived suppressor cells in human colorectal carcinoma. *World J. Gastroenterol.* **18**, 3303–9 (2012).
335. Diaz-Montero, C. M. *et al.* Increased circulating myeloid-derived suppressor cells correlate with clinical cancer stage, metastatic tumor burden, and doxorubicin-cyclophosphamide chemotherapy. *Cancer Immunol. Immunother.* **58**, 49–59 (2009).
336. Ribatti, D. & Crivellato, E. The controversial role of mast cells in tumor growth. *Int. Rev. Cell Mol. Biol.* **275**, 89–131 (2009).
337. Ruffell, B. & Coussens, L. M. Histamine restricts cancer: nothing to sneeze at. *Nat. Med.* **17**, 43–4 (2011).
338. McKenzie, G. J. *et al.* Impaired Development of Th2 Cells in IL-13-Deficient Mice. **9**, 423–432 (1998).
339. Greenblatt, M. B. *et al.* Interspecies comparison of human and murine scleroderma reveals IL-13 and CCL2 as disease subset-specific targets. *Am. J. Pathol.* **180**, 1080–94 (2012).
340. Wang, M. *et al.* Peanut-induced intestinal allergy is mediated through a mast cell-IgE-FcεRI-IL-13 pathway. *J. Allergy Clin. Immunol.* **126**, 306–16, 316.e1–12 (2010).
341. Goebeler, M. *et al.* Interleukin-13 selectively induces monocyte chemoattractant protein-1 synthesis and secretion by human endothelial cells. Involvement of IL-4R alpha and Stat6 phosphorylation. *Immunology* **91**, 450–7 (1997).
342. Gu, N. *et al.* Intelectin is required for IL-13-induced monocyte chemotactic protein-1 and -3 expression in lung epithelial cells and promotes allergic airway inflammation. *Am. J. Physiol. Lung Cell. Mol. Physiol.* **298**, L290–6 (2010).
343. Ma, C. *et al.* Anti-Gr-1 antibody depletion fails to eliminate hepatic myeloid-derived suppressor cells in tumor-bearing mice. *J. Leukoc. Biol.* **92**, 1199–206 (2012).
344. Kapanadze, T. *et al.* Regulation of accumulation and function of myeloid derived suppressor cells in different murine models of hepatocellular carcinoma. *J. Hepatol.* **59**, 1007–13 (2013).
345. Li, M., Knight, D. a, A Snyder, L., Smyth, M. J. & Stewart, T. J. A role for CCL2 in both tumor progression and immunosurveillance. *Oncoimmunology* **2**, e25474 (2013).

346. Cripps, J. G., Wang, J., Maria, A., Blumenthal, I. & Gorham, J. D. Type 1 T helper cells induce the accumulation of myeloid-derived suppressor cells in the inflamed Tgfb1 knockout mouse liver. *Hepatology* **52**, 1350–9 (2010).
347. Huang, B. *et al.* CCL2/CCR2 pathway mediates recruitment of myeloid suppressor cells to cancers. *Cancer Lett.* **252**, 86–92 (2007).
348. Obstfeld, A. E. *et al.* C-C chemokine receptor 2 (CCR2) regulates the hepatic recruitment of myeloid cells that promote obesity-induced hepatic steatosis. *Diabetes* **59**, 916–25 (2010).
349. Hansell, C. a H. *et al.* Universal expression and dual function of the atypical chemokine receptor D6 on innate-like B cells in mice. *Blood* **117**, 5413–24 (2011).
350. Bao, S., Husband, a J. & Beagley, K. W. B1 B cell numbers and antibodies against phosphorylcholine and LPS are increased in IL-6 gene knockout mice. *Cell. Immunol.* **198**, 139–42 (1999).
351. Kipps, T. J. The CD5 B cell. *Adv. Immunol.* **47**, 117–85 (1989).
352. Cinamon, G., Zachariah, M. A., Lam, O. M., Foss, F. W. & Cyster, J. G. Follicular shuttling of marginal zone B cells facilitates antigen transport. *Nat. Immunol.* **9**, 54–62 (2008).
353. Attanavanich, K. & Kearney, J. F. Marginal zone, but not follicular B cells, are potent activators of naive CD4 T cells. *J. Immunol.* **172**, 803–11 (2004).
354. Waldschmidt, T., Snapp, K., Foy, T., Tygrett, L. & Carpenter, C. B-cell subsets defined by the Fc epsilon R. *Ann. N. Y. Acad. Sci.* **651**, 84–98 (1992).
355. Baumgarth, N., Tung, J. W. & Herzenberg, L. A. Inherent specificities in natural antibodies: a key to immune defense against pathogen invasion. *Springer Semin. Immunopathol.* **26**, 347–62 (2005).
356. Haas, K. M., Poe, J. C., Steeber, D. A. & Tedder, T. F. B-1a and B-1b cells exhibit distinct developmental requirements and have unique functional roles in innate and adaptive immunity to *S. pneumoniae*. *Immunity* **23**, 7–18 (2005).
357. Baumgarth, N. *et al.* B-1 and B-2 cell-derived immunoglobulin M antibodies are nonredundant components of the protective response to influenza virus infection. *J. Exp. Med.* **192**, 271–80 (2000).
358. Alugupalli, K. R. *et al.* The resolution of relapsing fever borreliosis requires IgM and is concurrent with expansion of B1b lymphocytes. *J. Immunol.* **170**, 3819–27 (2003).

359. Binder, C. J. *et al.* Pneumococcal vaccination decreases atherosclerotic lesion formation: molecular mimicry between *Streptococcus pneumoniae* and oxidized LDL. *Nat. Med.* **9**, 736–43 (2003).
360. Takatsu, K. *et al.* Cytokine receptors on Ly-1 B cells. IL-5 and its receptor system. *Ann. N. Y. Acad. Sci.* **651**, 241–58 (1992).
361. Vink, A., Warnier, G., Brombacher, F. & Renauld, J. C. Interleukin 9-induced in vivo expansion of the B-1 lymphocyte population. *J. Exp. Med.* **189**, 1413–23 (1999).
362. Soriano, F. G., Barbeiro, H. V. & Barbeiro, D. F. Inflammatory response: role of B1 cells. *Shock* **39 Suppl 1**, 5–9 (2013).
363. Hayakawa, K. & Hardy, R. R. Normal, autoimmune, and malignant CD5+ B cells: the Ly-1 B lineage? *Annu. Rev. Immunol.* **6**, 197–218 (1988).
364. Förster, I. & Rajewsky, K. Expansion and functional activity of Ly-1+ B cells upon transfer of peritoneal cells into allotype-congenic, newborn mice. *Eur. J. Immunol.* **17**, 521–8 (1987).
365. Förster, I., Gu, H. & Rajewsky, K. Germline antibody V regions as determinants of clonal persistence and malignant growth in the B cell compartment. *EMBO J.* **7**, 3693–703 (1988).
366. Kocks, C. & Rajewsky, K. Stable expression and somatic hypermutation of antibody V regions in B-cell developmental pathways. *Annu. Rev. Immunol.* **7**, 537–59 (1989).
367. Amezcua Vesely, M. C., Bermejo, D. a, Montes, C. L., Acosta-Rodríguez, E. V & Gruppi, A. B-Cell Response during Protozoan Parasite Infections. *J. Parasitol. Res.* **2012**, 362131 (2012).
368. Minoprio, P., Coutinho, A., Spinella, S. & Hontebeyrie-Joskowicz, M. Xid immunodeficiency imparts increased parasite clearance and resistance to pathology in experimental Chagas' disease. *Int. Immunol.* **3**, 427–33 (1991).
369. Oliveira, F. L., Aguiar, A. M., Borojevic, R. & El-Cheikh, M. C. IgE expression on the surface of B1 and B2 lymphocytes in experimental murine schistosomiasis. *Braz. J. Med. Biol. Res.* **38**, 1033–42 (2005).
370. Komegae, E. N., Grund, L. Z., Lopes-Ferreira, M. & Lima, C. The longevity of Th2 humoral response induced by proteases natterins requires the participation of long-lasting innate-like B cells and plasma cells in spleen. *PLoS One* **8**, e67135 (2013).

371. Wilson, E. H., Katz, E., Goodridge, H. S., Harnett, M. M. & Harnett, W. In vivo activation of murine peritoneal B1 cells by the filarial nematode phosphorylcholine-containing glycoprotein ES-62. *Parasite Immunol.* **25**, 463–6 (2003).
372. Kaneko, Y. *et al.* CD40-mediated stimulation of B1 and B2 cells: implication in autoantibody production in murine lupus. *Eur. J. Immunol.* **26**, 3061–5 (1996).
373. Hastings, W. D., Tumang, J. R., Behrens, T. W. & Rothstein, T. L. Peritoneal B-2 cells comprise a distinct B-2 cell population with B-1b-like characteristics. *Eur. J. Immunol.* **36**, 1114–23 (2006).
374. Kitamura, D., Roes, J., Kühn, R. & Rajewsky, K. A B cell-deficient mouse by targeted disruption of the membrane exon of the immunoglobulin mu chain gene. *Nature* **350**, 423–6 (1991).
375. Ghosh, S., Hoselton, S. a & Schuh, J. M. μ -chain-deficient mice possess B-1 cells and produce IgG and IgE, but not IgA, following systemic sensitization and inhalational challenge in a fungal asthma model. *J. Immunol.* **189**, 1322–9 (2012).
376. Wu, L. C. & Zarrin, A. a. The production and regulation of IgE by the immune system. *Nat. Rev. Immunol.* **14**, 247–259 (2014).
377. Larché, M., Akdis, C. A. & Valenta, R. Immunological mechanisms of allergen-specific immunotherapy. *Nat. Rev. Immunol.* **6**, 761–71 (2006).
378. Zheng, Y., Shopes, B., Holowka, D. & Baird, B. Conformations of IgE bound to its receptor Fc epsilon RI and in solution. *Biochemistry* **30**, 9125–32 (1991).
379. Gustavsson, S., Hjulström, S., Liu, T. & Heyman, B. CD23/IgE-mediated regulation of the specific antibody response in vivo. *J. Immunol.* **152**, 4793–800 (1994).
380. Xiong, H., Dolpady, J., Wabl, M., Curotto de Lafaille, M. A. & Lafaille, J. J. Sequential class switching is required for the generation of high affinity IgE antibodies. *J. Exp. Med.* **209**, 353–64 (2012).
381. Worldwide variation in prevalence of symptoms of asthma, allergic rhinoconjunctivitis, and atopic eczema: ISAAC. The International Study of Asthma and Allergies in Childhood (ISAAC) Steering Committee. *Lancet* **351**, 1225–32 (1998).
382. Flohr, C., Quinnell, R. J. & Britton, J. Do helminth parasites protect against atopy and allergic disease? *Clin. Exp. Allergy* **39**, 20–32 (2009).

383. Yazdanbakhsh, M., Kremsner, P. G. & van Ree, R. Allergy, parasites, and the hygiene hypothesis. *Science* **296**, 490–4 (2002).
384. Mingomataj, E. C., Xhixha, F. & Gjata, E. Helminths can protect themselves against rejection inhibiting hostile respiratory allergy symptoms. *Allergy* **61**, 400–6 (2006).
385. Faulkner, H. *et al.* Age- and infection intensity-dependent cytokine and antibody production in human trichuriasis: the importance of IgE. *J. Infect. Dis.* **185**, 665–72 (2002).
386. Watanabe, N., Katakura, K., Kobayashi, A., Okumura, K. & Ovary, Z. Protective immunity and eosinophilia in IgE-deficient SJA/9 mice infected with *Nippostrongylus brasiliensis* and *Trichinella spiralis*. *Proc. Natl. Acad. Sci. U. S. A.* **85**, 4460–2 (1988).
387. Quinnell, R. J., Bethony, J. & Pritchard, D. I. The immunoepidemiology of human hookworm infection. *Parasite Immunol.* **26**, 443–54
388. Schönbeck, U., Mach, F. & Libby, P. CD154 (CD40 ligand). *Int. J. Biochem. Cell Biol.* **32**, 687–93 (2000).
389. Hjelm, F., Carlsson, F., Getahun, A. & Heyman, B. Antibody-mediated regulation of the immune response. *Scand. J. Immunol.* **64**, 177–84 (2006).
390. Getahun, A., Hjelm, F. & Heyman, B. IgE enhances antibody and T cell responses in vivo via CD23⁺ B cells. *J. Immunol.* **175**, 1473–82 (2005).
391. Hjelm, F., Karlsson, M. C. I. & Heyman, B. A novel B cell-mediated transport of IgE-immune complexes to the follicle of the spleen. *J. Immunol.* **180**, 6604–10 (2008).
392. Henningsson, F. *et al.* IgE-mediated enhancement of CD4⁺ T cell responses in mice requires antigen presentation by CD11c⁺ cells and not by B cells. *PLoS One* **6**, e21760 (2011).
393. Bobrie, A., Colombo, M., Raposo, G. & Théry, C. Exosome secretion: molecular mechanisms and roles in immune responses. *Traffic* **12**, 1659–68 (2011).
394. Padro, C. J., Shawler, T. M., Gormley, M. G. & Sanders, V. M. Adrenergic regulation of IgE involves modulation of CD23 and ADAM10 expression on exosomes. *J. Immunol.* **191**, 5383–97 (2013).
395. Qazi, K. R., Gehrman, U., Domange Jordö, E., Karlsson, M. C. I. & Gabrielsson, S. Antigen-loaded exosomes alone induce Th1-type memory through a B-cell-dependent mechanism. *Blood* **113**, 2673–83 (2009).

- 396. Kehry, M. R. & Yamashita, L. C. Low-affinity IgE receptor (CD23) function on mouse B cells: role in IgE-dependent antigen focusing. *Proc. Natl. Acad. Sci. U. S. A.* **86**, 7556–60 (1989).
- 397. Stief, A. *et al.* Mice deficient in CD23 reveal its modulatory role in IgE production but no role in T and B cell development. *J. Immunol.* **152**, 3378–90 (1994).
- 398. Rudolph, A. K., Burrows, P. D. & Wabl, M. R. Thirteen hybridomas secreting hapten-specific immunoglobulin E from mice with Iga or Igb heavy chain haplotype. *Eur. J. Immunol.* **11**, 527–9 (1981).
- 399. Kim, K. J., Kanellopoulos-Langevin, C., Merwin, R. M., Sachs, D. H. & Asofsky, R. Establishment and characterization of BALB/c lymphoma lines with B cell properties. *J. Immunol.* **122**, 549–54 (1979).
- 400. Liu, F. T. *et al.* Monoclonal dinitrophenyl-specific murine IgE antibody: preparation, isolation, and characterization. *J. Immunol.* **124**, 2728–37 (1980).
- 401. Chen, B.-H. *et al.* Necessity of the stalk region for immunoglobulin E interaction with CD23. *Immunology* **107**, 373–81 (2002).

VITA

Rebecca Kelley Martin was born on May 14, 1983 and grew up in Richmond, Virginia. She is an American citizen. She graduated from Mills E. Godwin High School in Richmond, Virginia in 2001. She attended Virginia Commonwealth University in Richmond, Virginia and graduated *cum laude* with a Bachelor's of Science in 2009.